
UNIVERSITY OF THE
WITWATERSRAND,
JOHANNESBURG

# *Metallic Equivalent of Aircraft Landing Gear Using Composite Materials*

***Marius Hugo Kotze***

(Student number: 2743834)

School of Mechanical, Industrial and Aeronautics

University of the Witwatersrand

Johannesburg, South Africa.

**Supervisor: Michael Boer**

A Research Project report submitted to the Faculty of Engineering and the Built Environment, University of the Witwatersrand, in fulfilment of the requirements for the degree of Masters of Science in Engineering.

*2024/07/15*

# Declaration

I declare that this Dissertation is my own, unaided work. It is being submitted for the Degree of Master of Science in Engineering at the University of Witwatersrand, Johannesburg. It has not been submitted before any degree of examination in any other University.

Signature: 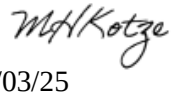

Date: 2024/03/25

# Abstract

There are two types of Light Sport Aircraft landing gear configuration. The taildragger and tricycle arrangement where the difference is specified by the position of the main landing gear. Shipment delay of the current Aluminium 7075 T6 landing gear has caused further delays in the manufacturing of the BushCat Light Sport Aircraft. Thus, a composite alternative was required which could be manufactured locally. The objective was to determine which locally available material was best suited as an alternative to the current Aluminium 7075 T6 design. This included estimation of the correct design loads acting on the BushCat aircraft main landing gear and to specify a composite alternative that could withstand these calculated design application loads. The loads that were used would be obtained from the ASTM F2245-14 regulations and EASA CS-23 amendments. The loads were validated by means of Finite Element Analysis and analytical calculations. Drop tests were also conducted by the company and image processing was used to compare the calculated deformations to the FEA results. This was used to validate the load and constraint applications in Ansys 2023 R2 software. The composite materials used for analysis were unidirectional epoxy e-glass wet layup and prepregs fibres. A coupon study was conducted on Aluminium 7075 T6 alloy and [0/90/90/0], [0/45/45/0], [0/90/45/0] layered unidirectional epoxy e-glass wet layup and prepreg coupons loaded under tension, compression, bending and torsion. The FEA results were validated using analytical calculations obtained from the Classical Lamination Theory. It was concluded that the unidirectional epoxy e-glass prepreg coupons were best suited as an alternative as better results in withstanding the applied load applications were obtained. The prepreg fibres also contained a lower void content in comparison to the wet layup fibres, thus increasing the fatigue life of the composite laminate as well as reducing the moisture absorption. The final composite landing gear was analysed using the Puck-failure criterion and it was found that after analysis and modifications were conducted, the newly designed composite landing gear could withstand the applied loads during limit load and ultimate load conditions without any fibre or inter-fibre failure in the strut of the landing gear. It was found that, failure had occurred in one of the fibre plies near the bolted regions of the axle section during ultimate (emergency) landing conditions and was thus concluded that the composite landing gear should still be inspected when attempting emergency landing at higher load conditions at an aircraft maximum take-off weight of 600 kg. The final composite landing gear design after modifications was 4.613 kg heavier than the Aluminium 7075 T6 landing gear. With regards to manufacturing the final composite landing gear a vacuum bagging process should be followed where the final vacuum bagging assembly containing the composite layup of the landing gear should be placed inside an oven or autoclave to start the curing process. Once the composite landing gear is cured, it could be machined into its final shape were non-destructive techniques such as ultrasound of thermography should be used to inspect the final composite landing gear for any air of volatile compounds withing the laminate. Static and dynamic destructive testing should also be used to validate if the final composite landing gear can withstand all landing conditions aircraft maximum weight without any fibre failure or delamination occurring.

# Table of Contents:

# List of Figures:

# List of Tables:

## 1. RESEARCH BACKGROUND

Aircraft landing gear plays an essential role during ground and landing operations [1]. The landing gear must withstand the loads during operation and absorb the impact energy of landing to ensure other components of the aircraft are not damaged in the process [1].

South African Civil Aviation Authority (SACAA) approved aircraft manufacturer is known for manufacturing the BushCat Light Sport Aircraft (LSA). The BushCat Aircraft main landing gear is manufactured using Aluminium alloy 7075 T6. The current landing gear is manufactured by Grove Aircraft Landing Gear Systems Inc. which is situated in United States of America. Due to the current landing gear being manufactured by a foreign company, the aircraft manufacturer has experienced delays in shipment of this specific landing gear which caused further delays in the assembly and delivering of the BushCat Aircraft. By finding a solution to the problem, shipment costs and manufacturing delays could be eliminated. The evidence of the main landing gear supply delay is contained in appendix C.

## 2. PROBLEM STATEMENT

The problem is created by frequent delays of the main landing gear supplied by Grove Landing Gear Systems Inc. and is significant for the manufacturing stages of the BushCat Aircraft. This component is an off-the-shelf product may exceed the required specifications for its application on the BushCat aircraft. Grove specialises in the manufacturing of Aluminium leaf spring landing gears by using their expertise, testing and machinery throughout the entire process. The product is not locally available in South Africa thus, a composite alternative is required since it can be manufactured locally, is cost effective and are used by various other local Light Sport Aircraft manufacturers.

## 3. RESEARCH QUESTIONS

### 3.1. Critical Research Question:

Can a main landing gear that is manufactured using composite materials withstand the loads acting on the current Aluminium alloy 7075 T6 landing gear design?

### 3.2. Sub Questions:

Which locally available composite material is best suited as an alternative to the current Aluminium 7075 T6 design?

## 4. RESEARCH OBJECTIVES

The objectives of this research are to:

a. Determine the correct design loads acting on the BushCat Aircraft main landing gear.
b. Validate Finite Element Analysis (FEA) results with numerical values and drop test results.
c. Specify a composite alternative that can withstand these calculated design application loads.

## 5. LITERATURE REVIEW

### 5.1. Introduction

The literature review will focus on the load conditions, landing conditions and the requirements of an aircraft landing gear specified by the Utility, Aerobatic and Commuter Category (EASA CS-23 Initial Issue) and (ASTM F2245 – 14) standard specifications for the design and performance of a Light Sport Airplane. It also includes literature regarding composite materials used for Light Sport Aircraft main landing gear.

### 5.2. Aircraft and Landing Gear Loads

#### 5.2.1. Loads/ Forces Acting on BushCat Aircraft Landing Gear:

There are two types of BushCat Aircraft landing gear configurations, namely Tricycle and Taildragger landing gear configuration as seen in Figure 1. Note that the main landing gear is positioned at different locations on the aircraft.

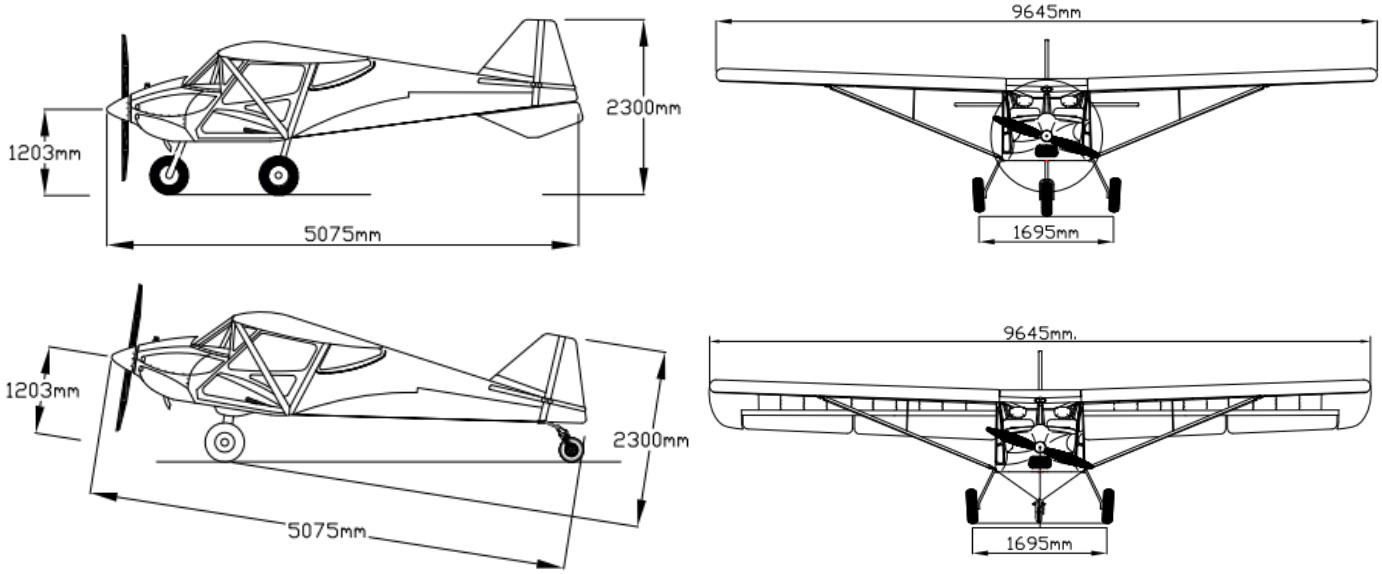


*Figure 1: BushCat Aircraft Tricycle and Taildragger Landing Gear Configuration and Aircraft Dimensions [2]*

In Figure 2, the current Aluminium 7075 T6 alloy landing gear is displayed as a leaf spring design with its load and deflection graph, which is important when considering the different landing conditions. The deflection ‘d’ denotes vertical deflection of the gear. It indicates the efficiency of the shock absorption by the landing gear and is directly correlated to the landing gear’s ability to absorb the impact forces during landing [3].

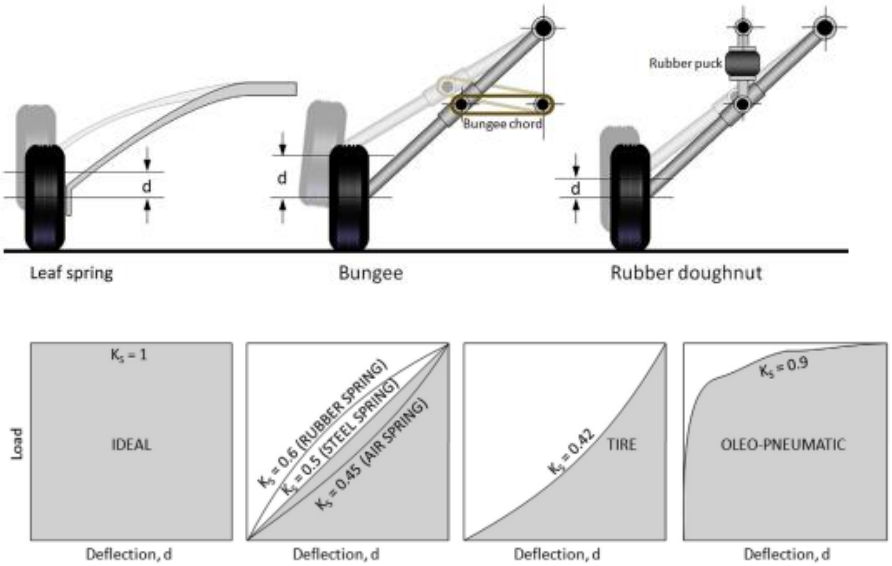


*Figure 2: Landing Gear Design and Load vs Deflection Graphs [3]*

In Figure 3, the basic landing conditions are indicated according to the ASTM F2245 – 14 and EASA CS – 23 regulations for the Tricycle and Taildragger configurations [4]. Each landing condition has its own Centre of Gravity (CG) position which influences load distribution of the aircraft and the loads experience on the main landing gear.

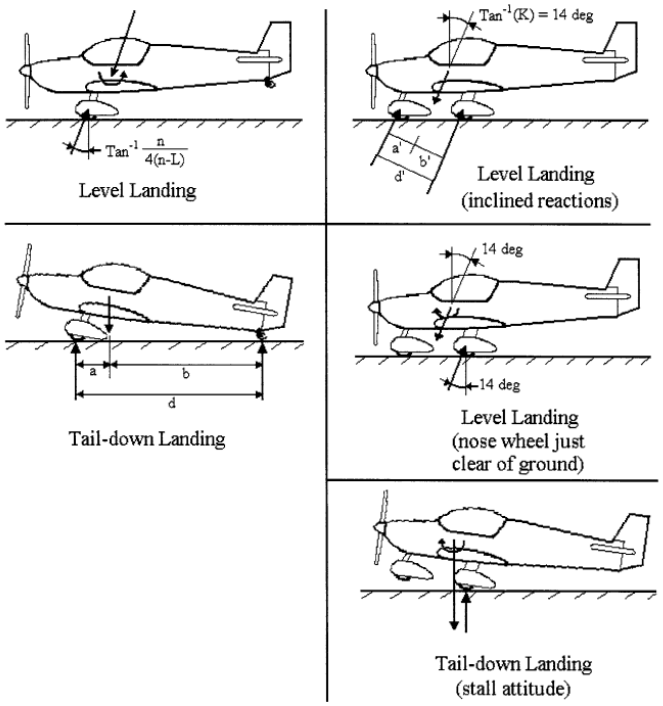


*Figure 3: Basic Landing Conditions [4]*

Table 1 contains a summary of Load/ Force applications for each landing condition. It is important to note the different landing conditions specified by the ASTM F2245 – 14 regulations [4]. When designing the main landing gear for any Aircraft, the design is required to withstand the worst landing condition specified in Figure 3 and Table 1. The safety factor required for each condition is 1.5 [4].

*Table 1: Description of Load/ Force Components for Each Landing Condition [4]*

| Condition | Tail Wheel Type | | Nose Wheel Type | | |
|---|---|---|---|---|---|
| | Level Landing | Tail-down Landing | Level Landing with Inclined Reactions | Level Landing with Nose Wheel Just Clear of Ground | Tail-Down Landing |
| Vertical component at CG | nW | nW | nW | nW | nW |
| Fore and aft component at CG | KnW | 0 | KnW | KnW | 0 |
| Lateral component in either direction at CG | 0 | 0 | 0 | 0 | 0 |
| Shock absorber deflection (rubber or spring shock absorber), % | 100 % | 100 % | 100 % | 100 % | 100 % |
| Tire deflection | Static | Static | Static | Static | Static |
| Main wheel loads ($V_r$) | (n-L)W | (n-L)Wb/d | (n–L)Wa'/d' | (n-L)W | (n-L)W |
| (both wheels) ($D_r$) | KnW | 0 | KnWa'/d' | KnW | 0 |
| Tail (nose) wheels ($V_r$) | 0 | (n-L)Wa/d | (n-L)Wb'/d' | 0 | 0 |
| Loads ($D_r$) | 0 | 0 | KnWb'/d' | 0 | 0 |

The following inputs are required to obtain the load/ force component at the Centre of Gravity (CG) and general loads for each landing scenario [4]:

$K = 0.25$

$L = {}^{2}/_{3} =$ Ratio of assumed wing lift to aircraft weight

$n_j =$ Load factor on wheels

$n = n_j + {}^{2}/_{3} =$ Load factor

$W =$ Maximum design weight of Aircraft (kg)

$a =$ Chord length of aircraft wing (m)

$b =$ Wing span of aircraft (m)

If $n_j > 3.33$, masses such as the engine, fuel tank, occupant, seats, and ballast must be designed for a limit load factor for landing $n_j + 0.67 = (n > 4)$.

According to the ASTM F2245 – 14 regulations, during emergency landing conditions the landing gear must be designed for the following ultimate load factors [4]:

$n = 3$ in the upwards direction

$n = 9$ or 10 (for engines) in the forwards direction

$n = 1.5$ in the lateral direction

According to the EASA CS – 23 and ASTM F2245 – 14 regulations, the following must be considered:

1) For side load conditions as seen in Figure 4, the limit vertical load factor = 1.34W, lateral inertia load factor = 0.83W and the vertical ground reaction force is divided between the main wheels. The lateral ground reaction frictional load is 0.5W acting inboard while 0.33W is acting outboard. The drag loads can be assumed to be zero [5].

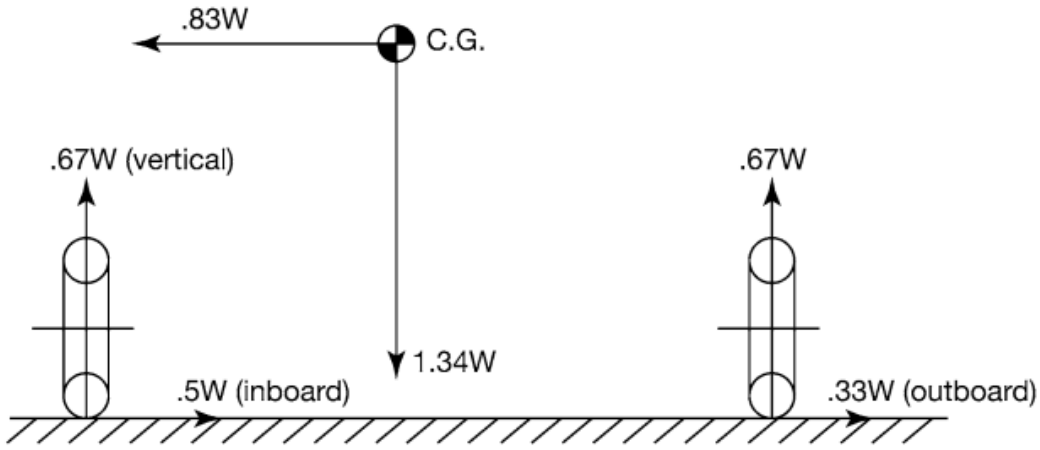


*Figure 4: Side Load Landing Conditions [4]*

2) During braked roll conditions as seen in Figure 5 with tyres in the static position, the limit vertical load factor = 1.33W. A drag reaction equals the vertical/ normal reaction is multiplied by the coefficient of friction of 0.8 at wheel contact point to the ground when brakes are applied [5].

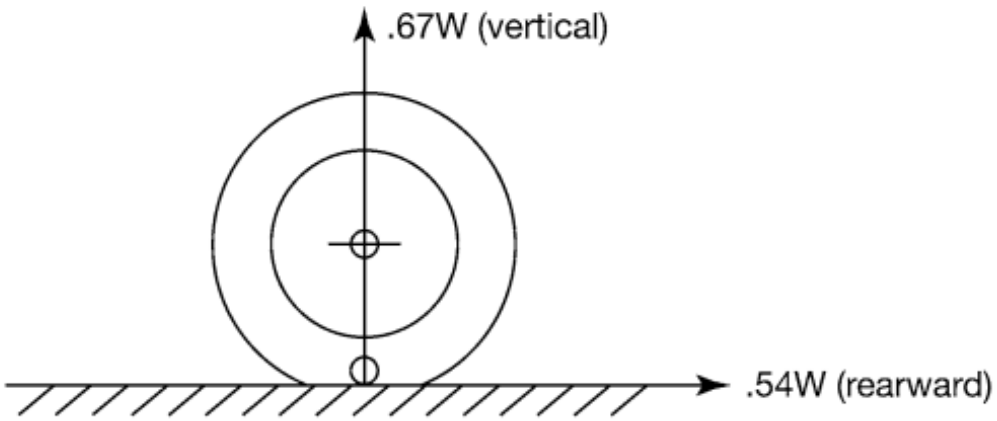


*Figure 5: Braked Roll Landing Condition [4]*

Figure 6 and Figure 7 provides the free body diagram for the loads exerted on both tricycle and taildragger landing gear. As seen in Figure 6 and Figure 7, the aircraft can land normally whilst during crosswind conditions the aircraft can be “skewed” during landing which is also known as a “crabbed” landing. When the crosswinds are strong enough, they can create a situation where the aircraft’s flight path is not directly aligned with the centreline of the runway.

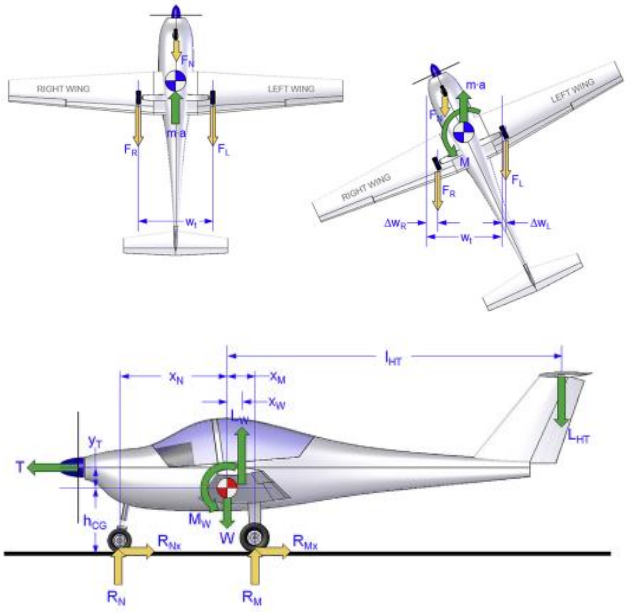


*Figure 6: Loads on Tricycle Configurated Aircraft During Landing [3]*

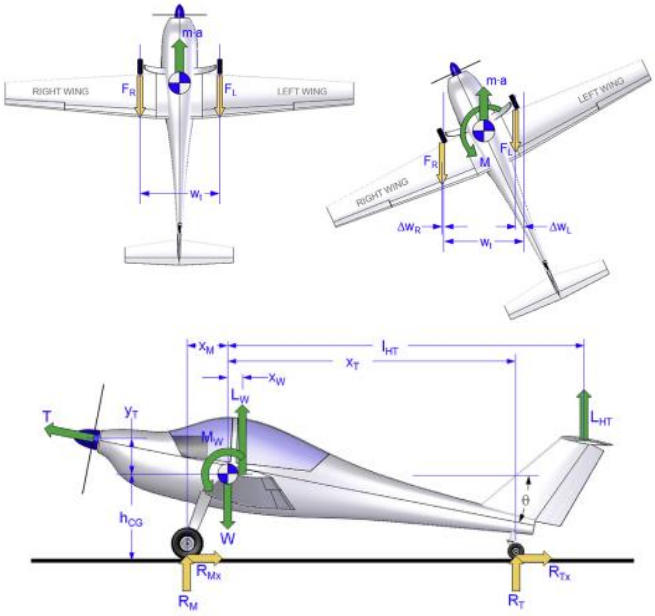


*Figure 7: Loads on Taildragger Configurated Aircraft During Landing [3]*

Figure 8 displays the mass and centre of gravity (CG) position graph obtained from the BushCat Pilot Operating Handbook (POH) [2]. Each specific mass that the aircraft may operate at has a forwards and rearwards CG limit. The percentage position at the CG is determined using the percentage Mean Aerodynamic Chord (MAC). A demonstration is shown in Figure 9. This graph is known to every pilot operating the BushCat Aircraft as well as the engineer designing the landing gear.

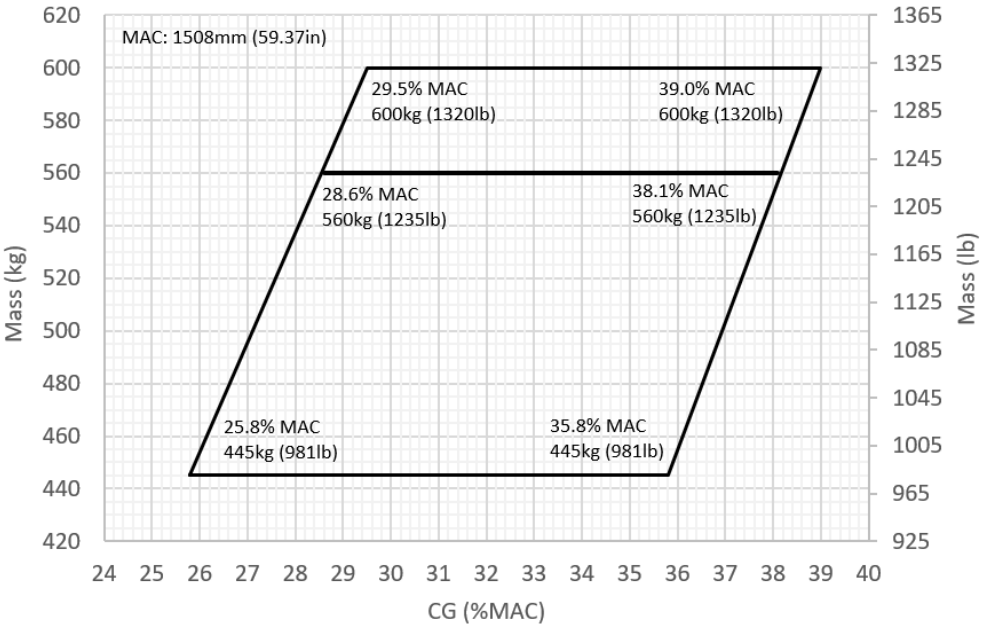


*Figure 8: Mass vs CG (%MAC) Graph for BushCat Aircraft [2]*

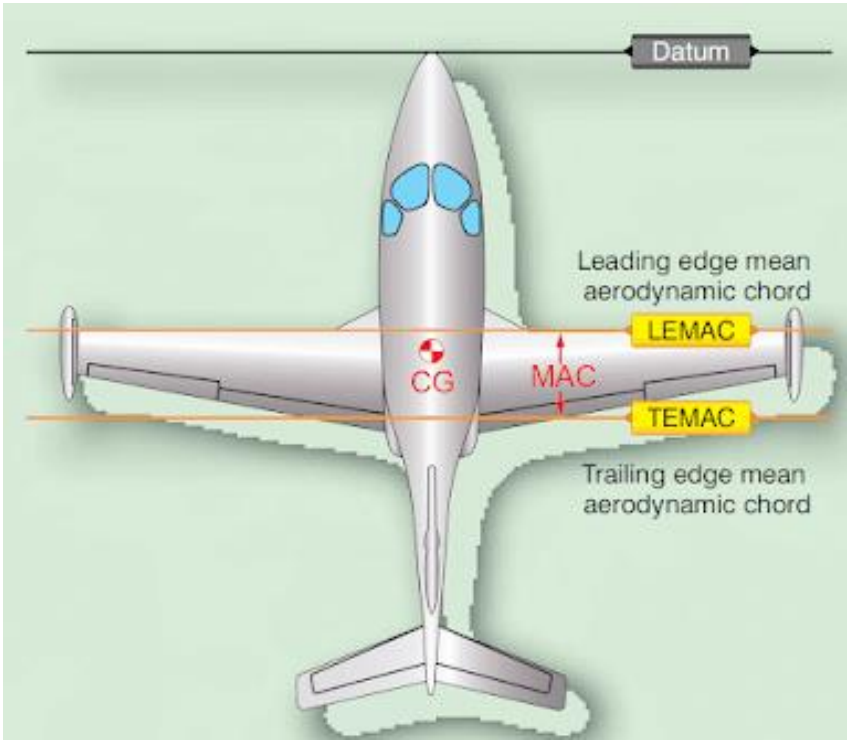


*Figure 9: MAC Chord Drawn Trough the Centre of the Area of the Wing [6]*

Wheel spin up loads must also be considered during landing. Equation 1 provides the wheel spin up loads during aircraft landing that are specified by the EASA CS – 23 regulations [5].

$$F_{Hmax} = \frac{1}{r_e}\sqrt{\frac{2Iw(V_H - V_C)_n F_{Vmax}}{t_z}} \quad (1)$$

Where:

$F_{Hmax}$ = Maximum rearward horizontal force acting on the wheel (lb)

$r_e$ = Effective rolling radius of wheel under impact based on tyre pressure during operation (ft)

$Iw$ = Rotation mass moment of inertia of rolling assembly (slug feet)

$V_H$ = Linear velocity of aircraft in the x-direction at instant of contact (ft/s)

$V_c$ = Peripheral speed of tyre (ft/s)

$n$ = Coefficient of friction

$F_{Vmax}$ = Maximum vertical force on wheel/ tyre (lb)

$tz$ = Time interval between wheel contact and maximum vertical force exerted on wheel (s)

According to the EASA CS-23 regulation the following requirements are necessary when testing the landing gear such as 1) limit shock absorption tests, 2) limit drop tests and 3) ground load dynamic test [5]. These tests are necessary after the new composite landing gear is installed to meet the safety requirements.

1) Limit shock absorption test

The landing gear may not fail, but yielding is allowed whilst simulating a descent velocity 1.2 times the limit descent velocity assuming that the wing lift force is the same as the weight of the aircraft [5].

2) Limit drop tests

Limit drop tests must be conducted using complete aircraft [4]. The drop height may not be less than the height calculated in the following formula:

$$\text{h (m)} = \ 0.0132 \left(\frac{\text{Mg}}{\text{S}}\right)^{½} \quad (2)$$

Where:

h = Drop height ($m$)
Mg = Mass × Gravity
S = Wing Area ($m^2$)

The drop height may also not be less than 0.234 m or more than 0.475 m [4].

If the wing lift is provided during free drop tests, then the weight for the landing gear drop height is calculated using Equation 3 [5]:

$$M_e = M \times \frac{h+(1-L)d}{h+d} \quad (3)$$

Where:

Me = Weight used during drop test (kg)

h = Specified free drop height (m)

d = Deflection of tyre + the vertical component of the axle distance travelled (m)

Mm = Weight of main landing gear (kg)

Mt = Weight of tail gear (kg)

Mn = Weight for nose gear assuming mass of aircraft acting at CG and exerts a force of 1g downwards and 0.33g forwards (kg)

L = Ratio of wing lift to aircraft weight, may not be more then 0.667g

3) Ground load dynamic test

For the ground load dynamic test, the test must be conducted using a complete aircraft and must adhere to the level landing conditions. The drop height must be 2.25 times the drop height that is calculated in the limit drop test section [5].

Composite Materials Used on Light Sport Aircraft Landing Gear:

A composite material is composed out of two elements that work together to achieve desired material properties [7]. Composites are divided into three main groups:

1) Polymer Matrix Composites (PMC)
2) Metal Matrix Composites (MMC)
3) Ceramic Matrix Composites (CMC)

However, for this project the focus will be on the PMC composites to design and manufacture a equivalent leaf spring landing gear. PMC use a polymer base resin as the matrix and for the reinforcement it uses glass fibre, carbon fibre or aramid [7]. The resins used can be epoxies or polyesters depending on the desired properties and application that is needed. The resin matrix better distributes the load across the fibres and protects it from abrasion or impact damage [7].

As seen in Figure 10, combining a composite fibre material with resin allows for a composite component that is highly resistant to both tensile stresses and strains. During loading of a composite structure/ component, the composite fibers are more effective in withstanding stresses whilst the resin is more effective in withstanding strain. Thus, a combination of both is needed inside a composite structure/ component to withstand the exerted loads.

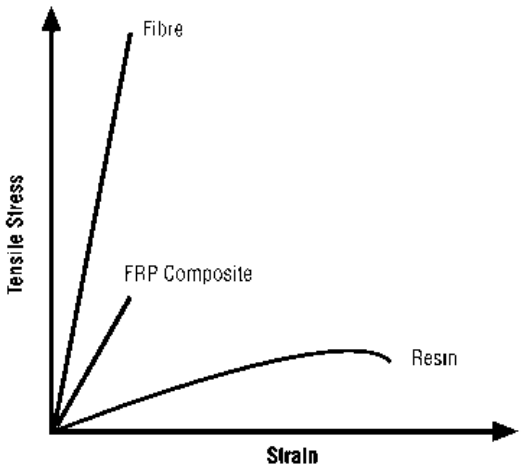


*Figure 10: Tensile vs Strain Graph for PMC [7]*

When using a fibre such as S-glass, the resin used must have a larger elongation to break percentage then the S-glass to achieve the maximum strain properties [7].

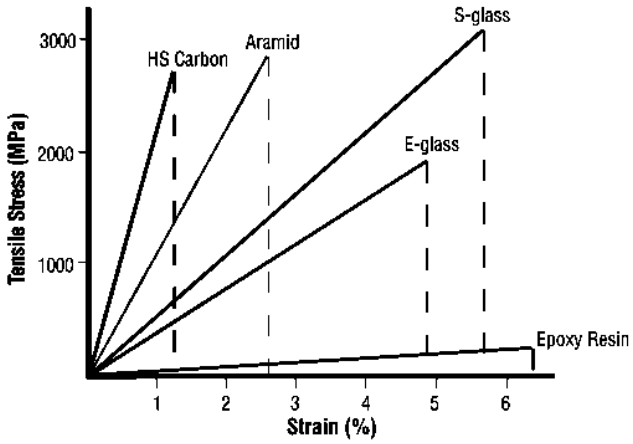


*Figure 11: Strains to Failure of PMC's [7]*

The overall material property for the composite is determined by the following [7]:

1) Properties of the fibre
2) Property of the resin
3) Fibre Volume Fraction (Ratio of the fibre to resin composite)
4) Orientation and geometry of the fibres inside the composite

Figure 12 provides the four main loads experienced by a composite component during load conditions [7]. The main loads that any composite structure or component will experience is tensile, compression, torsion and bending respectively.

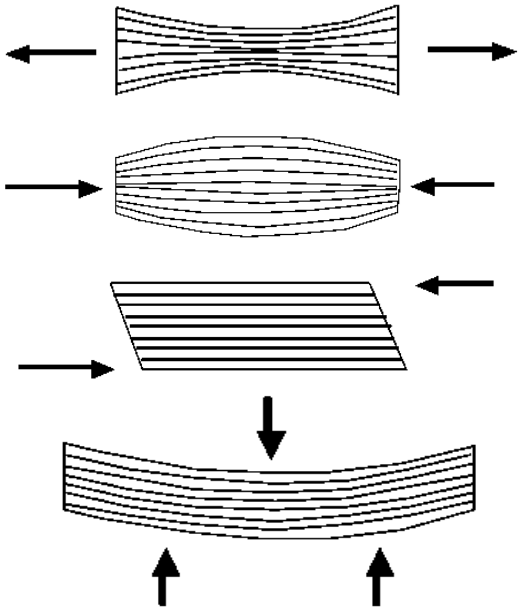

*Figure 12: Tensile, Compression, Shear and Flexural Loads Respectively [7]*

The resin normally used for aircraft landing gear applications is aircraft grade Epoxy resin. This is due to the highest stress and strain in comparison to Polyester and Vinylester resins that Epoxy resin can withstand. Polyester resins are considered a brittle resin which is not applicable for composite aircraft landing gear since its brittleness will not produce the spring action needed for the landing gear [7].

Composite materials demonstrate excellent fatigue resistance in comparison to most metals. The fatigue resistance of a composite is determined by the quality of the manufacturing process. As a result, epoxy-based resins are extremely resistant to fatigue in comparison to other resins used, thus it is very popular in the aviation industry when used for aircraft structures [7].

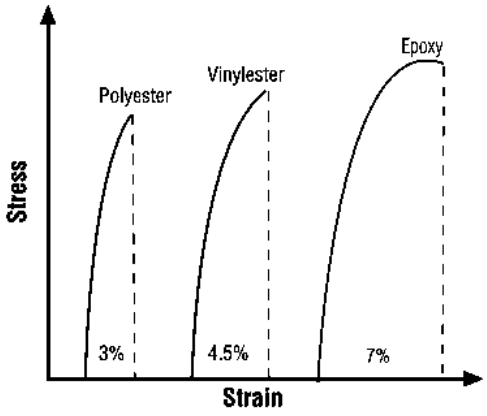


*Figure 13: Resin Comparison [7]*

Figure 14 shows how fibre laminates can be stacked to resist the load cases displayed in Figure 12. The symmetry and balance of the stack is important, the 45-degree stacks help with shear loads, whilst the 0 and 90-degree stacks help with bending loads acting on the structure [7].

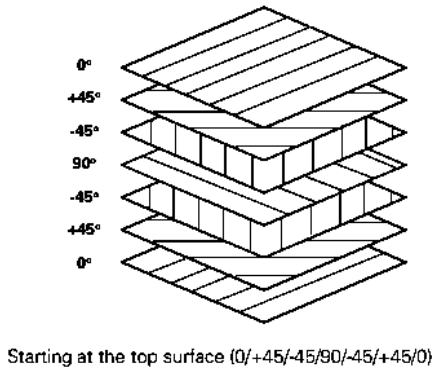


*Figure 14: Laminate Stacking Orientation [7]*

Table 2 provides a comparison between the different types of polymer matrix composites. The advantages, disadvantages, general cost provided by Toray Advanced Composites, availability, and ease of manufacturing were compared however, glass fibre reinforcement was studied and used during the design of the composite landing gear in this research report.

*Table 2: PMC Material Comparison*

| | **Glass Fibres** | **Carbon Fibres** | **Aramid Fibres** |
|---|---|---|---|
| Advantages | -High impact resistance (useful for applications requiring impact and shock absorbing effects) [8]<br>-High strain capacity [8] | -Exceptional strength to weight ratio<br>-Low corrosion<br>-High fatigue resistance [8]<br>-Good aesthetics<br>-Dimensional stability allowing fibres to maintain shape and dimension during changing environmental conditions. [8] | -Exceptional impact resistance<br>-Good fatigue resistance<br>-Good strength to weight ratio [8]<br>-Very low compressive strength (useful for only tensile and stiffness applications – less stiff than carbon fibre) [9] |
| Disadvantages | -Lower strength to weight ratio<br>-Can absorb moisture over time [8]<br>-Limited temperature resistance<br>-Can be susceptible to strong acids or alkalis [8] | -High Young's modulus<br>-High brittleness (susceptible to low strain failure) [8]<br>- Possibility to cause damage to structure during minor impact loads [8]<br>-High material and manufacturing costs. | -Degrades under prolonged exposure to UV-rays.<br>-Hybrid forms with other composites have increased delamination possibility [8]<br>-Possibility to not bond particularly well with most resin systems [9]<br>-Possibility to absorb water rapidly [9] |
| General Cost | E-glass 7581 (300 gsm) @ € 4.50/m^2 | Carbon 3K @ € 50/kg<br>Carbon 12K @ € 35/kg | Aramid (Twaron) (640 gsm) @ € 14.50/m^2 |
| Availability | -Widely used PMC, manufactured by Toray and Mitsubishi Chemical [9] | -Most widely used PMC, manufactured by Toray and Mitsubishi Chemical [9] | -Widely used PMC, manufactured by Toray and Mitsubishi Chemical [9] |
| Ease of Manufacturing | -Void content should be carefully controlled with regards to resin content application.<br>-May require oven or autoclave which increases production cost [10] | -Requires specialized manufacturing using autoclave curing. Can increase production cost [10] | -Mostly in hybrid forms with other PMC's, thus manufacturing process should be tailored to reduce delamination possibilities in final product [10] |

### 5.3. RX1E-A Aircraft Composite Undercarriage Case Study

In the following study conducted by the Chinese Society of Aeronautics and Astronautics (CSAA) a composite leaf spring landing gear was manufactured for the RX1E-A two-seater electric aircraft by means of autoclaving [11]. The ASTM 2245-14 standards were followed during the research conducted by CSAA.

*Figure 15: RX1E-A Two-Seater Electric Aircraft [11]*

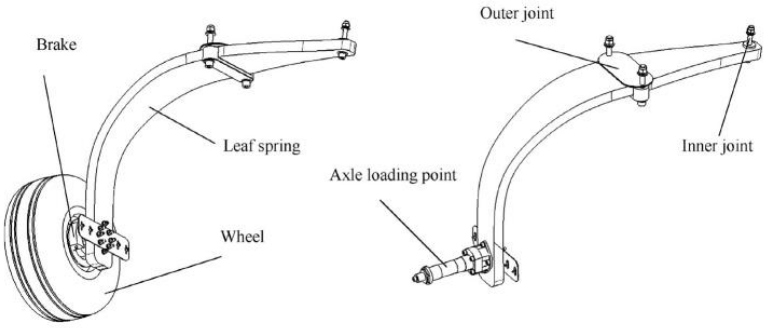


*Figure 16: RX1E-A Leaf Spring Landing Gear [11]*

Glass fibre unidirectional belt prepreg has a low modulus and high toughness. These characteristics are necessary to absorb the energy transferred to the landing gear [11]. The design of this composite landing gear must be able to minimise structural damage that can be caused by material deviation [11]. To obtain an optimum design, two stages need to be considered when constructing the composite gear. Stage 1 is the thickness optimisation of the composite fiber layers whilst Stage 2 is the fiber stack-up orientation optimisation of the layer [11].

Table 3 provides the material properties for the epoxy e-glass fibre composite prepreg. It includes the longitudinal modulus of elasticity ($E_1$), transverse modulus of elasticity ($E_2$). in-plane modulus of elasticity ($G_{12}$), in-plane Poisson's ratio ($\mu_{12}$), longitudinal tensile strength ($\sigma_1^t$), longitudinal compressive strength ($\sigma_1^c$), transverse tensile strength ($\sigma_2^t$), transverse compressive strength ($\sigma_2^c$ ) and the in-plane shear strength ($\sigma_{12}$) [11].

*Table 3: Properties of Glass Epoxy E-Glass Prepreg Fibre Material [8]*

| Parameter | $E_1$(GPa) | $E_2$(GPa) | $G_{12}$(GPa) | $\mu_{12}$ | $\sigma_1^t$(MPa) | $\sigma_1^c$(MPa) | $\sigma_2^t$(MPa) | $\sigma_2^c$(MPa) | $\bar{\sigma}_{12}$(MPa) |
|---|---|---|---|---|---|---|---|---|---|
| Value | 30 | 7.7 | 3.7 | 0.3 | 642 | 610 | 58 | 131 | 64 |

The following equations is used to obtain values of each landing load condition *[11]*:

1) Stiffness of leaf spring landing gear and tyre

$$k = \frac{k_t k_s}{k_t + k_s} \tag{4}$$

Where:

$k$ = Combined stiffness of leaf spring landing gear and tyre (-)
$k_t$ = Stiffness of wheel tyre (-)
$k_s$ = Stiffness of leaf spring gear (-)

2) Drop height of landing gear during drop test

$$h = 1.32\sqrt{\frac{W}{S}} \tag{5}$$

Where:

$h$ = Drop height ($m$)
$W$ = weight of aircraft ($kg$)
$S$ = Area of aircraft wing ($m^2$)

1) Load factor on the centre of gravity (CG) position

$$n = \frac{h + {}^{d}/_{3}}{e_d + d} + L \tag{6}$$

Where:

$n$ = Load factor on CG (-)
$h$ = Drop height ($m$)
$d$ = Total shock absorber travel ($m$)
$e_d$ = Shock efficiency (-)
$L$ = Ratio of assumed wing lift to aircraft weight (-)

2) Total shock absorber travel

$$d = \frac{nW}{k} \tag{7}$$

Where:

$d$ = Total shock absorber travel ($m$)

$n$ = Load factor on CG (-)

$W$ = weight of aircraft ($kg$)

$k$ = Combined stiffness of leaf spring landing gear and tyre (-)

Table 4 provides the weight of each layer of the composite that was adjusted by means of optimising the thickness for each layer. This reduced the weight of the leaf spring landing gear and an experiment was conducted to check what the displacement and ground load force in (Newtons) are for each optimisation [11]. To avoid crack propagation the number of continuous layers did not exceed four layers [11]. The angle of each layer in the continuous layer stack is also displayed.

*Table 4: Data Obtained/ Calculated of the Composite Material During Different Optimisations [8]*

| Model | Root layup & thickness(mm) | Ground load(N) | Displacement(mm) | Mass(kg) |
|---|---|---|---|---|
| Stiffness constrained leaf | [45/−45/0/45/90/−45/0/45/90/−45/0/45/90/−45/0]s<br>[0.8/0.8/3.2/0.8/0.8/0.8/3.2/0.8/0.8/0.8/1.6/0.8/0.8/0.8/1.6]s | 12973.483 | 156 | 4.9 |
| First-stage optimization | [45/−45/0/45/90/−45/0/45/90/−45/0/45/90/−45]s<br>[0.6/0.6/3.2/0.92/0.06/0.92/3.2/0.5/0.6/0.5/2.1/0.5/0.6/0.5]s | 8289.118 | 189 | 3.418 |
| Second-stage optimization | [45/−45/0/45/−45/0/45/90/−45/0/45/90/−45]s<br>[0.8/0.8/3.2/1.6/1.6/2.4/0.8/0.8/0.8/1.6/0.8/0.8/0.8]s | 9439.633 | 169.665 | 3.8 |

During the second stage optimisation shown in Figure 17, a comparison is presented regarding the area of the leaf spring landing gear where the thickness was adjusted. The thickness distribution before optimisation was focused near the bracket section of the gear connected to the aircraft fuselage and after optimisation the thickness distribution was modified to be more focused before the top bend section of the leaf spring gear strut.

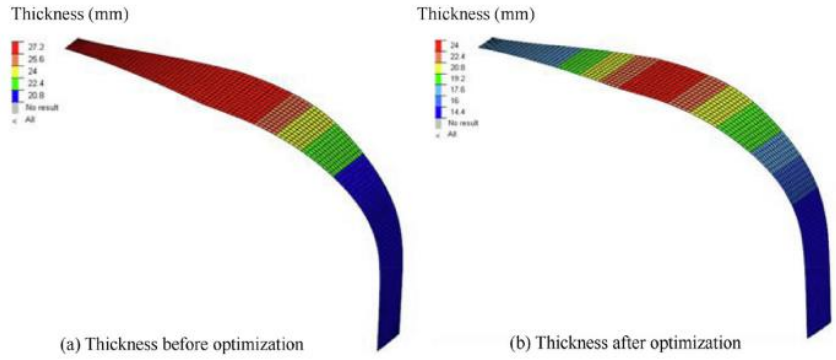


*Figure 17: Layer Thickness Optimisation [11]*

Figure 18 depicts the 3 modes namely tensile, compressive and shear failure respectively. The strength criterion of composite materials can be divided in two categories namely ultimate strength failure criteria such as the (maximum-stress and maximum-strain criterion), Tsai-Hill, Hoffman and Tsai-Wu which does not distinguish between failure modes whereas the second category distinguishes between failure modes such as the Hashin, Puck and LaRC03. The Puck failure criterion was used during the design since failure between fibre and inter-fibre is distinguished and can reasonably simulate the failure mechanisms between fibres whilst the theoretical prediction results agree well with obtained experimental results to ensure validity of the analysis. An addition to the Puck-failure criterion also included fibre and inter-fibre tension and compression failure making it an optimal choice for the analysis of the composite leaf spring landing gear [11].

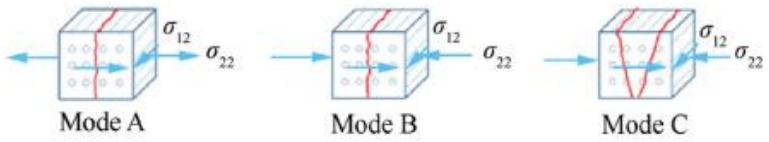


*Figure 18: 3 Failure Modes: Tensile, Compressive and Shear [11]*

In Figure 19, the FEA simulation results provide a visualisation on where the failure was most likely to occur for each failure parameter and mode. $ef_{modeA}$ is the inter-fibre failure Mode A damage parameter, $ef_{modeB}$ is the inter-fibre failure Mode B damage parameter, $ef_{modeC}$ is the inter-fibre failure Mode C damage parameter. $ef_{ft}$ is the fibre tensile Mode A damage parameter and $ef_{fc}$ is the fibre compressive failure Mode B damage parameter. The main composite gear was more prone to inter-fibre tensile failure ($ef_{modeA}$) and inter-fibre compression failure ($ef_{modeB}$) than inter-fibre shear failure ($ef_{modeC}$). Fibre tensile ($ef_{ft}$) and fibre compression ($ef_{fc}$) damage was also present during loading conditions on the modified gear. Thus, during loading of a composite leaf spring landing gear, the FEA results depict that the tensile and compressive load resulted in the failure of the composite leaf spring landing gear.

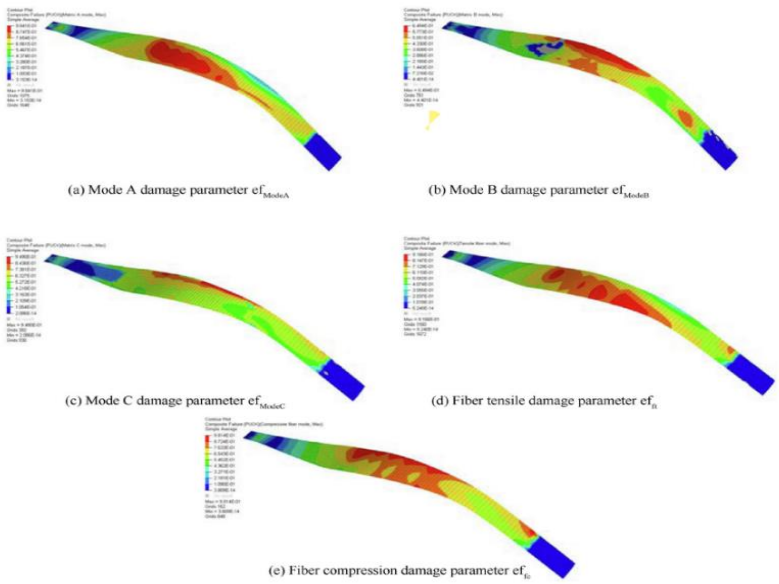


*Figure 19: FEM Simulation for Each Failure Parameter [11]*

Table 5 provides the FEA strain results of the composite leaf spring for each landing condition for both the tricycle and taildragger aircraft during ultimate (emergency) load conditions.

*Table 5: Maximum Strain of Leaf Spring in Tensile, Compressive and Shear Condition [8]*

| Condition | Tensile strain (με) | Compressive strain (με) | Shear strain (με) |
|---|---|---|---|
| Level landing with inclined reactions | 15340 | −15300 | 10170 |
| Level landing with nose wheel just clear of ground | 20700 | −20650 | 13720 |
| Tail-down landing | 18370 | −19460 | 13040 |
| Side load conditions (Inward load) | 2323 | −2497 | 1582 |
| Side load conditions (External load) | 9795 | −10140 | 6797 |
| Braked roll conditions | 8131 | −8241 | 5965 |

During the physical test conducted on the fibre composite landing gear, strain gauges were attached to the gear during the test. Figure 21 and Figure 22 shows the distribution of the strain gauges on the composite landing gear and the crane used to apply the load to the gear.

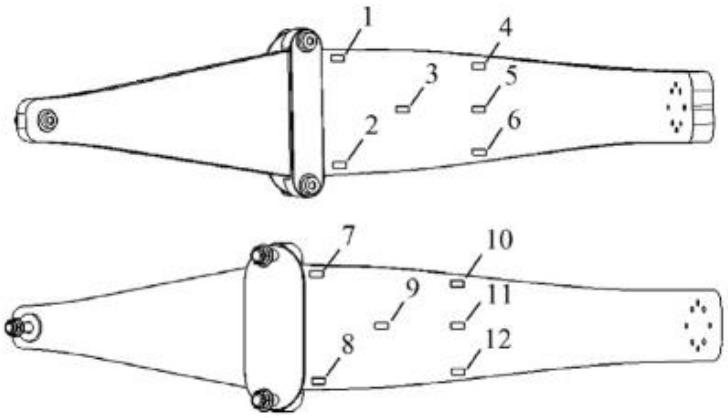


*Figure 20: Strain Gauge Distribution [11]*

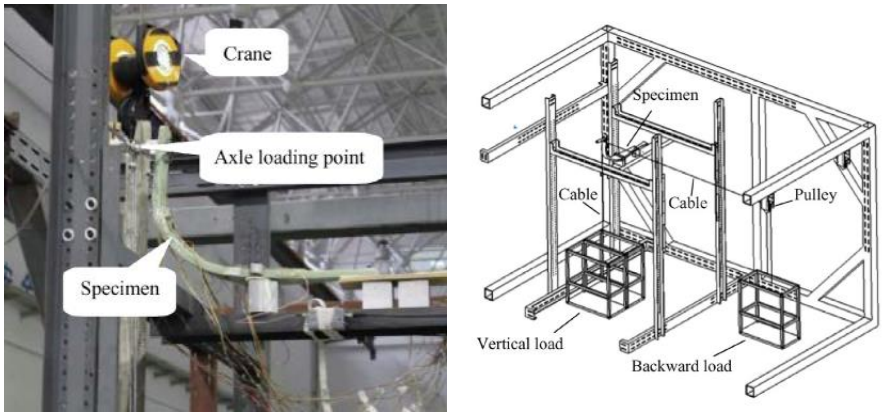


*Figure 21: Crane Loading Scheme [11]*

The experiment was conducted in two phases. The first phase was a static strength experiment that increased the load to the ultimate load [11]. This experiment was conducted to determine if the leaf spring gear met the stiffness and strength requirements and to record the displacement of the loading point on the axle together with the strain on the leaf spring [11]. The second phase was a failure experiment where the ultimate load was continuously applied to the gear until damage occurred. This was to determine the ultimate strength of the gear [11]. The load on the gear was maintained for 30 seconds at the limit load and the gear was then examined for any deformation or failure. It was found that if the gear was loaded 115% the ultimate load, the fibers failed due to tensile loads. The displacement of the gear in each direction is displayed up to 100% the ultimate load.

Figure 22 represents the failure experience by the -45-degree and 0-degree unidirectional fibers. The -45-degree fibers delaminated due to compressive loads and the 0-degree fibers failed due to tensile loads experienced during 115% the ultimate load condition.


*Figure 22: Tensile Failure on Landing Gear [11]*

Figure 23 provides the X, Y and Z displacements of the composite leaf spring landing gear during ultimate (emergency) load conditions. The maximum X, Y and Z displacements was 65mm, 250 mm, and 350 mm respectively.

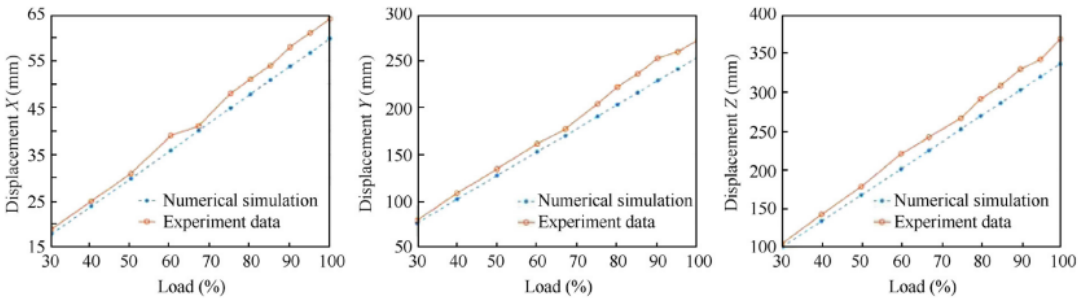


*Figure 23: Displacement Under 100% Ultimate Load in Each Direction [11]*

In conclusion, Table 6 shows the results obtained by the strain gauges compared to the simulation results. The maximum strain occurred on measurement points 10 and 12 which was near the side edges of the gear. This is an indication of where fibre and inter-fibre tensile and compressive failure is most likely to occur on this type of composite landing gear.

*Table 6: Comparison of Undercarriage Strain Results [8]*

| Measurement point | Numerical simulation data($\mu\varepsilon$) | Experiment data($\mu\varepsilon$) | Error |
|---|---|---|---|
| 1 | 14280 | 13298.964 | 6.87% |
| 2 | 16950 | 18226.335 | 7.53% |
| 3 | 17300 | 15533.67 | 11.21% |
| 4 | 12890 | 13448.137 | 4.33% |
| 5 | 18720 | 16874.208 | 9.86% |
| 6 | 18960 | 17278.248 | 8.87% |
| 7 | −13090 | −14048.188 | 7.32% |
| 8 | −19540 | −17906.456 | 8.36% |
| 9 | −16000 | −17545.6 | 9.66% |
| 10 | −19670 | −18550.777 | 5.69% |
| 11 | −17540 | −16415.686 | 6.41% |
| 12 | −19070 | −17634.029 | 7.53% |

### 5.4. Void Content and Fatigue Life of Composite Laminates

Voids or volatile compounds are considered as entrapped air inside the matrix of a composite structure. Figure 24, represents a visualisation of the fibres and matrix content inside a composite structure.

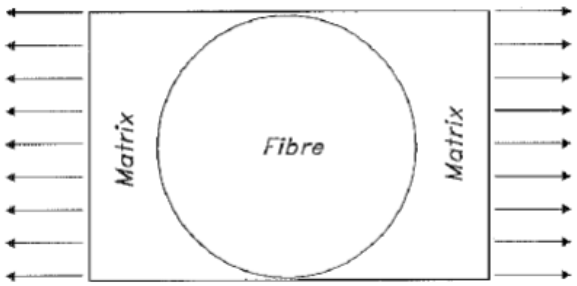


*Figure 24: Fibre and Matrix Representation Inside Composite Structures [9]*

It is considered virtually impossible to obtain a laminate that is totally void free as the actual void content present will depend on several factors such as the process used during manufacturing and the resin type [9]. Manufacturing methods such as hand lay-up will generally result in the highest void content whilst other methods such as autoclave manufacturing techniques result in the lowest void contents within the composite structure or component [9]. The resin type used during manufacturing is important since some resins (particularly phenolics) produce volatile compounds during the curing process. However, the higher the viscosity of the resin during manufacturing, the more difficult it becomes to remove the entrapped air and volatile compounds from the laminate [9].

The void content present within any composite structure is expressed as a volume fraction ($V_v$). The percentage void content can range anywhere from 0.05% up to 10% inside composite structures [9]. The presence of voids can be detrimental to the strength and elastic properties of the composite since the stiffness is reduced due to the volume of the composite carrying the applied loads are reduced. The transverse modulus ($E_2$) and in-plane shear modulus ($G_{12}$) are dominated by the matrix properties, thus the reduction in these properties is greater than $V_v$ in comparison to the longitudinal modulus ($E_1$). The longitudinal modulus is dominated by the fibre properties thus, it is not affected much by the void content [9]. However, if the void volume fraction exceeds 2%, the effects are more significant on the matrix dominated strength than its elastic properties. The voids tend to cause stress concentrations within the matrix which promotes failure such as cracking. Another significant impact of void content on the performance of composite structures is that it can reduce the fatigue life and moisture resistance of the structure [9]. Moisture absorption can cause swelling which in turn induces internal stresses that weaken the matrix. The moisture will ultimately degrade the bonding between the fibres and the matrix resulting in accelerated fatigue crack growth inside the structure [9].

Another factor leading to reduced fatigue life of the composite laminate is ultraviolet (UV) degradation. The UV radiation can break the polymer chains down within the matrix leading to embrittlement and reduced strength. Composite structures used outdoors or in environment with which UV exposure are more prone to fatigue crack initiation and propagation directly affecting the fatigue life of the composite [12].

### 5.5. Introduction, Literature Study and Case Study Summary

In conclusion, there are two types of light sport aircraft landing gear configurations namely the tricycle and taildragger aircraft configuration, the difference between the two is represented by the position of the main landing gear situated beneath the fuselage of the aircraft. Shipment delays of the current Aluminium 7075 T6 alloy landing gear has caused further delays in the manufacturing of the taildragger and tricycle Light Sport Aircraft. Thus, a composite alternative is required which could be manufactured locally to withstand the same load conditions as the Aluminium 7075 T6 alloy landing gear. According to the ASTM F2245 -14 and the EASA CS-23 regulations both the tricycle and taildragger aircraft has their own landing load conditions which should be considered when designing a main landing gear out of composite materials. The composite materials focused during design of a composite alternative to the current Aluminium 7075 T6 alloy landing gear is a polymer matrix in combination with E-glass fibres.

During the case study conducted on the Chinese RX1E-A Epoxy E-Glass belt prepreg leaf spring landing gear, the Puck failure criterion was used to analyse the failure present withing the composite gear. The Puck-failure criterion distinguishes between fibre and inter-fibre failure of a composite laminate. It was found that the composite leaf spring landing gear was more prone to inter-fibre tensile and inter-fibre compression failure than inter-fibre shear failure. The composite gear was also prone to fibre tensile and fibre compression failure. During structural testing of the gear, it is found that the -45-degree and 0-degree fibres failed due the above-

mentioned failure parameters at 115% the ultimate (emergency) load which corresponded to the Puck failure FEA analysis. This case study is relevant since it validated the Puck-failure criterion through experimental testing and confirmed its accuracy in predicting the failure modes in the composite laminate under specific load conditions. Secondly, it identified the different failure modes inside of the composite structure and highlighted the critical areas where the composite landing gear is vulnerable under limit and ultimate loads.

Lastly when manufacturing a composite structure, it is important to consider reducing the void content within the matrix as much as possible due the reduction in fatigue life when the void volume fraction increases. Voids and volatile compounds tend to cause stress concentrations withing the matrix which promotes failure such as crack initiation and crack propagation during continuous loading of the composite structure. Manufacturing methods such as hand lay-up results in high void and volatile content whilst autoclave manufacturing methods results in the lowest void and volatile content within the composite structure. The fatigue life of the composite structure will also depend on the moisture abortion and UV radiation exposure as it can significantly reduce the fatigue life of the composites structure or component.

# 6. RESEARCH METHODS

## 6.1. Research Design

For this proposed research, literature observations, calculations, FEA simulations, and advice from composite manufacturing experts have been used. This combined approach aimed to offer a more thorough analysis and addressed the research questions and objectives comprehensively.

The literature provides valuable knowledge on forces that act upon Light Sport Aircraft landing gear according to the correct EASA CS 23 amendments and ASTM F2245 – 14 standards. Calculations and numerical modelling can be used to simplify the complexity of using a composite design for landing gear by obtaining results regarding the stresses experienced by certain sections of the gear and to determine whether the material can safely withstand these loads. Advice from manufacturing experts can be valuable since manufacturing a component of composite materials needs practical experience and practical ideas to ensure that the design can be manufactured with what is locally available.

## 6.2. Instrumentation

The following software will be used during the duration of the research:

1) Ansys 2023 R2 Software - The software will be used to conduct an FEA analysis on the Aluminum 7075 T6 alloy and composite landing gear whilst it is subjected to the different landing loads conditions. Ansys software will also be used for the layering of the composite landing gear used in the FEA analysis.

2) Siemens NX 12 - The software was used to model the Aluminium 7075 T6 alloy landing gear components such as the brackets, axles, bolts, and nuts. It was also used to model the composite landing gear that was used for layering of the composite gear and FEA analysis inside of Ansys.

## 6.3. Data Collection/ Analysis

Data on various parameters was sourced to ensure that the design was valid. Some of the data that was collected by engineers at the company included aircraft weight, current landing gear dimensions, drop test results and the Pilot Operating Handbook (POH).

1) Aircraft weight - The weight is important when determining the loads on the landing gear. This data collection included maximum take-off weight, empty weight, and payload weight.

2) Landing gear dimensions - According to the aircraft manufacturer, the new design must be of similar dimensions as the current aluminum alloy landing gear so that minimal changes were required for brackets and aircraft modification.

3) Landing conditions - The landing conditions are important since they determine the forces that act in on the landing gear during different conditions for the taildragger and tricycle Bushcat aircraft. These landing conditions are determined using the EASA CS 23 amendments and ASTM F2245 – 14 standards.

4) Regulatory requirements - The regulatory requirements included the POH as it provided information regarding the limitations during the operation of the Bushcat aircraft. These limitations included aircraft airspeed, weight and balance which were important for calculations.

5) Stress analysis - Once the necessary data was collected, Ansys was used to perform a structural static stress analysis on the landing gear. This analysis was used to understand the forces acting on the landing gear and identify potential failure points.

### 6.4. Validity and Reliability

To validate and verify the composite landing gear design the following were conducted:

1) Landing gear drop test - Ansys simulations were compared to an actual drop test. The deformations were compared to the deformations presented in the simulations, this was done to check that the loads and constraints were applied correctly onto the gear. This was then transferred to the composite landing gear in the final design.

2) Landing gear deflection - The vertical stroke deflection was compared to the deflections obtained by FEA analysis to validate that the loads, application of loads and constraints were correctly applied in Ansys.

3) Mesh independence study – A mesh independence study was conducted during the landing gear deflection and bending stress analysis. This was done so that the correct mesh element size could determine the most accurate FEA result against the analytical calculations as well as the sensitivity of the stress and deflections obtained through FEA analysis when changing the mesh parameters.

4) Coupon simulations - Ansys software was used to conduct an FEA analysis on Aluminium 7075 T6 alloy during tensile, compression, bending and torsion load application. The results were compared to numerical calculations. The results were used during the composite gear optimisation to determine the correct fibre orientations that could withstand the loads more effectively.

# 7. LANDING GEAR LOAD CALCULATIONS

## 7.1. Introduction

In this section the loads calculations for the different side loads, brake loads, wheel spin up loads, self-aligning torque and for all landing conditions for the tricycle and taildragger gear configurations of the BushCat Aircraft were conducted. The effect that these forces have on the main landing gear were analysed and the loads calculated were used in chapter 8 and chapter 10 for the FEA-analysis of the Aluminium 7075 T6 and composite alternative landing gear. The loads were calculated for a maximum aircraft mass of 600 kg and a speed of 96.56 km/h (60 mph) obtained from the and BushCat Aircraft specifications as seen in Table 7 and Table 8.

Table 7 provides the specifications obtained from the documents of the BushCat Light Sport Aircraft regarding the maximum mass approved by the South African Civil Aviation Authority (SACAA) and Federal Aviation Administration (FAA). Table 7 and Table 8 provides the BushCat Aircraft weight and balance specifications as well as the final approach speed.

*Table 7: Light Sport Aircraft Maximum Take-off Weight [13]*

| Country | Authority | Operated as[1] | Max. Mass[1] |
|---|---|---|---|
| South Africa | South African Civil Aviation Authority (SACAA) / Recreational Aircraft Association of South Africa (RAASA) | NTCA | 560 kg (1230 lbs) |
| | | Microlight | 450 kg (992 lbs) |
| USA | Federal Aviation Administration (FAA) | S-LSA | 600 kg (1320 lbs) |
| | | E-LSA | |
| | | EAB | |

*Table 8: BushCat Aircraft Weight and Balance Specifications, Final Approach Speed [13]*

| Parameter | Mass | Arm |
|---|---|---|
| Empty Mass (Nosewheel) * | 340 kg | 310 mm |
| Empty Mass (Taildragger) * | 350 kg | 435 mm |
| Fuel Tank (Max Capacity – 94L) | 69 kg | 1060 mm |
| Maximum Take-Off Mass | 600 kg | 445 – 588 mm |
| Maximum Upper Baggage | 25 kg | 1060 mm |
| Maximum Lower Baggage | 20 kg | 1418-1624 mm |

Once airspeed of 56-60 mph IAS (600 kg) is obtained, the wing flaps should be set to the landing setting whilst confirming that the fuel pump is on and the fuel selector is on [13].

### 7.2. Aluminium 7075 T6 Alloy Landing Gear Assembly

Figure 25 provides the landing gear and wheel assembly annotations of the main landing gear on the BushCat taildragger aircraft. The same assembly applies for the tricycle aircraft. In Figure 25 the following annotations can be noted regarding the assembly of the main Aluminium 7075 T6 alloy landing gear:

**Aircraft main gear assembly**:

2. Spring gear
3. Brackets (radius plates)
4. Protection shims
8. M12 × 60 mm bolts
9. M12 washers
10. M12 nylock nut

**Wheel assembly**:

1. Wheel assembly (hub and tyre)
2. Calliper assembly
3. A3C axle nut with split pins
4. A3C axle
5. AN6 24A bolts
6. AN5 23A bolts
7. M8 × 16 × 1.6 mm washers
8. M10 × 18 × 2 mm washers
9. M10 nylock nut
10. M8 nylock nut

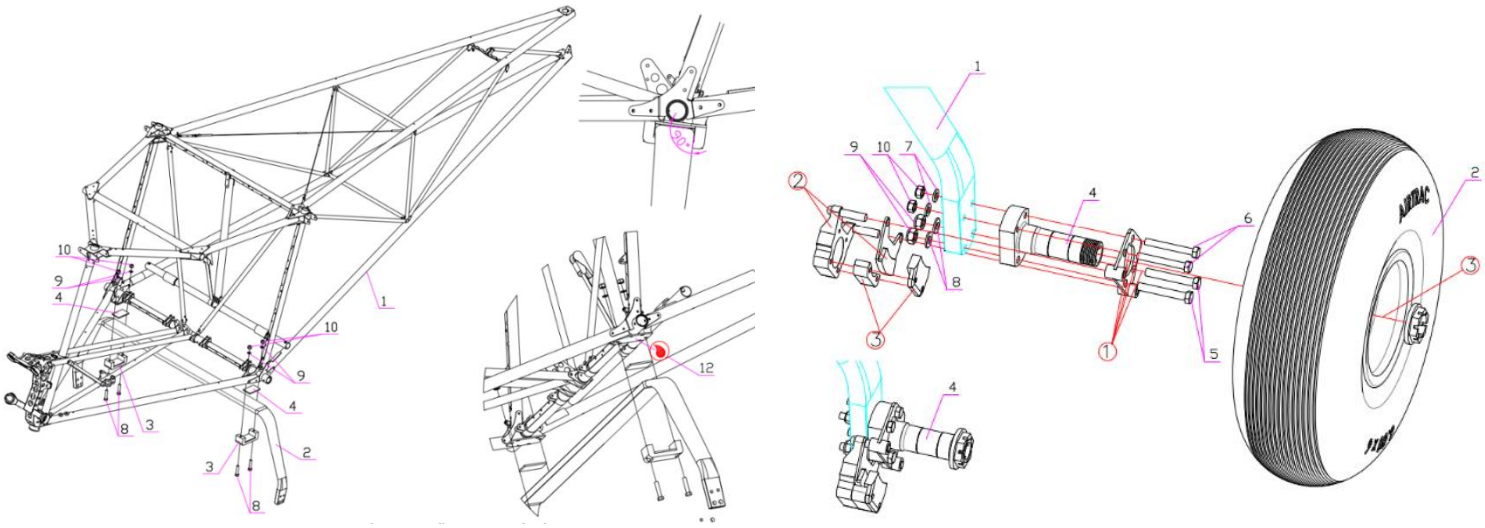

*Figure 25: BushCat Landing Gear Assembly to Aircraft [13]*

## 7.3. Analytical Calculations

### 7.3.1. Landing Condition Loads

Table 9 and Table 11 provides the different landing conditions for the nose wheel and taildragger aircraft configuration used with an aircraft maximum take-off weight (MOTW) of 600 kg with a limit ground reaction load factor of n = 2.1 on the landing gear according to CS 23.473 amendments. During emergency landing the ultimate load factor should be n = 3 in accordance with ASTM F2245. Refer to section 5.2.1, Figure 3 and Table 1 for different landing conditions and equations used.

*Table 9: Taildragger Aircraft Landing Loads (Limit Load Factor = 2.1)*

| **Taildragger Aircraft** | | | |
|---|---|---|---|
| | **Level Landing** | **Tail down landing** | **Units** |
| Vertical component at (CG) | 12360.6 | 12360.6 | N |
| Fore and aft component at (CG) | 14715 | 0 | N |
| Lateral component at (CG) | 0 | 0 | N |
| Shock absorber deflection | 100 | 100 | % |
| Tyre deflection | static | static | - |
| Main wheel loads (Vertical component) | 8436.6 | 7381.77 | N |
| Both wheels (friction) | 3090.15 | 0 | N |
| Tail/ nose wheel (Vertical component) | 0 | 1370.67 | N |

*Table 10: Taildragger Aircraft Landing Loads (Ultimate Load Factor = 3)*

| **Taildragger Aircraft** | | | |
|---|---|---|---|
| | **Level Landing** | **Tail down landing** | **Units** |
| Vertical component at (CG) | 17658 | 17658 | N |
| Fore and aft component at (CG) | 14715 | 0 | N |
| Lateral component at (CG) | 0 | 0 | N |
| Shock absorber deflection | 100 | 100 | % |
| Tyre deflection | static | static | - |
| Main wheel loads (Vertical component) | 13734 | 12016.84 | N |
| Both wheels (friction) | 4414.5 | 0 | N |
| Tail/ nose wheel (Vertical component) | 0 | 2231.32 | N |

*Table 11: Tricycle Aircraft Landing Loads (Limit Load Factor = 2.1)*

| Tricycle Aircraft | | | | |
|---|---|---|---|---|
| | **Level Landing with inclined reactions** | **Level landing with nose just clear of ground** | **Tail down landing (stall altitude)** | **Units** |
| Vertical component at (CG) | 12360.6 | 12360.6 | 12360.6 | N |
| Fore and aft component at (CG) | 14715 | 14715 | 0 | N |
| Lateral component at (CG) | 0 | 0 | 0 | N |
| Shock absorber deflection | 100 | 100 | 100 | % |
| Tyre deflection | static | static | static | - |
| Main wheel loads (Vertical component) | 4218.3 | 8436.6 | 8436.6 | N |
| Both wheel (friction) | 1545.08 | 3090.15 | 0 | N |
| Tail/ nose wheel (Vertical component) | 4218.3 | 0 | 0 | N |

*Table 12: Tricycle Aircraft Landing Loads (Ultimate Load Factor = 3)*

| Tricycle Aircraft | | | | |
|---|---|---|---|---|
| | **Level Landing with inclined reactions** | **Level landing with nose just clear of ground** | **Tail down landing (stall altitude)** | **Units** |
| Vertical component at (CG) | 17658 | 17658 | 17658 | N |
| Fore and aft component at (CG) | 14715 | 14715 | 0 | N |
| Lateral component at (CG) | 0 | 0 | 0 | N |
| Shock absorber deflection | 100 | 100 | 100 | % |
| Tyre deflection | static | static | static | - |
| Main wheel loads (Vertical component) | 6867 | 13734 | 13734 | N |
| Both wheel (friction) | 2207.25 | 4414.5 | 0 | N |
| Tail/ nose wheel (Vertical component) | 6867 | 0 | 0 | N |

Refer to section 5.2.1, Figure 4, and Figure 5 for side/ braked roll loads, equation 1 for wheel-spin up loads during a MOTW of 600 kg. Table 13 represents the loads obtained for side/ braked roll and wheel-spin up loads.

*Table 13: Side Loads, Wheel Spin-Up Load and Landing Gear Deflection*

| **Side Load Conditions** | | |
|---|---|---|
| Left Tyre | | |
| Vertical Load | 3943.62 | N |
| Inboard Load | 2943 | N |
| Right Tyre | | |
| Vertical Load | 3943.62 | N |
| Outboard Load | 1942.38 | N |
| **Braked Roll Conditions** | | |
| Both Tyres | | |
| Vertical Load | 3943.62 | N |
| Rearward Load | 3178.44 | N |
| **Wheel Spin-Up Loads** | | |
| Both Tyres | | |
| Rearward Load | 17616.52 | N |

From Table 9 to Table 12 according to the ASTM F2245-14 and EASA CS-23 regulations, for an aircraft MOTW of 600 kg the maximum ground reaction and torsional loads for limit load conditions were 8436.6 N and 3090.15 Nm respectively. For ultimate load conditions the maximum ground reaction and torsional loads were 13734 N and 4414.5 Nm respectively. Note that the angle of impact during landing varied for each load landing condition on both the tricycle and taildragger aircraft.

In Table 13 according to the ASTM F2245-14 and EASA CS-23 regulations, the maximum ground reaction load during side load and braked roll landing conditions were 3943.62 N whilst during side load “crabbed” landing conditions the maximum lateral load was the inboard load of 2943 N. During wheel spin-up loads it was assumed that the load is only active 1 second after impact before roll-out phase.

### 7.3.2. Landing Gear Stroke Deflection

Figure 26 presents how a force generates deflection when applied to the landing gear during the different landing conditions. As seen in the figure, the total stroke is a result of the perpendicular component of the ground reaction force. This diagram can be used for both the Aluminium 7075 T6 alloy and composite landing gear when calculating the stroke.

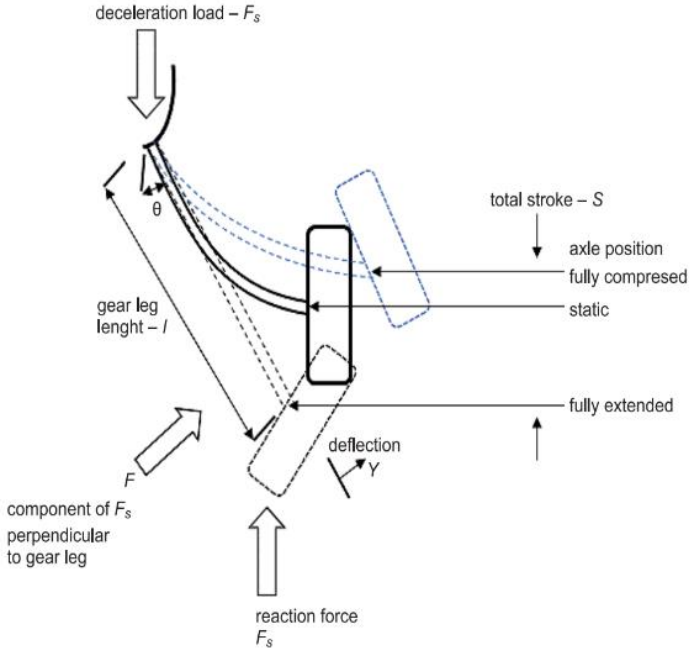


*Figure 26: Landing Gear Deflection Loads Diagram [14]*

Equation 8 was used to find the reaction force per tyre at different impact angles. Note that the frictional loads were not present in the calculations of the landing gear leg stroke deflection.

$$F_s = \frac{F_{vertical}(Cos\ \theta_{impact})}{2} \tag{8}$$

Where:

$F_s$ = Reaction force ($N$)
$F_{vertical}$ = Vertical ground reaction component (load factor integrated) ($N$)
$\theta_{impact}$ = Impact angle of landing gear ($degrees$)

During landing, the impact angle ranges from 0 to 14-degrees. Level landing conditions were presented by 0-degree impact angle and landing conditions that occur during tail down, inclined, nose wheel clear, and stall altitude conditions was presented by a 14-degree impact angle.

Equation 9 was used to calculate the stroke deflection of the leaf spring landing gear leg. Note that the stroke deflection calculated using equation 9 did not account for the added rotational deflection obtained by the radius plate brackets. When doing an FEA comparison, the radius plate bracket rotational deflections should be eliminated.

$$S = \frac{F_s(\sin^2\theta)l^3}{3EI_x} \tag{9}$$

Where:

$S$ = Stroke deflection ($mm$)

$\theta$ = Leg angle ($degrees$)

$l$ = Length of leg ($mm$)

$E$ = Youngs modulus ($MPa$)

$I_x$ = Moment on inertia ($mm^4$)

The ground reaction loads can be found from Table 9 to Table 12. The leg angle of the Aluminium 7075 T6 alloy landing gear was found to be approximately 23.6 degrees and the leg length was approximately 565.36 mm. See Appendix B (Aluminium 7075 T6 alloy gear and Composite gear drawings) for more information regarding the dimensions.

Equation 10 provides more information regarding the moment of inertia used during the stroke calculations:

$$I_x = \frac{bh^3}{12} \tag{10}$$

Where:

$b$ = leg thickness ($mm$)

$h$ = leg width ($mm$)

Due to the Aluminium 7075 T6 alloy landing gear leg not being uniform in thickness and width throughout, it was assumed that the section of the leg with the least thickness and maximum width should be taken since this section occupies the most stress during each landing condition as seen in chapter 9. The thickness was approximately 14.2 mm and the width was approximately 53.102 mm. By taking these dimensions, an approximation was obtained for the vertical stroke deflections occurring during each landing conditions as validated in chapter 8.

Equations 11 to 13 were used to obtain the reaction moment, bending stress, and safety factor within the landing gear leg:

$$M_{bending} = Fl \tag{11}$$

Where:

$M_{bending}$ = Moment reaction due to ground reaction force ($N.mm$)

$F$ = Perpendicular force component ($N$)

$$\sigma_{bending} = \frac{M_{bending}c}{I_x} \tag{12}$$

Where:

$\sigma_{bending}$ = Bending Stress ($MPa$)

$c$ = Distance from neutral axis to outermost fibre ($mm$)

$$SF_{flexural} = \frac{\sigma_{yield}}{\sigma_{flexural}} \tag{13}$$

Where:

$SF_{bending}$ = Flexural yield strength safety factor (-)

$\sigma_{yield}$ = Flexural yield strength ($MPa$)

Table 14 and Table 15 provides the stroke deflection of the Aluminium 7075 T6 Alloy landing gear during the different landing conditions.

*Table 14: Aluminium 7075 T6 Alloy Landing Gear Deflection (Limit Load Factor = 2,1)*

| Landing Condition | Deflection/ Stroke (mm) | Bending Stress (MPa) | Safety Factor (Yield) |
|---|---|---|---|
| **Taildragger Aircraft** | | | |
| Level Landing | 19.443 | 191.12 | 2.51 |
| Tail Down Landing | 16.507 | 162.26 | 2.96 |
| **Tricycle Aircraft** | | | |
| Level Landing (Inclined) | 9.433 | 92.26 | 5.18 |
| Level Landing (nose just clear of ground) | 18.865 | 185.45 | 2.59 |
| Tail Down Landing (stall-altitude) | 18.865 | 185.45 | 2.59 |
| Side, Braked and Wheel Spin-Up | 9.088 | 89.34 | 5.37 |

*Table 15: Aluminium 7075 T6 Alloy Landing Gear Deflection (Ultimate Load Factor = 3)*

| Landing Condition | Deflection/ Stroke (mm) | Bending Stress (MPa) | Safety Factor (Yield) |
|---|---|---|---|
| **Taildragger Aircraft** | | | |
| Level Landing | 31.651 | 311.13 | 1.54 |
| Tail Down Landing | 26.871 | 264.14 | 1.82 |
| **Tricycle Aircraft** | | | |
| Level Landing (Inclined) | 15.356 | 150.94 | 3.18 |
| Level Landing (nose just clear of ground) | 30.711 | 301.89 | 1.59 |
| Tail Down Landing (stall-altitude) | 30.711 | 301.89 | 1.59 |
| Side, Braked and Wheel Spin-Up | 9.088 | 89.34 | 5.37 |

From the analytical results obtained the maximum stress occurred on the taildragger aircraft during level landing. The stress will differ during the Aluminium 7075 T6 alloy landing gear FEA analysis as seen in chapter 9 due to the frictional loads being present and radius plate brackets having rotational deflection.

### 7.3.3. Self-Aligning Torque (Tow-in)

Torque occurs on the landing gear strut as aircraft wheel touches the runway as seen in Figure 27. Frictional loads on the wheels in contact with the runway, braking during landing and flex of the leaf spring landing gear results in the inner surface of the tyre touching the runway. This action subjects the landing gear strut to torsion. The gear will then counteract the torsional loads to realign the wheels straight again.

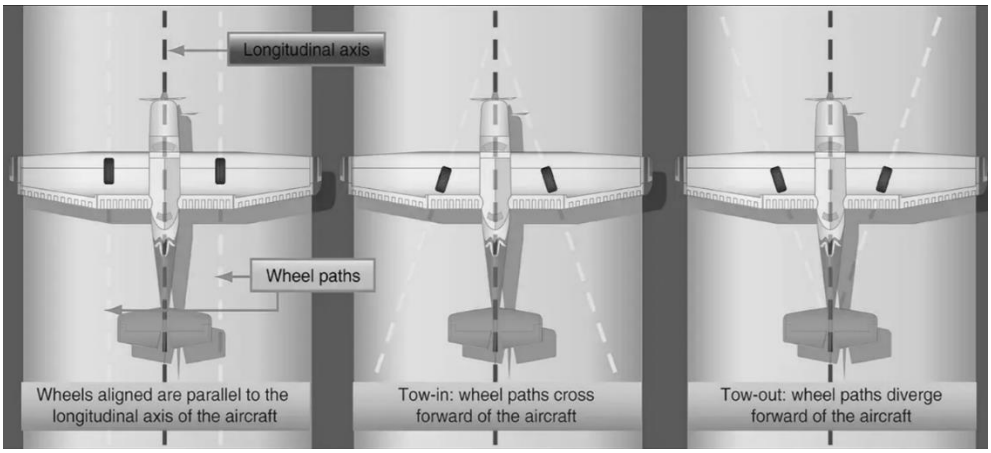


*Figure 27: Aircraft Landing Tow-In and Tow-Out Wheel Self-Alignment [15]*

Figure 28, provides the free-body diagram regarding the frictional force due to the tyres impacting the runway creating tow-out loads on the landing gear leg.

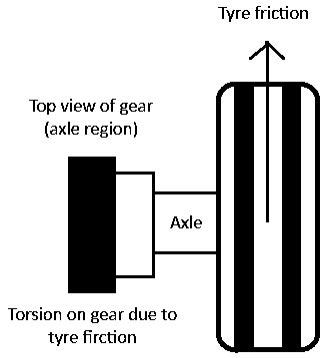


*Figure 28: Self-Aligning Torque Free-Body Diagram*

Equation 14 were used to calculate the tow-in torsional loads on the aircraft:

$$M_{tow\ load} = F_{friction\ tyre} \times (L_{axle\ shaft}/2 + L_{axle\ head} + L_{gear\ thickness}/2) \quad (14)$$

Where:

$M_{tow\ load}$ = Torque created due to tyre frictional load ($N.mm$)

$F_{friction\ tyre}$ = Tyre frictional load ($N$)

$L_{axle\ shaft}$ = Length of A3C stub axle shaft ($mm$)

$L_{axle\ head}$ = Thickness of A3C axle head ($mm$)

$L_{gear\ thickness}$ = Thickness of the gear at axle region ($mm$)

Equation 15 was used to calculate the torsional stress on the gear leg during landing. Note that the torsional stress was only an estimate since landing gear leg has a leg arc angle was not uniform in thickness. The gear thickness and gear width used was 14.2 mm and 53.102 mm respectively.

$$\tau_{torsion} = \frac{M_{tow\ load}}{C_1 ab^2} \quad (15)$$

Where:

$\tau_{torsion}$ = Torsional stress ($MPa$)

$C_1$ = 1st value obtained through $^{a}/_{b}$ ratio (-)

$a$ = Gear thickness ($mm$)

$b$ = Gear width ($mm$)

Equation 16 was used to obtain the rotational deflection of the landing gear leg due to tyre frictional resulting in two-out conditions.

$$\theta_{torsion} = \frac{M_{tow\ load} l}{C_2 a b^3 G} \times \frac{180}{\pi} \quad (16)$$

Where:

$\theta_{torsion}$ = Torsional deflection ($degrees$)

$l$ = Length of gear leg ($mm$)

$C_2$ = 2nd value obtained through $a/b$ ratio (-)

$G$ = Shear Modulus ($mm$)

Equation 17 was used to obtain $C_1$ and equation 18 was used to obtain $C_2$ used in equation 15. These values are influenced by the ratio of $a/b$ and follow a linear line plotted on a graph. The $a/b$ ratio used during the calculations was 3.740. Thus, $C_1$ = 0.141 and $C_2$ = 0.405.

$$C_1 = 0.033\left(a/b\right) + 0.0175 \quad (17)$$

$$C_2 = 0.072\left(a/b\right) + 0.136 \quad (18)$$

Equation 19 was used to obtain the torsional yield safety factor of the landing gear leg:

$$SF_{torsion} = \frac{\sigma_{yield}}{\tau_{torsion}} \quad (19)$$

Where:

$SF_{torsion}$ = Torsional yield strength safety factor (-)

$\sigma_{yield}$ = Torsional yield strength ($MPa$)

In Table 16, the wheels of the aircraft were in tow-in position causing torsion on landing gear legs thus, during impact the wheels will be in tow-in alignment.

*Table 16: Self Aligning Torque Experienced by Landing Gear (Limit Load Factor = 2,1)*

| Landing Condition | Torque (Nm) | Torsional Stress (MPa) | Deflection (Degrees) | Safety Factor (Torsion Yield) |
|---|---|---|---|---|
| **Taildragger Aircraft** | | | | |
| Level Landing | 237.632 | 157.40 | 4.58 | 2.10 |
| Tail Down Landing | 0 | 0 | 0 | - |
| **Tricycle Aircraft** | | | | |
| Level Landing (Inclined) | 118.82 | 72,29 | 2.29 | 4.21 |
| Level Landing (nose just clear of ground) | 237.63 | 144,57 | 4.58 | 2.10 |
| Tail Down Landing (stall-altitude) | 0 | 0 | 0 | - |
| Side, Braked and Wheel Spin-Up | 244.42 | 148,70 | 4.71 | 2.04 |

*Table 17: Self Aligning Torque Experienced by Landing Gear (Ultimate Load Factor = 3)*

| Landing Condition | Torque (Nm) | Torsional Stress (MPa) | Deflection (Degrees) | Safety Factor (Torsion Yield) |
|---|---|---|---|---|
| **Taildragger Aircraft** | | | | |
| Level Landing | 339.48 | 224.85 | 6.55 | 1.47 |
| Tail Down Landing | 0 | 0 | 0 | - |
| **Tricycle Aircraft** | | | | |
| Level Landing (Inclined) | 169.74 | 112.43 | 3.27 | 2.94 |
| Level Landing (nose just clear of ground) | 339.48 | 224.85 | 6.55 | 1.47 |
| Tail Down Landing (stall-altitude) | 0 | 0 | 0 | - |
| Side, Braked and Wheel Spin-Up | 244.42 | 161.90 | 4.71 | 2.04 |

### 7.3.4. Bolt Bearing Stress

AN5-23A and AN6-24A bolts manufactured using 8740 alloy steel were used when attaching the stub axle to the main gear as well as the brackets. The AN6-24A bolts were used at the bottom and the AN5-23A are used at the top of the stub axle. The AN5-23A and AN6-24A bolts were only used for the Aluminium 7075 T6 alloy landing gear. When designing the composite landing gear in chapter 11, different bolts were used since the shank length of the current bolts were too short. Figure 29 represents bearing stresses of the bolts acting on the material. The material must be able to withstand these loads especially when using composite materials.

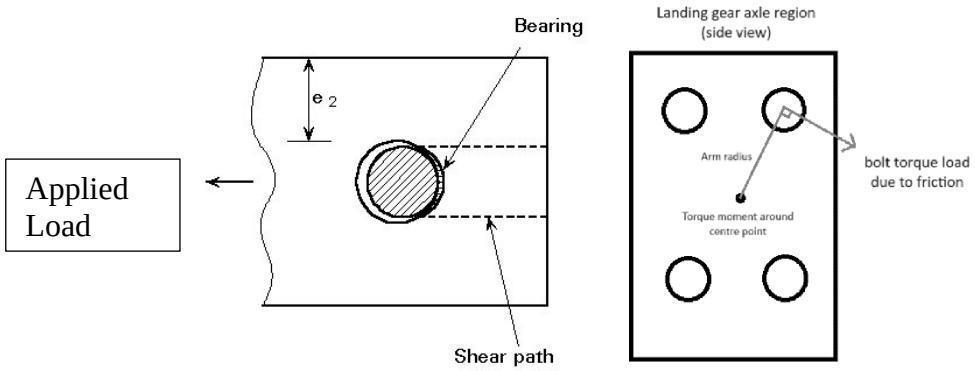


*Figure 29: Bearing Stresses Experience by Landing Gear Material [16]*

Equation 20 was used to obtain the bearing stress exerted onto the main landing gear bolted region. Note the area that was used was the side surface of the bolt in contact with the landing gear.

$$\sigma_{bearing} = \frac{(F_{friction} \times R_{tyre})}{4 R_{arm} t_{gear} d_{bolt}} \tag{20}$$

Where:

$\sigma_{bearing}$ = Bearing stress ($MPa$)

$R_{tyre}$ = Radius of tyre ($mm$)

$R_{arm}$ = Arm radius ($mm$)

$F_{friction}$ = Frictional load ($N$)

$t_{gear}$ = Landing gear axle region thickness ($mm$)

$d_{bolt}$ = Bolt diameter ($mm$)

Equation 21 was used to obtain the safety factor of the gear being subjected to bearing stresses:

$$SF_{bearing} = \frac{\sigma_{yield}}{\sigma_{bearing}} \tag{21}$$

Where:

$SF_{bearing}$ = Bearing stress safety factor (-)

$\sigma_{yield}$ = Yield strength ($MPa$)

*Table 18: Landing Gear Material Bearing Stress (Limit Load Factor = 2,1)*

| Landing Condition | Bearing Stress (MPa) AN5 | Safety Factor (Yield) | Bearing Stress (MPa) AN6 | Safety Factor (Yield) |
|---|---|---|---|---|
| **Taildragger Aircraft** | | | | |
| Level Landing | 16.71 | 28.48 | 13.93 | 34.48 |
| Tail Down Landing | 0 | - | 0 | - |
| **Tricycle Aircraft** | | | | |
| Level Landing (Inclined) | 8.36 | 56.97 | 6.96 | 68.36 |
| Level Landing (nose just clear of ground) | 16.71 | 28.48 | 13.93 | 34.48 |
| Tail Down Landing (stall-altitude) | 0 | - | 0 | - |
| **Side Load and Braked Roll** | | | | |
| - | 17.19 | 27.69 | 14.32 | 33.23 |

*Table 19: Landing Gear Material Bearing Stress (Ultimate Load Factor = 3)*

| Landing Condition | Bearing Stress (MPa) AN5 | Safety Factor (Yield) | Bearing Stress (MPa) AN6 | Safety Factor (Yield) |
|---|---|---|---|---|
| **Taildragger Aircraft** | | | | |
| Level Landing | 23.87 | 19.94 | 19.90 | 23.93 |
| Tail Down Landing | 0 | - | 0 | - |
| **Tricycle Aircraft** | | | | |
| Level Landing (Inclined) | 11.94 | 39.88 | 9.95 | 47.85 |
| Level Landing (nose just clear of ground) | 23.87 | 19.94 | 19.90 | 23.93 |
| Tail Down Landing (stall-altitude) | 0 | - | 0 | - |
| **Side Load and Braked Roll** | | | | |
| - | 17.19 | 27.69 | 14.32 | 33.23 |

From results obtained, the Aluminium 7075 T6 alloy landing gear withstands the bearing loads exceptionally well by having a minimum safety factor of 23.93 during level landing at ultimate load conditions.

# 8. FEA VALIDATIONS AND MESH INDEPENDENCE STUDY

## 8.1. Introduction

In this section the validation of the FEA analysis and mesh independence study is presented. The application of loads, constraints and mesh refinements were validated by comparison with drop tests and landing gear deflection calculations. The landing gear and its components was modelled and assembled using Siemens NX 12 and the FEA analysis was done with Ansys 2023 R2 Mechanical.

## 8.2. Landing Gear Leg Vertical Deflection Validation

Figure 30 displays the main landing gear with the components that were used for the validation. The no-separation contact type were used for the landing gear in contact with the stub axles, axle bolts, and nylock nuts whilst the bonded contact type was used for the radius plate brackets in contact the M12 bracket bolts. See Appendix B for dimensions of the landing gear

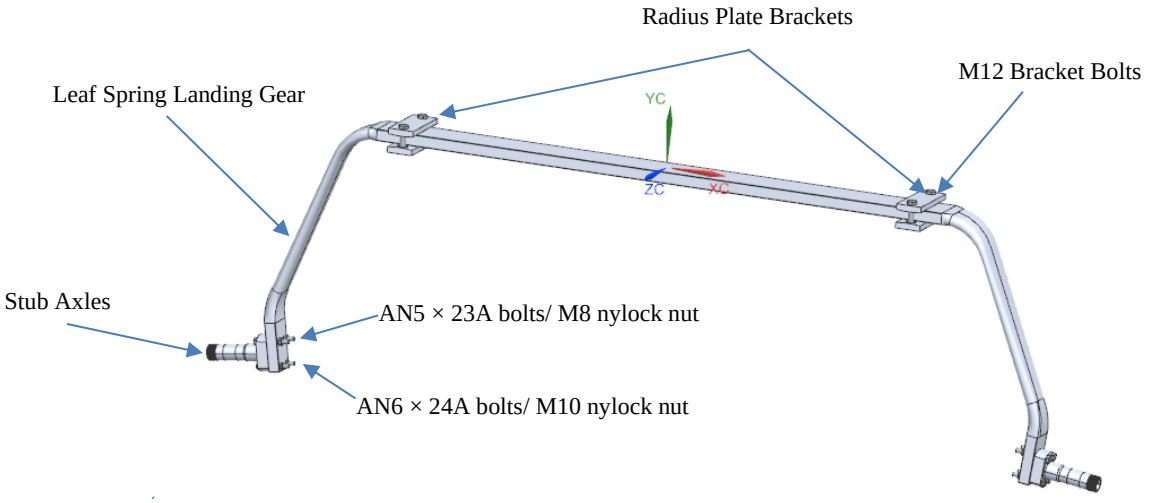


*Figure 30: Main Landing Gear Assembly*

Table 20 provides the material properties for the landing gear and its assembled components.

*Table 20: Material Properties (Landing Gear Assembly)*

| - | Al 7075 T6 (Landing Gear) | Al 6061 T6 (Stub Axle) | Al 6082 T6 (Radius Plates) | 8740 Steel (Bolts and Nuts) | Units |
|---|---|---|---|---|---|
| **Density** | 2800 | 2698.8 | 2698.8 | 7861.1 | $kg/m^3$ |
| **Young's Modulus** | 72000 | 68900 | 69000 | 205 | MPa |
| **Poisson's Ratio** | 0.32 | 0.33 | 0.33 | 0.29 | (-) |
| **Bulk Modulus** | 66667 | 67549 | 67647 | 162.7 | MPa |
| **Shear Modulus** | 27273 | 25902 | 25940 | 79.457 | MPa |
| **Tensile Yield Strength** | 503 | 276 | 276 | 861.84 | MPa |
| **Tensile Ultimate Strength** | 572 | 310 | 310 | 930 | MPa |

### 8.2.1. Landing Gear Vertical Deflection FEA Load and Constraint Setup

Figure 31, provides a 90-degree impact load application to the Aluminium 7075 T6 undercarriage whilst no frictional loads were applied to the stub axles. The impact angle was adjusted for each landing condition for both the tricycle and taildragger aircraft whereas the maximum impact-angle were 14-degrees. The limit load applied is equal to 4218.3 N per tyre for taildragger level landing as seen in Figure 31.


*Figure 31: Taildragger Aircraft Level Landing Load Application (Deflection Validation)*

Figure 32 provides the constrain application to the radius plates of aircraft landing gear. Equation 9 used to calculate the deflections does not include the rotational deflections occurring on the radius plates brackets thus, the fixed support is used over its surface. Equation 9 only accounts for landing gear leg deflection as the rotation of the radius plate brackets added an additional vertical deflection to the landing gear leg.

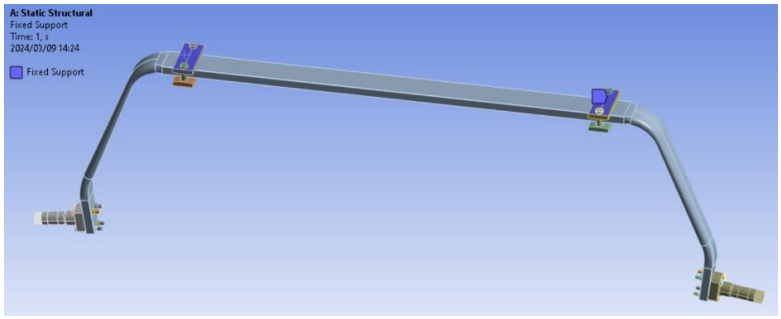


*Figure 32: FEA Vertical Deflection Validation (Constraint Application)*

Figure 33 provides the FEA results for vertical limit load and ultimate load deflections of the taildragger aircraft level landing. Note that the rotational deflection of the radius plate brackets was not included.

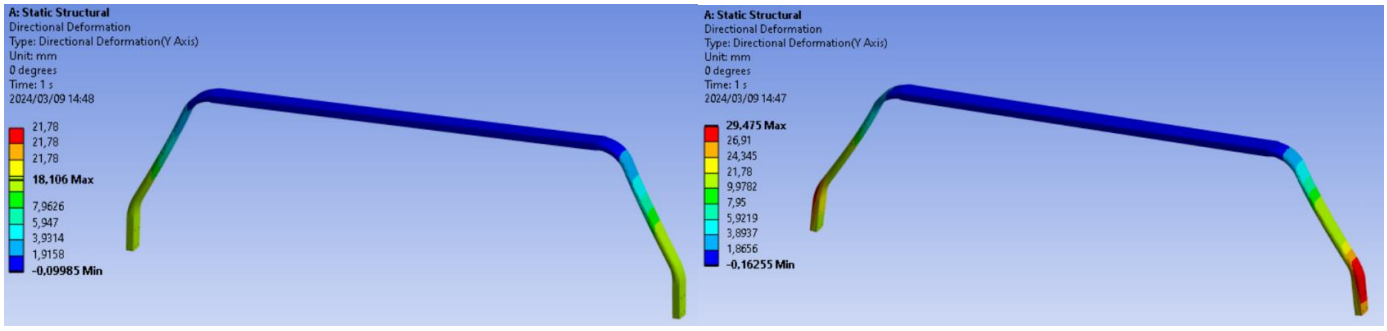


*Figure 33: FEA Vertical Deflection Validation (Taildragger Aircraft Level Landing) Limit and Ultimate Load Results*

Table 21 and Table 22 provides the comparison between the FEA and analytical results for the landing gear leg deflection during limit and ultimate loads respectively.

*Table 21: Validation of Results and Mesh Independence Study (Landing Gear Deflection – Limit Load)*

| - | **Calculated Results (mm)** | **23 mm Mesh (%error)** | **20 mm Mesh (%error)** | **16 mm Mesh (%error)** | **13 mm Mesh (%error)** | **10 mm Mesh (%error)** |
|---|---|---|---|---|---|---|
| **Landing Gear Deflection (Taildragger Aircraft)** | | | | | | |
| Level Landing | 19.443 | 17.998<br>7.432 % | 18.150<br>6.650 % | 18.183<br>6.480 % | 18.101<br>6.902 % | 18.106<br>6.877 % |
| Tail Down Landing | 16.507 | 15.352<br>6.997 % | 15.377<br>6.846 % | 15.400<br>6.706 % | 15.410<br>6.646 % | 15.412<br>6.634 % |
| **Landing Gear Deflection (Tricycle Aircraft)** | | | | | | |
| Level Landing (Inclined) | 9.433 | 8.512<br>9.764 % | 8.522<br>9.658 % | 8.536<br>9.509 % | 8.539<br>9.477 % | 8.546<br>9.403 % |
| Level Landing (Nose Clear) | 18.865 | 17.554<br>7.002 % | 17.565<br>6.891 % | 17.570<br>6.865 % | 17.926<br>4.977 % | 17.615<br>6.626 % |
| Tail Down Landing (Stall Altitude) | 18.865 | 17.554<br>7.002 % | 17.565<br>6.891 % | 17.570<br>6.865 % | 17.926<br>4.977 % | 17.615<br>6.626 % |
| **Side Load and Braked Roll** | | | | | | |
| Side Load | 9.088 | 8.401<br>7.559 % | 8.412<br>7.438 % | 8.426<br>7.284 % | 8.436<br>7.174 % | 8.464<br>6.866 % |
| Braked Roll | 9.088 | 8.401<br>7.559 % | 8.412<br>7.438 % | 8.426<br>7.284 % | 8.436<br>7.174 % | 8.464<br>6.866 % |

*Table 22: Validation of Results and Mesh Independence Study (Landing Gear Deflection – Ultimate Load)*

| - | **Calculated Results (mm)** | **23 mm Mesh (%error)** | **20 mm Mesh (%error)** | **16 mm Mesh (%error)** | **13 mm Mesh (%error)** | **10 mm Mesh (%error)** |
|---|---|---|---|---|---|---|
| **Landing Gear Deflection (Taildragger Aircraft)** | | | | | | |
| Level Landing | 31.651 | 29.367<br>7.216 % | 29.519<br>6.736 % | 29.552<br>6.632 % | 29.470<br>6.891 % | 29.475<br>6.875 % |
| Tail Down Landing | 26.871 | 25.030<br>6.851 % | 25.055<br>6.758 % | 25.078<br>6.673 % | 25.088<br>6.635 % | 25.090<br>6.628 % |
| **Landing Gear Deflection (Tricycle Aircraft)** | | | | | | |
| Level Landing (Inclined) | 15.356 | 14.303<br>6.857 % | 14.313<br>6.792 % | 14.327<br>6.701 % | 14.330<br>6.681 % | 14.337<br>6.636 % |
| Level Landing (Nose Clear) | 30.711 | 28.614<br>6.828 % | 28.625<br>71.916 % | 28.630<br>6.776 % | 28.986<br>5.617 % | 28.675<br>6.630 % |
| Tail Down Landing (Stall Altitude) | 30.711 | 28.614<br>6.828 % | 28.625<br>71.916 % | 28.630<br>6.776 % | 28.986<br>5.617 % | 28.675<br>6.630 % |
| **Side Load and Braked Roll** | | | | | | |
| Side Load | 9.088 | 8.401<br>7.559 % | 8.412<br>7.438 % | 8.426<br>7.284 % | 8.436<br>7.174 % | 8.464<br>6.866 % |
| Braked Roll | 9.088 | 8.401<br>7.559 % | 8.412<br>7.438 % | 8.426<br>7.284 % | 8.436<br>7.174 % | 8.464<br>6.866 % |

## 8.3. Landing Gear Drop Test FEA Validation

### 8.3.1. Drop test setup, by the company

Drop tests were conducted on the taildragger setup loaded with 375 kg of sand bags. The aircraft frame drop height was 0.3 m to represent an ultimate load (emergency landing) condition and a camera was placed in front of the aircraft frame to capture the drop test being conducted. The tailwheel was secured onto a block to replicate a taildragger level landing. A 2-ton lever block weight was used to lift the aircraft frame using a chain and a hook attached to a steel structure. A 3-ton maximum weight crane scale was used to measure the weight of the aircraft frame loaded with sand bags.

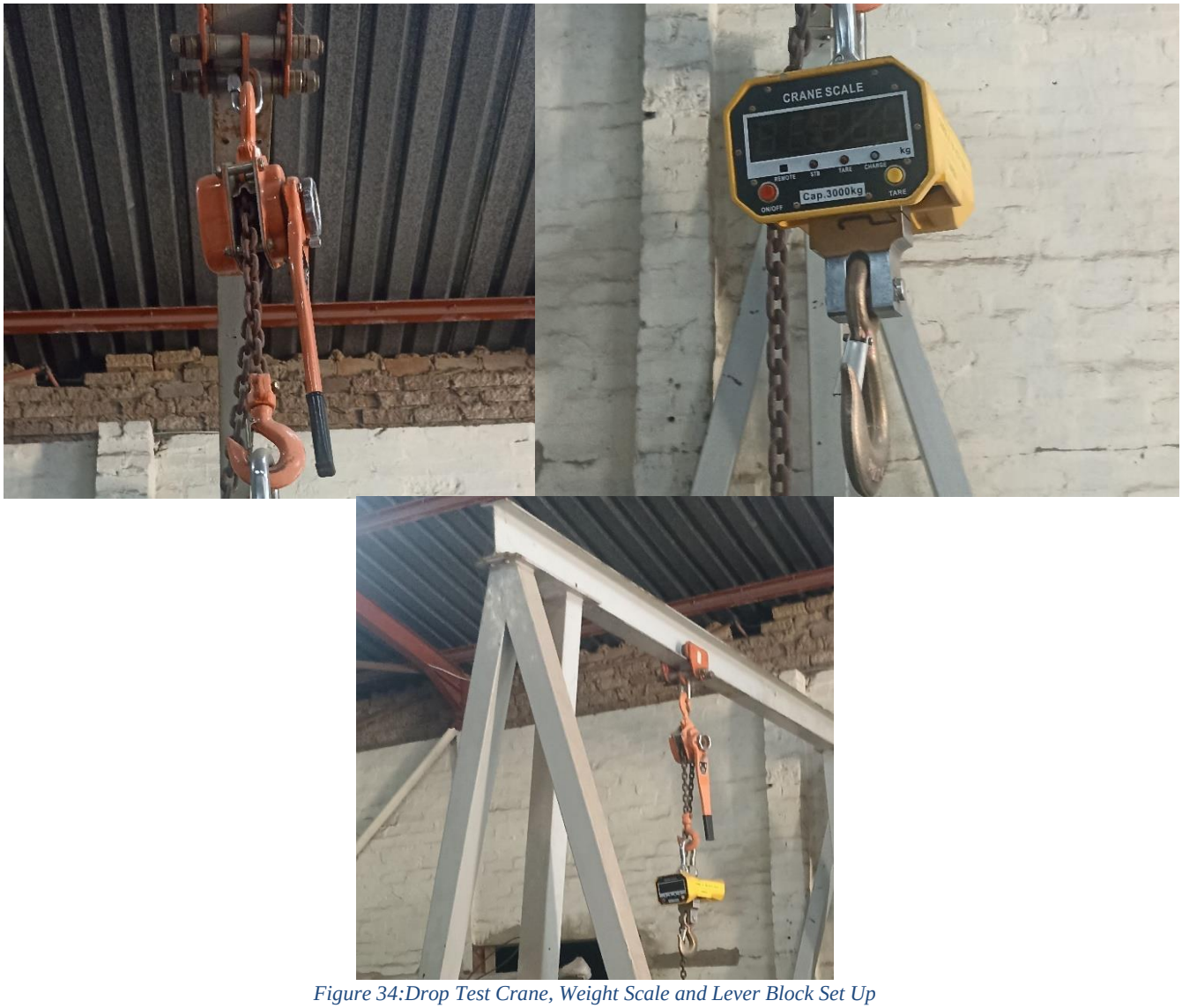


*Figure 34:Drop Test Crane, Weight Scale and Lever Block Set Up*

### 8.3.2. Drop Test FEA Load and Constraint Setup

The drop test setup and load application method represent a taildragger level landing thus, the loads were applied the same way as in section 8.3.1. The constraint setup will differ since the drop test validation takes the rotational deflection of the radius plate brackets into account. As seen in Figure 35, during heavy landing conditions, the gear strut will deflect upwards whilst the centre section of the gear deflects downwards [17]. If the gear is attached too rigidly, the load will transmit to the fuselage resulting in failure in the lower longerons near the attached points [17].

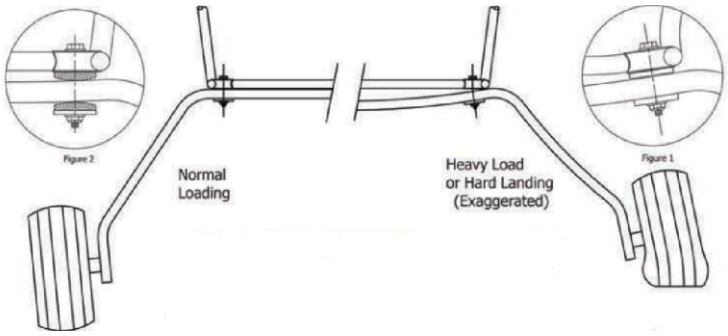


*Figure 35: Radius Plate Brackets Rotational Deflection [17]*

Figure 36 provides the fixed support application method used for the drop test FEA validation. It is applied in the centre of the radius plate brackets to introduce rotation deflection during landing.

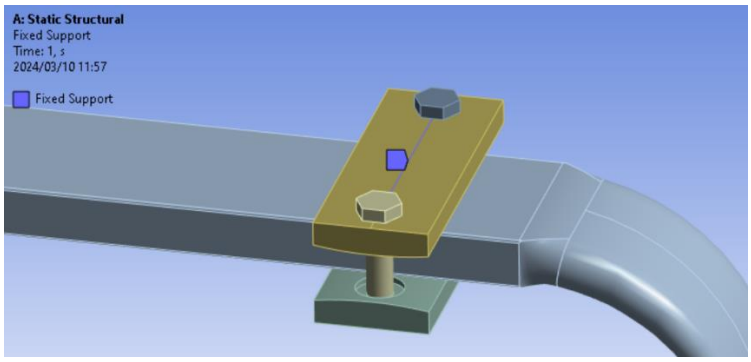


*Figure 36: Drop Test Fixed Support Application*

Figure 37 provides the drop test FEA vertical and horizontal deflection results at a drop weight of 375 kg and drop height of 0.3 m.

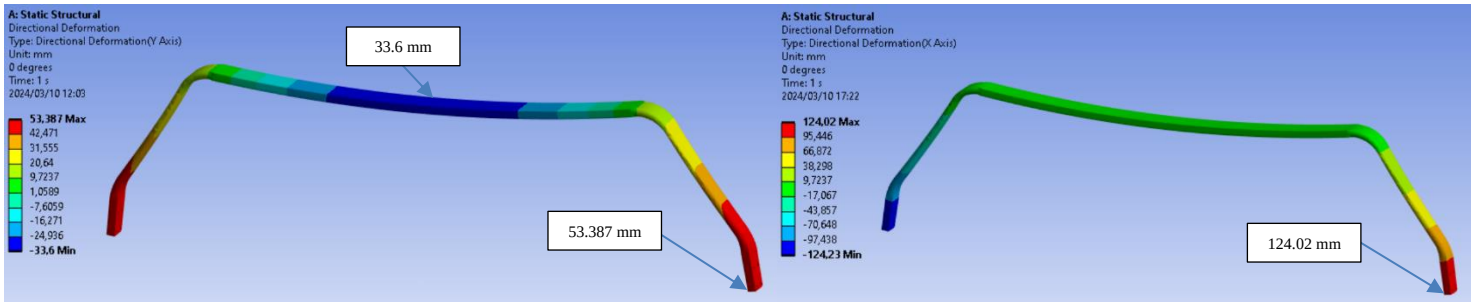


*Figure 37: Drop Test FEA Vertical and Horizontal Deflection Results*

The deflections were calculated from the images by taking the actual length and dividing it by the pixel length to obtain a pixel to length scale. This scale can be used to obtain deflections for any other part of the landing gear during the drop tests. These lengths obtained from the images are also compared to the FEA results to ensure validation. In Figure 38 we can see the dimension of the current Aluminium 7075 T6 alloy landing gear that were used during the drop test validation. In Figure 39, the we can see the dimensions calculated using the calculated pixel to length scale. These calculated dimensions were compared to Figure 38 to make sure the calculated dimensions using the scale are of similar value. Note that the distance between the tyres varies between Figure 38 and Figure 39 since before the gear is dropped the weight of tyres bends the landing gear legs inwards.

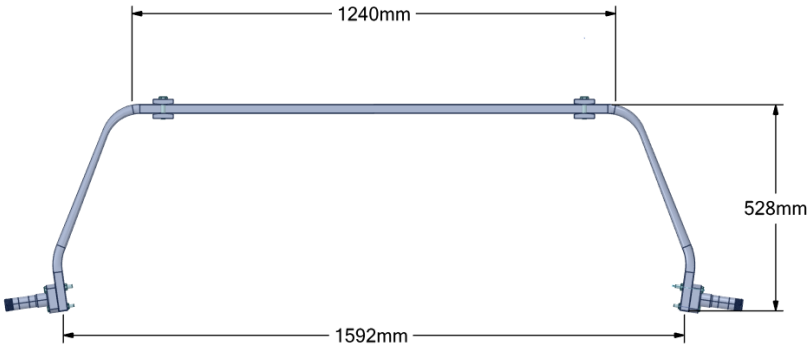


*Figure 38: Aluminium 7075 T6 Landing Gear Drop Test Dimension*

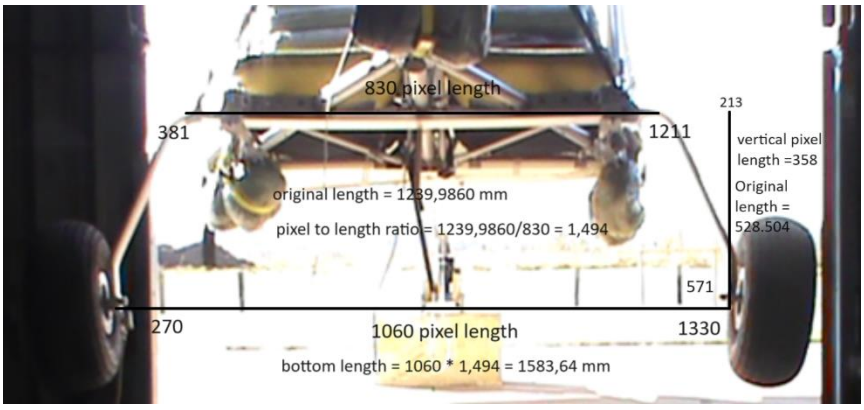


*Figure 39: Aluminium 7075T6 Landing Gear Pre-Drop Test (0,3 m at 375 kg)*

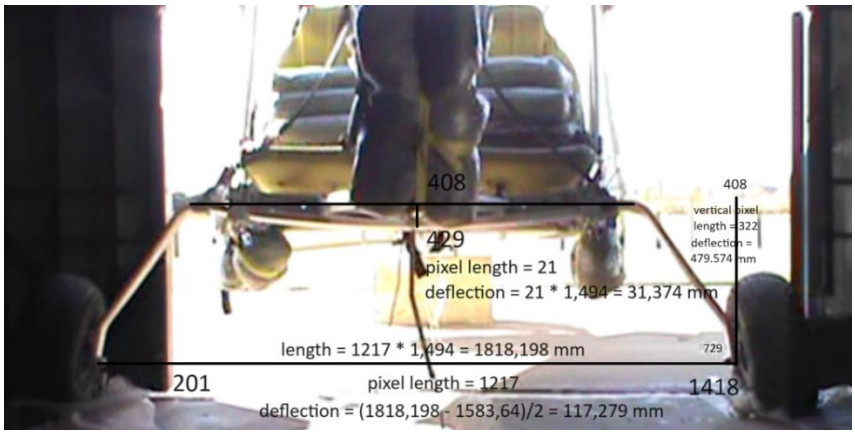


*Figure 40: Aluminium 7075T6 Landing Gear Drop Test Maximum Horizontal and Vertical Deflection*

The following calculations were done as seen in Figure 39 and Figure 40:

### 1) Pixel to Length Reference Scale and Original Distances

To find the pixel to length reference scale, the actual measured length was divided by the pixel length as seen in Figure 39. Note that this calculation was done before the landing gear is dropped and underwent deflection.

Top Beam Section (Reference):

$$1211\ pixles - 381\ pixels = 830\ pixel\ length$$

$$Original\ Length = 1239.9860\ mm$$

$$pixel\ to\ length\ ratio = \frac{1239.9860\ mm}{830\ pixel\ length} = 1.494$$

Original Horizontal Distance Between Tyres:

The pixel length is multiplied by the pixel to length scale to find the horizontal distance.

$$1330\ pixles - 270\ pixels = 1060\ pixel\ length$$

$$Distance\ between\ tyres = 1060\ pixel\ length\ \times 1.494 =\ 1583.64\ mm$$

Original Vertical Distance:

$$571\ pixles - 213\ pixels = 358\ pixel\ length$$

$$Distance\ between\ tyres = 358\ pixel\ length\ \times 1.494 =\ 534.852\ mm$$

### 2) Vertical Top Beam Deflection

As seen in Figure 40, the top beam section was located just beneath the aircraft fuselage.

$$429\ pixels - 408\ pixels = 21\ pixel\ length$$

$$Vertical\ top\ beam\ deflection = 21\ pixel\ length\ \times 1.494 =\ 31.374\ mm$$

### 3) Landing Gear Vertical Deflection

$$729\ pixels - 408\ pixels = 321\ pixel\ length$$

$$Vertical\ distance = 321\ pixel\ length\ \times 1.494 =\ 479.574\ mm$$

$$Actual\ vertical\ deflection = 534.852\ mm - 479.574\ = 55.278\ mm$$

**4) Landing Gear Horizontal Deflection**

$$1418\,pixels - 201\,pixels = 1217\,pixel\,length$$

$$Horizontal\,distance = 1217\,pixel\,length \times 1.494 = 1818.198\,mm$$

$$Actual\,horizontal\,deflection = 1818.198\,mm - 1583.64\,mm = 234.558\,mm$$

$$Divide\,by\,two\,to\,get\,horizontal\,deflection\,per\,tyre\,thus, giving\,117.279\,mm$$

Table 23 provides the error percentage between the mesh independence study comparison between the analytical and FEA results for the drop test validation.

*Table 23: Validation of Results and Mesh Dependence Study (Drop Test)*

| - | **Calculated Results (mm)** | **23 mm Mesh (%error)** | **20 mm Mesh (%error)** | **16 mm Mesh (%error)** | **13 mm Mesh (%error)** | **10 mm Mesh (%error)** |
|---|---|---|---|---|---|---|
| **Drop Test** | | | | | | |
| Vertical Deflection (Top Beam) | 31.374 | 33.484<br>6.899 % | 33.50<br>6.943 % | 33.507<br>6.963 % | 33.529<br>7.024 % | 33.6<br>7.220 % |
| Vertical Deflection (Landing Gear) | 55.276 | 53.051<br>4.025 % | 53.185<br>3.783 % | 53.230<br>3.701 % | 53.29<br>3.593 % | 53.387<br>3.417 % |
| Horizontal Deflection (Landing Gear) | 117.279 | 123.833<br>5.293 % | 123.99<br>5.413 % | 124.082<br>5.483 % | 124.136<br>5.524 % | 124.23<br>5.595 % |

To ensure reliability of the findings presented in Table 23, the uncertainty was calculated below based on the margin of error when taking the pixel length measurements as seen in Figure 39 and Figure 40. The aim is to predict the inherent inaccuracies in the results to evaluate the conclusions drawn from the data presented in Table 23. In this study presented, a change in 5% to 10% of the original pixel length was evaluated to see the change occurring in the pixel to length ratio and its effect on the calculated deflections. This is due to the pixel to length ratio making use of the actual length of the landing gear section. Note that the original pixel to length ratio calculated was 1.494 with a corresponding pixel length of 830.

*Table 24: Drop Test Pixel to Length Ratio Uncertainties*

| Percentage change | **-10%** | **-5%** | **0%** | **+5%** | **+10%** |
|---|---|---|---|---|---|
| Calculated Pixel Length | 747 | 788.5 | 830 | 871.5 | 913 |
| Pixel to Length Ratio | **1.660** | **1.573** | **1.494** | **1.423** | **1.358** |
| Vertical Deflection (Top Beam) | 34.859 | 33.024 | 31.374 | 29.879 | 28.521 |
| Vertical Deflection (Landing Gear) | 61.418 | 58.186 | 55.276 | 52.644 | 50.251 |
| Horizontal Deflection (Landing Gear) | 106.614 | 111.691 | 117.279 | 123.448 | 130.306 |

Figure 41 provides a visualisation with regards to the uncertainty of the pixel to length ratio and the deflection compairsons betweent the FEA and analytical results.

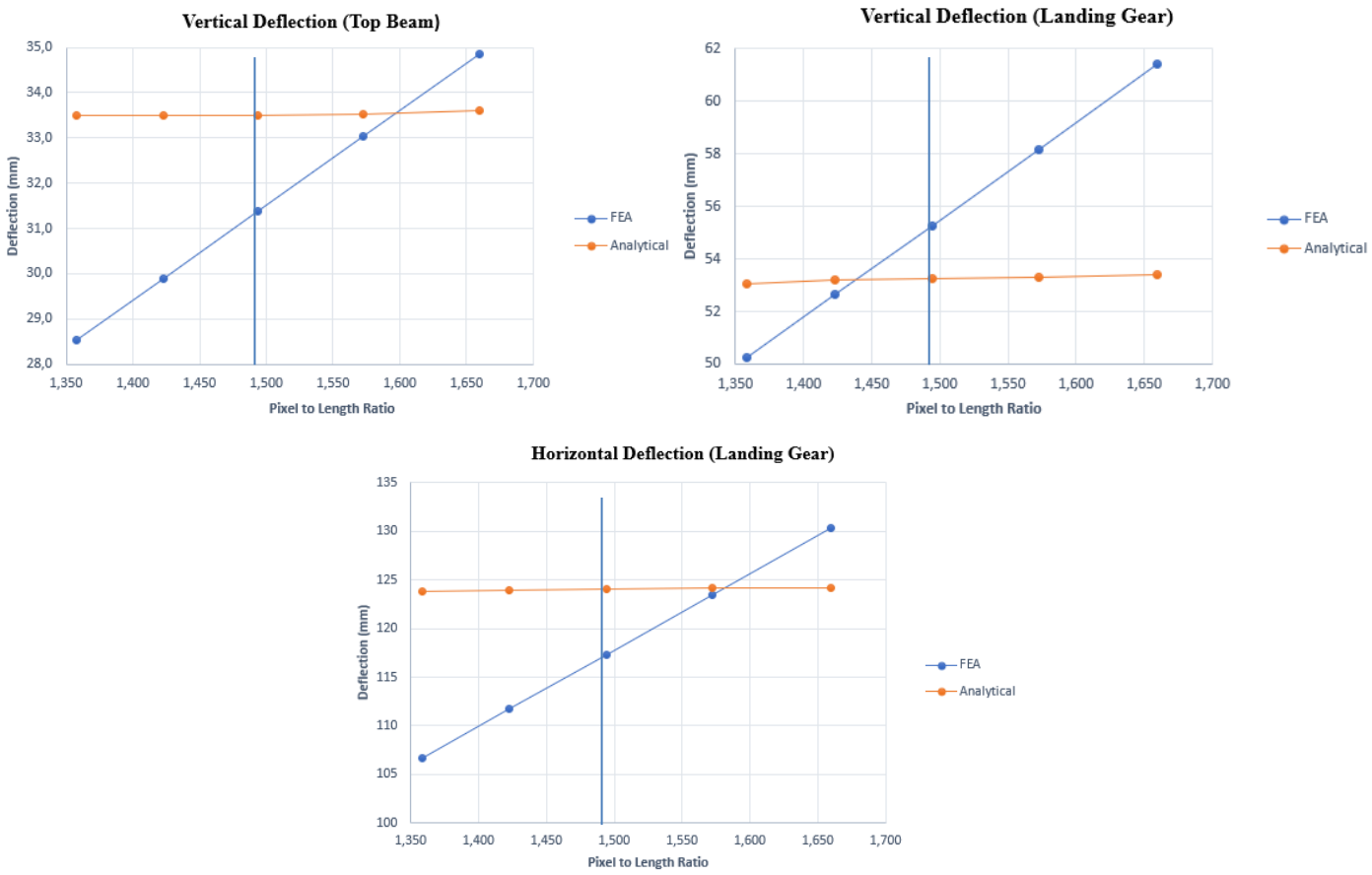


*Figure 41: Drop Test Pixel to Length Ratio vs Deflection Uncertainties*

## 8.4. Load/ Constrain Application and Mesh Independence Study Summary

In conclusion, the analysis conducted through FEA assumed that the load was applied gradually and remained constant whereas the physical drop test involved dynamic loading where the gear experienced sudden impact and varying loads during the impact phase which resulted in initial impact, rebound and possibly secondary impacts. Another uncertainty which could be presented was the boundary conditions defined during the FEA analysis such as the constraint application at the radius plate brackets. During the physical tests, the boundary conditions were more complex and less controlled, considering the frictional forces between the tyres and ground during impact. The deflection results obtained through FEA analysis and analytical pixel calculations were within a 10% error range. The usage of the 10% error range signified a reasonable level of agreement between the numerical and analytical results due to the complexities and uncertainties inherent between the FEA results and physical tests. Thus, it should be considered that the static FEA provided valuable insights with regards to the structural behaviour of the landing gear, but physical drop tests were crucial for validating these simulations by capturing the dynamic effects that occur during a real-world drop test scenario. Thus, we can conclude that the load application on the stub axles and constraint application to the radius plate brackets in Ansys were a close approximate according to the real-world physical drop tests conducted.

# 9. ALUMINIUM LANDING GEAR ANALYSIS

## 9.1. Introduction

In this section a FEA analysis was conducted on the current Aluminium 7075T6 alloy landing gear loaded with all landing conditions at a maximum weight of 600 kg at limit load and ultimate load conditions. All loads were presented in Table 9 and Table 12. All load/constraint and mesh application were done using validated methods conducted in chapter 8.

## 9.2. Mesh Application

A 10 mm mesh size were used on the Aluminium 7075 T6 alloy landing gear, stub axle, bolts, and nuts as validated in chapter 8. Figure 42 presents the 10 mm mesh application to the landing gear and assembled components.

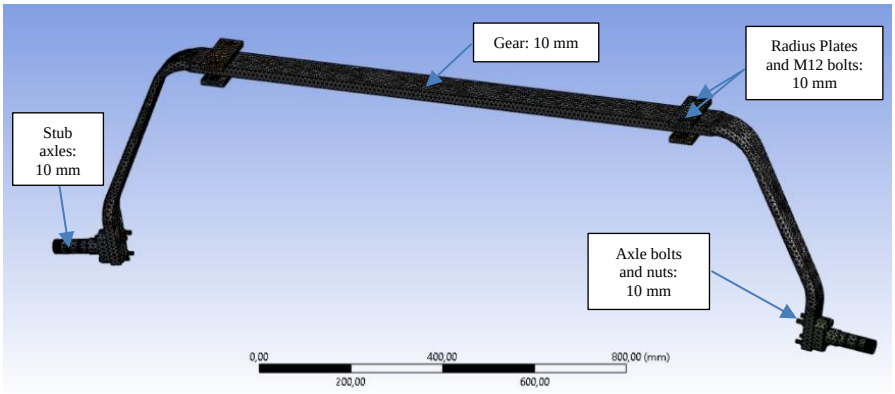


*Figure 42: Mesh Application to Aluminium 7075 T6 Alloy Landing Gear*

### 9.2.1. Taildragger Aircraft

9.2.1.1. Taildragger Level landing

The landing gear at limit load conditions was subjected to main wheel ground reaction loads of 8436.6 N and 3090.15 N in frictional loads on the main tyres. The average wheel size with hub and tyre is 10 inches thus, a 5-inch radius with resulting torque loads on the stub axles being 392.449 Nm. At ultimate load the ground reaction load was 13734 N and 4414.5 N in frictional loads thus, applying a torque load on the stub axles of 560.642 Nm. It was assumed that the landing gear impacted the runway vertically with a 90-degree angle.

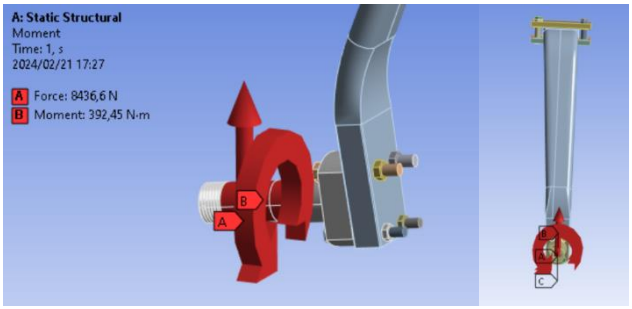


*Figure 43: Taildragger Level Landing Aluminium Landing Gear Load Application (FEA Limit Load)*

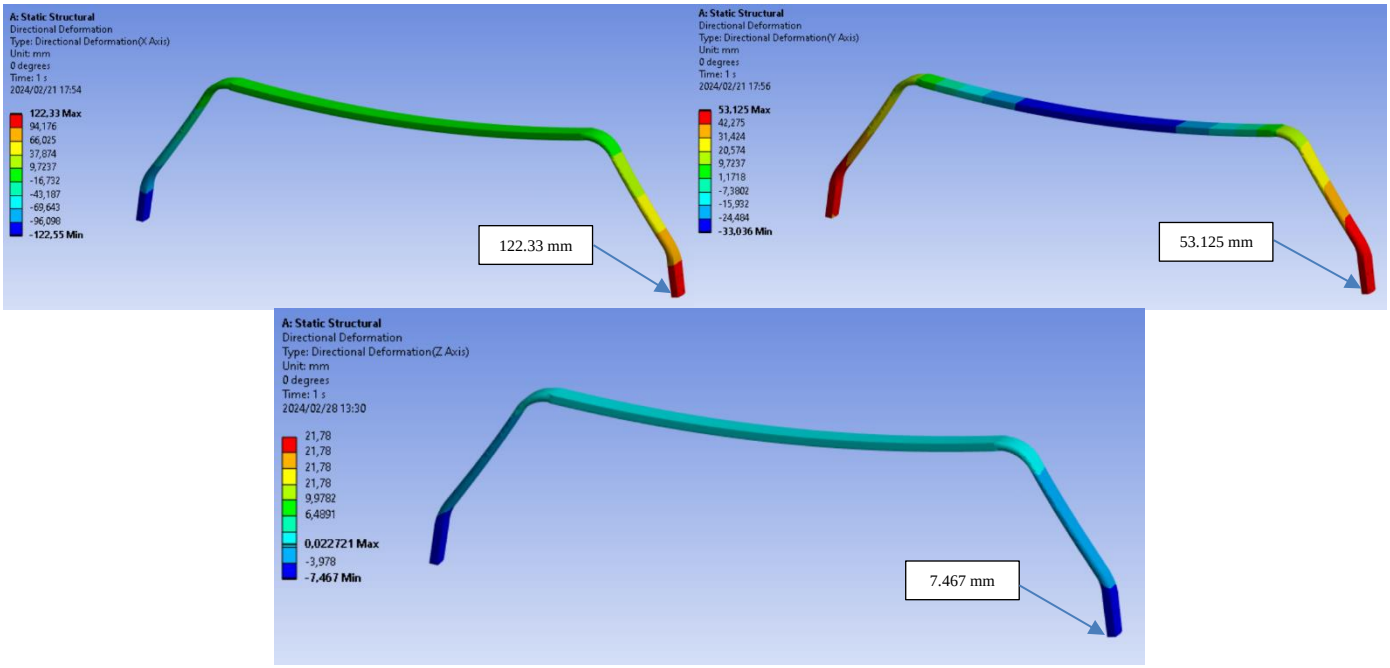


*Figure 44: Aluminium Landing Gear Level Landing FEA Limit Load X, Y, Z Deformation Results (Taildragger)*

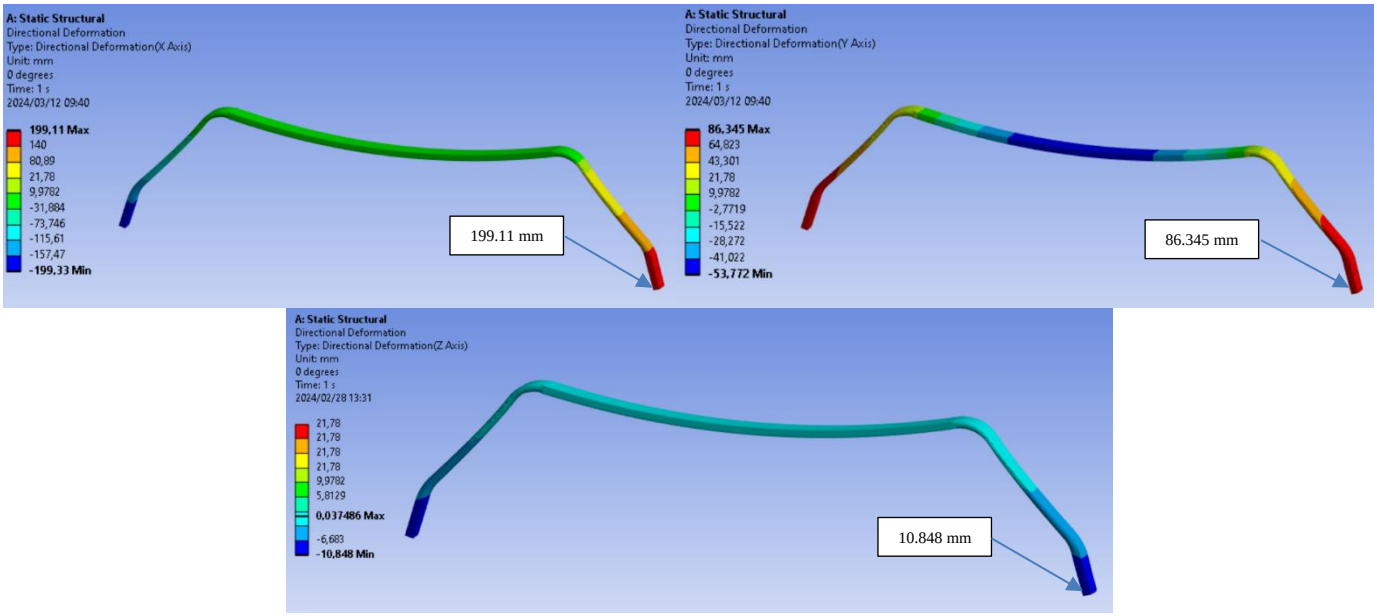


*Figure 45: Aluminium Landing Gear Level Landing FEA Ultimate Load X, Y, Z Deformation Results (Taildragger)*

During level landing of the taildragger aircraft, at limit load conditions the observed stress on the surface of the main gear was 375.29 MPa, whereas the maximum was stress through the main gear leg was approximately 291.9 MPa as seen in Figure 55. The yield strength of Aluminium 7075 T6 was 480 MPa thus, having a yield safety factor of 1.644 at limit load landing conditions. For ultimate load conditions seen in Figure 47 in the stress was 606.17 MPa on the surface whereas for the maximum stress throughout the main gear, the FEA results show approximately 471.47 MPa. The ultimate strength of Aluminium 7075 T6 was 540 MPa resulting in an ultimate strength safety factor of 1.145 near the surface of the gear at ultimate load landing conditions. The stress reduces as the measurement was taken closer to the middle of the gear strut increasing the ultimate safety factor during ultimate (emergency loads).

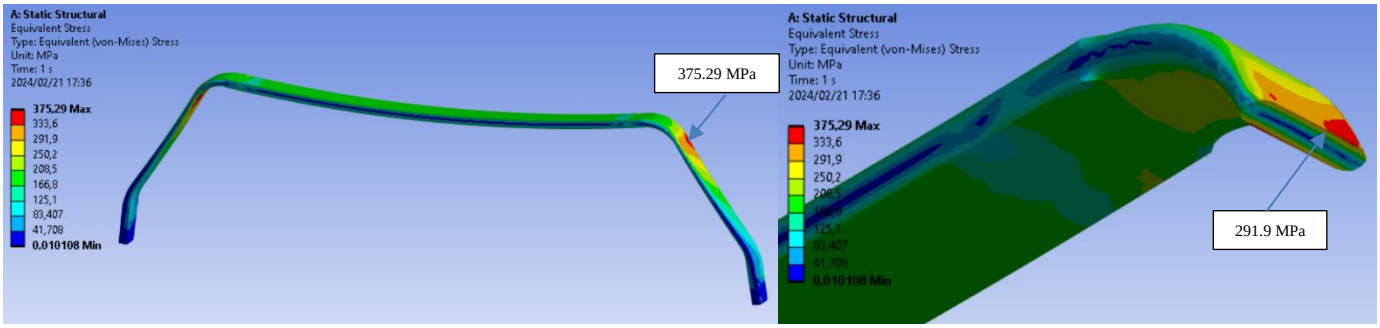


*Figure 46: Aluminium Landing Gear Level Landing Limit Load FEA Stress Results (Taildragger)*

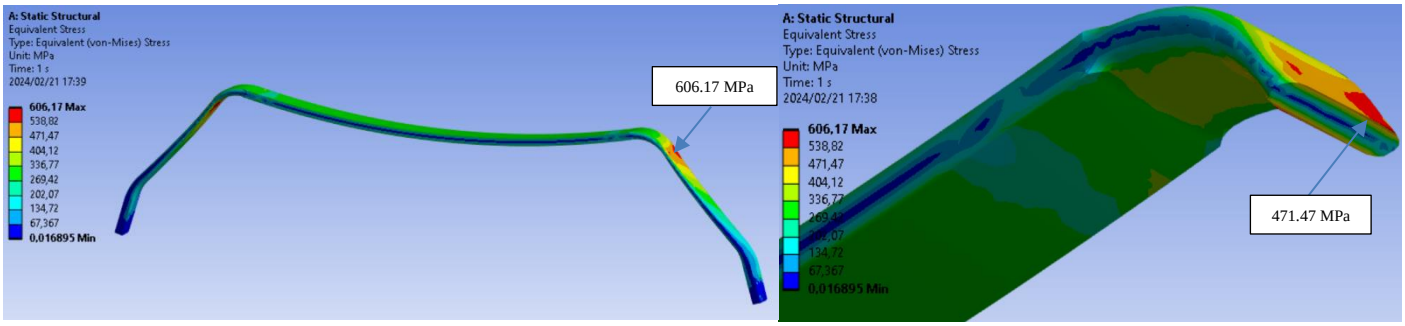


*Figure 47: Aluminium Landing Gear Level Landing Ultimate Load FEA Stress Results (Taildragger)*

In Figure 48, the left image provides equivalent elastic strain for limit loads and right image for ultimate loads during taildragger aircraft level landing.

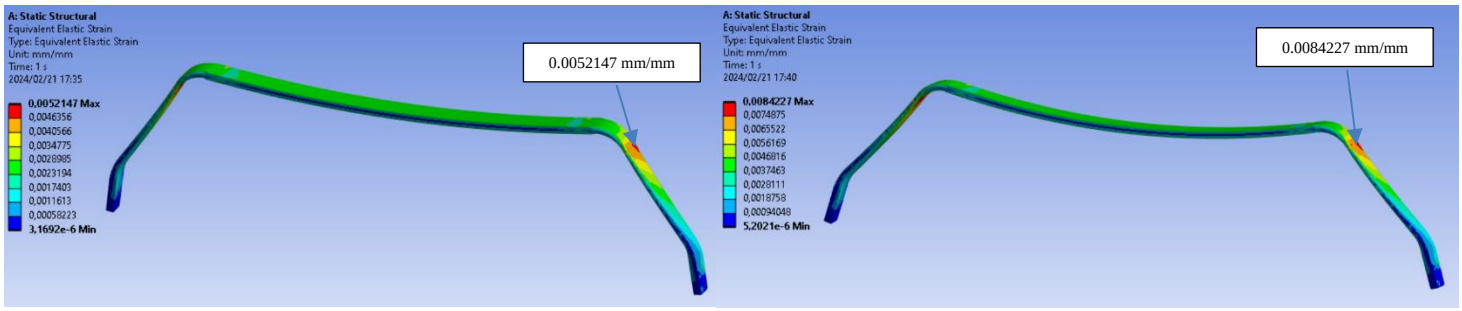


*Figure 48: Aluminium Landing Gear Level Landing Limit and Ultimate Load FEA Strain Results (Taildragger)*

In conclusion, during level landing of the taildragger aircraft, the X, Y and Z limit load deformations were 122.33 mm, 53.125 mm and, 7.464 mm respectively. The limit load stress on landing gear was approximately 291.9 MPa resulting in a yield strength safety factor of 1.644 whilst the limit load strain on the gear was 0.0052147 mm/mm. At ultimate load conditions the X, Y and Z deformations were 199.11 mm, 86.345 mm and, 10.848 mm respectively. The ultimate load stress on the landing gear was approximately 471.47 MPa resulting in an ultimate strength safety factor of 1.145 whilst the strain on the gear was 0.0084227 mm/mm.

9.2.1.2. Taildragger Tail down landing

The landing gear was subjected to main wheel ground reaction loads of 7381.8 N during limit load conditions and 12016.84 N during ultimate load conditions according to Table 9 and Table 10. There were no frictional loads applied to the main wheels according to ASTM standards. It was assumed that the main landing gear would impact the runway at a 14-degree angle for a taildragger tail down landing according to Figure 3.

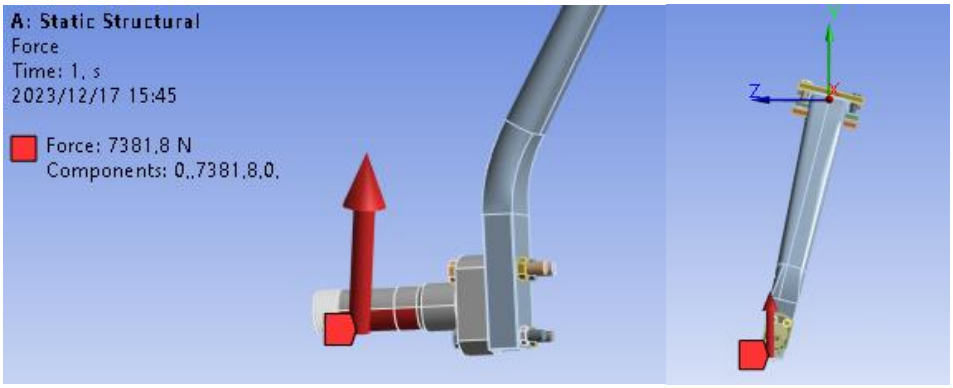


*Figure 49: Taildragger Tail Down Landing Aluminium Landing Gear Load Application (FEA)*

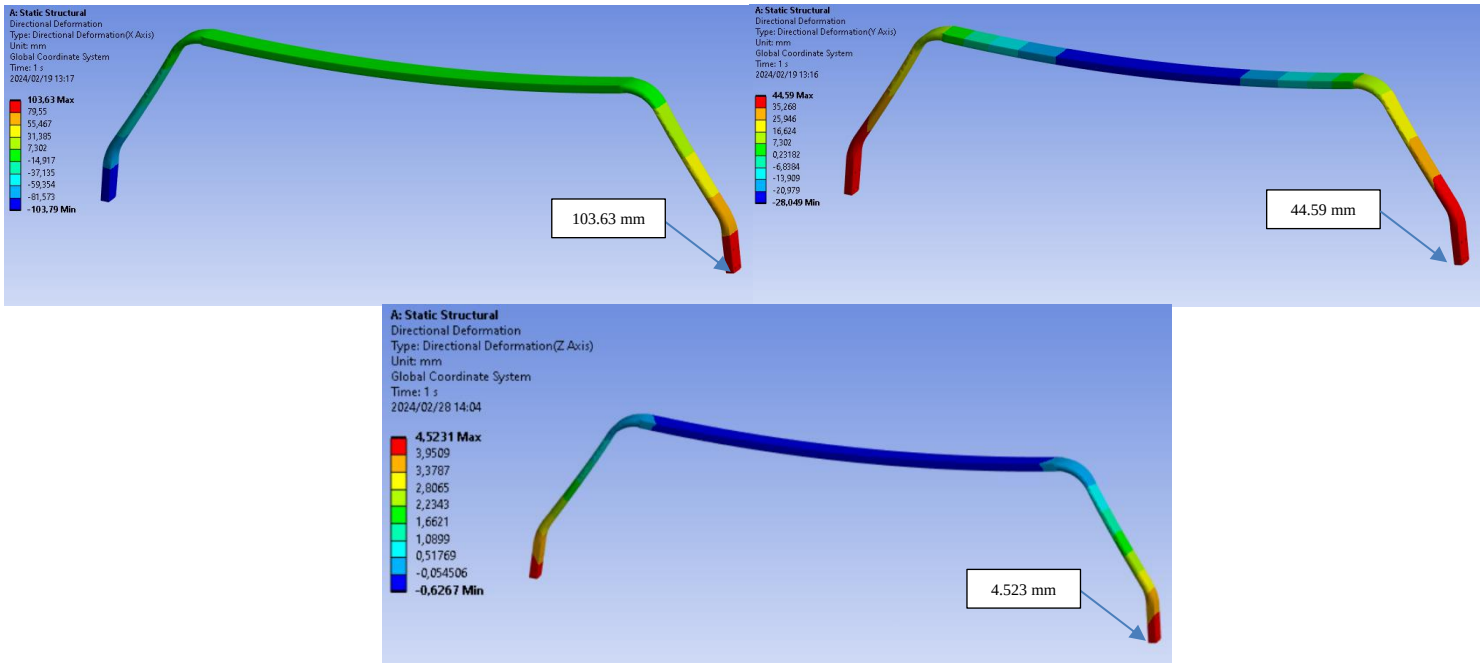


*Figure 50: Aluminium Landing Gear Tail Down Landing Limit Load FEA X, Y, Z Deformation Results (Taildragger)*

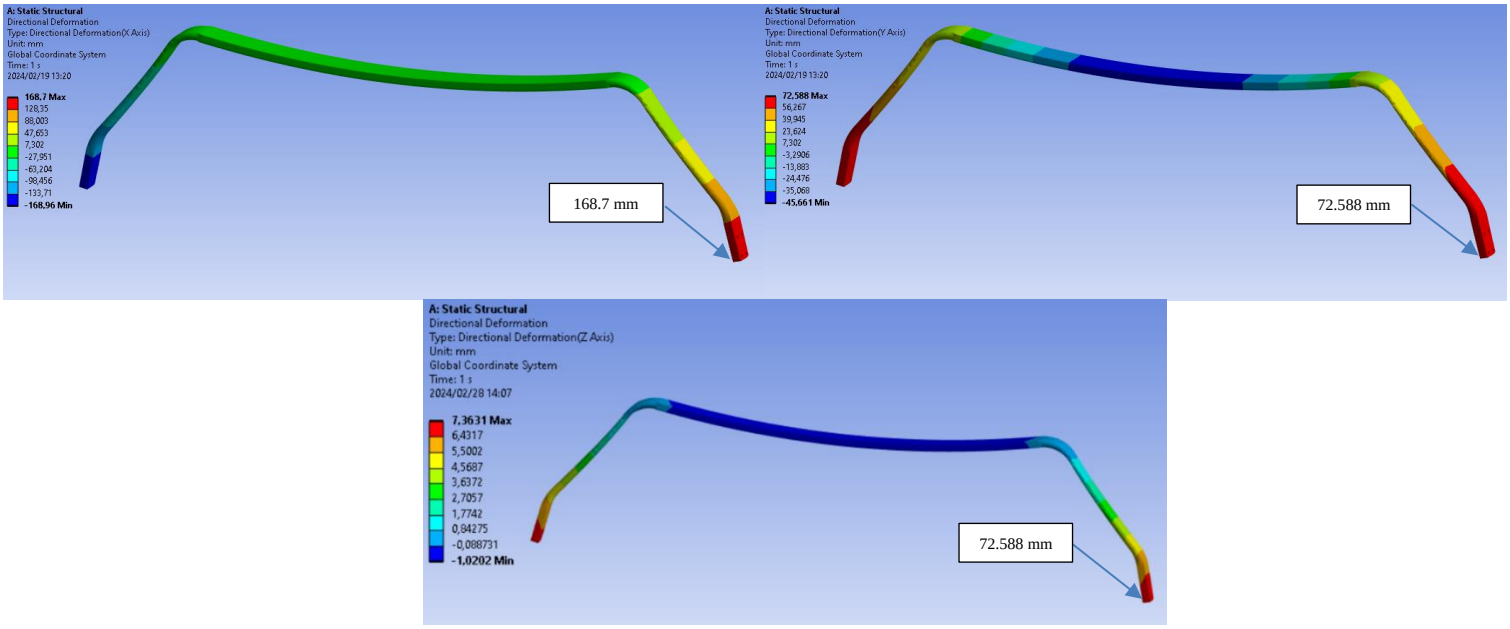


*Figure 51:Aluminium Landing Gear Tail Down Landing Ultimate Load FEA X, Y, Z Deformation Results (Taildragger)*

During the taildragger tail down landing at limit load condition the stress on the surface of the main gear was 328.78 MPa. The stress within the gear was approximately 255.72 MPa resulting in a yield safety factor of 1.877. During ultimate load conditions the maximum stress were on the surface of the gear at 535,22 MPa. The stress throughout the gear was approximately 416.29 MPa resulting in a yield safety factor of 1.153 in the leg strut whilst having an ultimate safety factor of 1.393 near the surface of the landing gear strut.

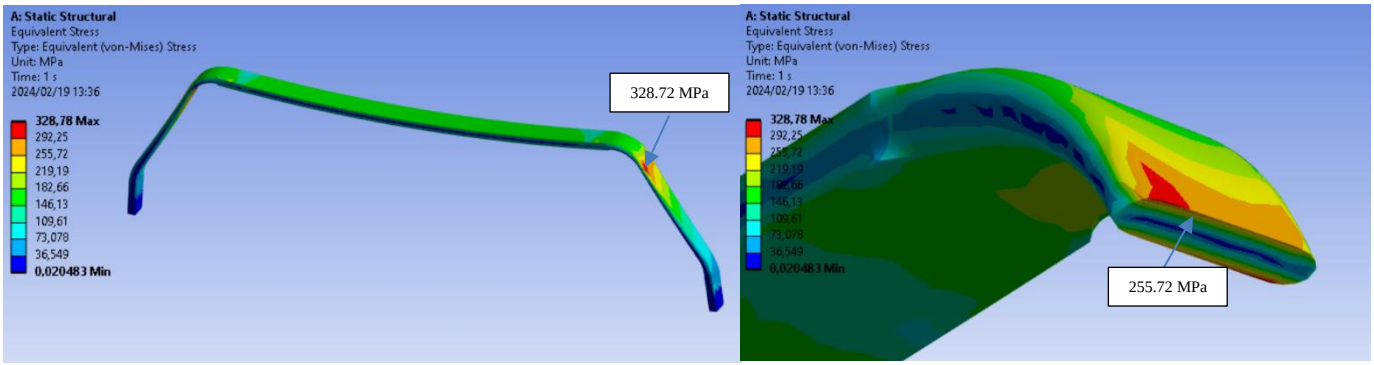


*Figure 52: Aluminium Landing Gear Tail Down Limit Load Landing FEA Stress Results (Taildragger)*

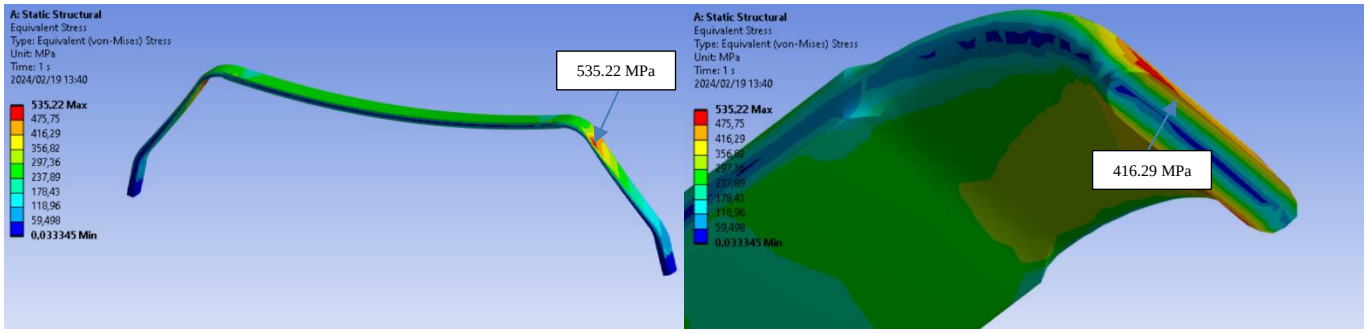


*Figure 53: Aluminium Landing Gear Tail Down Ultimate Load Landing FEA Stress Results (Taildragger)*

In Figure 54 the left image provides equivalent elastic strain for limit loads and right image for ultimate loads during taildragger aircraft tail down landing.

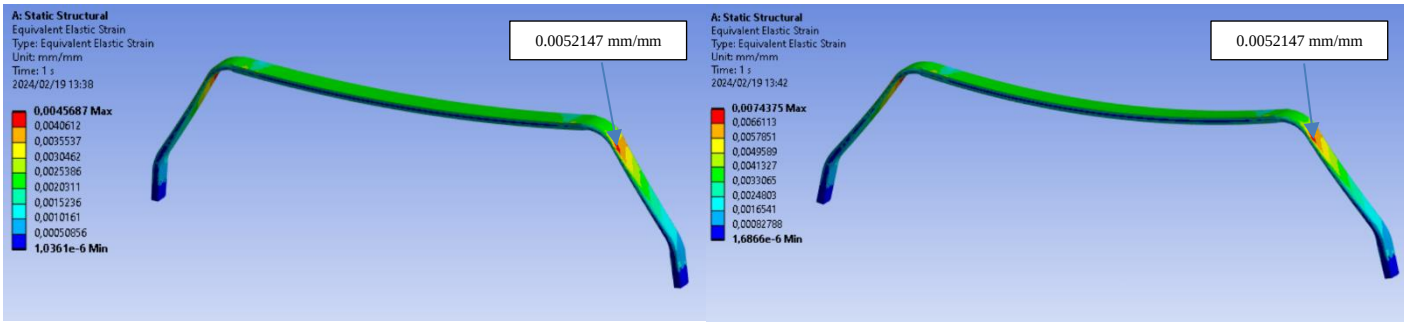


*Figure 54: Aluminium Landing Gear Tail Down Limit and Ultimate Load Landing FEA Strain Results (Taildragger)*

In conclusion, during tail down landing of the taildragger aircraft at limit load conditions, the X, Y and Z deformations were 103.63 mm, 44.59 mm and, 4.5231 mm respectively. The limit load stress on landing gear was approximately 255.72 MPa resulting in a yield strength safety factor of 1.877 whilst the strain on the gear was 0.004569 mm/mm. At ultimate load conditions the X, Y and Z deformations were 168.7 mm, 72.588 mm and, 7.363 mm respectively. The ultimate load stress on the landing gear was approximately 416.29 MPa resulting in an ultimate strength safety factor of 1.393 whilst the strain on the gear was 0.0074375 mm/mm.

### 9.2.2 Tricycle Aircraft

#### 9.2.2.1 Tricycle Level landing with Inclined Reactions

The landing gear at limit load conditions was subjected to main wheel ground reaction loads of 4218.3 N and 1545.08 N in frictional loads on the main tyres in contact with the runway during level landing of the tricycle aircraft. The torque loads on each stub axle were 196.225 Nm. At ultimate load the ground reaction load was 6867 N and 2207.25 N in frictional loads thus, applying a torque load on each stub axle of 280.321 Nm. It was assumed that the landing gear impacts the runway with a 14-degree angle during tricycle aircraft level landing with inclined reactions.

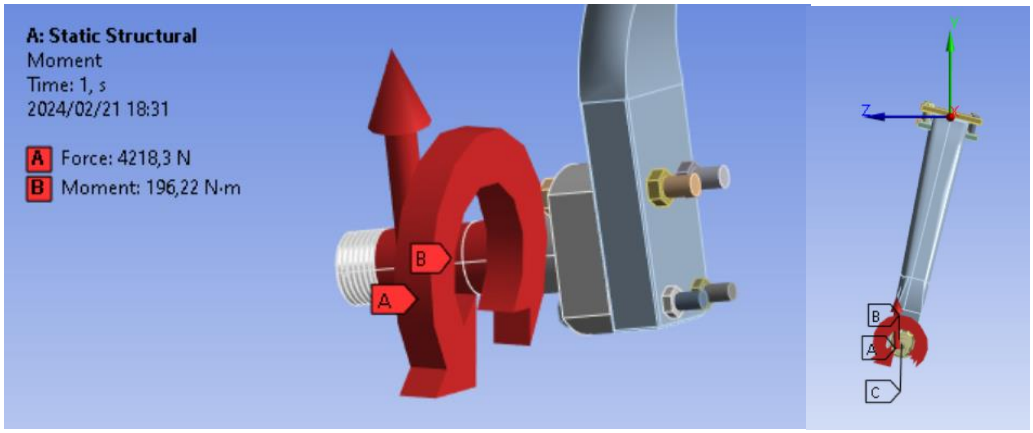


*Figure 55: Tricycle Level Landing (Inclined Reactions) Aluminium Landing Gear Load Application (FEA)*

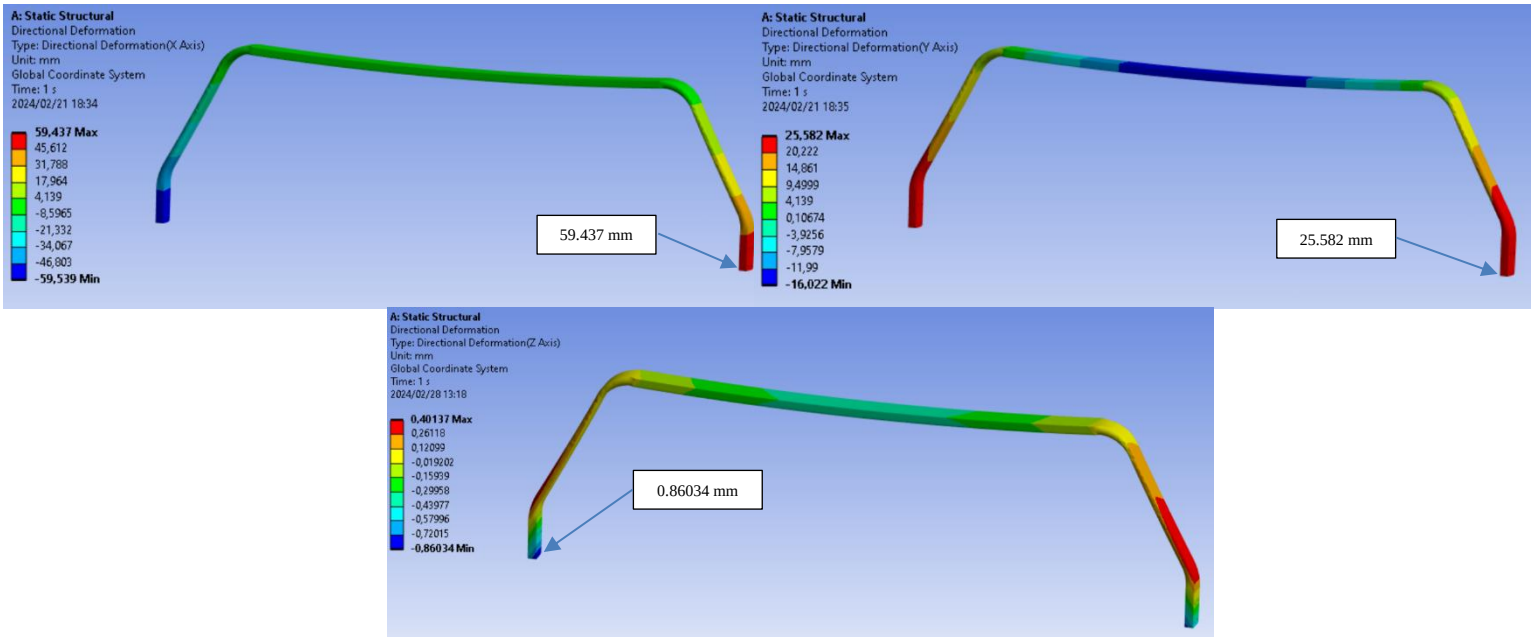


*Figure 56: Aluminium Landing Gear Level Landing (Inclined Reactions) Limit Load FEA X, Y, Z Deformation Results (Tricycle)*

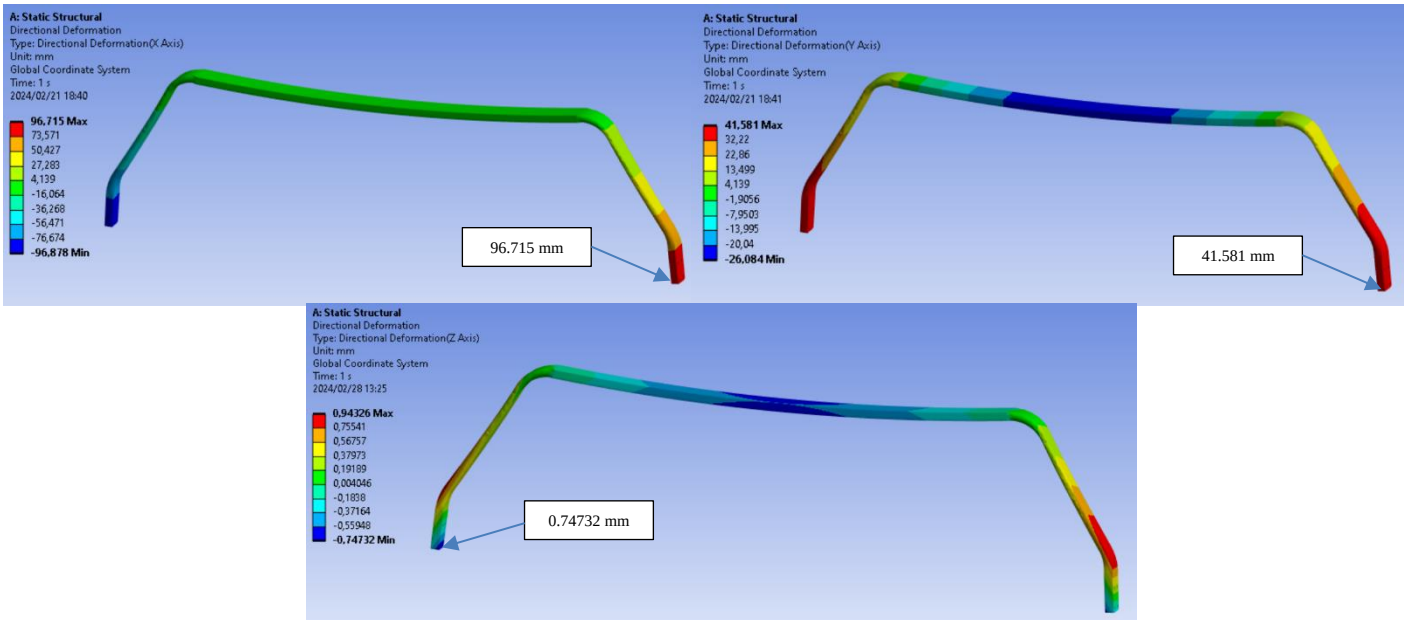


*Figure 57: Aluminium Landing Gear Level Landing (Inclined Reactions) Ultimate Load FEA X, Y, Z Deformation Results (Tricycle)*

During tricycle aircraft level landing with inclined reactions for the limit load condition the stress on the surface of the main gear was 176.28 MPa. The stress throughout the gear was approximately 137.1 MPa resulting in a yield safety factor of 3.501. For the ultimate load condition, the stress on the surface of the gear was 289.01 MPa. The stress throughout the gear was approximately 224.79 MPa resulting in a yield safety factor of 2.135 thus, the gear would survive emergency landing conditions during tricycle level landing with inclined reactions.

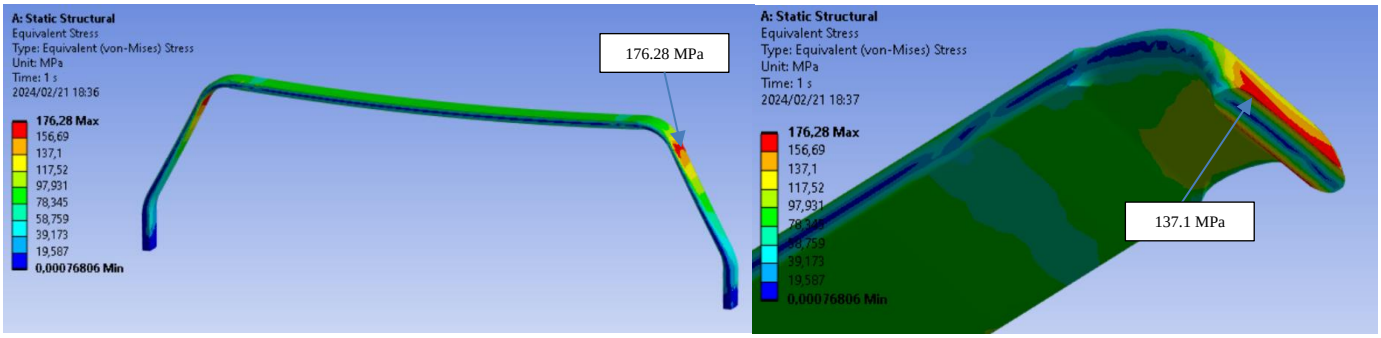


*Figure 58: Aluminium Landing Gear Level Landing (Inclined Reactions) Limit Load FEA Stress Results (Tricycle)*

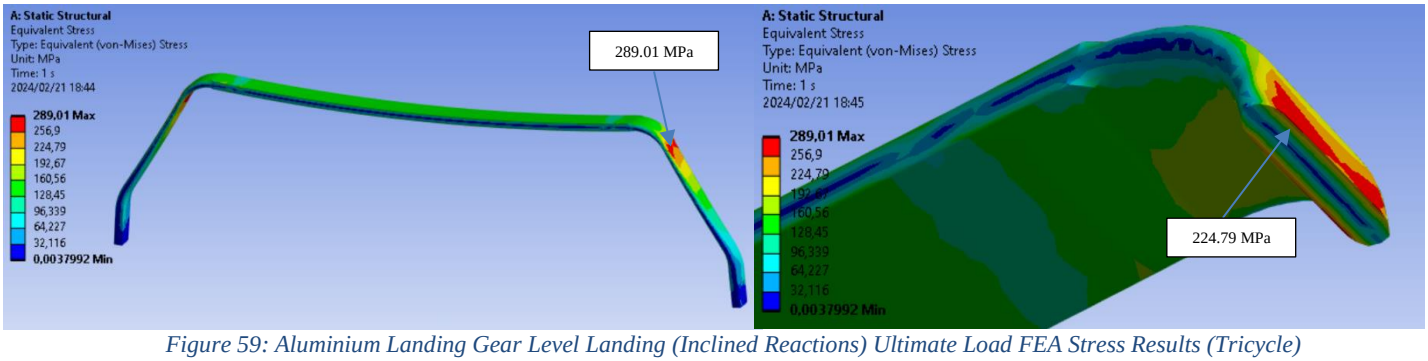


*Figure 59: Aluminium Landing Gear Level Landing (Inclined Reactions) Ultimate Load FEA Stress Results (Tricycle)*

Figure 60 provides equivalent elastic strain for limit loads and right image for ultimate loads during tricycle aircraft level landing with inclined reactions.

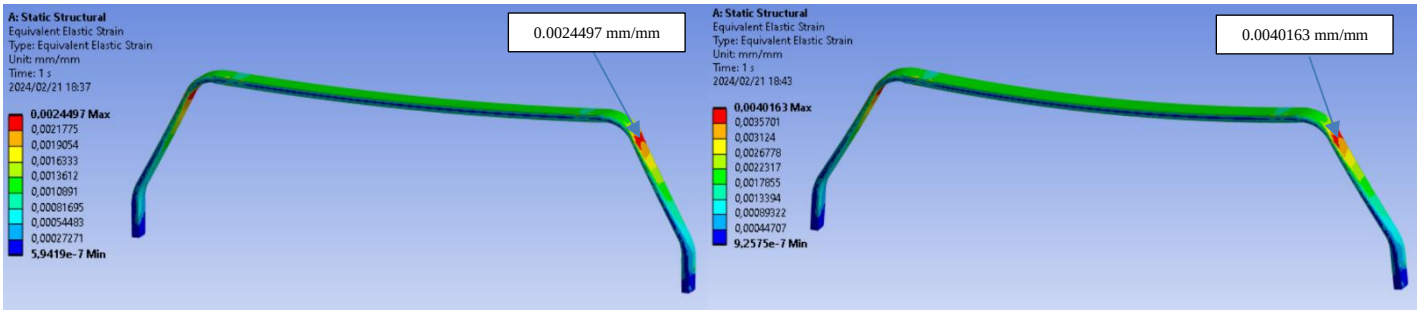


*Figure 60: Aluminium Landing Gear Level Landing (Inclined Reactions) Limit and Ultimate Load FEA Strain Results (Tricycle)*

In conclusion, during level landing (inclined reactions) of the tricycle aircraft at limit load conditions, the X, Y and Z deformations were 59.437 mm, 25.582 mm and, 0.86034 mm respectively. The stress on landing gear was approximately 137.1 MPa resulting in a yield strength safety factor of 3.501 whilst the strain on the gear was 0.0024497 mm/mm. At ultimate load conditions the X, Y and Z deformations were 96.715 mm, 41.581 mm and, 0.74732 mm respectively. The stress on the landing gear was approximately 224.79 MPa resulting in a yield strength safety factor of 2.135 whilst the strain on the gear was 0.0040163 mm/mm.

### 9.2.2.2 Tricycle Level landing with Nose Wheel Just Clear of Ground

The landing gear under limit load conditions was subjected to main wheel ground reaction loads of 8436.6 N and 3090.6 N in frictional loads on the main tyres in contact with the runway during tricycle aircraft level landing with nose wheel just clear of ground. The torque loads on each stub axle were 392.449 Nm. At ultimate load the ground reaction load was 13734 N and 4414.5 N in frictional loads thus, applying a torque load on each stub axle of 560.641 Nm. It was assumed that the landing gear impacts the runway with a 14-degree angle during tricycle aircraft level landing with nose wheel just clear of ground.

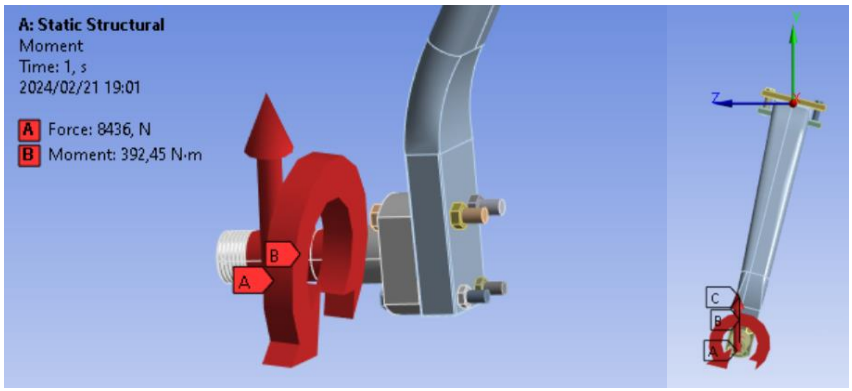


*Figure 61: Tricycle Level Landing (Nose Wheel Clear) Aluminium Landing Gear Load Application (FEA)*

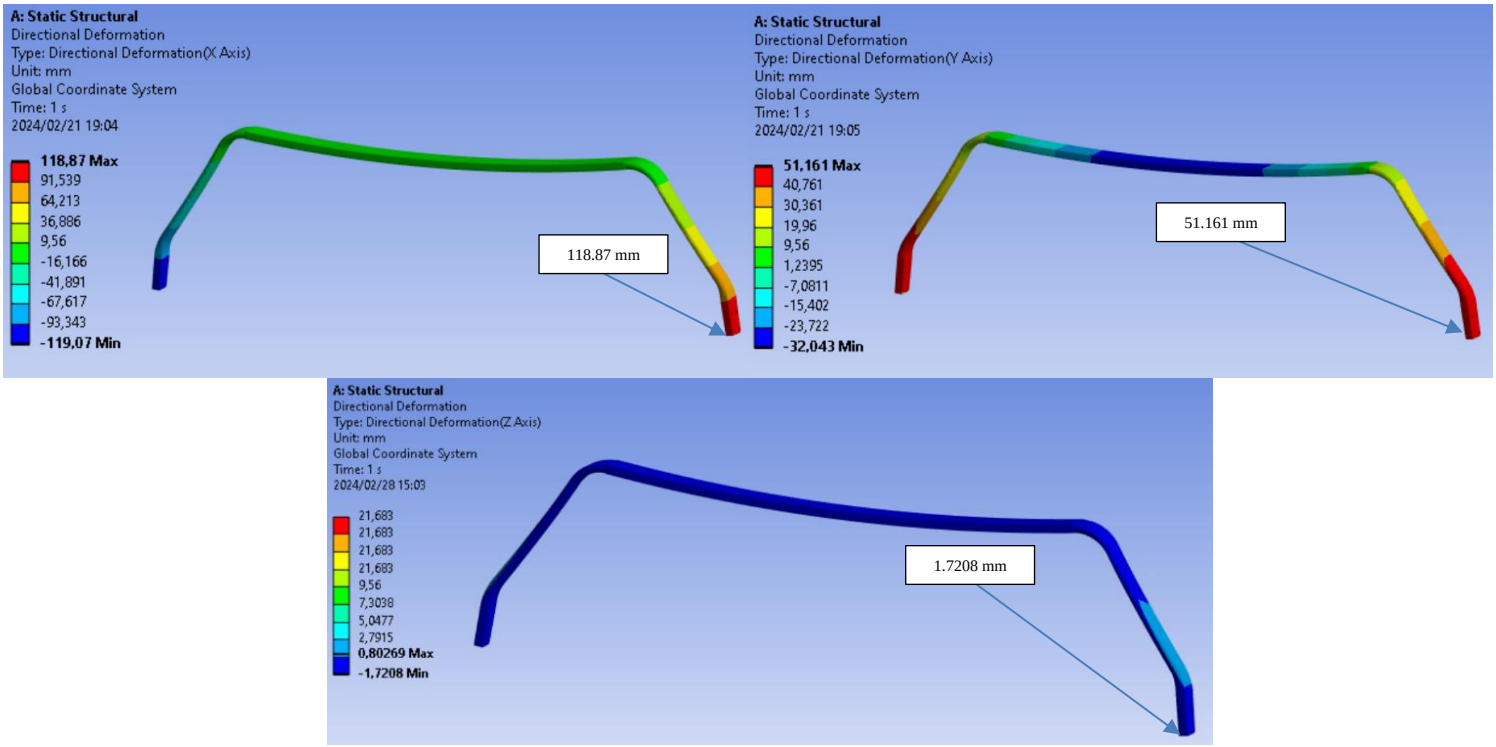


*Figure 62: Aluminium Landing Gear Level Landing (Nose Wheel Clear) Limit Load FEA X, Y, Z Deformation Results (Tricycle)*

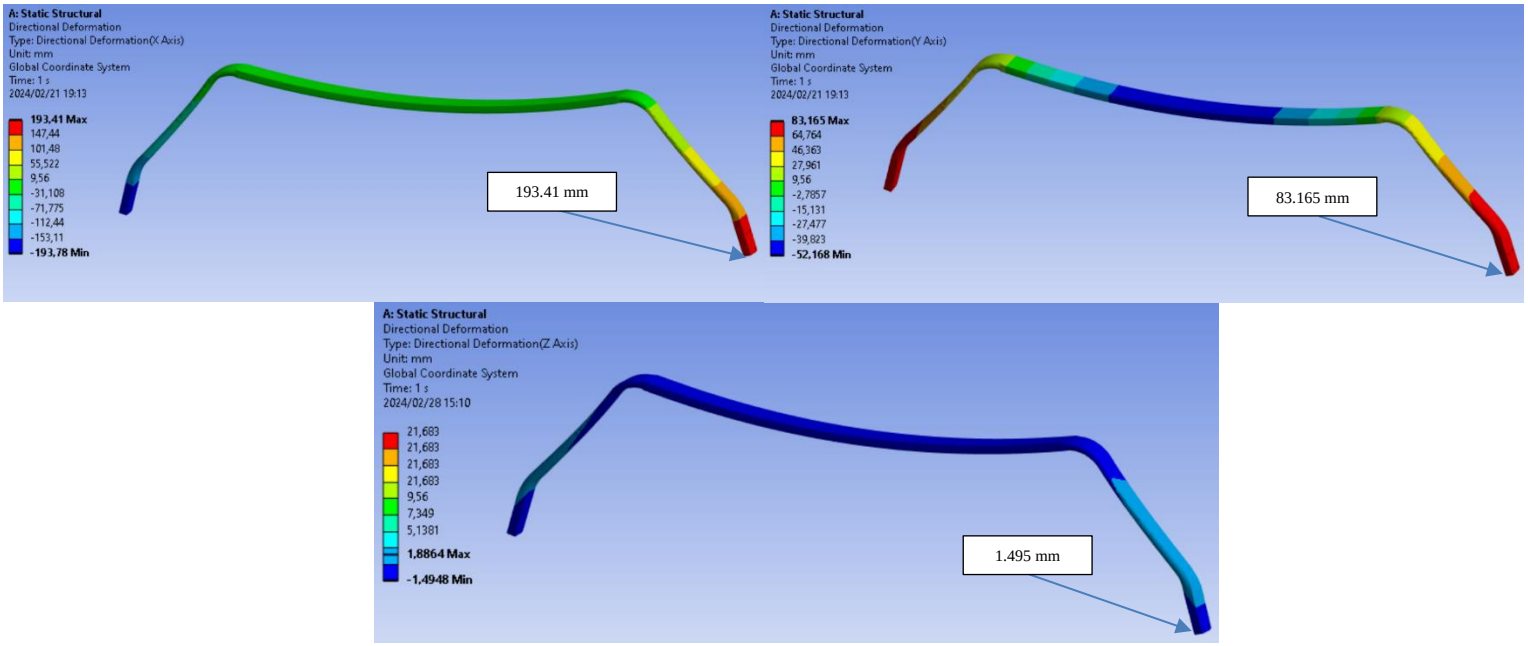


*Figure 63: Aluminium Landing Gear Level Landing (Nose Wheel Clear) Ultimate Load FEA X, Y, Z Deformation Results (Tricycle)*

During tricycle aircraft level landing with nose wheel just clear of ground for the limit load condition the stress on the surface of the main gear was 352.53 MPa. The stress throughout the gear was approximately 274.19 MPa resulting in a yield safety factor of 1.751. For ultimate load conditions the stress on the surface of the gear was 578.02 MPa. The stress throughout the gear was approximately 449.57 MPa resulting in an ultimate safety factor of 1.201.

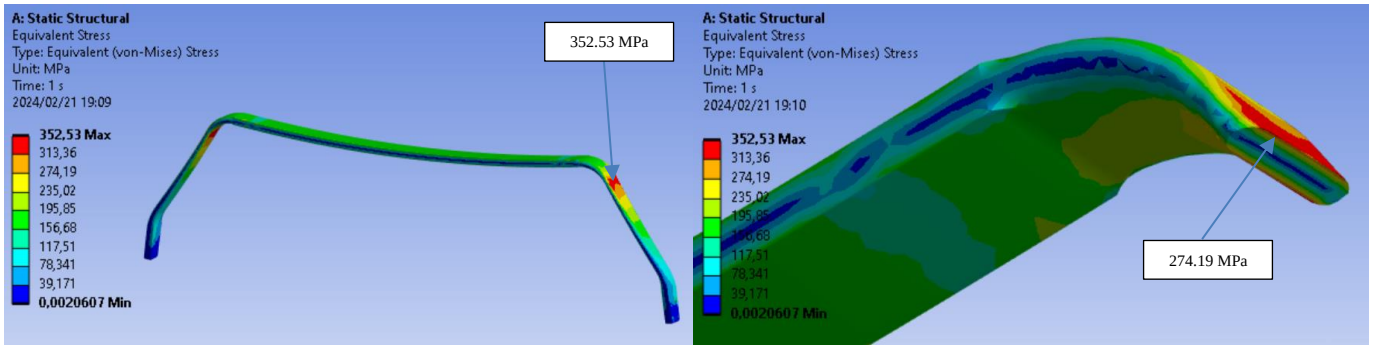


*Figure 64: Aluminium Landing Gear Level Landing (Nose Wheel Clear) Limit Load FEA Stress Results (Tricycle)*

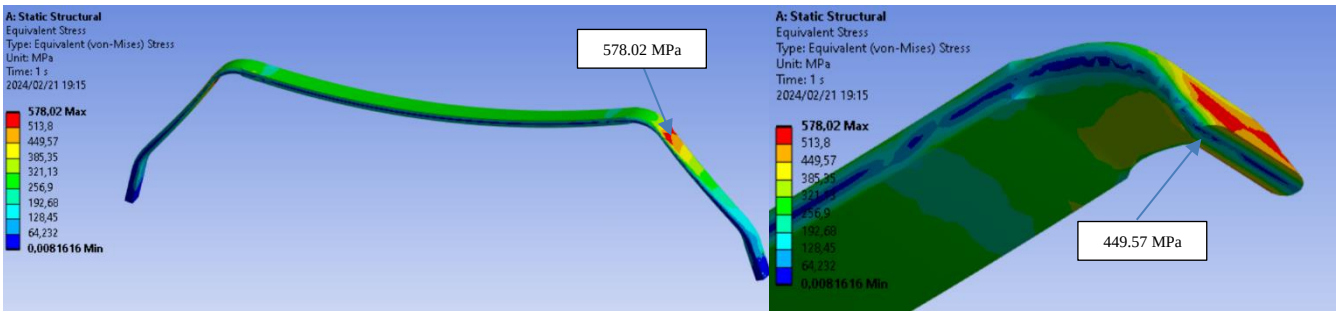


*Figure 65: Aluminium Landing Gear Level Landing (Nose Wheel Clear) Ultimate Load FEA Stress Results (Tricycle)*

Figure 66 provides the equivalent elastic strain for limit load and ultimate load conditions during tricycle aircraft level landing with nose wheel just clear of ground.

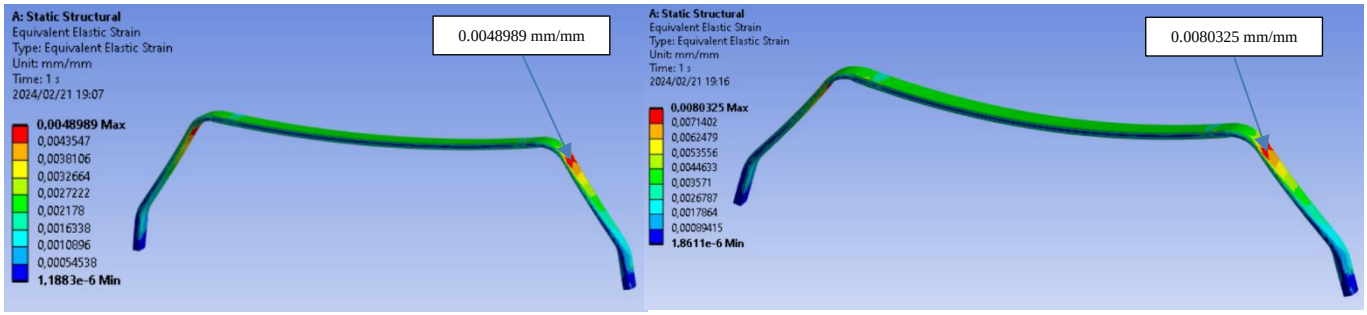


*Figure 66: Aluminium Landing Gear Level Landing (Nose Wheel Clear) Limit and Ultimate Load FEA Strain Results (Tricycle)*

In conclusion, during level landing with nose wheel just clear of ground for the tricycle aircraft at limit load conditions, the X, Y and Z deformations were 118.87 mm, 51.161 mm and, 1.721 mm respectively. The stress on landing gear was approximately 274.14 MPa resulting in a yield strength safety factor of 1.751 whilst the strain on the gear was 0.00490 mm/mm. At ultimate load conditions the X, Y and Z deformations were 193.41 mm, 83.165 mm and, 1.495 mm respectively. The stress on the landing gear was approximately 449.57 MPa resulting in an ultimate strength safety factor of 1.201 whilst the strain on the gear was 0.0080325 mm/mm.

### 9.2.2.3 Tricycle Tail Down Landing (Stall Attitude)

The landing gear was subjected to main wheel ground reaction loads of 8436.6 N during limit load conditions and 13734 N during ultimate load conditions. There were no frictional loads on the main wheels according to ASTM standards. It was assumed that the main landing gear would impact the runway at a maximum 14-degree angle for a tricycle aircraft tail down landing during stalling attitude conditions.

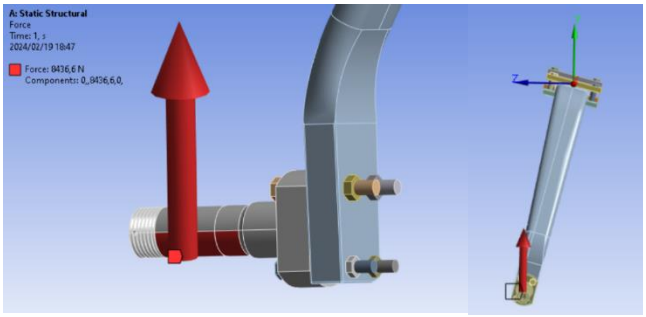


*Figure 67:Tricycle Level Landing (Stall Attitude) Aluminium Landing Gear Load Application (FEA)*

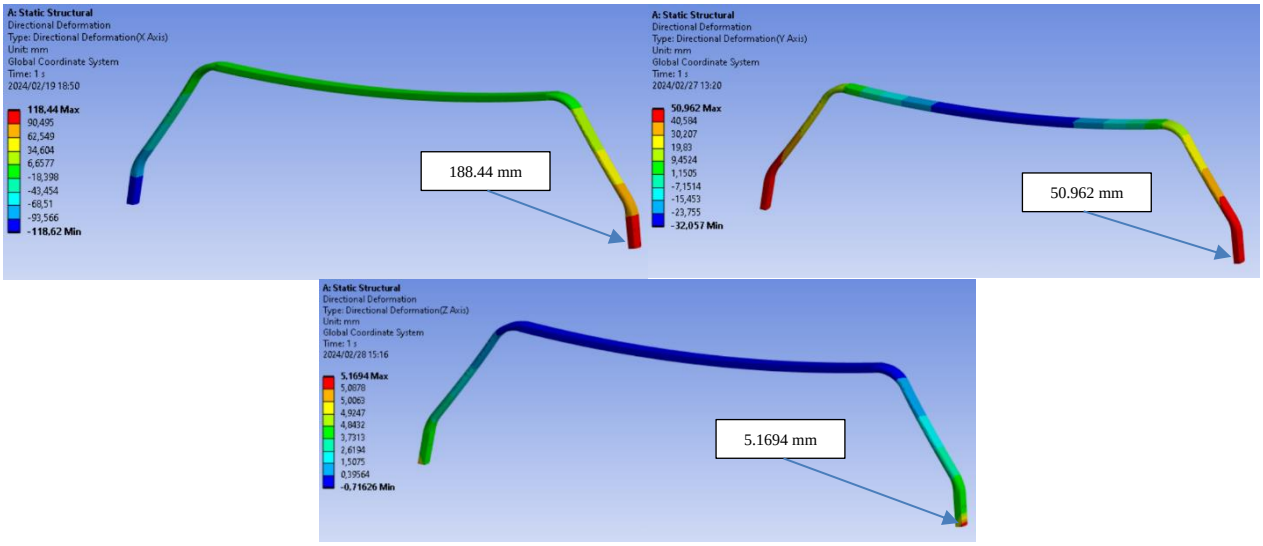


*Figure 68: Aluminium Landing Gear Level Landing (Stall Attitude) Limit Load FEA X, Y, Z Deformation Results (Tricycle*

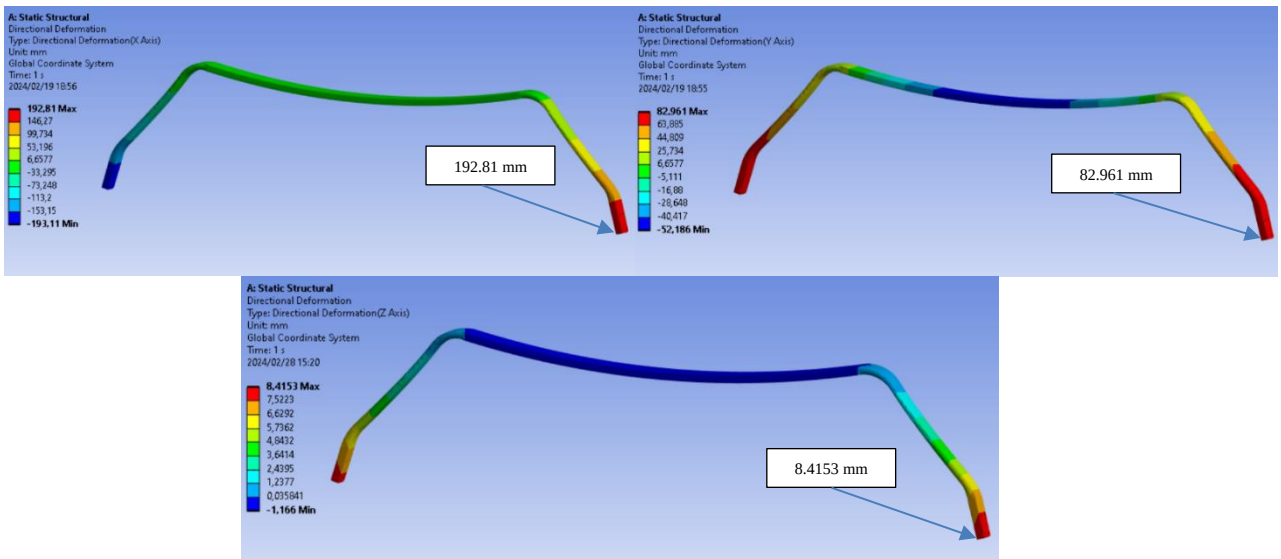


*Figure 69: Aluminium Landing Gear Level Landing (Stall Attitude) Ultimate Load FEA X, Y, Z Deformation Results (Tricycle)*

During tricycle aircraft level landing for stalling attitude conditions during limit load condition the stress on the surface of the main gear was 375.67 MPa. The stress throughout the gear was approximately 292.26 MPa resulting in a yield strength safety factor of 1.642. For ultimate load conditions the stress on the surface of the gear was 634.67 MPa. The stress throughout the gear was approximately 475.77 MPa resulting in an ultimate strength safety factor of 1.135.

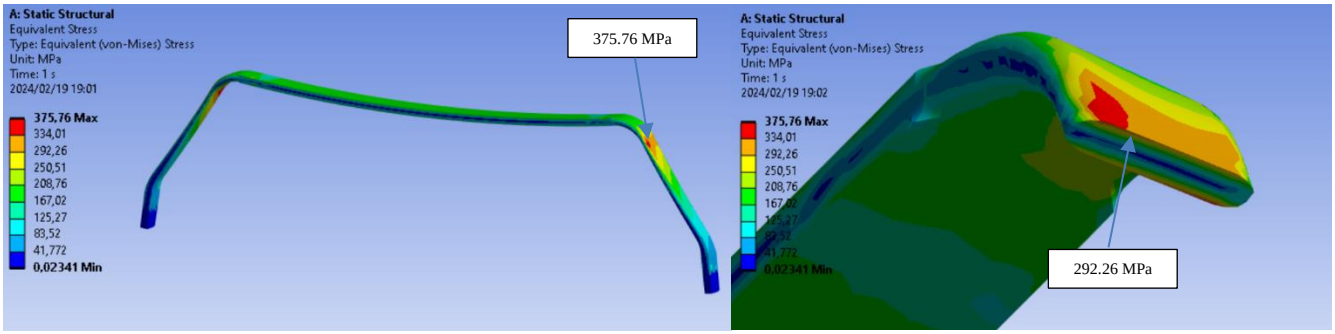


*Figure 70: Aluminium Landing Gear Level Landing (Stall Attitude) Limit Load FEA Stress Results (Tricycle)*

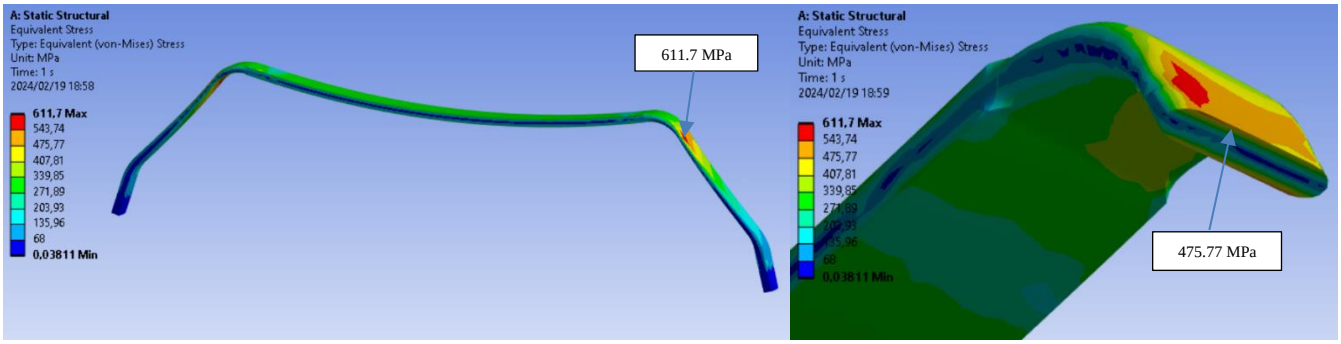


*Figure 71: Aluminium Landing Gear Level Landing (Stall Attitude) Ultimate Load FEA Stress Results (Tricycle)*

In Figure 72 the left image provides equivalent elastic strain for limit loads and right image for ultimate loads during tricycle aircraft stall attitude landing.

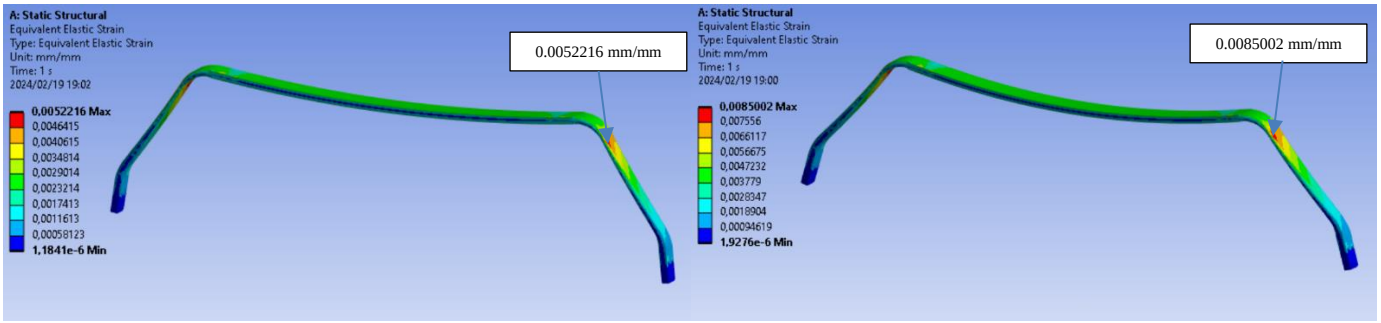


*Figure 72: Aluminium Landing Gear Level Landing (Stall Attitude) Limit and Ultimate Load FEA Strain Results (Tricycle)*

In conclusion, during (stall attitude) level landing for the tricycle aircraft at limit load conditions, the X, Y and Z deformations were 118.44 mm, 50.962 mm and, 5.169 mm respectively. The stress on landing gear was approximately 292.26 MPa resulting in a yield strength safety factor of 1.642 whilst the strain on the gear was 0.00522 mm/mm. At ultimate load conditions the X, Y and Z deformations were 192.81 mm, 82.961 mm and, 8.415 mm respectively. The stress on the landing gear was approximately 475.77 MPa resulting in an ultimate strength safety factor of 1.135 whilst the strain on the gear was 0.0085002 mm/mm.

### 9.2.3 Side Load and Braked Roll

#### 9.2.3.1 Taildragger and Tricycle Side Loads

During side load landing condition at a maximum aircraft take-off weight of 600 kg, the landing gear was subjected to main wheel ground reaction loads of 3943.62 N. The inboard frictional load was 2943 N resulting in torque loads of 373.761 Nm whilst the outboard frictional load was 1942.38 N resulting in a torque load of 246.682 Nm. It was assumed that the landing gear impacts the runway at a 90-degree angle. See Figure 4, for representation of side load condition.

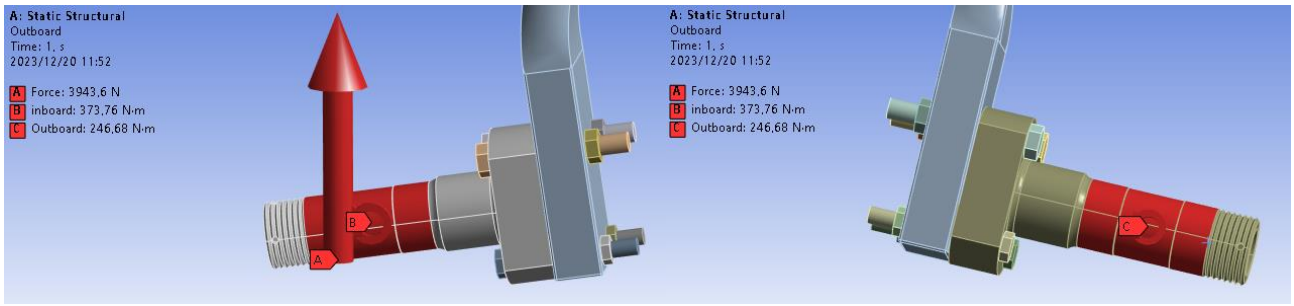


*Figure 73: Aluminium Landing Gear Side Loads FEA Load Application*

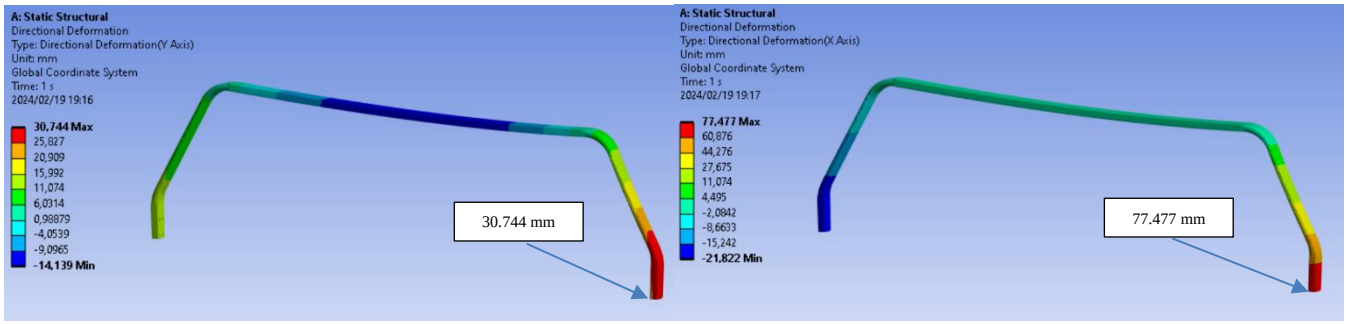


*Figure 74: Aluminium Landing Gear Side Load FEA Stress Results*

As seen in Figure 75, during side load conditions when landing with a MTOW of 600 kg, the stress experienced on the surface of the gear was 262.95 MPa. The stress experience throughout the main gear was approximately 204.55 MPa which results in a yield strength safety factor of 2.347.

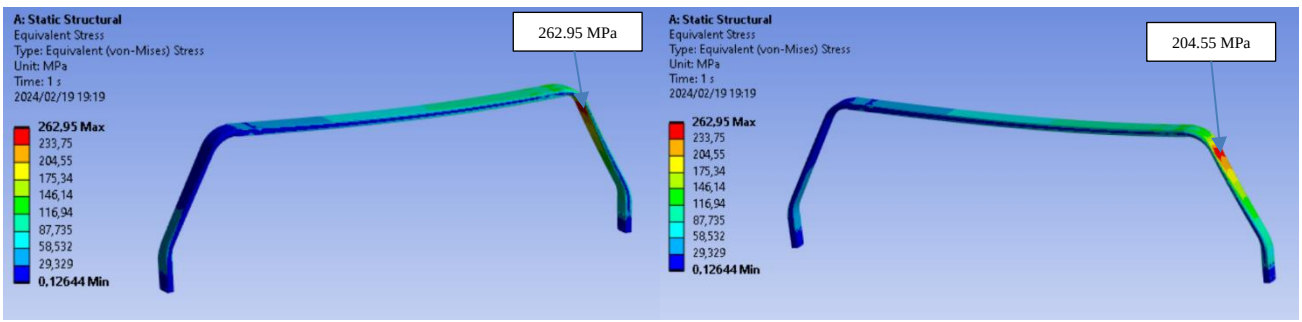


*Figure 75: Aluminium Landing Gear Side Loads FEA Deformation Results*

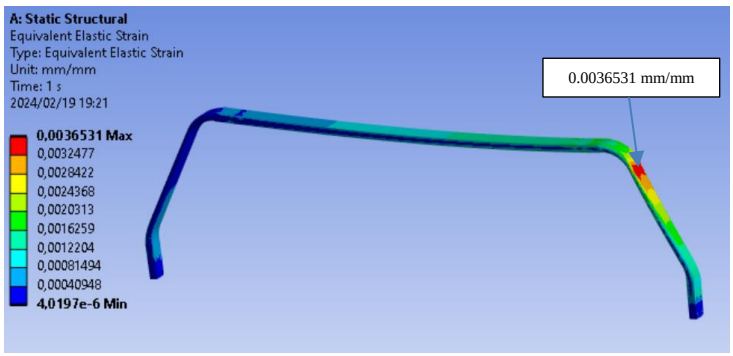


*Figure 76: Aluminium Landing Gear Side Loads FEA Strain Results*

In conclusion, during side load landing for the taildragger and tricycle aircraft at MTOW of 600 kg, the X, Y and Z deformations were 77.477 mm, 30.744 mm and, 0 mm respectively. The stress on landing gear was approximately 204.55 MPa resulting in a yield strength safety factor of 2.347 whilst the strain on the gear was 0.00365 mm/mm.

### 9.2.3.2 Taildragger and Tricycle Braked Roll Loads

During side load landing condition, the landing gear was subjected to main wheel ground reaction loads of 3943.62 N. The rearward frictional loads on both tyres were 3178.44 N resulting in a torque load around both the stub axles of 246.682 Nm. It was assumed that the landing gear impacts the runway at a 90-degree angle.

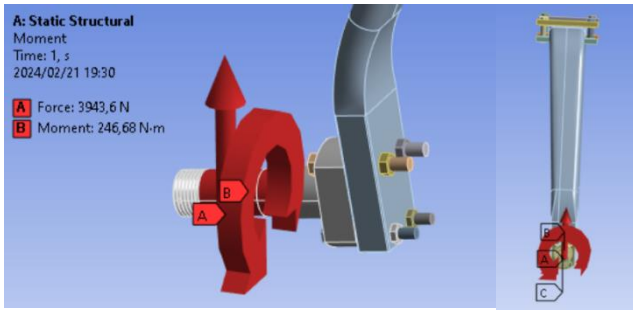


*Figure 77: Aluminium Landing Gear Braked Roll Loads FEA Load Application*

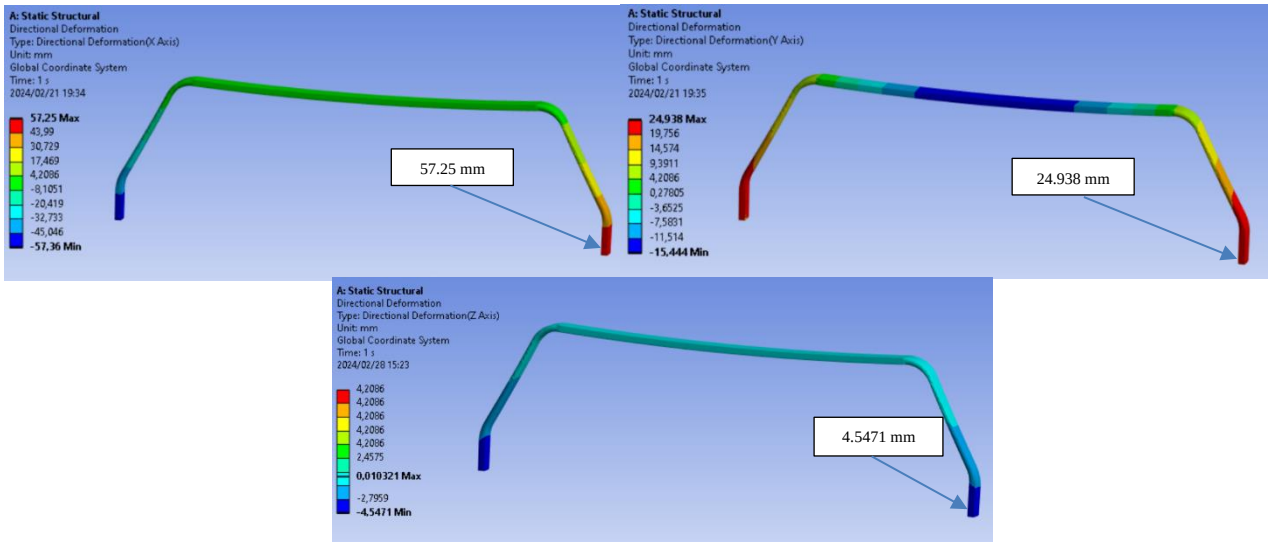


*Figure 78: Aluminium Landing Gear Braked Roll Loads FEA Deformation Results*

As seen in Figure 79, during side load conditions when landing with a MOTW of 600 kg, the stress experienced on the surface of the gear was 179.48 MPa. The stress experience throughout the main gear was approximately 139.6 MPa which resulting in a yield strength safety factor of 3.438.

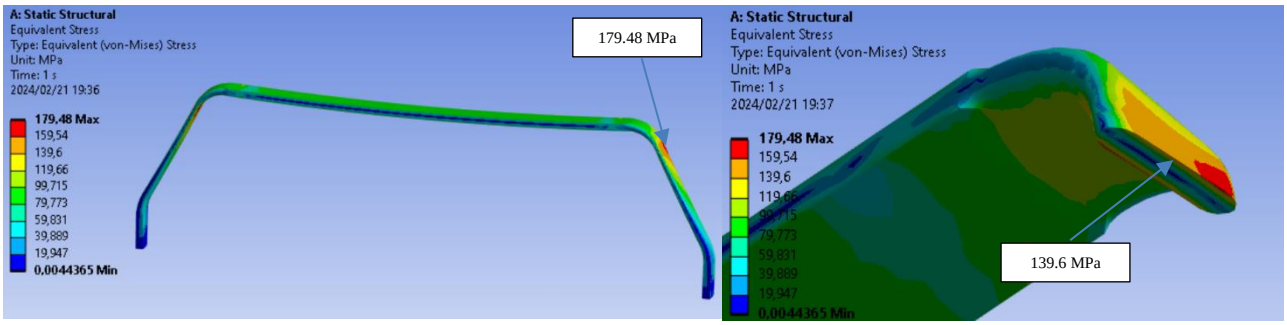


*Figure 79: Aluminium Landing Gear Landing Braked Roll Loads FEA Stress Results*

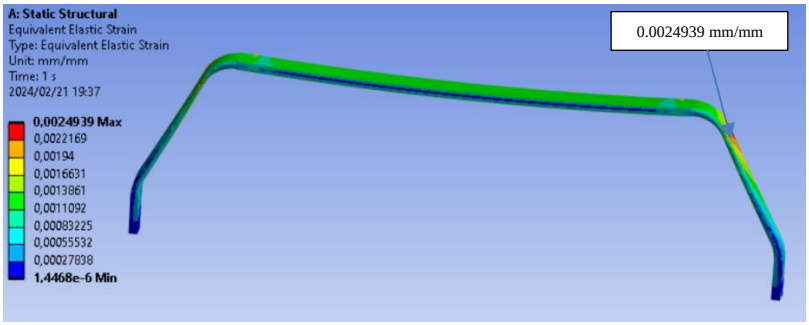


*Figure 80: Aluminium Landing Gear Braked Roll Loads FEA Strain Results*

In conclusion, during braked roll landing for the taildragger and tricycle aircraft at MTOW of 600 kg, the X, Y and Z deformations were 57.25 mm, 24.938 mm and, 4.547 mm respectively. The stress on landing gear was approximately 139.6 MPa resulting in a yield strength safety factor of 3.438 whilst the strain on the gear was 0.0024939 mm/mm.

### 9.3 Aluminium 7075 T6 Landing Conditions FEA Results

Table 25 and Table 26 provides a summary of all the FEA results obtained for the Aluminium 7075 T6 landing gear during limit and ultimate load conditions. The maximum stress occurred during a taildragger level landing and tricycle tail down landing (stall altitude) due to higher ground reaction loads. These two landing conditions should be further inspected when conducting physical tests to obtain a new composite design

*Table 25: Aluminium 7075T6 Landing Gear Limit Loads FEA Results*

| Landing Condition | x-deform | y-deform | z-deform | Stress | Strain | Yield SF | Ultimate SF |
|---|---|---|---|---|---|---|---|
| - | mm | mm | mm | MPa | mm/mm | - | - |
| **Taildragger Aircraft** | | | | | | | |
| Level Landing | 122.33 | 53.125 | 7.467 | 291.9 | 0.00521 | **1.644** | **1.850** |
| Tail Down Landing | 103.63 | 44.59 | 4.523 | 255.72 | 0.00457 | **1.877** | **2.392** |
| **Tricycle Aircraft** | | | | | | | |
| Level Landing (Inclined Reactions) | 59.437 | 25.582 | 0.860 | 137.1 | 0.00245 | **3.501** | **3.939** |
| Level Landing (Nose Clear) | 118.87 | 51.161 | 1.721 | 274.19 | 0.00490 | **1.751** | **1.969** |
| Tail Down Landing (Stall Attitude) | 118.44 | 50.962 | 5.169 | 292.26 | 0.00522 | **1.642** | **1.848** |
| **Additional Landing** | | | | | | | |
| Side Load | 77.477 | 30.744 | 0 | 204.55 | 0.00365 | **2.347** | **2.640** |
| Braked Roll | 57.25 | 24.938 | 4.547 | 139.6 | 0.00249 | **3.438** | **3.725** |

*Table 26: Aluminium 7075T6 Landing Gear Ultimate Loads FEA Results (Emergency Landing)*

| Landing Condition | x-deform | y-deform | z-deform | Stress | Strain | Yield SF | Ultimate SF |
|---|---|---|---|---|---|---|---|
| - | mm | mm | mm | MPa | mm/mm | - | - |
| **Taildragger Aircraft** | | | | | | | |
| Level Landing | 199.05 | 86.345 | 10.848 | 471.47 | 0.00842 | **1.018** | **1.145** |
| Tail Down Landing | 168.7 | 72.588 | 7.363 | 416.29 | 0.00744 | **1.153** | **1.393** |
| **Tricycle Aircraft** | | | | | | | |
| Level Landing (Inclined Reactions) | 96.715 | 41.581 | 0.747 | 224.79 | 0.00402 | **2.135** | **2.402** |
| Level Landing (Nose Clear) | 193.41 | 83.165 | 1.495 | 449.57 | 0.008033 | **1.068** | **1.201** |
| Tail Down Landing (Stall Attitude) | 192.81 | 82.961 | 8.415 | 475.77 | 0.00850 | **0.991** | **1.135** |
| **Additional Landing** | | | | | | | |
| Side Load | 77.477 | 30.744 | 0 | 204.55 | 0.00365 | **2.347** | **2.640** |
| Braked Roll | 57.25 | 24.938 | 4.547 | 139.6 | 0.00249 | **3.438** | **3.725** |

# 10 COUPON STUDY

## 10.2 Introduction

In this section coupons consisting of (wet layup and prepreg) epoxy e-glass fibres were compared to an Aluminium 7075 T6 coupon under tension, compression, bending and torsion. With regards to manufacturing the main undercarriage, different combinations of fibre orientations could also be used to provide information on the desired stack-up sequence based on loads experienced during landing. The analytical calculations were also compared to the FEA results using classical lamination theory to ensure that the FEA results obtained were correct.

## 10.3 Coupon Setup

All coupons will have the dimensions of 250×25×4 mm. The composite coupons have 3 different layups such as [0/90/90/0, 0/45/45/0, and 0/90/45/0] and a mesh element size of 2 mm was used during FEA analysis. The coupon load application is as follows: 5000 N for tensile and compressive loads, -18750 N.mm for bending and 5000 N.mm for torsion on the coupons. These loads were specifically chosen to reach the maximum stress and strain limits of epoxy e-glass fibres during tension, compression, bending and, torsion before failure.

## 10.4 Coupon Material Specification

Table 27 and Table 28 provides the material specifications for unidirectional epoxy e-glass (prepreg) and unidirectional and epoxy e-glass (wet). The material data was taken from Ansys material library. The material specifications for Aluminium 7075 T6 can be found in Table 20.

*Table 27: Epoxy E-Glass UD Prepreg Material Specification in Ansys*

| | | |
|---|---|---|
| Density | 2000 | kg m^-3 |
| Orthotropic Elasticity | | |
| Young's Modulus X direction | 45000 | MPa |
| Young's Modulus Y direction | 10000 | MPa |
| Young's Modulus Z direction | 10000 | MPa |
| Poisson's Ratio XY | 0,3 | |
| Poisson's Ratio YZ | 0,4 | |
| Poisson's Ratio XZ | 0,3 | |
| Shear Modulus XY | 5000 | MPa |
| Shear Modulus YZ | 3846,2 | MPa |
| Shear Modulus XZ | 5000 | MPa |
| Orthotropic Stress Limits | | |
| Tensile X direction | 1100 | MPa |
| Tensile Y direction | 35 | MPa |
| Tensile Z direction | 35 | MPa |
| Compressive X direction | -675 | MPa |
| Compressive Y direction | -120 | MPa |
| Compressive Z direction | -120 | MPa |
| Shear XY | 80 | MPa |
| Shear YZ | 46,154 | MPa |
| Shear XZ | 80 | MPa |
| Orthotropic Strain Limits | | |
| Tensile X direction | 0,0244 | |
| Tensile Y direction | 0,0035 | |
| Tensile Z direction | 0,0035 | |
| Compressive X direction | -0,015 | |
| Compressive Y direction | -0,012 | |
| Compressive Z direction | -0,012 | |
| Shear XY | 0,016 | |
| Shear YZ | 0,012 | |
| Shear XZ | 0,016 | |

*Table 28: Epoxy E-Glass UD Wet Layup Material Specification in Ansys*

| | | |
|---|---|---|
| Density | 1850 | kg m^-3 |
| Orthotropic Secant Coefficient of Thermal Expansion | | |
| Orthotropic Elasticity | | |
| Young's Modulus X direction | 35000 | MPa |
| Young's Modulus Y direction | 9000 | MPa |
| Young's Modulus Z direction | 9000 | MPa |
| Poisson's Ratio XY | 0,28 | |
| Poisson's Ratio YZ | 0,4 | |
| Poisson's Ratio XZ | 0,28 | |
| Shear Modulus XY | 4700 | MPa |
| Shear Modulus YZ | 3500 | MPa |
| Shear Modulus XZ | 4700 | MPa |
| Orthotropic Stress Limits | | |
| Tensile X direction | 780 | MPa |
| Tensile Y direction | 31 | MPa |
| Tensile Z direction | 31 | MPa |
| Compressive X direction | -480 | MPa |
| Compressive Y direction | -100 | MPa |
| Compressive Z direction | -100 | MPa |
| Shear XY | 60 | MPa |
| Shear YZ | 35 | MPa |
| Shear XZ | 60 | MPa |
| Orthotropic Strain Limits | | |
| Tensile X direction | 0,0244 | |
| Tensile Y direction | 0,0038 | |
| Tensile Z direction | 0,0038 | |
| Compressive X direction | -0,015 | |
| Compressive Y direction | -0,0125 | |
| Compressive Z direction | -0,0125 | |
| Shear XY | 0,015 | |
| Shear YZ | 0,012 | |
| Shear XZ | 0,015 | |

The weight comparison between the Aluminium 7075 T6 coupon, epoxy e-glass wet layup and epoxy e-glass prepreg shown in Figure 81. Epoxy e-glass wet layups typically consist of a 50:50 percent weight ratio between the resin epoxy and fibres whilst the epoxy e-glass prepregs consist of a 35:65 resin epoxy to fibre weight ratio percentage. The epoxy e-glass prepreg was determined to be approximately 28% lighter and the epoxy e-glass wet layup approximately 34% lighter than Aluminium 7075 T6 coupon. The stress, strain and safety factors were analysed for different fibre orientations for both the wet layup and prepreg to conclude a final decision for a composite alternative.

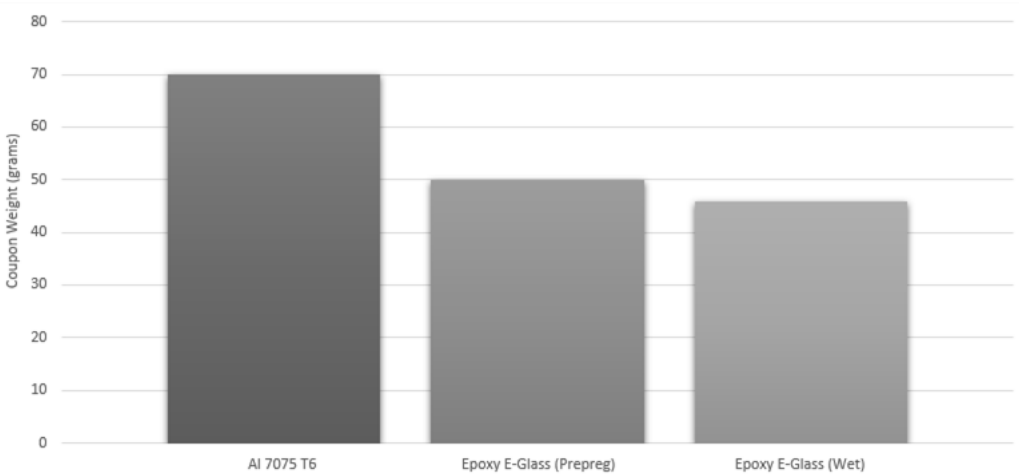


*Figure 81: Coupons Specimen Weight Comparison*

## 10.5 Aluminium 7075 T6 Calculation Theory and Load Application

In this section the method and theory are provided for the stress, strain, and safety factor calculations which was used to validate the Aluminium 7075 T6 coupon FEA analysis. The load applications seen from Figure 82 to Figure 84 was also used during the composite coupon analysis.

1) **Aluminium 7075 T6 Coupon Tensile and Compressive Load**:

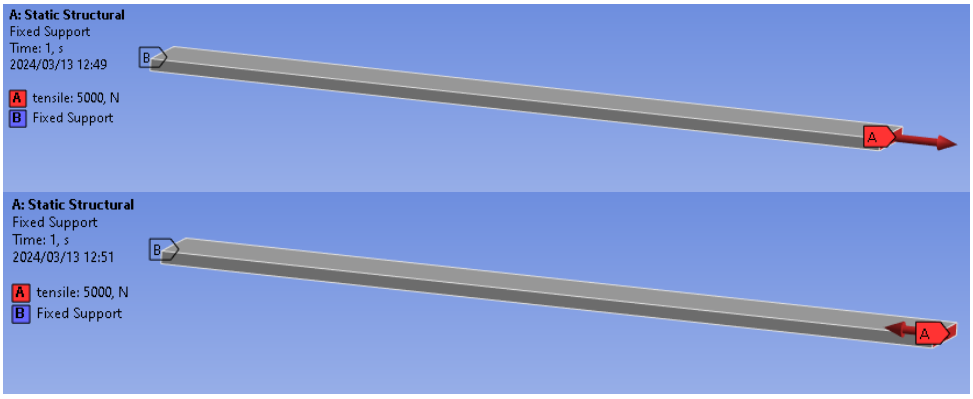


*Figure 82: Coupons Tensile and Compressive Load Application*

$$\sigma_{tensile/compressive} = \frac{F_{tensile/compressive}}{A} \tag{22}$$

Where:

$\sigma_{tensile/compressive}$ = Tensile/ compressive stress ($MPa$)
$F_{tensile/compressive}$ = Tensile/ compressive force ($N$)
$A$ = Area of load application ($mm^2$)

$$\varepsilon_{tensile/compressive} = \frac{\sigma_{tensile/compressive}}{E} \tag{23}$$

Where:

$\varepsilon_{tensile/compressive}$ = Tensile/ compressive strain ($mm/mm$)
$E$ = Young's modulus ($MPa$)

2) **Aluminium 7075 T6 Beam Bending Load**:

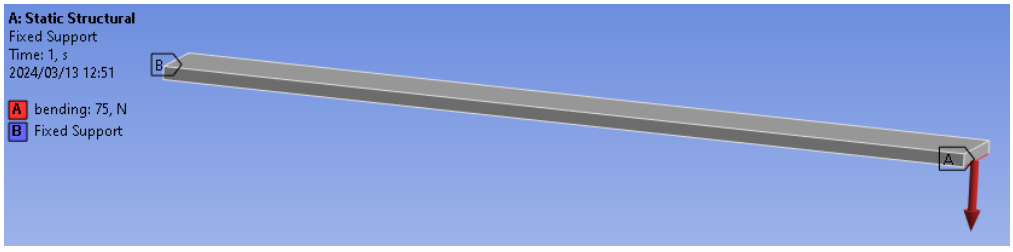


*Figure 83: Coupons Bending Load Application*

$$M_{bending} = F_{bending} L \tag{24}$$

Where:

$M_{bending}$ = Bending moment $(N.mm)$
$F_{bending}$ = Applied bending force $(N)$
$L$ = Length of coupon $(mm)$

$$\sigma_{bending} = \frac{M_{bending} c}{I} \tag{25}$$

Where:

$\sigma_{bending}$ = Bending stress $(MPa)$
$c$ = Distance from neutral axis to outermost fibre $(mm)$
$I$ = Moment of inertia $(mm^4)$

$$\varepsilon_{bending} = \frac{\sigma_{bending}}{E} \tag{26}$$

Where:

$\varepsilon_{bending}$ = Bending strain $(mm/mm)$

### 3) Aluminium 7075 T6 Beam Torsion:

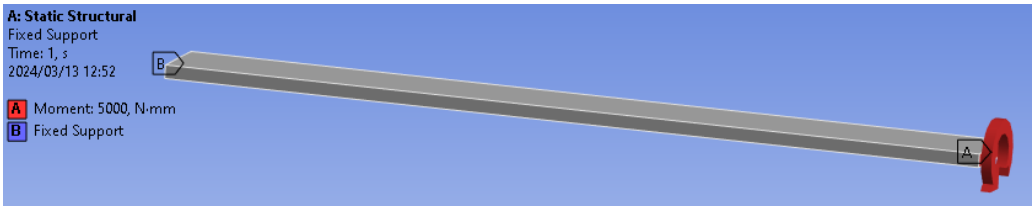


*Figure 84: Coupons Torsional Load Application*

$$\tau_{torsion} = \frac{T}{C_1 a b^2} \qquad \frac{a}{b} = 0{,}16 \; gives \; C_1 = 0{,}028 \tag{27}$$

Where:

$\tau_{torsion}$ = Torsional stress $(MPa)$
$T$ = Torsional moment $(N.mm)$
$C_1$ = 1st value obtained through $^{a}/_{b}$ ratio, refer to equation 17 to obtain values for $C_1$ (-)
$a$ = Coupons thickness $(mm)$
$b$ = Coupon width $(mm)$

$$\varepsilon_{torsion} = \frac{\tau_{torsion}}{E} \tag{28}$$

Where:

$\varepsilon_{torsion}$ = Torsional strain $(mm/mm)$

### 10.6 Aluminium 7075 T6 Coupon

The following analysis is used as a reference example that was compared to both the epoxy e-glass wet layup and epoxy e-glass prepreg coupons in section 10.7.

### 10.6.2 Aluminium 7075 T6 Coupon FEA Results

In Figure 85 the stress and strain on the coupons were 49.875 MPa and 0.0006927 mm/mm respectively during a 5000 N tensile load.

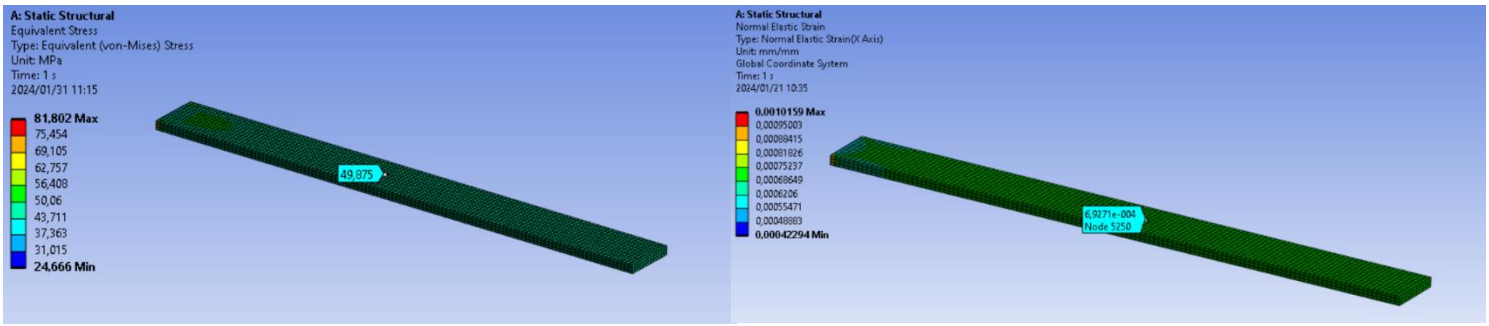


*Figure 85: Aluminium 7075 T6 Coupon, Stress and Strain (Tension)*

In Figure 86 the stress and strain on the coupons were -49.875 MPa and -0.0006927 mm/mm respectively during a 5000 N compressive load.

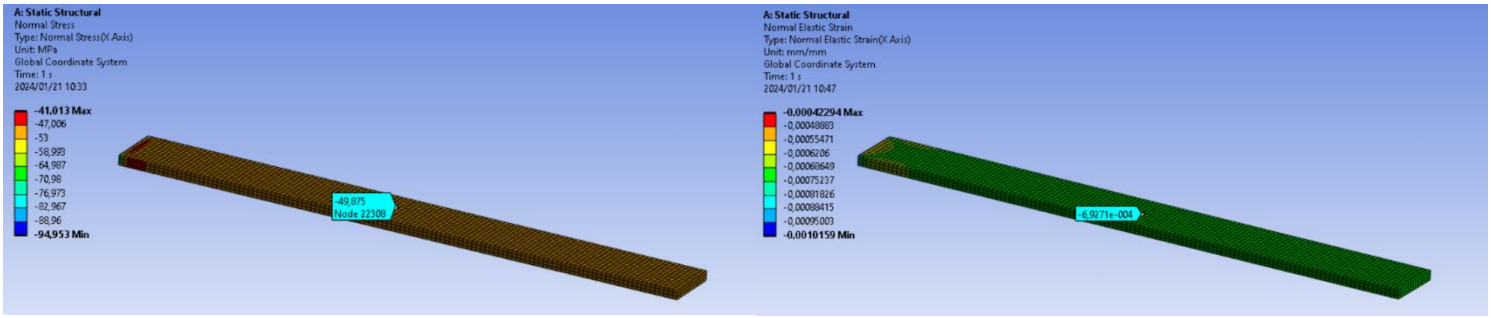


*Figure 86: Aluminium 7075 T6 Coupon Stress and Strain (Compression)*

Figure 87 provides the results for the Aluminium 7075 T6 coupon under -75 N bending load resulting in an 18750 N.mm moment around the fixed support on the opposite end. The stress and strain on the coupons were-141.05 MPa and 0.0019434 mm/mm respectively.

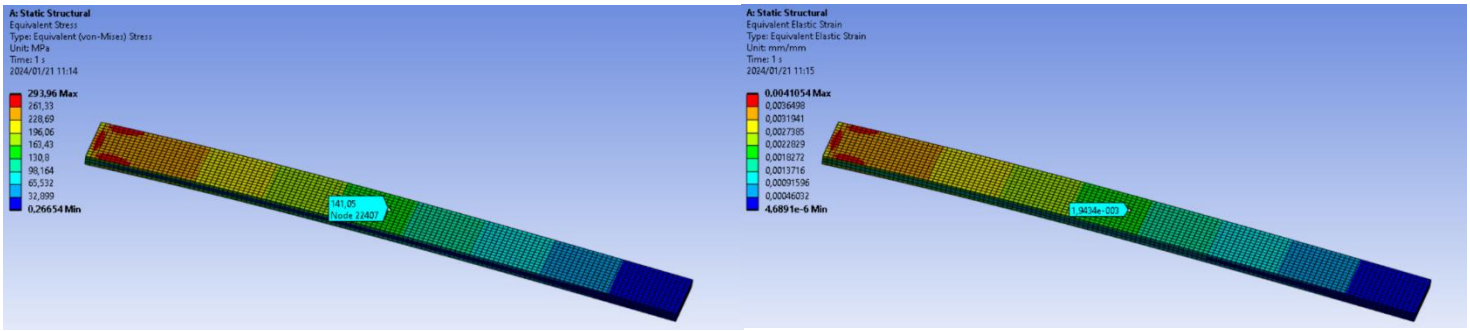


*Figure 87: Aluminium 7075 T6 Coupon Stress and Strain (Beam Bending)*

Figure 88 provides the results for the Aluminium 7075 T6 coupon under 5000 N.mm torsional load. The stress and strain on the coupons were 71.882 MPa and 0.00099836 mm/mm respectively.

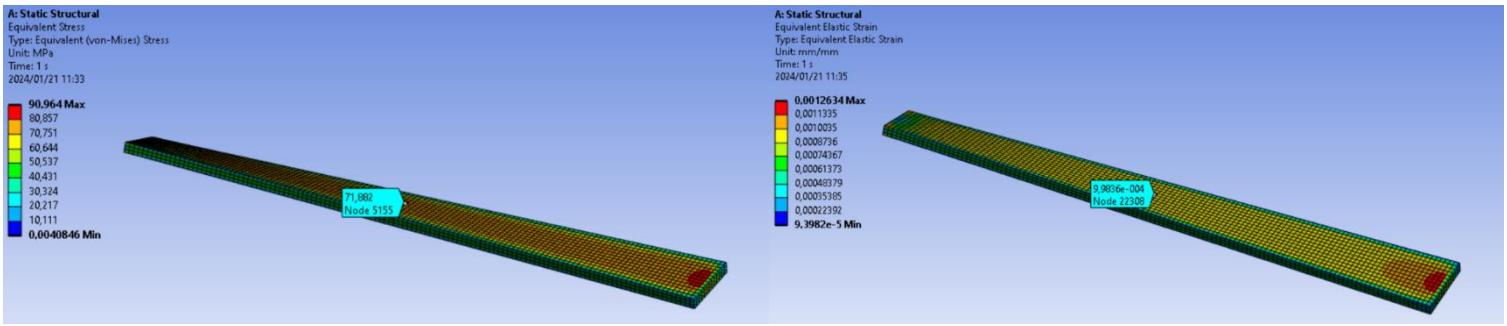


*Figure 88: Aluminium 7075 T6 Coupon Stress and Strain (Beam Torsion)*

Table 29, provide the FEA results, hand calculations and percentage error results for the Aluminium 7075 T6 coupon under tension, compression, bending, and torsion.

*Table 29: Aluminium 7075 T6 and Epoxy E-Glass Coupon Analysis Results*

| **Load Type** | **Stress (FEA)** | **Stress (Analytical)** | **Strain (FEA)** | **Strain (Analytical)** | **Yield Safety Factor** |
|---|---|---|---|---|---|
| **-** | **MPa** | **MPa** | **mm/mm** | **mm/mm** | **-** |
| **Tension** | 49.875 | 50<br>0.25 % | 0.0006927 | 0.0006944<br>0,24 % | 9.624 |
| **Compression** | -49.875 | -50<br>0.25 % | -0.0006927 | -0.0006944<br>0,24 % | 9.624 |
| **Bending** | 141.05 | 140.625<br>0.3 % | 0.009434 | 0.009531<br>1,02 % | 3.403 |
| **Torsion** | 71.882 | 71.685<br>0.274 % | 0.0099836 | 0.0099562<br>0.275 % | 6.678 |

In conclusion, from FEA results obtained in Table 29, the Aluminium 7075 T6 alloy coupon had the highest yield strength safety factors for tension and compression loads whereas being the weakest during bending loads. The coupon experienced the least strain during tension and compression loads whilst experiencing the most strain during torsional load conditions.

## 10.7 Composite Matrix Calculation (Classical Lamination Theory)

In this section the method and theory are provided for composite matrix calculations which was used to validate the epoxy e-glass (prepreg and wet layup) FEA analysis.

Equation 30 is referred to the Reduced Stiffness (or Constitutive) matrix. This matrix was used since it formed the basis for all subsequent laminate stress analysis, and was the first step taken once the elastic constants were known. Note that $[Q]$ can be different for each layer in the laminate. Thus, while the strain variation through the laminate was linear, the stress variations were not necessarily so [9].

$$[Q] = \begin{bmatrix} Q_{11} & Q_{12} & 0 \\ Q_{12} & Q_{22} & 0 \\ 0 & 0 & Q_{66} \end{bmatrix} \tag{30}$$

The following equations was used to find the elastic constants of the composite. The find the values used in equation 31 to equation 35, the refer to Table 27 or Table 28 depending on wet layup or prepreg calculation.

$$Q_{11} = \frac{E_1}{1-v_{12}v_{21}} \tag{31}$$

$$Q_{12} = \frac{v_{12}E_2}{1-v_{12}v_{21}} \tag{32}$$

$$Q_{22} = \frac{E_2}{1-v_{12}v_{21}} \tag{33}$$

$$Q_{66} = G_{12} \tag{34}$$

$$v_{21} = \frac{E_1}{E_1}v_{12} \tag{35}$$

Table 30 provides the coupon fibre orientations used in the transformation matrices $[T]^1$ and $[T]^{-1}$ to find the transformed reduced stiffness matrix $[\bar{Q}]$.

*Table 30: Coupons Fibre Orientations for Composite Matrix Calculations*

| Fibre Layer | Fibre Orientations (Degrees) | | |
|---|---|---|---|
| (-) | Coupon 1 | Coupon 2 | Coupon 3 |
| 1 | 0 | 0 | 0 |
| 2 | 90 | 45 | 90 |
| 3 | 90 | 45 | 45 |
| 4 | 0 | 0 | 0 |

As seen in Figure 89, consider the fibre layer at an angle $\theta$ to the reference axis. This angle was used in the transformation matrices to obtain the transformed reduced stiffness matrix for each fibre layer as shown by equation 36.

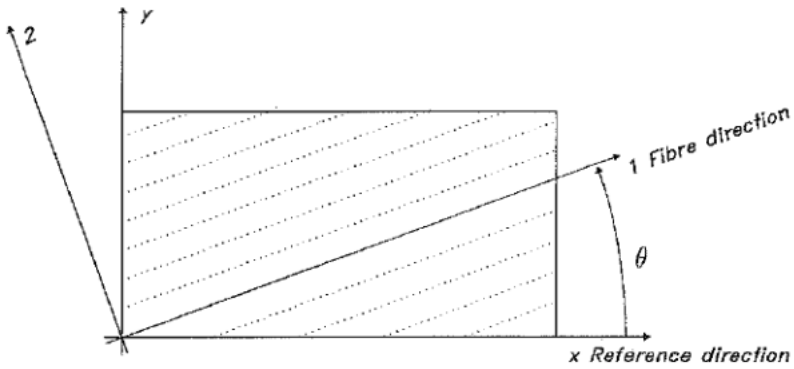


*Figure 89: Unidirectional Material at an Angle to Reference Axis [9]*

Equation 36 was used to find the transformed reduced stiffness matrix for each individual fibre layer 1 to fibre layer 4. The transformation matrices and Reuter's matrices were also used.

$$[\bar{Q}]_{1\ to\ 4} = [T]^{-1}[Q][R][T]^{1}[R]^{-1} \tag{36}$$

Transformation matrices:

$$[T]^{1} = \begin{bmatrix} \cos^2\theta & \sin^2\theta & 2sin\theta cos\theta \\ \sin^2\theta & \cos^2\theta & -2sin\theta cos\theta \\ -sin\theta cos\theta & sin\theta cos\theta & \cos^2\theta - \sin^2\theta \end{bmatrix} \tag{37}$$

$$[T]^{-1} = \begin{bmatrix} \cos^2\theta & \sin^2\theta & -2sin\theta cos\theta \\ \sin^2\theta & \cos^2\theta & 2sin\theta cos\theta \\ sin\theta cos\theta & -sin\theta cos\theta & \cos^2\theta - \sin^2\theta \end{bmatrix} \tag{38}$$

Reuter's matrices:

$$[R]^{1} = \begin{bmatrix} 1 & 0 & 0 \\ 0 & 1 & 0 \\ 0 & 0 & 2 \end{bmatrix} \tag{39}$$

$$[R]^{-1} = \begin{bmatrix} 1 & 0 & 0 \\ 0 & 1 & 0 \\ 0 & 0 & 0.5 \end{bmatrix} \tag{40}$$

Once the transformed reduced stiffness matrices were obtained for each fibre layer the following $[A]$, $[B]$ and, $[D]$ matrices were obtained.

In Figure 90 the through thickness visualization is provided for the coupons. The thickness provided in Figure 90 was used to obtain matrices $[A]$, $[B]$ and $[D]$.

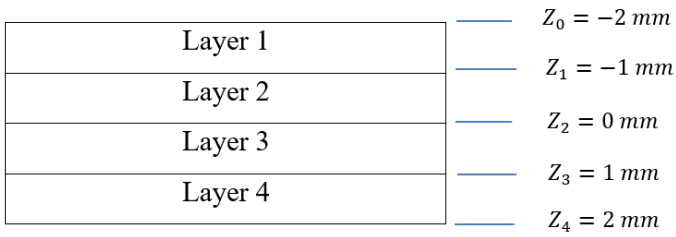


*Figure 90: Coupon Through Thickness Visualization*

The $[A]$ matrix relates in-plane forces directly with in-plane strains and is referred to as the extensional stiffness matrix.

- $A_{11}$, $A_{22}$ and $A_{66}$ relates to a force resultant in a particular direction with a strain in the same direction [9].

- $A_{12}$ is the Poisson's ratio term and relates forces in one direction with strains perpendicular to the force direction [9].

- $A_{16}$ and $A_{26}$ are the in-plane coupling terms which relates the axial forces to shear strains and vice versa. These terms imply that under an axial force, shear will develop in addition to the axial and Poisson's strain [9]. Where the Poisson's term couples axial forces with transverse strains, $A_{16}$ and $A_{26}$ couples axial forces with shear strains [9]. These terms can be eliminated by making the matrix balanced meaning that for every $+\theta$ layer there is a $-\theta$ layer.

$$[A] = \begin{bmatrix} A_{11} & A_{12} & A_{16} \\ A_{12} & A_{22} & A_{26} \\ A_{16} & A_{26} & A_{66} \end{bmatrix} \tag{41}$$

To obtain the $[A]$ matrix equation 43 was used:

$$\left[A_{iy}\right] = \Sigma_{k=1}^{N}\left[\bar{Q}_{iy}\right]_k (z_k - Z_{k-1}) \tag{42}$$

$$[A] = [\bar{Q}]_1(z_1 - z_0) + [\bar{Q}]_2(z_2 - z_1) + [\bar{Q}]_3(z_3 - z_2) + [\bar{Q}]_4(z_4 - z_3) \tag{43}$$

The $[B]$ matrix is referred to as the coupling matrix. It relates the in-plane forces with curvatures and moments with in-plane strains.

- $B_{11}$, $B_{22}$ and $B_{66}$ couples in-plane forces with the curvatures in the same direction [9].
- $B_{12}$ couples the in-plane forces with curvatures in a direction perpendicular to the force [9].
- $B_{16}$ and $B_{26}$ couple axial in-plane forces with twisting curvatures/ twisting moments with in-plane strains.

$$[B] = \begin{bmatrix} B_{11} & B_{12} & B_{16} \\ B_{12} & B_{22} & B_{26} \\ B_{16} & B_{26} & B_{66} \end{bmatrix} \tag{44}$$

It is important to note that the $[B]$ matrix can be eliminated by ensuring that the laminate is symmetric about its mid-plane meaning that the one half of the laminate should mirror the other half.

To obtain the $[B]$ matrix equation 46 was used:

$$\left[B_{iy}\right] = 0.5\left(\sum_{k=1}^{N}\left[\bar{Q}_{iy}\right]_k (z_k - Z_{k-1})\right) \tag{45}$$

$$[B] = 0.5[\bar{Q}]_1(z_1 - z_0) + 0.5[\bar{Q}]_2(z_2 - z_1) + 0.5[\bar{Q}]_3(z_3 - z_2) + 0.5[\bar{Q}]_4(z_4 - z_3) \tag{46}$$

The $[D]$ matrix is referred to as the bending of flexural stiffness matrix and relates moments directly to curvatures.

- $D_{11}$, $D_{22}$ and $D_{66}$ are the direct flexural stiffness terms which relates the bending moments with the curvatures in the same directions [9].
- $D_{12}$ is a Poisson's type term for bending which relates a moment in one direction with curvatures in the perpendicular direction [9].
- $D_{16}$ and $D_{26}$ are referred to as the coupling terms relating the bending moments with twisting curvatures [9].

$$[D] = \begin{bmatrix} D_{11} & D_{12} & D_{16} \\ D_{12} & D_{22} & D_{26} \\ D_{16} & D_{26} & D_{66} \end{bmatrix} \tag{47}$$

To obtain the $[D]$ matrix equation 49 was used:

$$\left[D_{iy}\right] = 0.333\left(\sum_{k=1}^{N}\left[\bar{Q}_{iy}\right]_k (z_k - Z_{k-1})\right) \tag{48}$$

$$[D] = 0.333[\bar{Q}]_1(z_1 - z_0) + 0.333[\bar{Q}]_2(z_2 - z_1) + 0.333[\bar{Q}]_3(z_3 - z_2) + 0.333[\bar{Q}]_4(z_4 - z_3) \tag{49}$$

Once matrices $[A]$, $[B]$ and $[D]$ were obtained, the inverse of equation 50 was used in equation 51 to determine the strains and curvatures given known forces and moments.

$$\begin{bmatrix} A & B \\ B & D \end{bmatrix} = \begin{bmatrix} A_{11} & A_{12} & A_{16} & B_{11} & B_{12} & B_{16} \\ A_{12} & A_{22} & A_{26} & B_{12} & B_{22} & B_{26} \\ A_{16} & A_{26} & A_{66} & B_{16} & B_{26} & B_{66} \\ B_{11} & B_{12} & B_{16} & D_{11} & D_{12} & D_{16} \\ B_{12} & B_{22} & B_{26} & D_{12} & D_{22} & D_{26} \\ B_{16} & B_{26} & B_{66} & D_{16} & D_{26} & D_{66} \end{bmatrix} \tag{50}$$

$$\begin{bmatrix} \epsilon_x^0 \\ \epsilon_y^0 \\ \epsilon_z^0 \\ k_x \\ k_y \\ k_z \end{bmatrix} = \begin{bmatrix} A & B \\ B & D \end{bmatrix}^{-1} \begin{bmatrix} N_x \\ N_y \\ N_z \\ M_x \\ M_y \\ M_z \end{bmatrix} \tag{51}$$

To find the strains in the global X, Y and Z direction for different fibre layers through thickness, equation 52 was used:

$$[\epsilon]_k^{xy} = [\epsilon^0]^{xy} + z_k[k]^{xy} \tag{52}$$

To find the strains in the X, Y and Z fibre directions for different fibre layers through thickness, equation 53 was used:

$$[\epsilon]_k^{12} = [T]_k[\epsilon]_k^{xy} \tag{53}$$

To find the stresses in the global X, Y and Z direction for different fibre layers through thickness, equation 54 was used:

$$[\sigma]_k^{xy} = [\bar{Q}]_k[\epsilon]_k^{xy} \tag{54}$$

To find the stresses in the X, Y and Z fibre directions for different fibre layers through thickness, equation 55 was used:

$$[\sigma]_k^{12} = [T]_k[\sigma]_k^{xy} \tag{55}$$

### 10.8 UD Epoxy E- Glass Coupon FEA Analysis

In this section the FEA and analytical results were provided for the epoxy e-glass UD prepreg and wet-layup coupons [0/90/90/0, 0/45/45/0, 0/90/45/0] and Aluminium 7075 T6 coupons under tension, compression, bending and torsion. The results for all fibre layers in the laminate were compared and analysed in section 10.9 to obtain a composite material alternative to the current Aluminium 7075 T6 landing gear.

### 10.9 UD Epoxy E-Glass [0/90/90/0] Coupons FEA and Analytical Results

1) Tensile Analysis

Figure 91 and Figure 92 illustrates the FEA stress results for [0/90/90/0] prepreg and wet layup coupons under beam tension. Note that the stress in fibre 1 = fibre 4 and fibre 2 = fibre 3 due to same fibre orientation. The stress, strain, and Puck-failure safety factor obtained from the FEA results for the prepreg coupon fibre layer 1 was 82.259 MPa, 0.008045 mm/mm and 8.0413 respectively. The stress, strain, and Puck-failure safety factor for the wet layup coupon fibre layer 1 was 79.986 MPa, 0.002579 mm/mm and 9.0346 respectively.

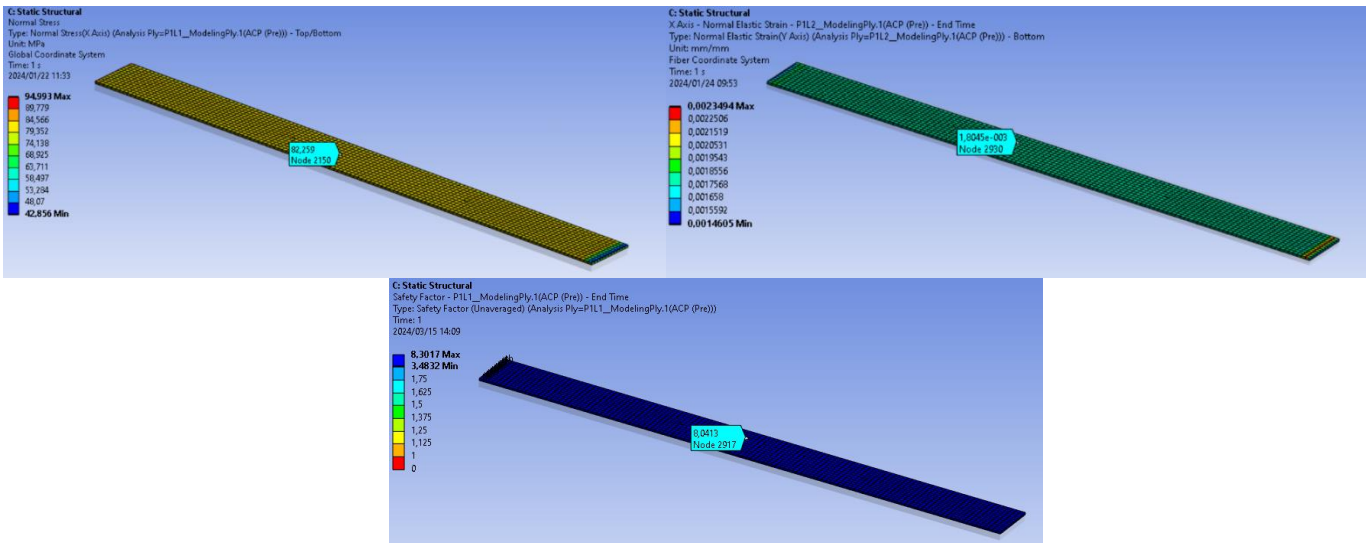


*Figure 91: [0/90/90/0] Epoxy E-Glass UD Prepreg Coupon Beam Tensile Stress, Strain and Safety Factor (Fibre Layer 1)*

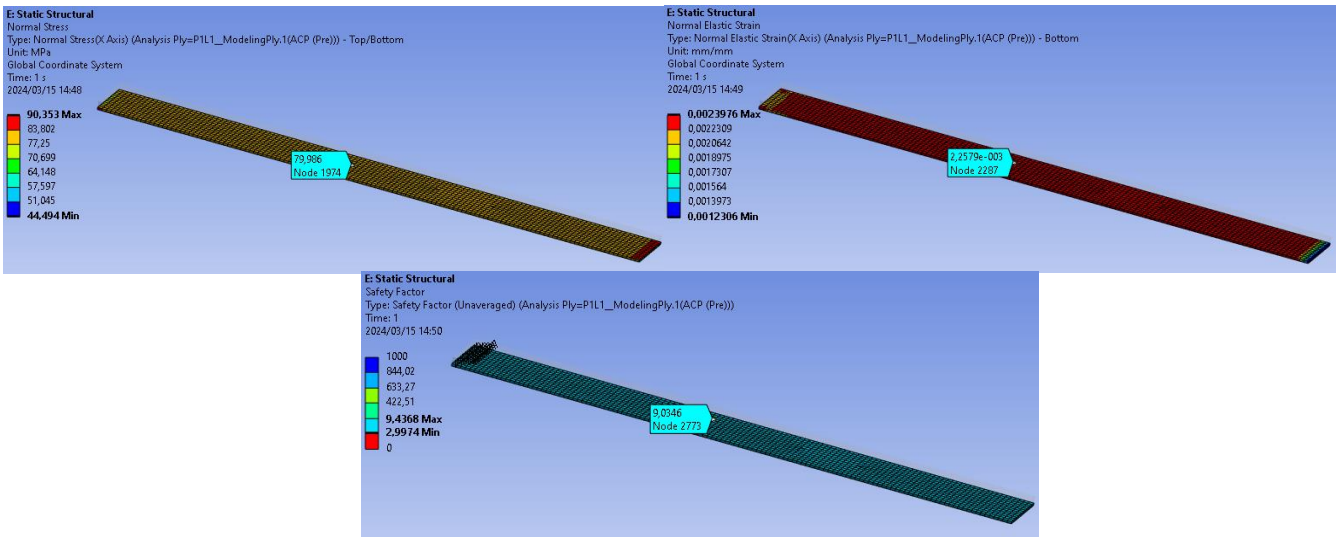


*Figure 92: [0/90/90/0] Epoxy E-Glass UD Wet Layup Coupon Beam Tensile Stress, Strain and Safety Factor (Fibre Layer 1)*

2) Compressive Analysis

Figure 93 and Figure 94 illustrate the FEA stress results for [0/90/90/0] prepreg and wet layup coupons under beam compression. Note that the stress in fibre 1 = fibre 4 and fibre 2 = fibre 3 due to same fibre orientation. The stress, strain, and Puck-failure safety factor obtained from the FEA results for the prepreg coupon fibre layer 1 was 82.259 MPa, 0.008045 mm/mm and 8.1448 respectively. The stress, strain, and Puck-failure safety factor for the wet layup coupon fibre layer 1 was 79.986 MPa, 0.0022579 mm/mm and 6.001 respectively.

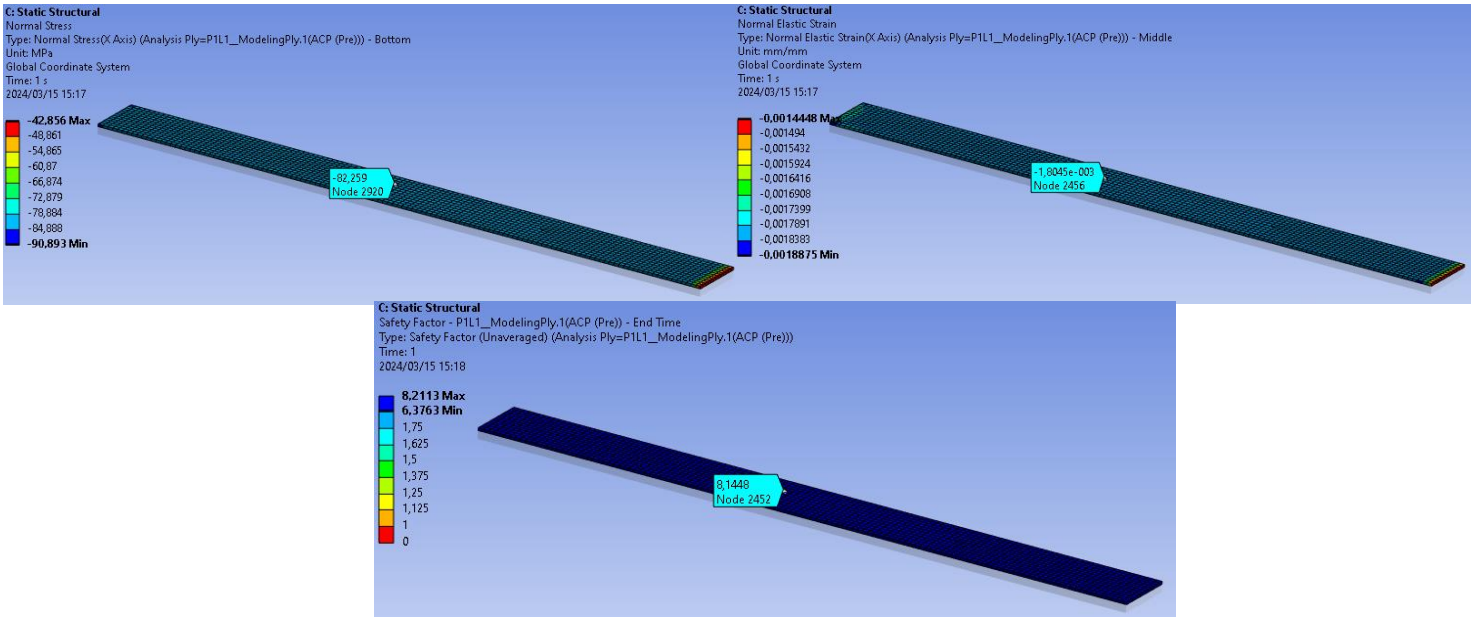


*Figure 93: [0/90/90/0] Epoxy E-Glass Prepreg Coupon Beam Compression Stress, Strain and Safety Factor (Fibre Layer 1)*

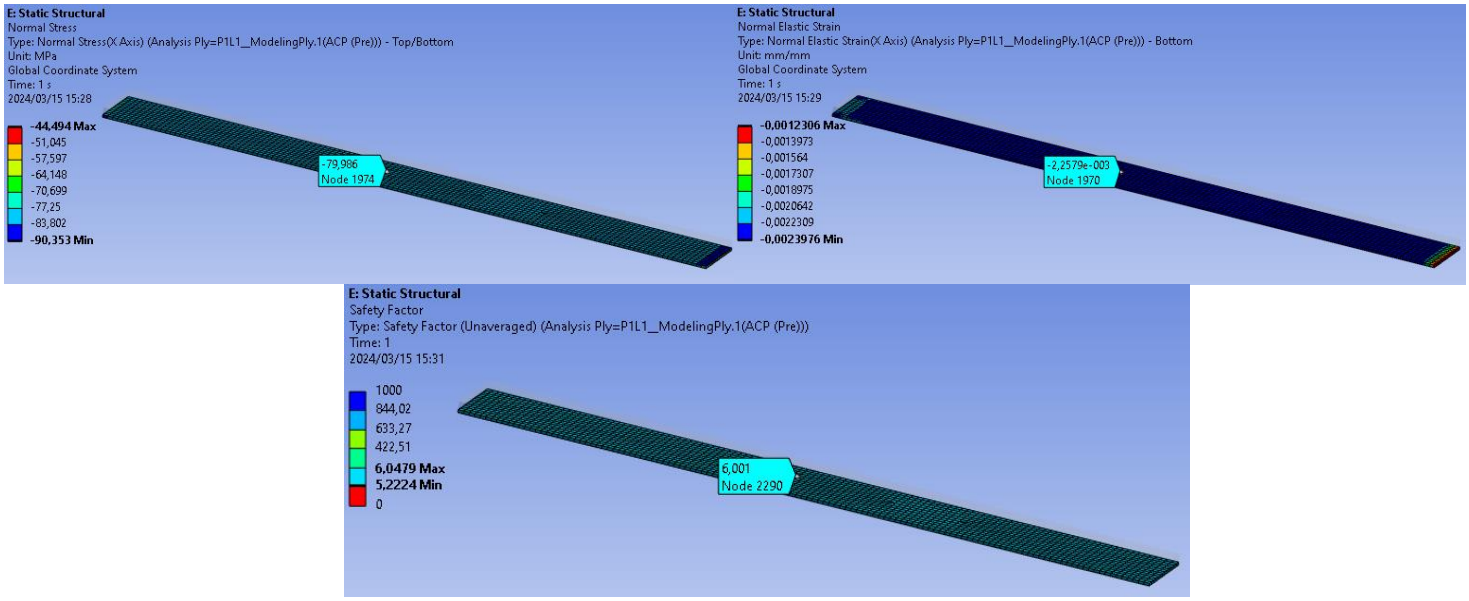


*Figure 94: [0/90/90/0] Epoxy E-Glass Wet Layup Coupon Beam Compression Stress, Strain and Safety Factor (Fibre Layer 1)*

3) Bending/ Flexural Analysis

Figure 95 and Figure 96 illustrates the FEA results for [0/90/90/0] prepreg and wet layup coupons under beam bending. Note that stress and strains in fibre 1 = fibre 4 and fibre 2 = fibre 3 due to the same fibre orientations and same position from mid-plane, but Puck-failure safety factors differ due to fibre 1 and fibre 2 experiencing tension and fibre 3 and fibre 4 experiencing compression. The stress, strain, and Puck-failure safety factor for the prepreg coupon fibre layer 1 was 152.29 MPa, 0.0034467 mm/mm and 5.9102 respectively. The stress, strain, and Puck-failure safety factor for the wet layup coupon fibre layer 1 was 156.53 MPa, 0.0044437 mm/mm and 4.8653 respectively.

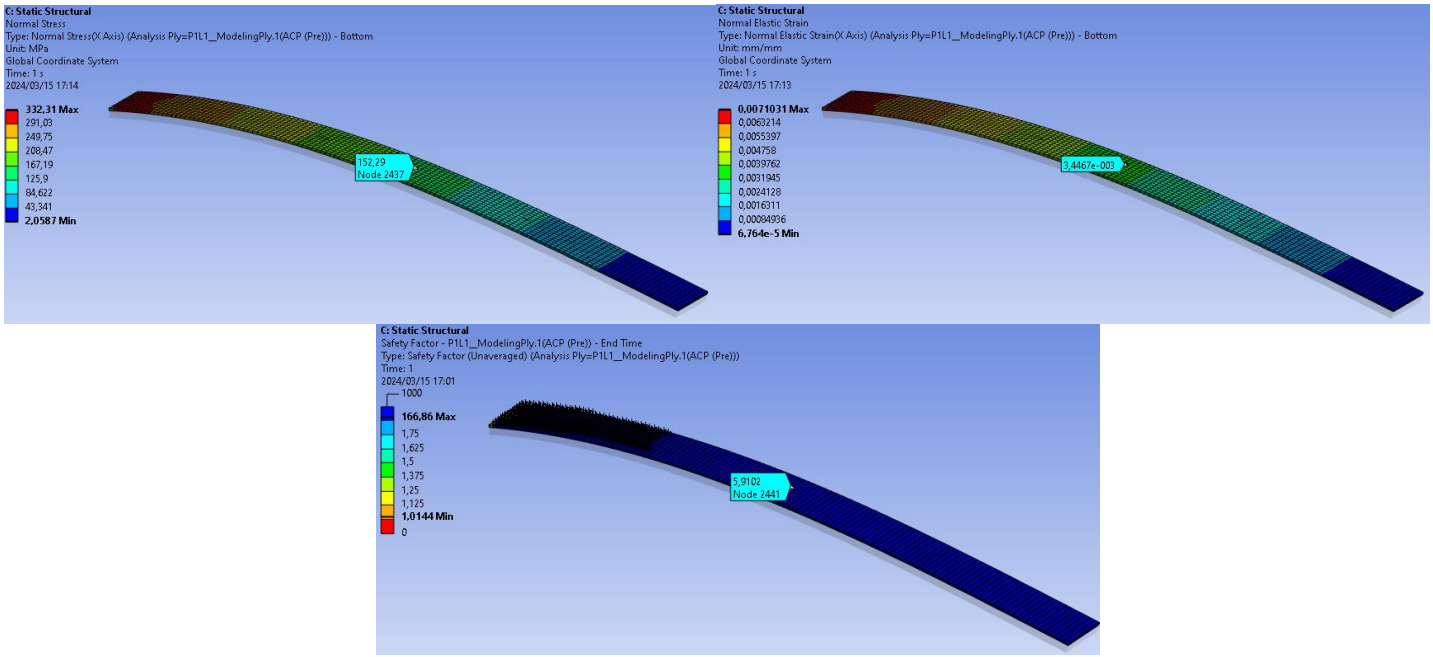


*Figure 95: [0/90/90/0] Epoxy E-Glass Prepreg Coupon Beam Bending Stress, Strain and Safety Factor (Fibre Layer 1)*

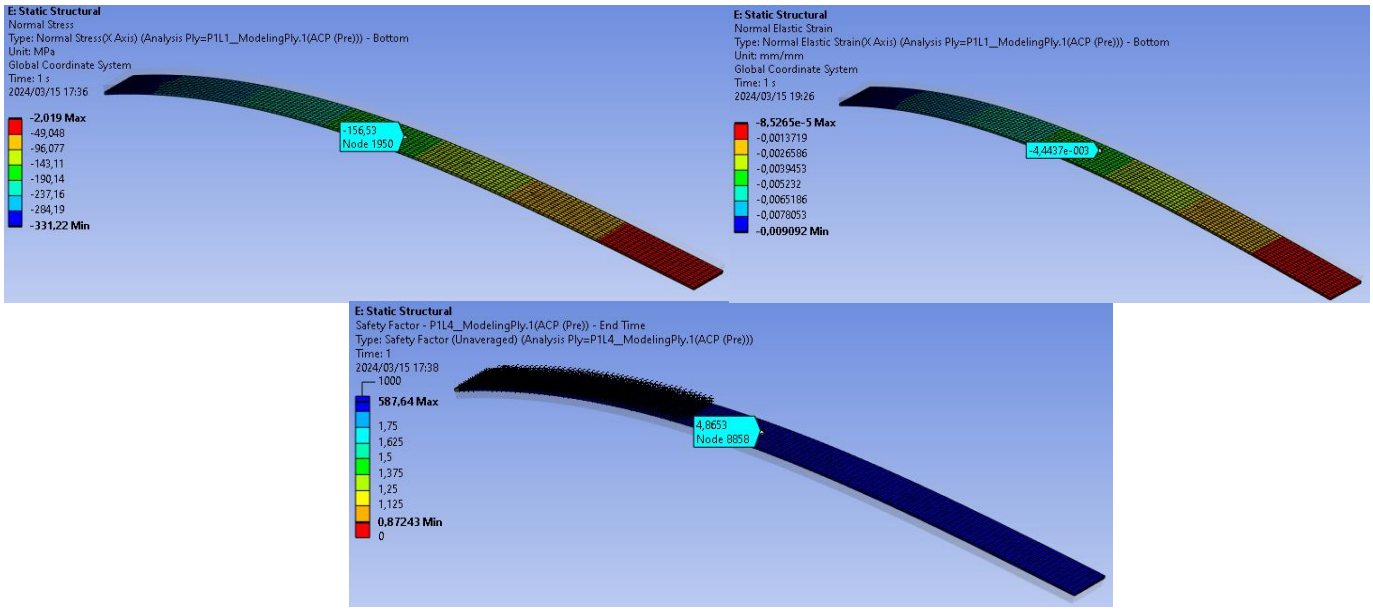


*Figure 96: [0/90/90/0] Epoxy E-Glass Wet Layup Coupon Beam Bending Stress, Strain and Safety Factor (Fibre Layer 1)*

4) Torsion Analysis

Figure 97 and Figure 98 illustrates the FEA results for [0/90/90/0] prepreg and wet layup coupons under beam torsion. Note that stress and strains in fibre 1 = fibre 4 and fibre 2 = fibre 3 due to the same fibre orientations and shear strain that increases from the mid-plane to the outermost fibre. The stress, strain, and Puck-failure safety factor for the prepreg coupon fibre layer 1 was 72.199 MPa, 0.0067695 mm/mm and 1.9185 respectively. The stress, strain, and Puck-failure safety factor for the wet layup coupon fibre layer 1 was 72.374 MPa, 0.0071824 mm/mm and 1.4359 respectively.

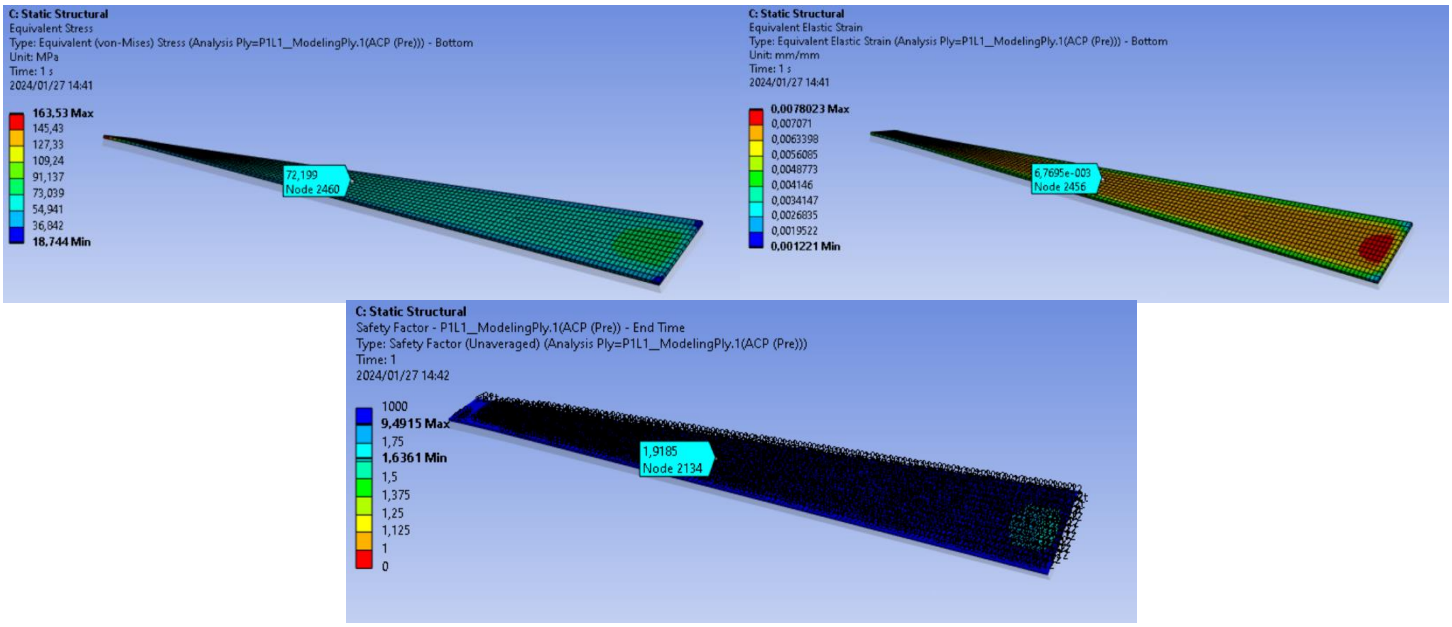


*Figure 97: [0/90/90/0] Epoxy E-Glass Prepreg Coupon Beam Torsional Stress, Strain and Safety Factor (Fibre Layer 1)*

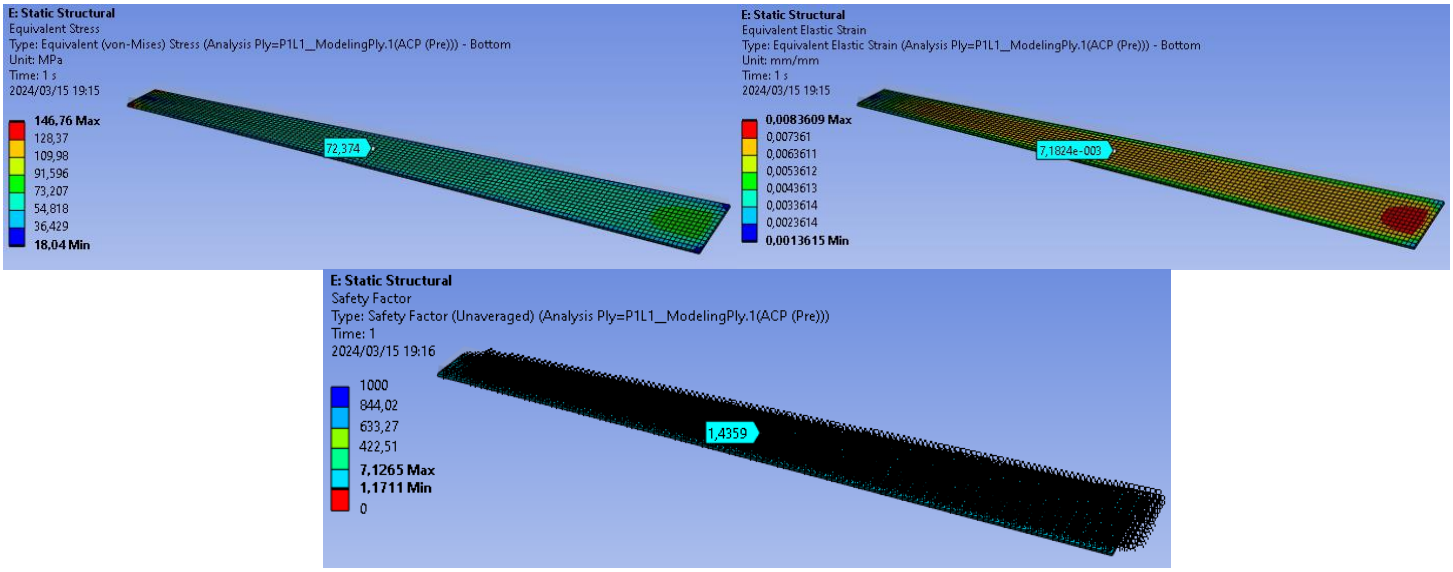


*Figure 98: [0/90/90/0] Epoxy E-Glass Wet Layup Coupon Beam Torsional Stress, Strain and Safety Factor (Fibre Layer 1)*

Table 31 to Table 34 provides the FEA and analytical results obtained for [0/90/90/0] layered Epoxy E-Glass UD prepreg and Epoxy E-Glass UD wet layup coupons during tension, compression, bending and torsion. See Appendix A for the [0/45/45/0] and [0/90/45/0] layered coupons FEA and analytical results.

*Table 31: Prepreg and Wet Layup Coupon [0/90/90/0] Results (Tensile Load)*

| Load Type | Stress (FEA) | Stress (Analytical) | Strain (FEA) | Strain (Analytical) | Safety Factor |
|---|---|---|---|---|---|
| - | MPa | MPa | mm/mm | mm/mm | - |
| **[0/90/90/0] Prepreg Coupon (Tension)** | | | | | |
| Layer 1 | 82.259 | 82.201<br>0.071 % | 0.0018045 | 0.001803<br>0.083 % | **8.0413** |
| Layer 2 | 17.811 | 17.799<br>0.067 % | 0.0018045 | 0.001803<br>0.083 % | **1.9644** |
| Layer 3 | 17.811 | 17.799<br>0.067 % | 0.0018045 | 0.001803<br>0.083 % | **1.9644** |
| Layer 4 | 82.259 | 82.201<br>0.071 % | 0.0018045 | 0.001803<br>0.083 % | **8.0413** |
| **[0/90/90/0] Wet Layup Coupon (Tension)** | | | | | |
| Layer 1 | 79.986 | 79.903<br>0.104 % | 0.002579 | 0.002594<br>0.582 % | **9.0346** |
| Layer 2 | 20.074 | 20,097<br>0.115 % | 0.002579 | 0.002594<br>0.582 % | **1.5434** |
| Layer 3 | 20.074 | 20,097<br>0.115 % | 0.002579 | 0.002594<br>0.582 % | **1.5434** |
| Layer 4 | 79.986 | 79.903<br>0.104 % | 0.002579 | 0.002594<br>0.582 % | **9.0345** |

*Table 32: Prepreg and Wet Layup Coupon Results [0/90/90/0] (Compressive Load)*

| Load Type | Stress (FEA) | Stress (Analytical) | Strain (FEA) | Strain (Analytical) | Safety Factor |
|---|---|---|---|---|---|
| - | MPa | MPa | mm/mm | mm/mm | - |
| **[0/90/90/0] Prepreg Coupon (Compression)** | | | | | |
| Layer 1 | -82.259 | -82.201<br>0.071 % | -0.001805 | -0.001803<br>0.011 % | **8.1448** |
| Layer 2 | -17.811 | -17.799<br>0.067 % | -0.001805 | -0.001803<br>0.112 % | **6.7279** |
| Layer 3 | -17.811 | -17.799<br>0.067 % | -0.001805 | -0.001803<br>0.112 % | **6.7279** |
| Layer 4 | -82.259 | -82.201<br>0.071 % | -0.001805 | -0.001803<br>0.0112 % | **8.1448** |
| **[0/90/90/0] Wet Layup Coupon (Compression)** | | | | | |
| Layer 1 | -79.986 | -79.903<br>0.104 % | -0.0022579 | -0.002594<br>0.582 % | **6.001** |
| Layer 2 | -20.074 | -20.094<br>0.115 % | -0.0022579 | -0.002594<br>0.582 % | **4.982** |
| Layer 3 | -20.074 | -20.094<br>0.115 % | -0.0022579 | -0.002594<br>0.582 % | **4.982** |
| Layer 4 | -79.986 | -79.903<br>0.104 % | -0.0022579 | -0.002594<br>0.582 % | **6.001** |

*Table 33: Prepreg and Wet Layup Coupon Results [0/90/90/0] (Bending Load)*

| Load Type | Stress (FEA) | Stress (Analytical) | Strain (FEA) | Strain (Analytical) | Safety Factor |
|---|---|---|---|---|---|
| - | MPa | MPa | mm/mm | mm/mm | - |
| **[0/90/90/0] Prepreg Coupon (Bending)** | | | | | |
| Layer 1 | 157.29 | 156.01<br>0.814 % | 0.0034467 | 0.0034451<br>0.046 % | **5.9102** |
| Layer 2 | 16.878 | 16.478<br>2.370 % | 0.0017241 | 0.0017226<br>0.087 % | **1.933** |
| Layer 3 | -16.878 | -16.478<br>2.370 % | -0.0017241 | -0.0017226<br>0.087 % | **6.691** |
| Layer 4 | -157.29 | -156.01<br>0.814 % | -0.0034467 | -0.0034451<br>0.046 % | **4.065** |
| **[0/90/90/0] Wet Layup Coupon (Bending)** | | | | | |
| Layer 1 | 156.53 | 155.249<br>0.818 % | 0.0044437 | 0.004422<br>0.491 % | **4.8653** |
| Layer 2 | 21.086 | 21.073<br>0.062 % | 0.0022177 | 0.002211<br>0.303 % | **1.4802** |
| Layer 3 | -21.086 | -21.073<br>0.062 % | -0.0022177 | -0.002211<br>0.303 % | **5.0703** |
| Layer 4 | -156.53 | -155.249<br>0.818 % | -0.0044437 | -0.004422<br>0.491 % | **2.8616** |

*Table 34: Prepreg and Wet Layup Coupon Results [0/90/90/0] (Torsional Load)*

| Load Type | Stress (FEA) | Stress (Analytical) | Strain (FEA) | Strain (Analytical) | Safety Factor |
|---|---|---|---|---|---|
| - | MPa | MPa | mm/mm | mm/mm | - |
| **[0/90/90/0] Prepreg Coupon (Torsion)** | | | | | |
| Layer 1 | 72.199 | 75.002<br>3.882 % | 0.0067695 | 0.007106<br>4.971 % | **1.9185** |
| Layer 2 | 36.108 | 37.501<br>3.858 % | 0.003852 | 0.004019<br>4.335 % | **3.8367** |
| Layer 3 | 36.108 | 37.501<br>3.858 % | 0.003852 | 0.004019<br>4.335 % | **3.8367** |
| Layer 4 | 72.199 | 75.002<br>3.882 % | 0.0067695 | 0.007106<br>4.971 % | **1.9185** |
| **[0/90/90/0] Wet Layup Coupon (Torsion)** | | | | | |
| Layer 1 | 72.374 | 75.002<br>3.504 % | 0.0071824 | 0.0075328<br>4.879 % | **1.4359** |
| Layer 2 | 36.166 | 37.501<br>3.691 % | 0.0035902 | 0.0037360<br>3.903 % | **2.8724** |
| Layer 3 | 36.166 | 37.501<br>3.691 % | 0.0035902 | 0.0037244<br>3.903 % | **2.8724** |
| Layer 4 | 72.374 | 75.002<br>3.504 % | 0.0071824 | 0.0075328<br>4.879 % | **1.4359** |

## 10.10 UD Epoxy E-Glass Prepreg and Wet Layup Coupons FEA Results

In this section the FEA stress, strain and Puck-failure safety factor results are provided for the [0/90/90/0], [0/45/45/0] and [0/90/45/0] layered Epoxy E-Glass UD prepreg and Epoxy E-Glass UD wet layup coupons during tension, compression, bending and torsion.

### 10.10.2 Coupon Tensile FEA Results

In Figure 99, the stress, strain and Puck-failure safety factor results are provided the prepreg and wet layup coupons during tensile loading. For the [0/90/90/0] layered coupons, the stress was the largest for the 0-degree unidirectional fibre. For the [0/45/45/0] layered coupon the stress on 0-degree unidirectional fibre was less due to the 45-degree fibres being able to carry more of the tensile load than the 90-degree fibres. The strain was also less for [0/45/45/0] layered coupon than the [0/90/90/0] layered coupon. These results were further represented by the [0/90/45/0] layered coupon during tensile loading. From results obtained regarding the Puck-failure for the coupons, all fibre layers in the [0/45/45/0] layered coupon had higher safety factors than the [0/90/90/0] layered coupon, thus making this fibre layup orientation more effective during tensile loading. Overall, the prepregs obtained less strain and higher Puck-failure safety factors when experiencing tensile loading, making it more resistant to failure in comparison to the wet layup coupons.

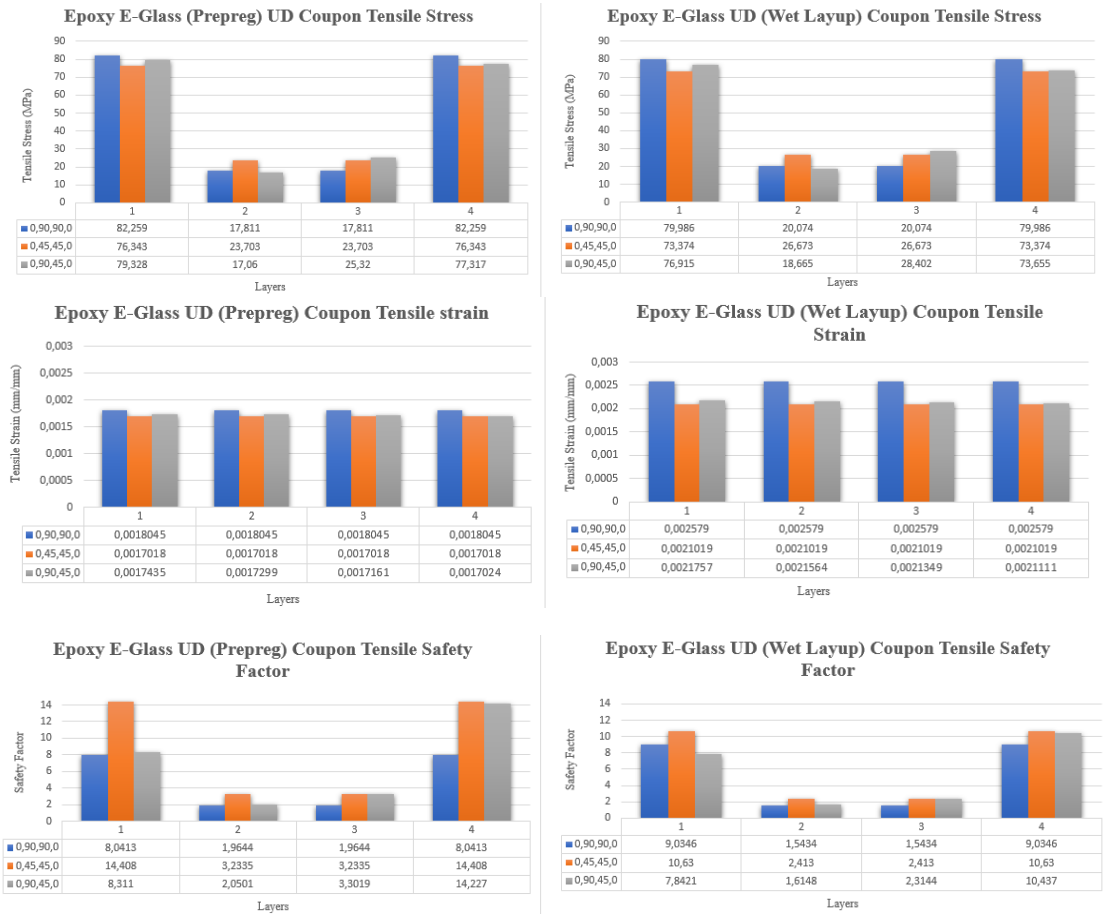


*Figure 99: UD Epoxy E-Glass Prepreg and UD Epoxy E-Glass Wet Layup Coupons Tensile Stress, Strain and Puck-Failure Safety Factor Results*

In Figure 100, the stress, strain and Puck-failure safety factor results are provided the prepreg and wet layup coupons during compression loading. For the [0/90/90/0] layered coupons, the stress was the largest for the 0-degree unidirectional fibre. For the [0/45/45/0] layered coupon the stress on 0-degree unidirectional fibre was less due to the 45-degree fibres being able to carry more of the compressive load than the 90-degree fibres. The strain was also less for [0/45/45/0] layered coupon than the [0/90/90/0] layered coupon. These results were further represented by the [0/90/45/0] layered coupon during compressive loading. From results obtained regarding the Puck-failure for the coupons, all fibre layers in the [0/45/45/0] layered coupon had higher safety factors than the [0/90/90/0] layered coupon, thus making this fibre layup orientation more effective during compression loading. Overall, the prepregs obtained less strain and higher Puck-failure safety factors when experiencing compression loading, making it more resistant to failure in comparison to the wet layup coupons.

In comparison to the tensile analysis, the 0-degree unidirectional fibres had a higher safety factor for [0/45/45/0] layered coupon during tensile loading whilst the 45-degree fibres had a higher safety factor for compression loading. The 90-degree fibres obtained higher safety factor results when experiencing compression loads than tensile loads. In conclusion, the [0/45/45/0] layered coupons were much more effective during compression loading than the [0/90/90/0] and [0/90/45/0] layered coupons.

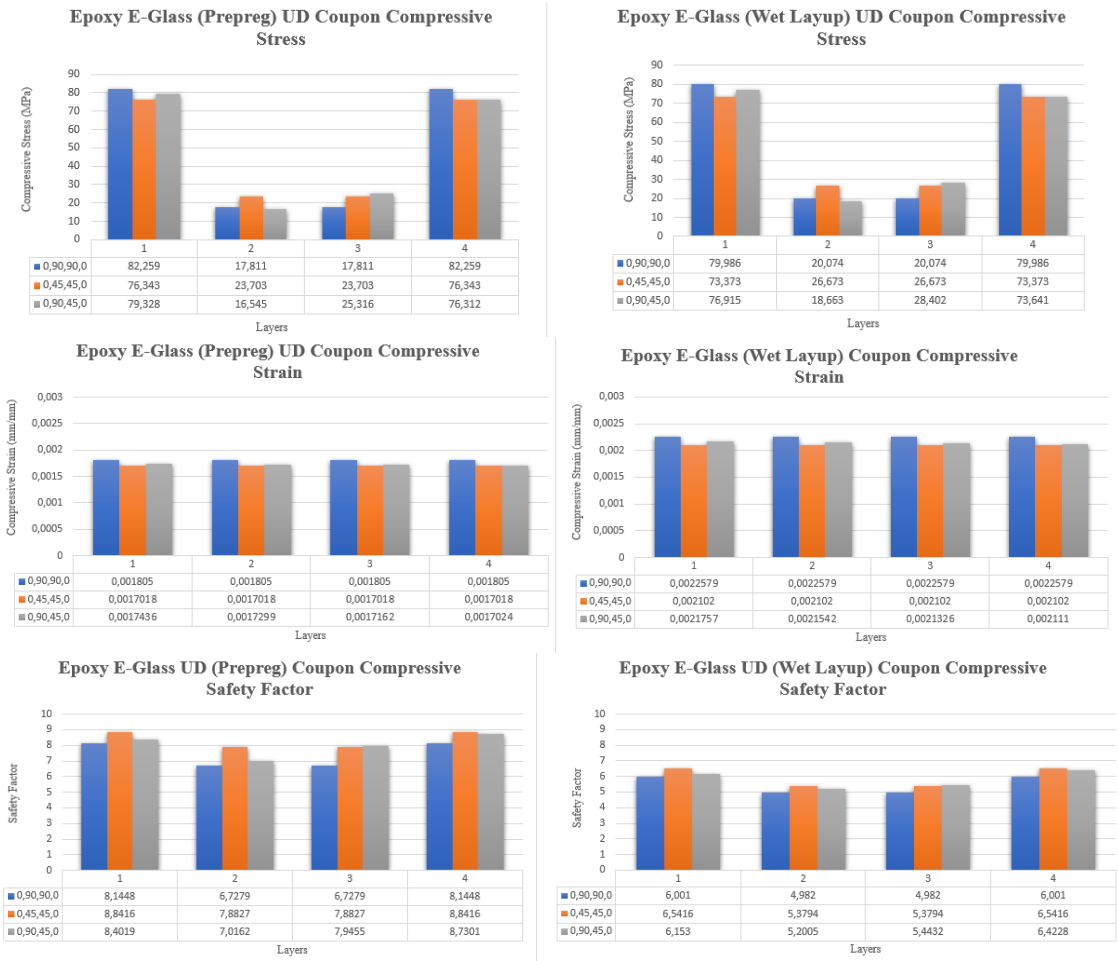


*Figure 100: UD Epoxy E-Glass Prepreg and UD Epoxy E-Glass Wet Layup Coupons Compressive Stress, Strain and Puck-Failure Safety Factor Results*

In Figure 101, the stress, strain and Puck-failure safety factor results are provided the prepreg and wet layup coupons during flexural loading. For the [0/90/90/0] degree layered coupons, the 0-degree unidirectional fibres had higher stress results in comparison to the 0-degree unidirectional fibres in the [0/45/45/0] degree layered coupons. The 45-degree fibres also had higher stress results in comparison to the 90-degree fibres during flexural loading for the [0/90/45/0] degree layered coupons. The [0/45/45/0] degree layered coupons resulted in less strain in comparison to the [0/90/90/0] degree layered coupons since the 45-degree fibres are much more effective in resisting flexural deformation than the 90-degree fibres, thus being more effective in withstanding deformation. This deformation results were further represented by the [0/90/45/0] degree layered coupons as fibre 3 and fibre 4 resulting in less flexural deformation. During flexural loading the Puck-failure safety factors differed for each fibre since fibre 1 and fibre 2 underwent tension whilst fibre 3 and fibre 4 underwent compression. The safety factor results for the fibres undergoing tension and fibres undergoing compression could be further analysed as discussed in Figure 99 and Figure 100.

Overall, the prepreg coupons resulted in less strain and higher Puck-failure safety factors in comparison wet layup coupons, thus making it more effective in withstanding flexural loads.

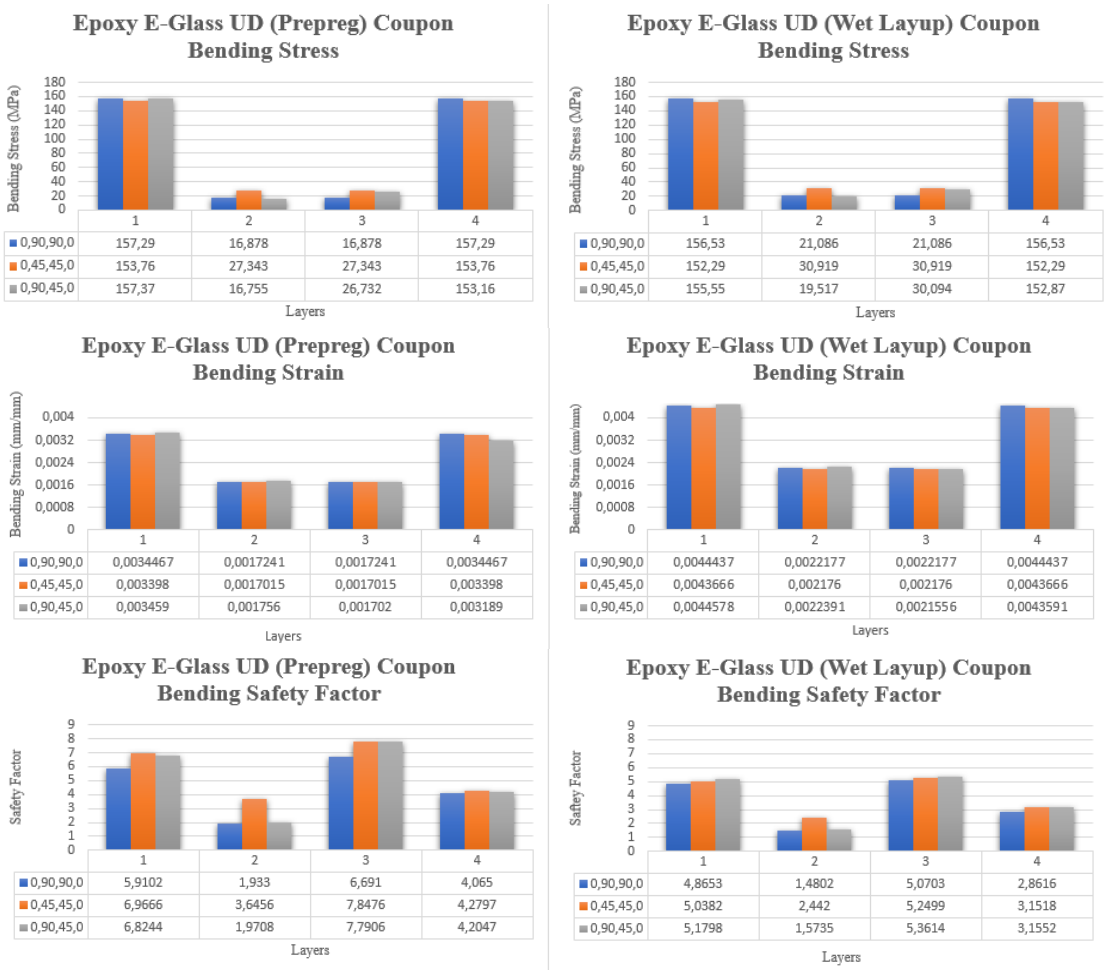


*Figure 101: UD Epoxy E-Glass Prepreg and UD Epoxy E-Glass Wet Layup Coupons Bending Stress, Strain and Puck-Failure Safety Factor Results*

In Figure 102, the stress, strain and Puck-failure safety factor results are provided the prepreg and wet layup coupons during torsional loading. For the [0/45/45/0] degree layered coupons, the 45-degree fibres had the highest torsional stress in comparison to the 0-degree unidirectional fibres. For the [0/90/90/0] degree layered coupons, the 0-degree unidirectional fibres resulted in a higher torsional stress than the 90-degree fibres. The [0/45/45/0] degree layered coupons resulted in less torsional strain then the [0/90/90/0] degree layered coupons due the 45-degree fibres withstanding the torsional deformation more effective than the 90-degree fibres. With regards to the Puck-failure safety factors, the 45-degree fibres were the most effective in withstanding shear failure in comparison to the 0-degree unidirectional and 90-degree fibre layers.

Overall, the prepreg fibres obtained better results with regards to safety factors for all coupons in comparison to the wet layup coupons. The prepreg fibres also resulted in less strain than the wet layup coupons.

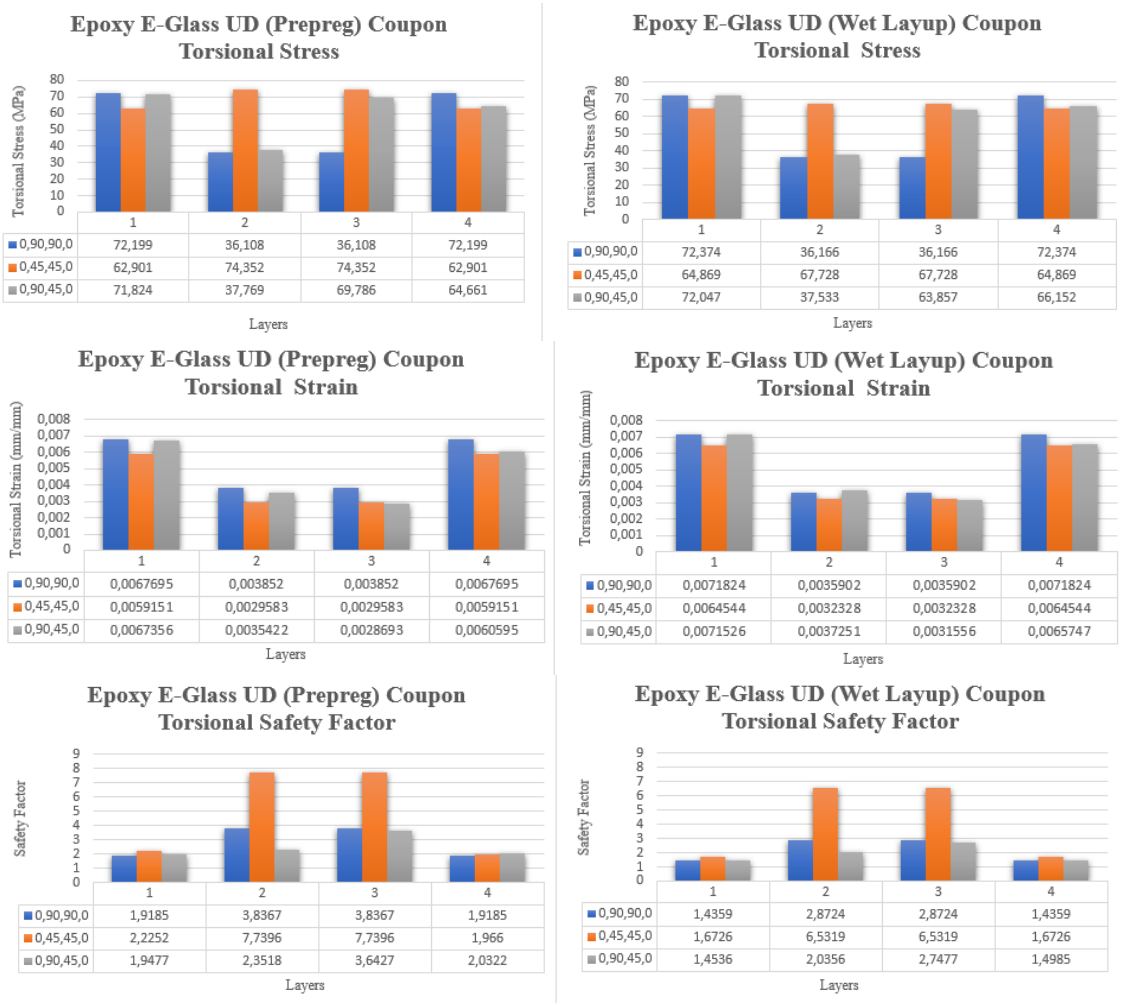


*Figure 102: UD Epoxy E-Glass Prepreg and UD Epoxy E-Glass Wet Layup Coupons Torsional Stress, Strain and Puck-Failure Safety Factor Results*

### 10.11 Coupon Study Summary

In conclusion, UD Epoxy E-Glass Prepreg and UD Epoxy E-Glass wet layup coupons consisting out of [0/90/90/0], [0/45/45/0] and [0/90/45/0] were loaded in tension, compression, bending and torsion to analyse and compare the differences in stress, strain, and Puck-failure safety factor for each individual fibre layer for both the prepreg and wet layup coupons. The FEA results were validated using composite Classical Lamination Theory. Aluminium 7075 T6 coupons were also loaded under the same load conditions and FEA results were validated and compared to the composite coupons consisting out of different fibre orientations. From FEA results obtained for both the composite and Aluminium 7075 T6 coupons, the analytical results were within a 5% error range thus, ensuring that the FEA results obtained were correct.

From FEA results obtained for the composite coupons loaded under tension, compression, bending, and torsion it was found that the [0/45/45/0] layered coupons obtained least strain and the highest Puck-failure safety factors in comparison to the [0/90/90/0] layer coupons. From FEA results obtained from the [0/90/45/0] layers coupons, the stress, strain, and Puck-failure safety factor results directly correlated to the results obtained from the [0/90/90/0] and [0/45/45/0] layered coupons. The wet layup coupons resulted in higher strain results and lower safety factors for each individual fibre layer for all tests conducted. Thus, the usage of UD Epoxy E-Glass Prepreg material was more preferred in comparison to a wet layup manufacturing of a composite aircraft landing gear using UD E-Glass and Epoxy Resin. The prepreg fibres were slightly heavier than the wet layup fibres, but less prepreg fibres could be used since it had less strain during loading whilst maintaining higher resistance to failure. In terms of fibre layup, it can be concluded that the usage of 90-degree orientated fibres should be eliminated when designing the composite aircraft landing gear since it was more prone to failure in comparison to the 45-degree and 0-degree unidirectional fibres during tension, compression, bending and torsion. Wet layup fibres generally consist out of a 1-10% void content which decreases its fatigue life and increases moisture absorption whereas prepreg fibres generally consist out of less than 1% void content increasing its fatigue life whilst decreasing moisture absorption.

With regards to the weight, the Aluminium 7075 was approximately 28% heavier than prepreg composite coupons. The strain in the Aluminium 7075 T6 coupons were also higher in comparison to the prepreg coupons during tensile, compression, bending and torsional loading. During tensile loading the 0-degree unidirectional fibres in the [0/45/45/0] layered coupons obtained higher safety factor results whereas the 45-degree fibres were weaker during tensile loading whilst all the individual fibres in the coupon were weaker than the Aluminium 7075 T6 coupon during compression loading. The [0/45/45/0] layered coupon obtained much higher safety factor results for all individual fibres in comparison to the Aluminium 7075 T6 coupons during flexural loading. The 45-degree fibres also obtained higher safety factor results than the Aluminium 7075 T6 coupons during torsional loading whereas the 0-degree unidirectional fibres were weaker.

## 11 COMPOSITE UNDERCARRIAGE DESIGN AND ANALYSIS

### 11.2 Introduction

In this section the final composite landing gear has been modelled and analysed. The load and constraint application to the main undercarriage validated in chapter 8 and composite material chosen from analysis in chapter 10 were applied to obtain a composite undercarriage alternative to the current Aluminium 7075 T6 design.

### 11.3 Composite Undercarriage Design Method

Figure 103, illustrates the correlation between a positive wheel camber angle, undercarriage leg arc and the high stress areas on the landing gear strut. The positive wheel camber angle enhances the stability and control of the aircraft during landing by improving its lateral stability by promoting better ground contact of the wheel during landing [18]. Additionally, the greater leg arc angle and leg arc radius the more shock absorption and strut deflection occurs during touchdown by minimising the stresses on the airframe. This results in a smoother ride during the different landing conditions for both the tricycle and taildragger aircraft [18]. Figure 103 also illustrates the section of the landing gear strut with the highest stresses that occur during landing which should be modified to withstand matrix and fibre failure at limit load and ultimate load conditions. For the bolted regions, holes must be drilled into the composite gear and by introducing shims the stresses can be distributed over a larger surface area which eliminates concentrated stress regions near the bolted areas of the gear [18].

The landing gear was analysed by means of leg arc angle, leg arc radius, wheel camber angle, gear length, gear width and layup optimization to find the most optimal composite alternative to the current Aluminium 7075 T6 design. A limit load factor of 2.1 and an ultimate load factor of 3 was used for the alternative analysis according to the CS 23 amendments and ASTM F2245 – 14 standards.

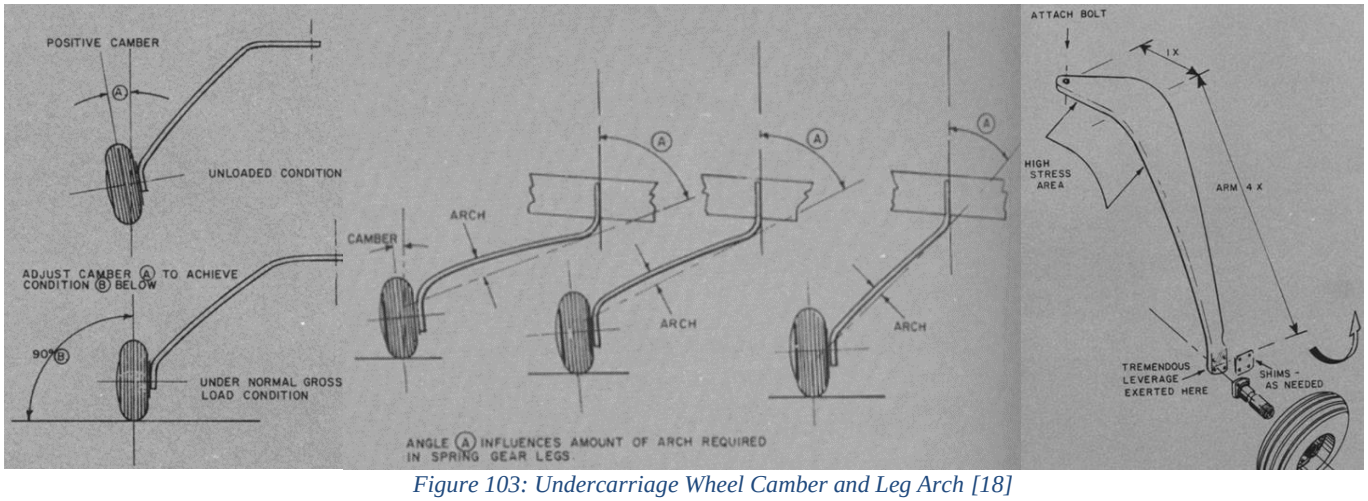


*Figure 103: Undercarriage Wheel Camber and Leg Arch [18]*

## 11.4 Composite Undercarriage Ansys Setup and Modelling Type

### 11.4.2 Ansys Workbench Setup

In Figure 104, the system setup used in Ansys for the composite gear is shown. In System A (Geometry) a model of the composite gear was imported and cleaned up by imprinting the brackets and axles onto the surface for FEA support and load application. It was also used to create the coordinate systems for the stub axles to which the ground load was applied to. System B (ACP Pre) was used to create the Epoxy E-glass UD prepreg fibre layup and specify the desired fibre orientations and thickness of the composite gear. System C (Static Structural) was used to apply the ground reaction and frictional loads together with the supports onto the shell composite model. System D (ACP Post) was used to analyse the deflection and Puck-failure of the composite gear per layer of fibre in the epoxy e-glass UD prepreg layup. Based on analysed results from ACP Post, the gear was optimized to withstand the loads during landing more effectively without failure whilst maintaining enough flexure in the gear struts for a smooth landing.

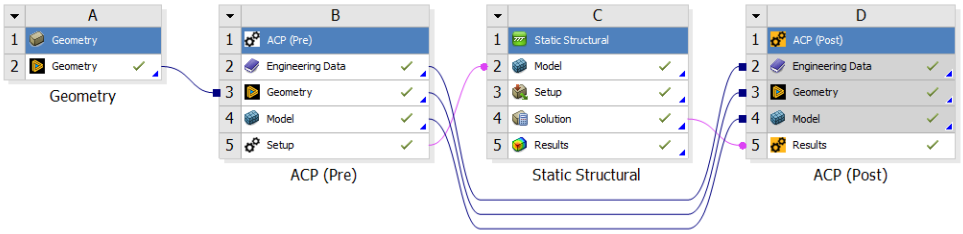


*Figure 104: Composite Undercarriage Ansys Systems Setup*

Figure 105, illustrates the imprinted faces of the stub axles and brackets on the surface of the 1st stage optimization base model gear. These faces were used to apply loads and constraints on the composite shell model during FEA analysis. In Figure 105, the coordinate systems are also visible indicating where the ground reaction loads were applied to the stub axles. The undercarriage model seen in Figure 105, was used as a reference model for analysis, which would provide insight to the changes needed to make the alternative composite undercarriage more effective in withstanding the load conditions specified.

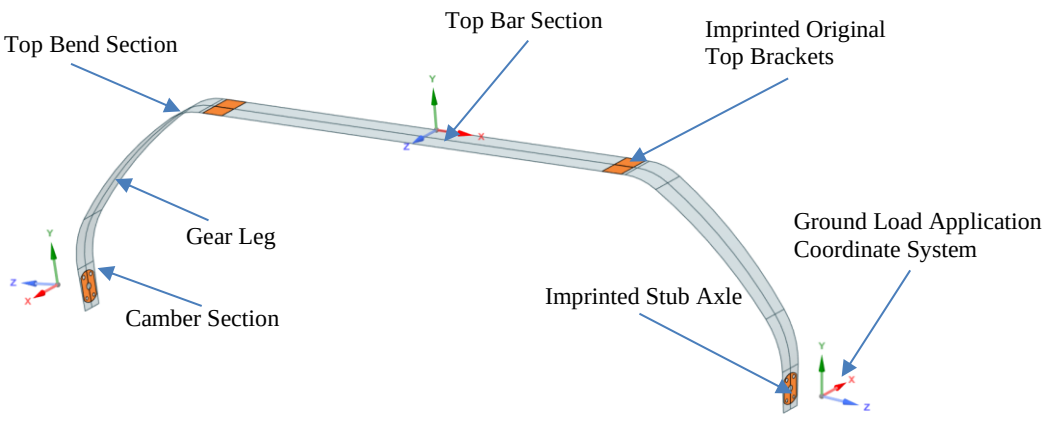


*Figure 105: Imprinted Stub Axles and Mounting Brackets on 1st Stage Composite Gear Surface*

### 11.4.3 Shell Element Modelling vs Solid Element Modelling in Ansys

1) Shell Element Modelling

Shell elements were suitable for modelling thin-walled structures to structures occupying a moderate thickness. The usage of shell elements was compliant in bending analysis and provided good deformation results whilst being computational inexpensive [19]. Due to shell elements being computational inexpensive, meshing requirements were reduced resulting in easier setup during optimization and quicker simulations. The downside to shell element modelling is that it could not accurately capture stress concentrations or complex 3D effects in thick structures [19]. Shell element modelling was not well suited for all geometries thus, a combination of different modelling techniques was required to obtain better accuracy.

2) Solid Element Modelling

Solid element modelling was aimed at modelling thick-walled structures. As the thickness of the laminate increased, the out of-plane stresses became more significant. The shortcoming of using solid element modelling is that they could become too stiff during bending when elements are thin [19]. This can result in the displacements results not being accurate due to elements undergoing a phenomenon called element locking [19]. As seen in Figure 106, the most common type of element locking due to flexural loads were shear element locking. When the elements had fewer integration points than what was needed for an exact solution or when the shear stresses became significant during bending, the elements did not have enough degrees of freedom to capture the shear behaviour accurately resulting in the elements becoming overly stiff during FEA. The usage of quadratic solid elements (SOLID186) in Ansys provides a better solution during FEA, but increases computational cost [19].

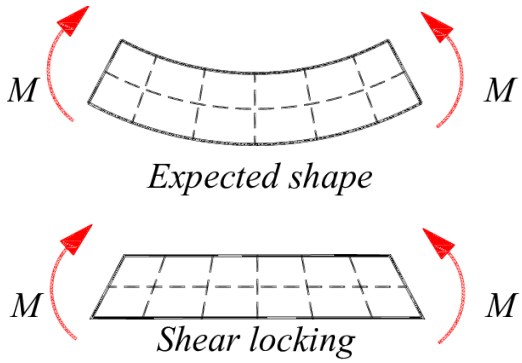


*Figure 106: Element Shear Locking Due to Flexural Loads [20]*

In conclusion, the leaf spring undercarriage undergoes bending during landing to increase shock-absorption thus, shell element modelling was used during the analysis and modification of the composite undercarriage as it was less computational expensive and reduced the probability of element shear locking during FEA.

## 11.5 Ansys (ACP Post) - Failure Criteria

As a result of the research conducted on the Chinese RX1E two-seater electric aircraft, the Puck Failure Criterion has been employed to examine the structural integrity and durability of the composite leaf spring undercarriage. The Puck Failure Criterion distinguishes between fibre and inter-fibre tension, compression, and shear failure. Additionally, it enables for the delamination within the composite structure to be analysed by using this criterion. Utilising Ansys (ACP Post), the Puck Failure analysis employed specialised codes to differentiate and assess the distinct failure modes occurring within the composite undercarriage. The inverse reserve factor, integral to the puck failure analysis, represented the reciprocal of the reserve factor and served as a precise gauge of how close the composite structure is to its failure limit during specified loading conditions. Additionally, the inverse reserve factor was used during the analysis process of the composite undercarriage to modify the structure to withstand the limit and ultimate loads exerted on the structure more effectively.

The following codes facilitate the differentiation and analysis of the failure modes:

a) pf = fibre failure
b) pmA = matrix tensile failure
c) pmB = matrix compression failure
d) pmC = matrix shear failure
e) pd = fibre delamination

Figure 107 represents the inverse reserve factor Puck Failure plot codes of a shell composite structure experiencing matrix tensile failure during loading. This method of analysis was used during the modification of the composite undercarriage alternative.

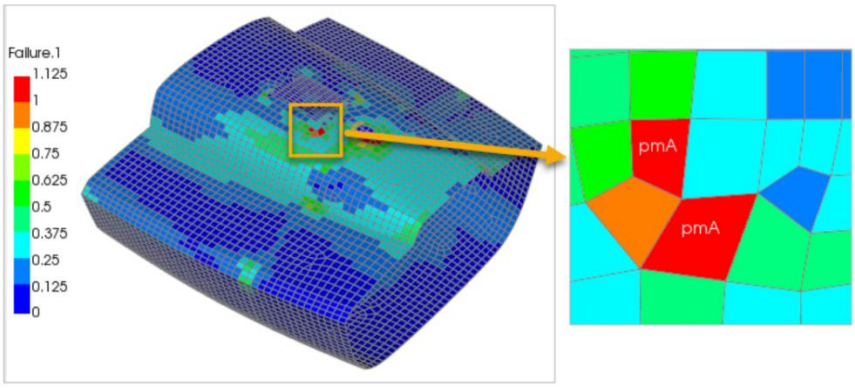


*Figure 107: ACP Post - Puck Failure Plot*

## 11.6 Composite Undercarriage Analysis and Optimization

### 11.6.2 1st Stage Analysis (Reference Composite Undercarriage)

The fibre layup consisted out of 3 epoxy e-glass UD prepreg stack ups namely the top stack up of 20 fibre plies, core stack up of 30 fibre plies and the bottom stack up out of 20 fibre plies. The thickness of UD Epoxy E-Glass prepreg fibres was approximately 0.254 mm (0.010 inches) and after manufacturing phase (compression and cure) the prepreg fibre thickness was approximately (0.0085 inches) 0.2159 mm. For the 1st stage analysis, the orientation of the UD Epoxy E-Glass prepreg fibres was 0-degree and ±45-degree as seen in Table 35. The usage of 90-degre fibres was eliminated as summarised during the coupon study. The 1st stage composite undercarriage had a thickness of 28.067 mm and 130 UD Epoxy E-Glass prepreg fibre layers whilst the thickness was uniform throughout the composite undercarriage.

*Table 35: Composite Undercarriage 1st Stage Analysis UD Epoxy E-Glass Prepreg Layup*

| Stack Up Section | Ply Amount | UD Epoxy E-Glass Prepreg (0.2159 mm) Layup sequence | Thickness (mm) |
|---|---|---|---|
| Top | 1 | [0/0/0/45/-45/0/0/45/-45/0/0/-45/45/0/0/-45/45/0/0/0] | 4.318 |
| Core | 3 | [45/-45/0/0/45/-45/0/-45/0/45/45/0/-45/0-45/-45/0/-45/0/45/45/0/-45/0/-45/45/0/0/-45/45] | 19.431 |
| Bottom | 1 | [0/0/0/45/-45/0/0/45/-45/0/0/-45/45/0/0/-45/-45/0/0/0] | 4.318 |

Figure 108 provides the dimensions for the base model composite gear used during the 1st stage analysis. This composite gear was used as a reference to determine what modifications were needed to improve its effectiveness in withstanding laminate fibre and matrix failure during landing. The landing gear leg had an arc radius of 140 mm, 1000 mm, and 200 mm respectively, positive camber angle of 5° and a gear length of 1900 mm. The top bar section had a length of 1160mm. The gear arc angle was approximately 34.92°. The gear leg width was tapered from 100 mm to 56 mm and the height remains the same as the current Aluminium 7075 T6 Alloy undercarriage.

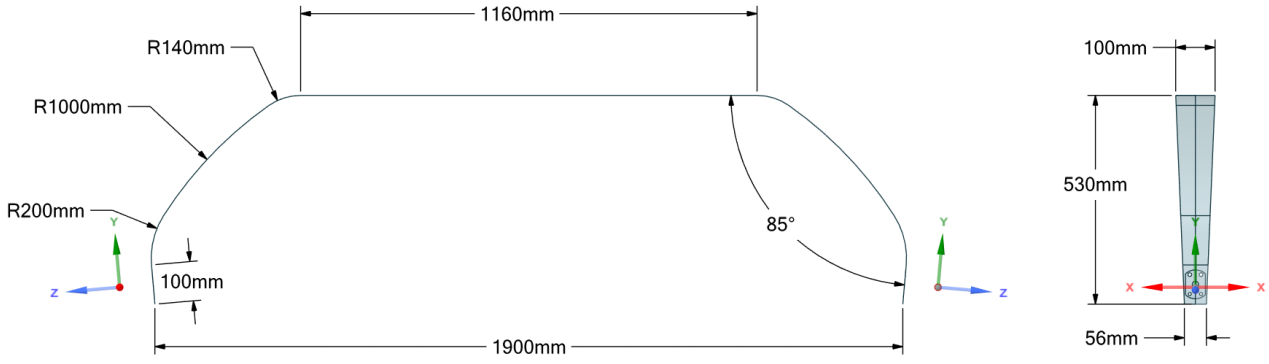


*Figure 108: 1st Stage Analysis Composite Undercarriage Dimensions*

Figure 109, illustrates the load and constraint application for the composite gear. The gear was fixed at the top bar section to reduce the bending stress in this section during impact. The remote displacement was put on the bracket section since bracket mountings used on composite gears situated in this region had some flexibility to rotate by reducing the stresses in undercarriage leg and increase flexibility during landing. The ground reaction loads from the tyres were applied to the axle coordinate system created and was linked to the imprinted face of the stub axle attachment illustrated in Figure 105. The frictional moment exerted on the stub axles were shifted towards the face of the imprinted axle. The applied ground and frictional loads would represent a level landing of the taildragger aircraft at a MTOW of 600 kg during limit load and ultimate load conditions. The load magnitudes could be found in Table 9 to Table 12. Note that the mesh element size was 10 mm as validated for the Aluminium 7075 T6 alloy undercarriage.

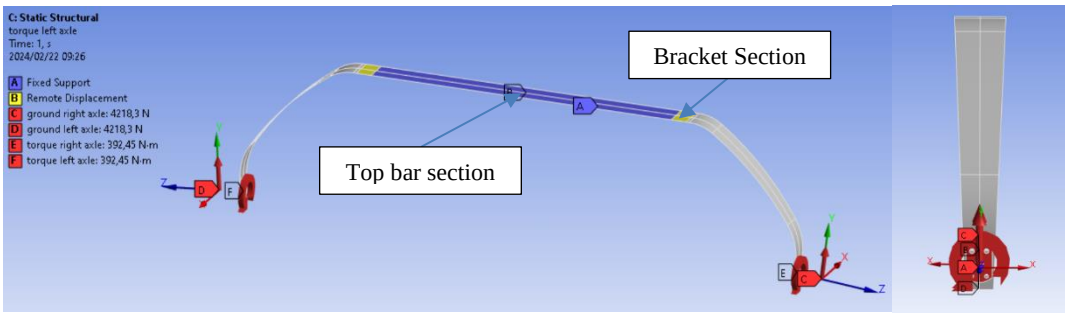


*Figure 109: Composite Undercarriage 1st Stage Analysis Load Application (Limit Load)*

Figure 110 illustrates the deflection of the composite undercarriage at limit load conditions. The limit load X, Y, Z deflections of the 1st stage analysis was 61.454 mm, 34.932 mm, and 8.879 mm respectively. During ultimate load conditions the deflections were 99.942 mm, 56.661 mm, and 12.72 mm respectively.

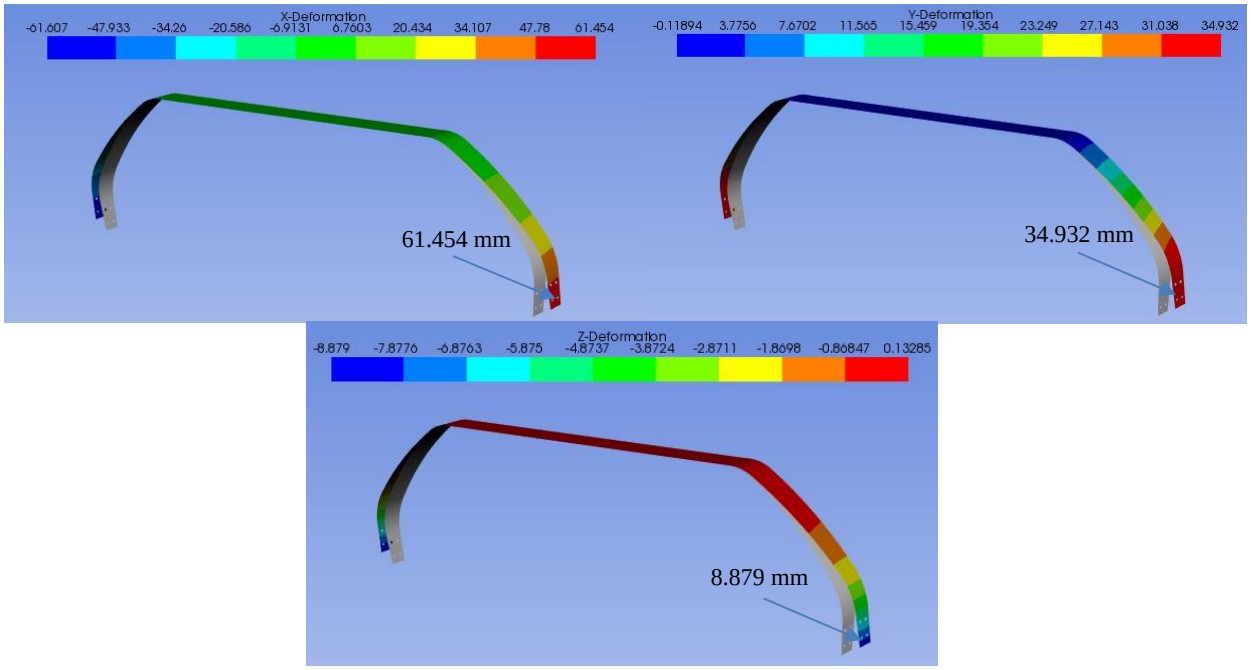


*Figure 110: Composite Undercarriage 1st Stage Analysis X, Y, Z Deformation (Limit Load)*

Figure 111 and Figure 112 illustrates the inverse reserve factor of the Puck-failure criterion for the 20 plies situated in the top stack up which was the least effective in withstanding the ground reaction loads and frictional loads during limit load and ultimate load conditions. During limit and ultimate load conditions the 0-degree plies more were prone to matrix tensile failure than fibre failure whilst the ±45-degree plies were more prone to matrix shear failure than matrix compressive failure. Note that if the inverse reserve factor exceeded 1, then failure occurred either in the fibre or matrix of the laminate indicated by Ansys. Also note that matrix tensile failure could occur in a compressive region since the strut undergoes combined loading conditions.

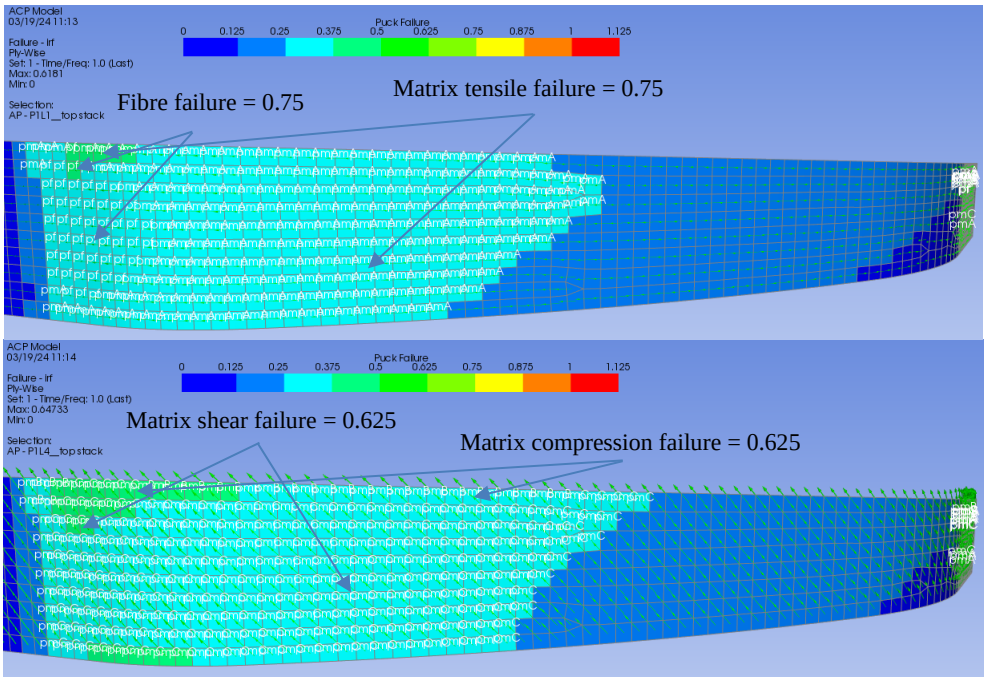


*Figure 111: Composite Undercarriage 1st Stage Analysis Puck Failure Worst Ply (Top Stack Up-Limit Load)*

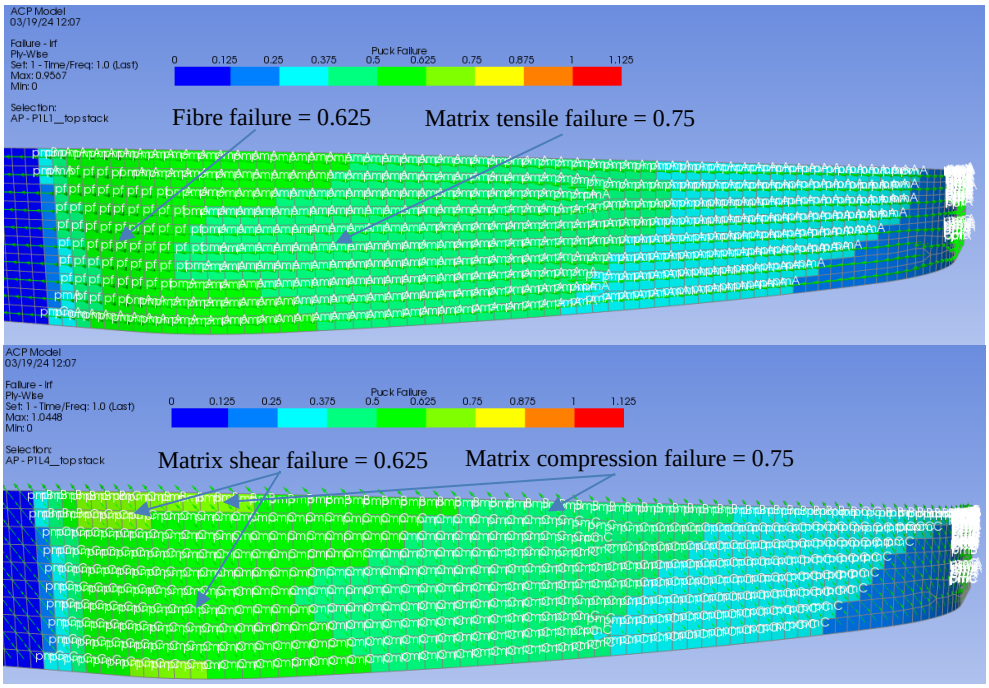


*Figure 112: Composite Undercarriage 1st Stage Analysis Puck Failure Worst Ply (Top Stack Up-Ultimate Load)*

Figure 113 and Figure 114 illustrates the inverse reserve factor of the Puck-failure criterion for the 90 fibre plies situated in the core stack up which was the least effective in withstanding the ground reaction loads and frictional loads during limit load and ultimate load conditions. During ultimate load conditions, matrix tensile failure/ cracking occurred in ±45-degree fibre layers. Note that the 0-degree unidirectional fibres were able to withstand failure during ultimate load conditions as the maximum inverse reserve factor was 0.75 for both fibre failure and matrix tensile failure. Note that most of the stress was concentrated near the bend section next to the bracket region during ultimate load conditions. Thus, during ultimate load conditions the gear would fail in its bottom core region resulting in the landing gear not being able to endure further operation.

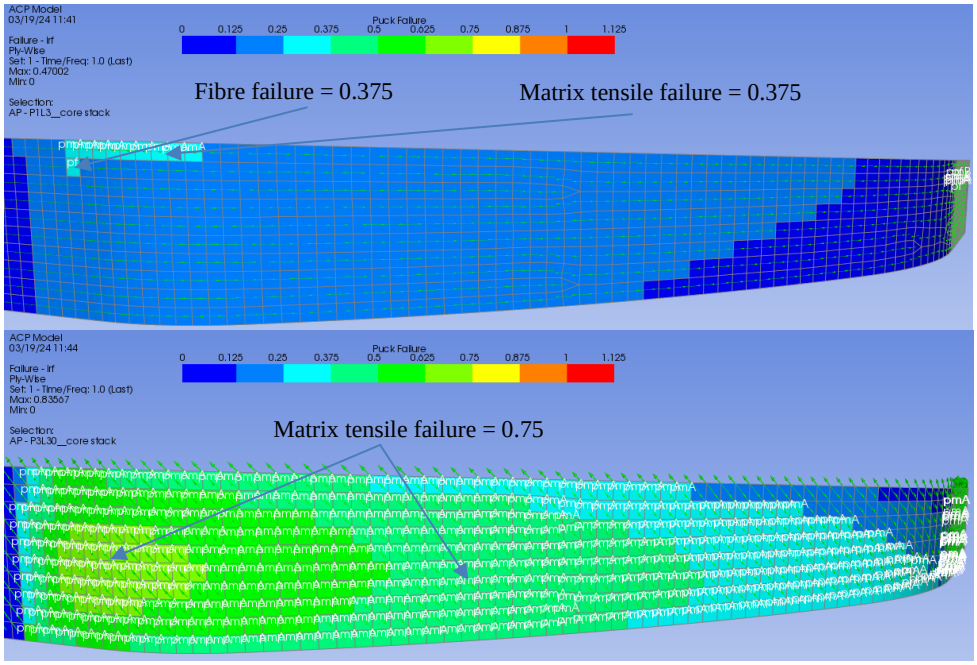


*Figure 113: Composite Undercarriage 1st Stage Analysis Puck Failure Worst Ply (Core Stack Up-Limit Load)*

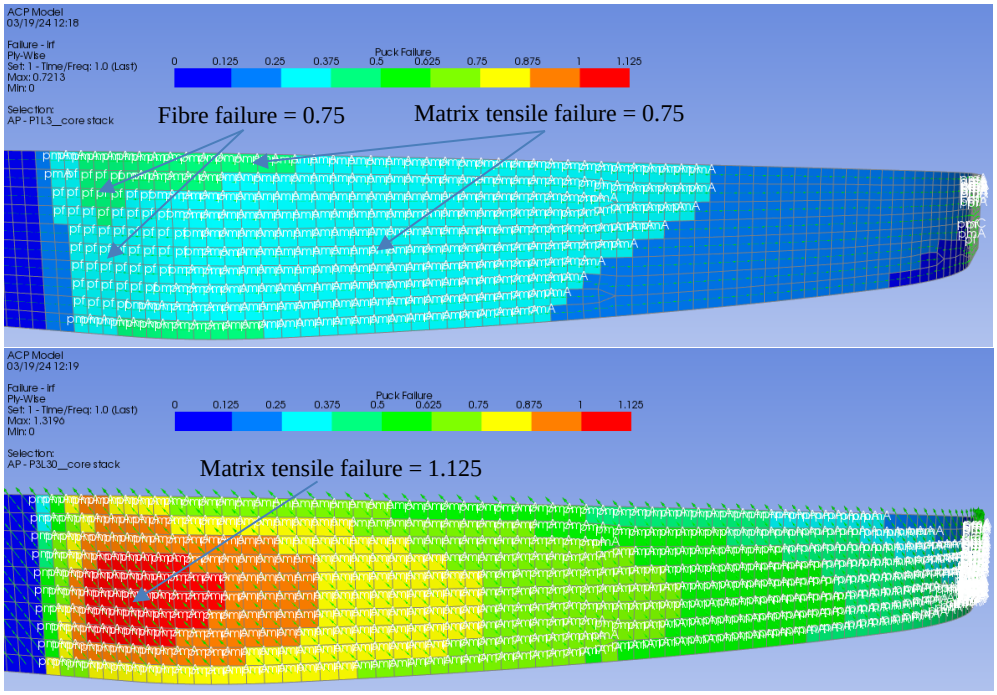


*Figure 114: Composite Undercarriage 1st Stage Analysis Puck Failure Worst Ply (Core Stack Up-Ultimate Load)*

Figure 115 and Figure 116 illustrates the inverse reserve factor of the Puck-failure criterion for the 20 plies situated in the bottom stack up which was the least effective in withstanding the ground reaction loads and frictional loads during limit load and ultimate load conditions. The 0-degree UD fibres were able to withstand the loads as the maximum inverse reserve factor was 0.75 for matrix tensile failure. During ultimate load conditions, the ±45-degree plies failed significantly due to matrix tensile failure and cracking. Thus, during ultimate load conditions the bottom stack up will not survive the ground reaction and frictional loads.

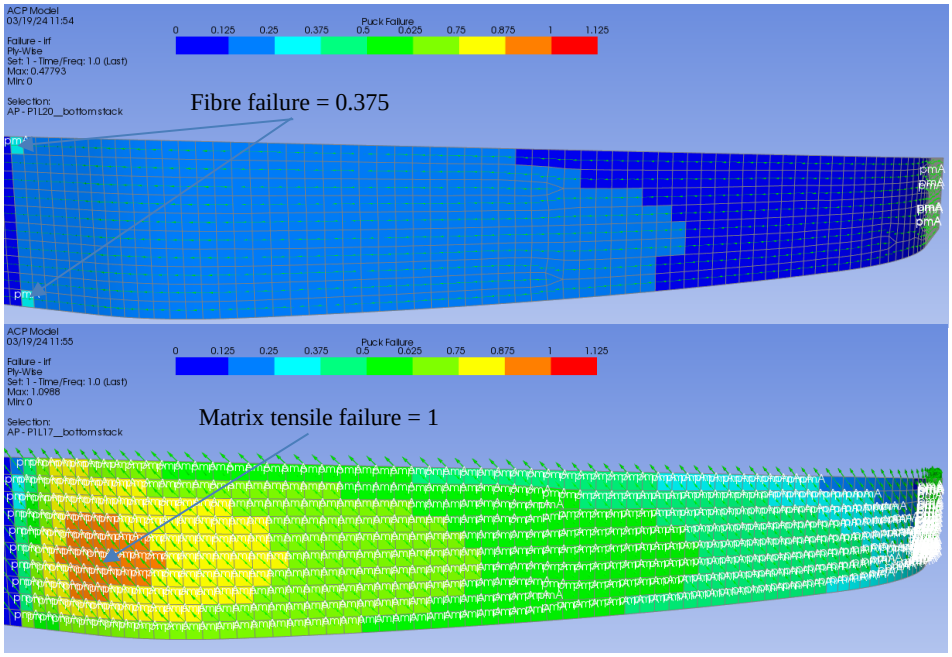


*Figure 115: Composite Undercarriage 1st Stage Analysis Puck Failure Worst Ply (Bottom Stack Up-Limit Load)*

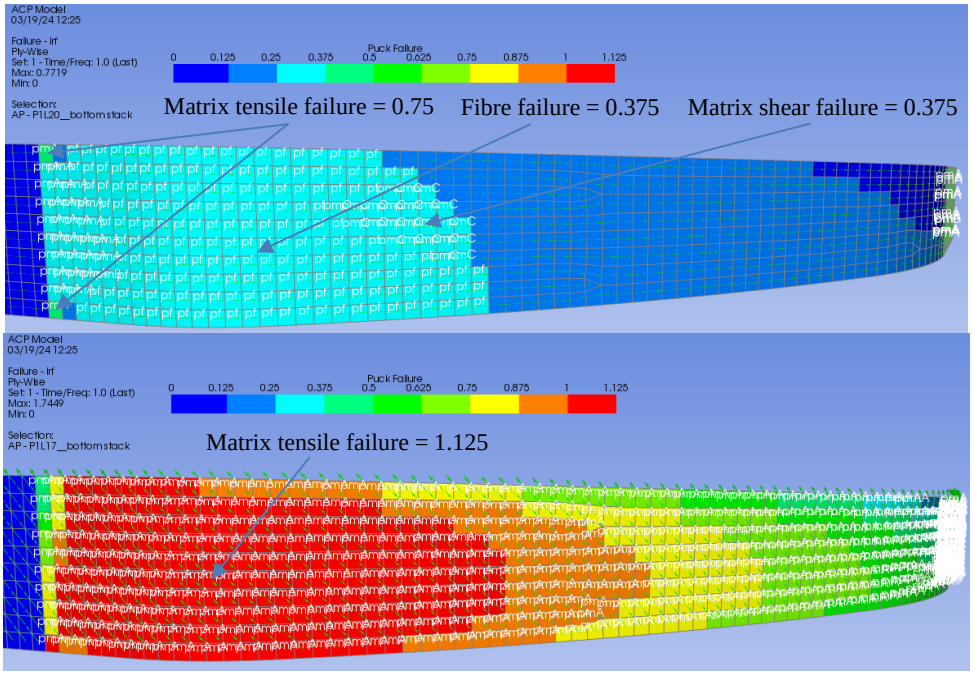


*Figure 116: Composite Undercarriage 1st Stage Analysis Puck Failure Worst Ply (Bottom Stack Up-Ultimate Load)*

In Figure 117 illustrates that the ±45-degree fibre plies near the bottom region of the fibre stack up would result in a combination of matrix tensile failure and cracking during limit and ultimate load conditions.

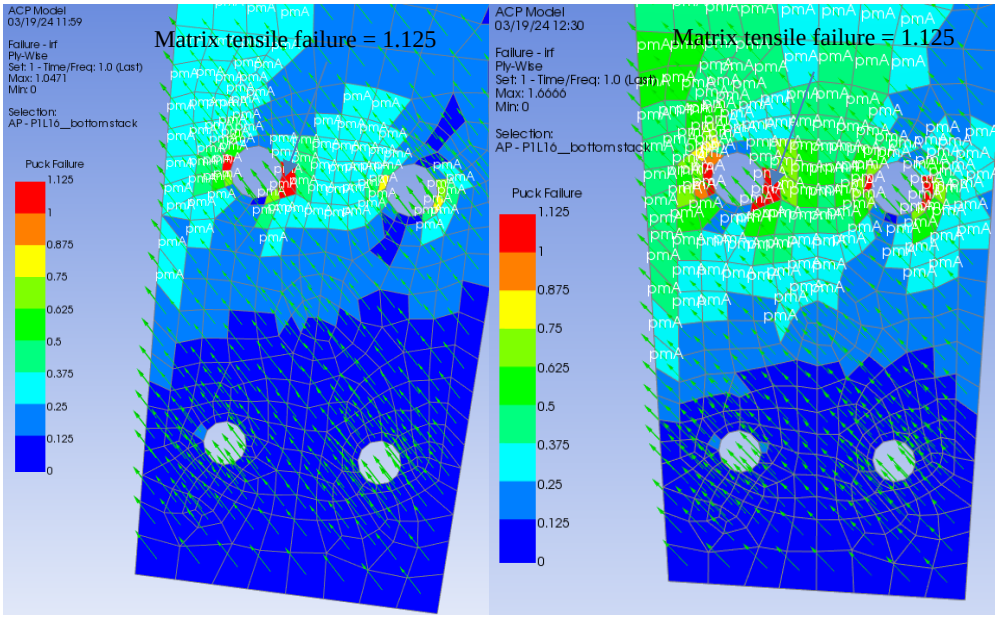


*Figure 117: Composite Undercarriage 1st Stage Analysis in Axle Region Puck Failure (Limit and Ultimate Load)*

In conclusion with regards to the 1st stage analysis of the composite undercarriage alternative, the gear of similar dimension and fibre layup orientation would not survive a level landing condition at MTOW of 600 kg at ultimate load conditions for the tricycle and taildragger light sport aircraft. During these load conditions the ±45-degree fibre layups at the bottom stack up failed due to Puck inter-fibre tensile failure and cracking. These fibres also resulted in matrix tensile failure and cracking near the bolted regions drilled for the stub axles. Thus, the fibre orientations needed to be adjusted to survive the ultimate load (emergency) conditions at MTOW of 600 kg. From the results obtained it could be concluded that the top leg arc radius should be increased to better distribute the load over a larger surface area in the composite undercarriage top bend section. The damping of the composite gear during landing should be modified by increasing the gear length that would increase vertical deflection to obtain a smoother landing.

### 11.6.3 2nd Stage Analysis (Fibre Orientation, Leg Arc Angle, Gear Length/ Width)

In the 2nd stage analysis, the fibre orientations were adjusted for the top, core, and bottom layups whilst a fibre thickness of 0.2159 mm was used. The ±45-degree critical fibre plies were replaced with ±15-degree fibre layers and the non-critical ±45-degree fibres were replaced with ±30-degree fibre layers. The usage of 90-degree plies were eliminated since they did not have enough strength to withstand the type of stresses and strains experienced during landing conditions at higher load factors. The symmetry of fibre layup from the mid-plane of the laminate to outermost fibres was obtained when changing the fibre orientations. This layup orientation should decrease the strain of the landing gear as validated by the coupon study. The thickness of the gear remained the same as well as being uniform in thickness throughout.

*Table 36: Composite Undercarriage 2nd Stage Analysis Epoxy E-Glass UD Prepreg Layup*

| Stack Up Section | Ply Amount | UD Epoxy E-Glass Prepreg (0.254 mm) Layup sequence | Thickness (mm) |
|---|---|---|---|
| Top | 1 | [0/0/0/15/-15/0/0/15/-15/0/0/-15/15/0/0/-15/15/0/0/0] | 4.318 |
| Core | 3 | [15/-15/0/0/15/-15/0/-30/0/30/30/0/-30/0/-15/-15/0/-30/0/30/30/0/-30/0/-15/15/0/0/-15/15] | 19.431 |
| Bottom | 1 | [0/0/0/15/-15/0/0/15/-15/0/0/-15/15/0/0/-15/15/0/0/0] | 4.318 |

In Figure 118, the radius of the top bending section was increased from 140 mm to 250 mm to better distribute the concentrated stress during level landing at ultimate load conditions. The gear length was increased to 2060 mm making the gear wider however, this could increase the stresses and strains experienced by the matrix and fibres further along the strut due to an increase in vertical deformation. The top beam length remained the same as increasing the gear length would increase the leg arc angle to approximately 40.333° as seen in Figure 103. This would provide better damping of the gear at limit load and ultimate load conditions. The camber angle also remained the same at a positive 5°. The composite gear strut was tapered from 100 mm down to 60 mm to slightly increase the leg width. This was due to the gear having no ±45-degree fibre plies to reduce the strain exerted on the gear because of frictional loads exerted on the tyres.

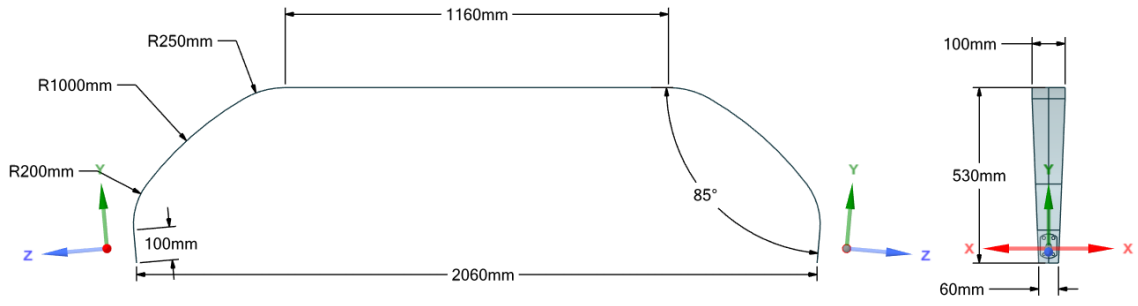


*Figure 118:2nd Stage Analysis Composite Undercarriage Dimensions*

Figure 119 illustrates the limit load application the modified 2nd stage composite undercarriage. The load application was applied using the same method as was used during the 1st stage analysis. The ground reaction and tyre frictional loads can be found in Table 9 to Table 12 for both limit load and ultimate load conditions.

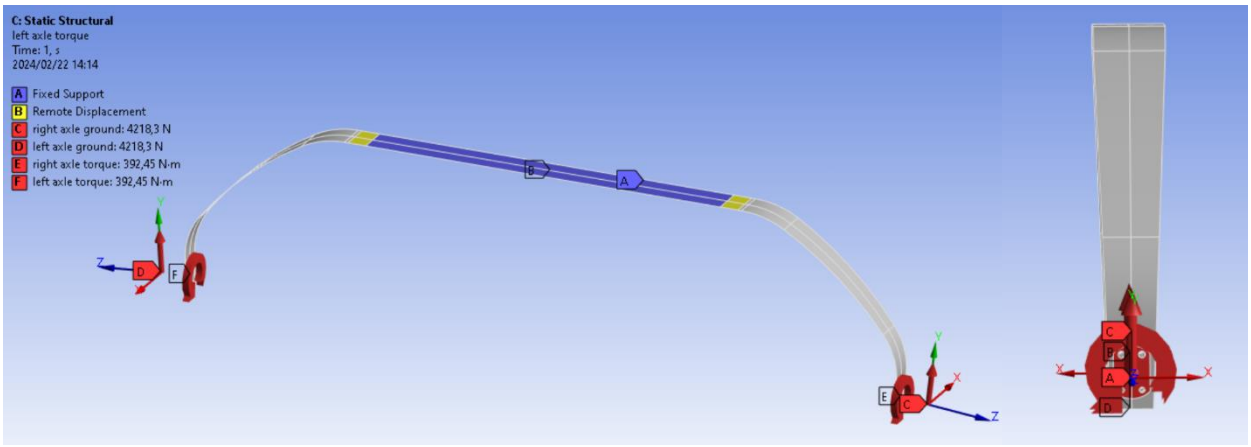


*Figure 119: Composite Undercarriage 2nd Stage Analysis Load Application (Limit Load)*

In Figure 120, the limit load X, Y, Z deflection of the modified 2nd stage composite undercarriage was 57.825 mm, 39.705 mm, and 13.132 mm respectively. During ultimate load conditions, the X, Y and Z deflections were 93.987 mm, 64.318 mm, and 18.827 mm respectively.

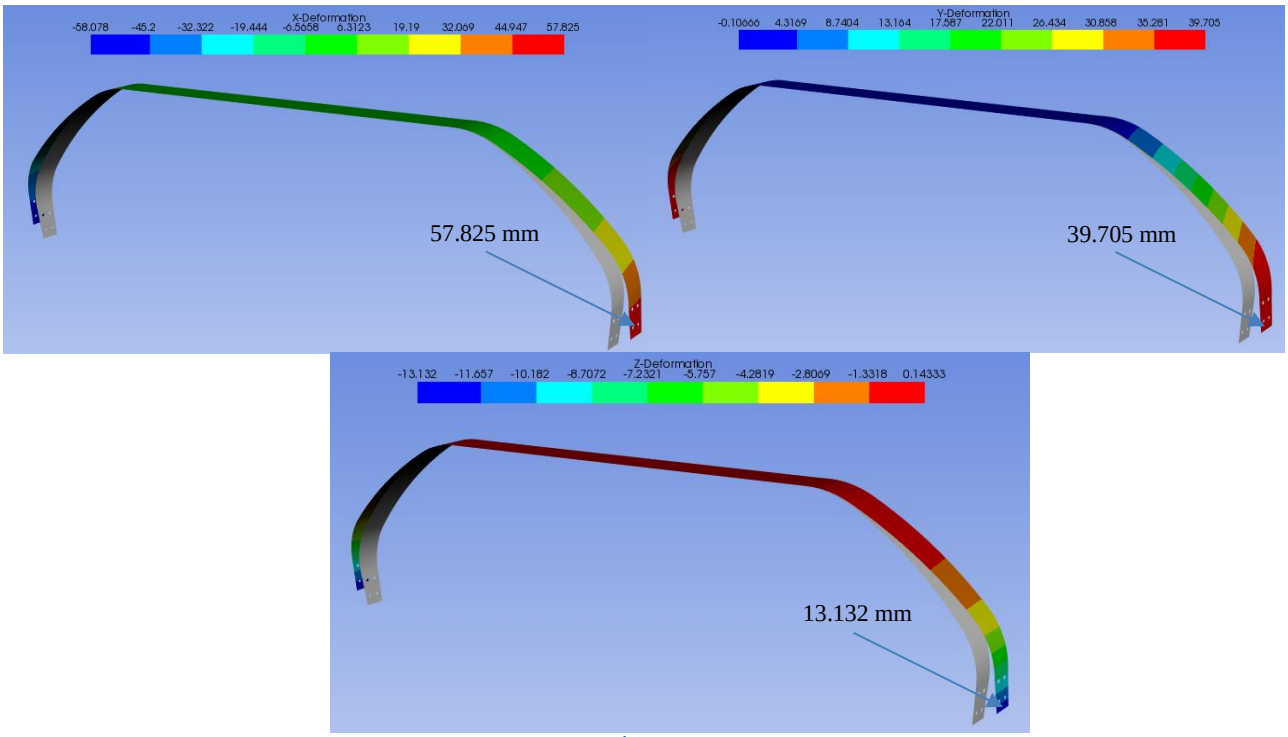


*Figure 120: Composite Undercarriage 2nd Stage Analysis X, Y, Z Deformation (Limit Load)*

In comparison to the 1st stage composite landing gear, the deformation in the X-direction decreased with 3.629 mm whilst the deformation in the Y direction increased with 4.773 mm and Z-direction with 4.253 mm.

In Figure 121 and Figure 122, the exposed 0-degree unidirectional top fibre layer was more prone to fibre failure and matrix tensile cracking whilst the ±15-degree fibre layers were more prone to matrix compressive failure and cracking. The maximum inverse reserve factor for limit load conditions were 0.375 and for ultimate load conditions 0.75. Thus, the fibres represented in the first 20 plies of the top stack up was strong enough to resist failure during high load factors at an aircraft MTOW of 600 kg.

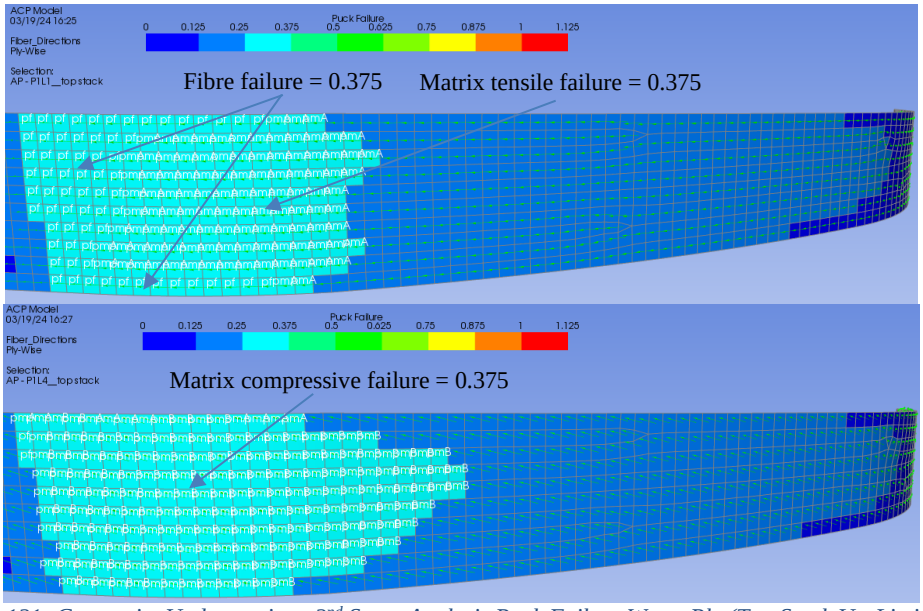


*Figure 121: Composite Undercarriage 2nd Stage Analysis Puck Failure Worst Ply (Top Stack Up-Limit Load)*

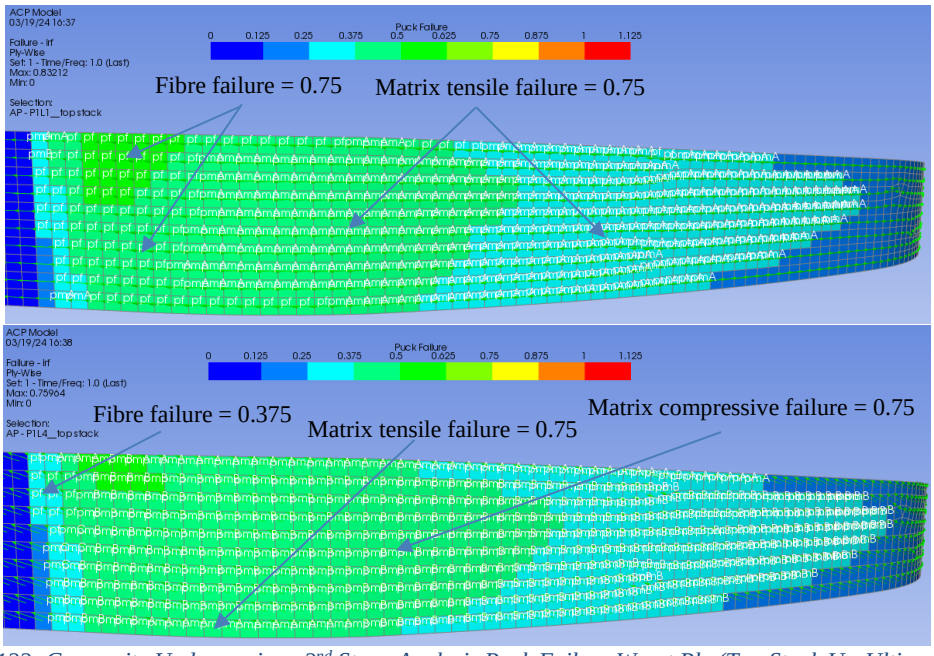


*Figure 122: Composite Undercarriage 2nd Stage Analysis Puck Failure Worst Ply (Top Stack Up-Ultimate Load)*

In Figure 123, the 0-degree UD fibre plies were not prone to any significant fibre-, tensile-, compressive and shear failure during limit load conditions whilst the ±30-degree fibre plies were more prone the matrix tensile failure. Figure 124 illustrates that during ultimate load conditions, the maximum Puck failure inverse reserve factor was 0.75 for the ±30-degree plies near the bottom of the core stack up. The 0-degree UD fibre at the top of the core stack up during ultimate load conditions was more prone to fibre failure and matrix tensile cracking by having a maximum Puck inverse reserve factor of 0.375. Thus, the fibres in the core stack up was able to resist failure during higher load conditions.

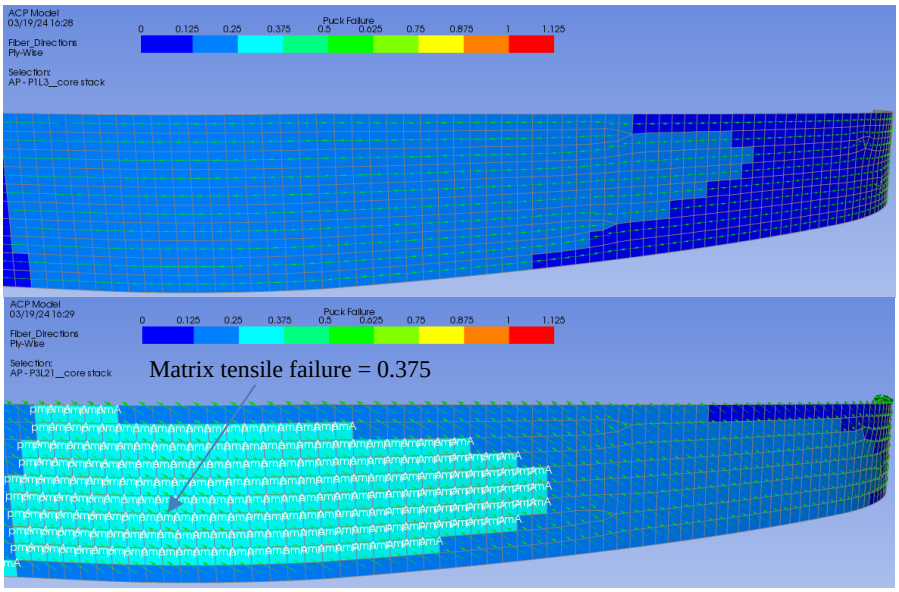


*Figure 123: Composite Undercarriage 2nd Stage Analysis Puck Failure Worst Ply (Core Stack Up-Limit Load)*

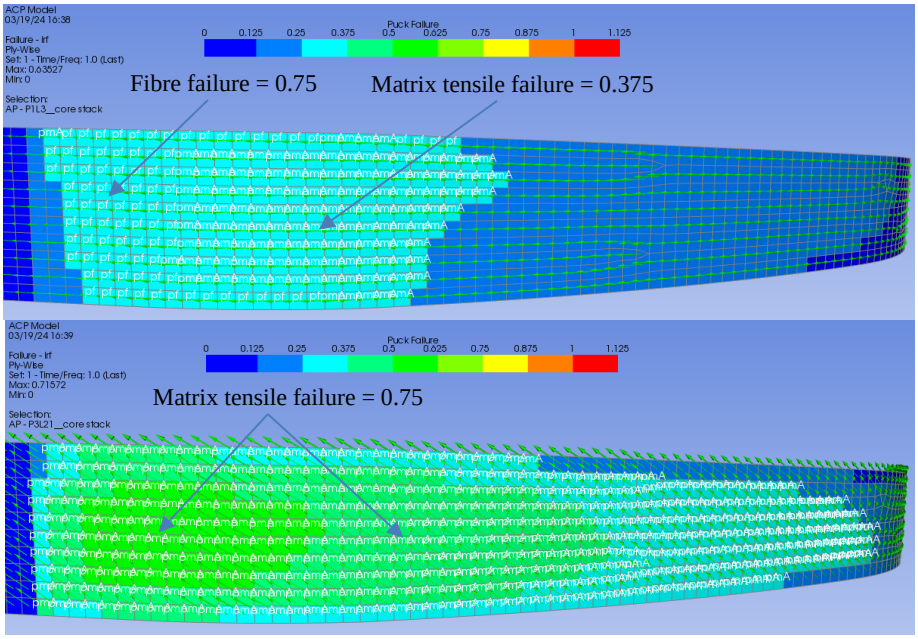


*Figure 124: Composite Undercarriage 2nd Stage Analysis Puck Failure Worst Ply (Core Stack Up-Ultimate Load)*

In Figure 125, the ±15-degree fibre plies in the bottom stack up were more prone to matrix tensile failure whilst the 0-degree unidirectional fibres were not prone to any significant matrix or fibre failure. In Figure 126, the 0-degree UD plies were prone to both matrix tensile- and compressive failure. The bottom section of the undercarriage experienced tension due to bending, but compression was also present due to the torsional load due to the friction on the tyres which created a combined loading scenario or of axis-loading. The ±15-degree fibre plies in the bottom stack were more prone the matrix tensile failure during ultimate load conditions

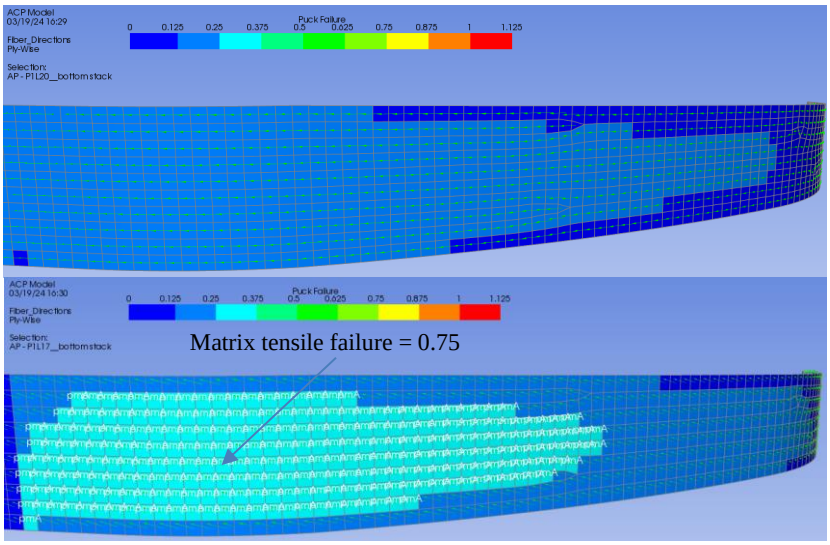


*Figure 125: Composite Undercarriage 2nd Stage Analysis Puck Failure Worst Ply (Bottom Stack Up-Limit Load)*

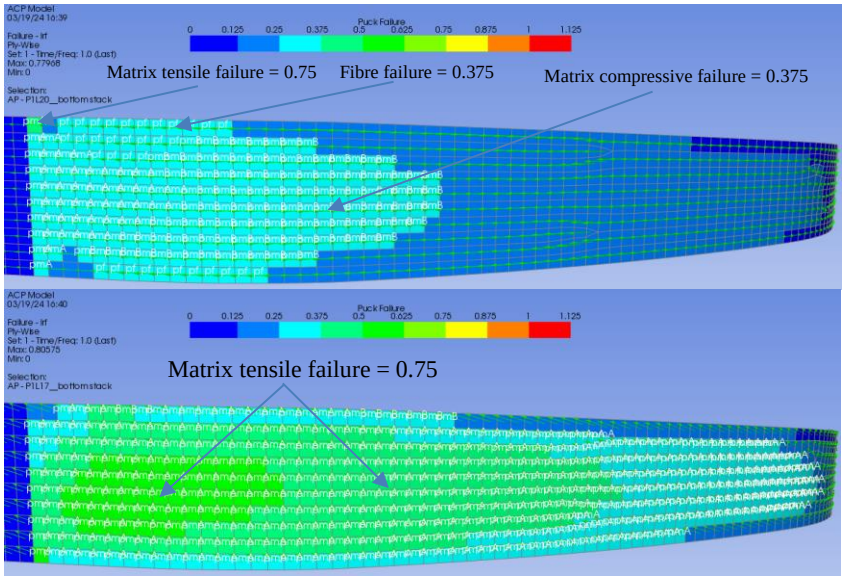


*Figure 126: Composite Undercarriage 2nd Stage Analysis Puck Failure Worst Ply (Bottom Stack Up-Ultimate Load)*

Figure 127 illustrates that during ultimate load conditions, matrix tensile failure was more likely to occur at the bolted regions resulting in failure. During ultimate load conditions the Puck failure inverse reserve factor was 1 which indicated that failure was present. This region should be modified to distribute the concentrated load of the stub axles across a wider surface area.

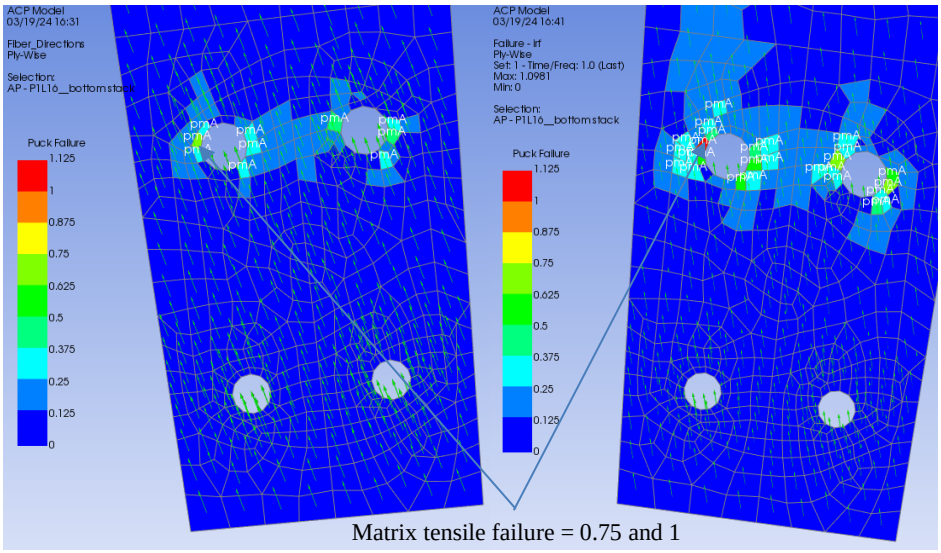


*Figure 127: Composite Undercarriage 2nd Stage Analysis in Axle Region Puck Failure (Limit and Ultimate Load)*

In conclusion by replacing the ±45-degree plies with ±15-degree and ±30-degree plies, the composite gear had a higher resistance to matrix tensile, compression and shear failure as well as fibre tensile, compressive, and shear failure. From the results obtained, distributing the stress throughout the gear strut resulted in the composite undercarriage being less prone to any matrix or fibre failure. This would increase the life span of the gear during everyday operations and make the gear strong enough to withstand emergency load conditions at a MTOW of 600 kg. At the axle region in the bottom stack up the fibres could be crushed at higher load conditions. Thus, to prevent matrix failure and crushing of fibres occurring during ultimate load conditions near the bolted section, the loads could to be distributed across a wider surface area. Steel alloy shims could be manufactured and placed beneath the stub axles and nuts to prevent shear out of the matrix and fibres near bolted regions during landing. Note that the teel alloy shims could corrode over an extended period thus, adequate protection is needed by means of protective coatings.

### 11.6.4 3rd Stage Analysis (Camber Angle and Axle Plates)

In 3rd stage analysis, the camber angle was adjusted to a positive 8 degrees to analyse the effect it had on the X, Y, Z deflections of the modified 3rd stage composite undercarriage. This was the same positive camber angle used on the Aluminium 7075 T6 undercarriage. The leg arc angle remained the same at 40.333 degrees. The loads were applied onto a wider surface area at the axle region which represented the 2 mm Steel alloy shims that distributed the stresses more effectively across a wider surface area to prevent cracking at the bolted regions. The fibre orientations remained the same as used during the 2nd stage analysis.

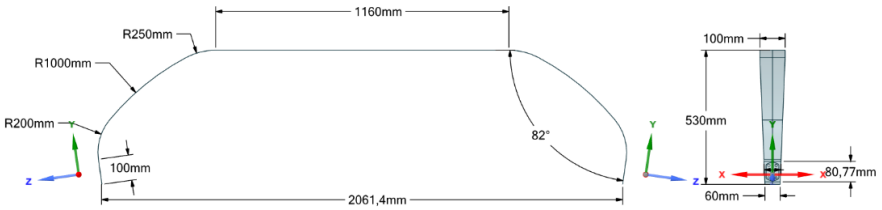


*Figure 128: 3rd Stage Analysis Composite Undercarriage Dimensions*

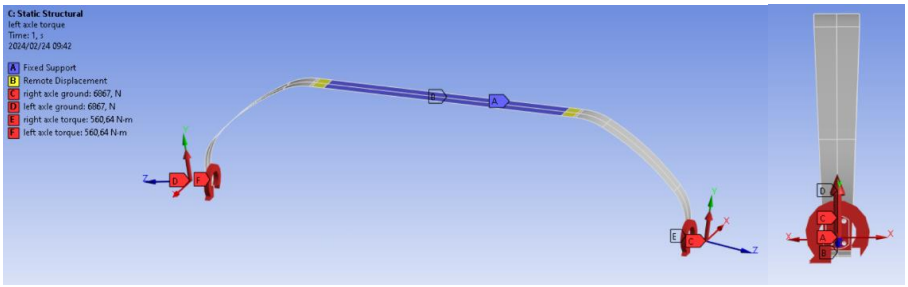


*Figure 129: Composite Undercarriage 3rd Stage Analysis Load Application (Limit Load)*

In Figure 130 the limit load X, Y, Z deflection of the modified 3rd stage composite undercarriage was 60.903 mm, 42.133 mm, and 13.937 mm respectively. During ultimate load conditions, the X, Y and Z deflections were 99.005 mm, 68.26 mm, and 19.981 mm respectively.

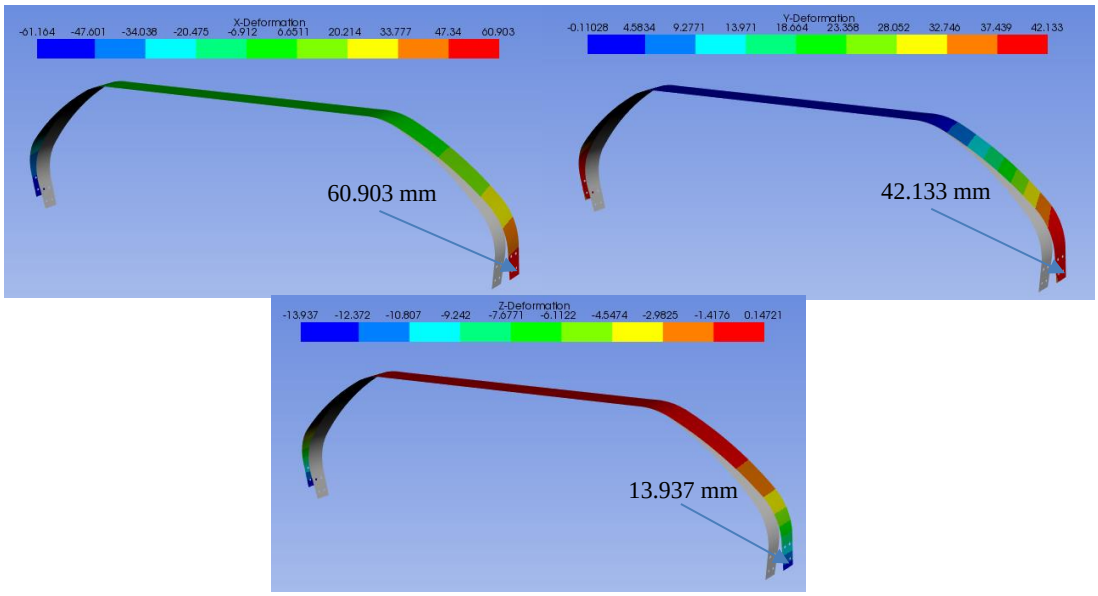


*Figure 130: Composite Undercarriage 3rd Stage Analysis X, Y, Z Deformation (Limit Load)*

In comparison to the 2nd stage analysis, the modified 3rd stage composite landing gear illustrated in Figure 128 had 3.078 mm increase in deformation in the X-direction. The deformation in the Y-direction increased with 2.428 mm and increased with 0.805 mm in the Z-direction.

Figure 131 illustrates that the stress and strains were distributed over a slightly larger surface area due loads being transferred directly to the shims at the axle region. This region was still prone to matrix tensile failure in the 16th fibre ply in the bottom stack up during limit load conditions, but resulted in matrix tensile failure at ultimate load conditions. The fibre plies in the top- and core stack up were prone to a combination of matrix tensile, compression and shear failure but no significant failure occurred. It was concluded that this region of the gear should still be inspected after a landing condition during ultimate (emergency) conditions has been attempted to make sure the landing gear was still in a working condition.

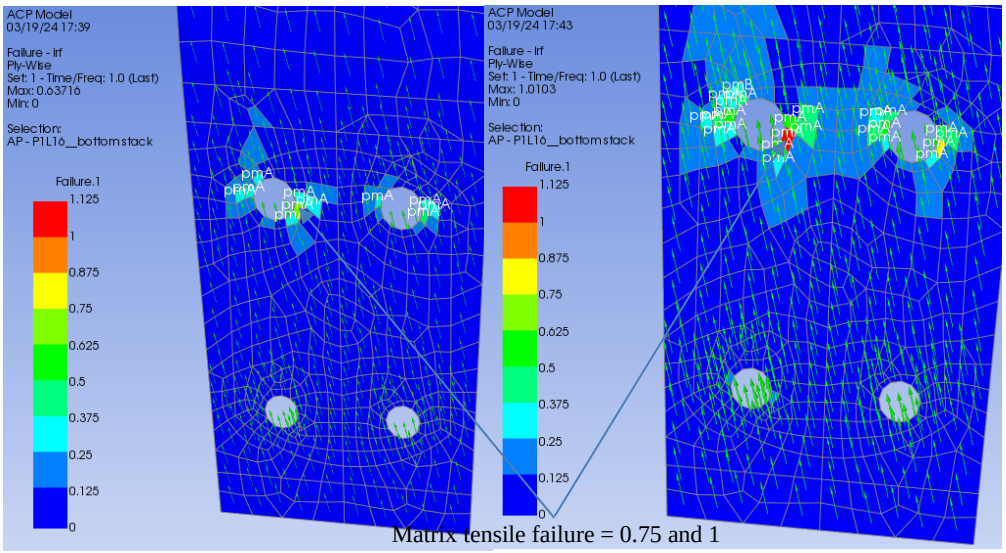


*Figure 131: Composite Undercarriage 3rd Stage Analysis in Axle Region Puck Failure (Limit and Ultimate Load)*

In summary, increasing the positive camber angle by 3 degrees resulted in an increase in the X, Y and Z deflections under limit- and ultimate load conditions thus, increasing the shock absorption to ensure a smoother landing. From FEA results obtain, the incorporation of 2 mm Steel alloy shims at the axle region of the composite undercarriage structure reduced failure in the plies. The matrix tensile failure still occurred during ultimate load conditions. By attempting an emergency landing it would still be crucial to inspect the composite undercarriage for any signs of failure represented by cracks or delamination of the fibers. Small cracks in the composite undercarriage would reduce the fatigue life of the gear.

### 11.6.5 Composite Undercarriage Deformation Analysis Results

In Table 37, the deformation of the 1st, 2nd, and 3rd stage analysis were provided and compared. For the 3rd stage analysis, the vertical deformation was modified to absorb the most impact during limit and ultimate load conditions whilst the horizontal deformation increased. The deflection near the bolted regions also increased on the modified 3rd stage composite landing gear. See section 11.5.5 for deformation comparisons between the modified composite landing gear and Aluminium 7075 T6 alloy gear.

*Table 37:Composite Undercarriage Analysis Stage Deformation Comparisons*

| Analysis Stage | X-Deformation (mm) | Y-Deformation (mm) | Z-Deformation (mm) |
|---|---|---|---|
| **Limit Load Conditions (2.1)** | | | |
| 1st Stage | 61.454 | 34.932 | 8.879 |
| 2nd Stage | 57.825 | 39.705 | 13.132 |
| 3rd Stage | 60.903 | 42.133 | 13.937 |
| **Ultimate Load Conditions (3)** | | | |
| 1st Stage | 99.942 | 56.661 | 12.72 |
| 2nd Stage | 93.987 | 64.318 | 18.827 |
| 3rd Stage | 99.005 | 68.26 | 19.981 |

### 11.6.6 Taildragger Undercarriage Deformation Results Comparison

Figure 132 and Figure 133 provides the deformations of taildragger aircraft current Aluminium 7075 T6 alloy landing gear and the modified composite landing gear for both level landing and tail down landing at different aircraft weight during limit load and ultimate load conditions. The vertical deflection for the composite landing gear was stiffer in comparison to the Aluminium 7075 T6 landing gear. This is due to Aluminium landing gear radius plate brackets that rotate during landing thus, increasing deflection of the strut. The composite landing gear did not use radius plate brackets thus, eliminating the added deformation obtained. From coupon analysis conducted it was found that strain in the Aluminium 7075 T6 coupons were higher in comparison to the UD Epoxy E-Glass fibre coupons. Thus, it could be concluded that using UD Epoxy E-Glass prepreg fibres for the composite landing gear design resulted in the gear becoming stiffer. Note that increasing the strain in the composite landing gear to increase the strut deflection will result in the prepreg fibres experiencing more stress and result in higher Puck-failure inverse reserve factors.

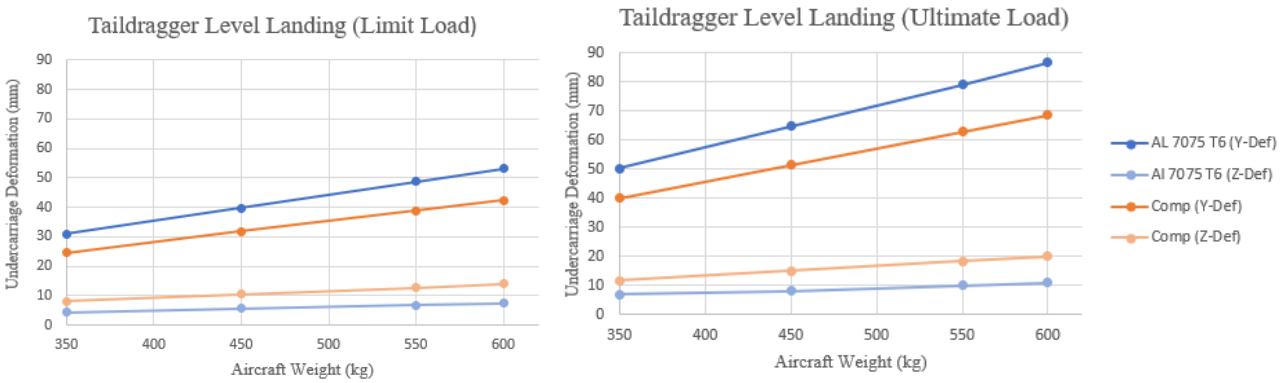


*Figure 132: Taildragger Level Landing (Al 7075 T6 vs Epoxy E-Glass UD Prepreg Undercarriage Deformations)*

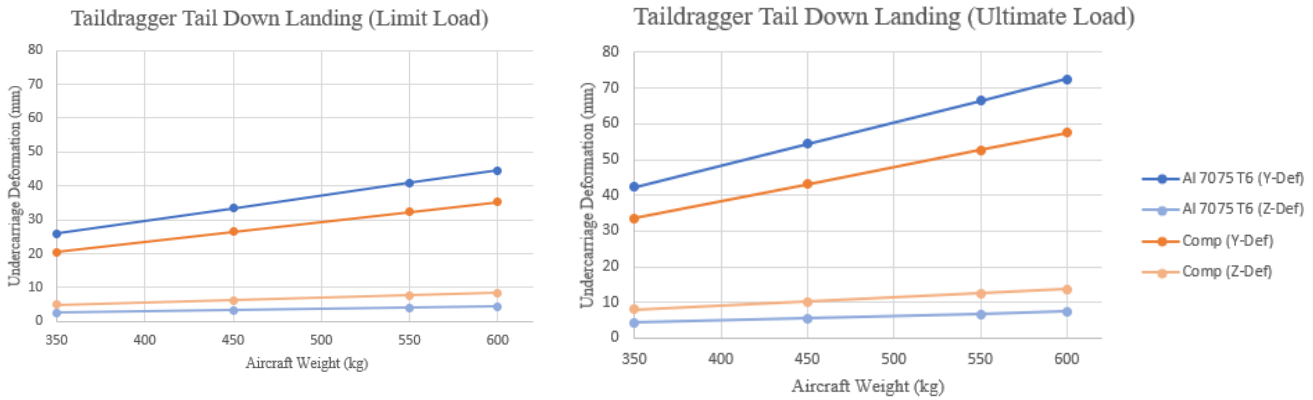


*Figure 133: Taildragger Tail Down Landing (Al 7075 T6 vs Epoxy E-Glass UD Prepreg Undercarriage Deformations)*

### 11.6.7 Tricycle Undercarriage Deflection Results

Figure 134 to Figure 136 provides the Aluminium 7075 T6 alloy and composite landing gear deformation comparisons for the taildragger aircraft at limit load and ultimate load conditions for different aircraft take-off weight. The Aluminium 7075 T6 landing gear obtained greater vertical and less axle region (Z-deformation) deflections in comparison to the composite landing gear. The composite landing gear was modified in both dimensions and fibre orientation to withstand the flexural and torsional load exerted on the strut. These modifications increased the stiffness of the strut to decrease the stresses and strains so that matrix or fibre failure does not occur during limit load and ultimate load conditions. The usage of 0-degree, 15-degree, and 30-degree prepreg fibres obtained better resistance to flexural loads thus, increasing the bending stiffness. The usage of these fibre orientations to withstand the large flexural stress and strains, decreased the torsional strength of the strut due to frictional loads on the tyre thus, increasing the strain in the axle region. In conclusion, the usage of less prepreg fibre plies will increase the vertical deflection of the strut up until it has obtained equivalent deflection in comparison the Aluminium 7075 T6 alloy landing gear, but will result in the prepreg fibre plies experiencing higher stresses and strains making it more prone the matrix and fibre failure.

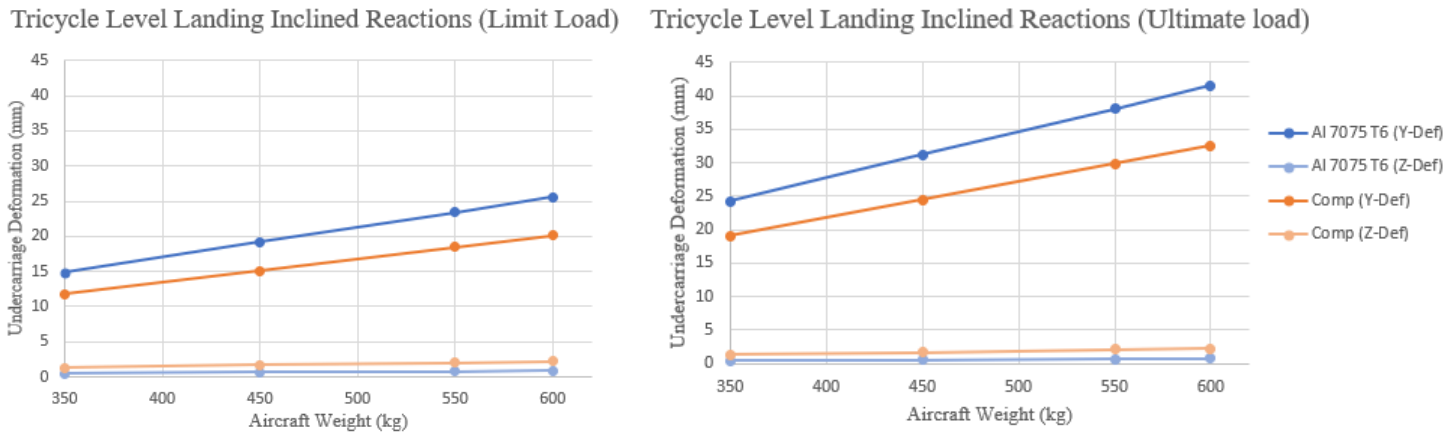


*Figure 134: Tricycle Level Landing Inclined Reactions (Al 7075 T6 vs Epoxy E-Glass UD Prepreg Undercarriage Deformations)*

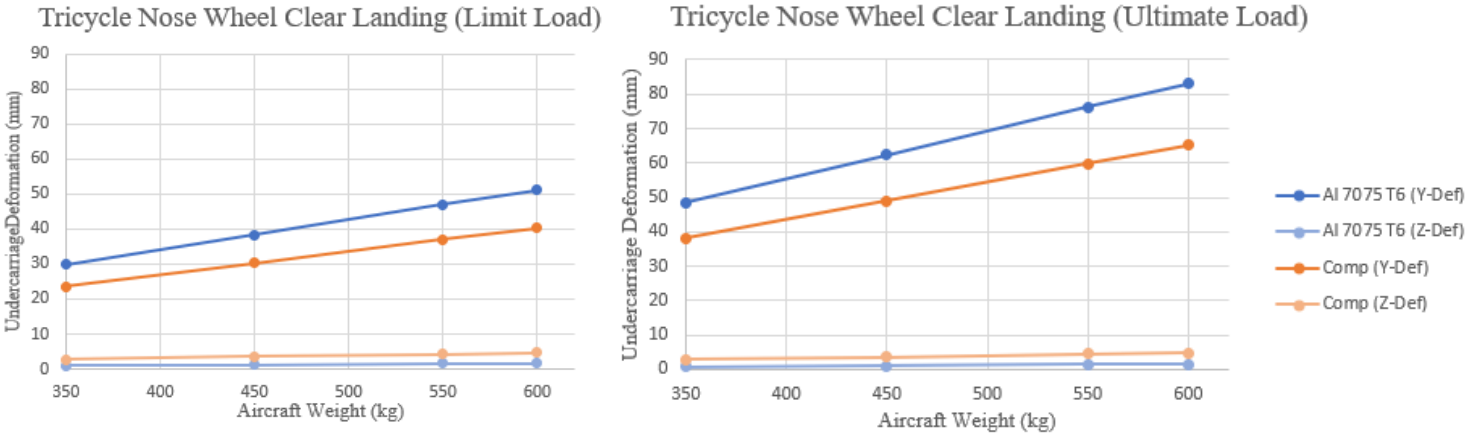


*Figure 135: Tricycle Nose Wheel Clear Landing (Al 7075 T6 vs Epoxy E-Glass UD Prepreg Undercarriage Deformations)*

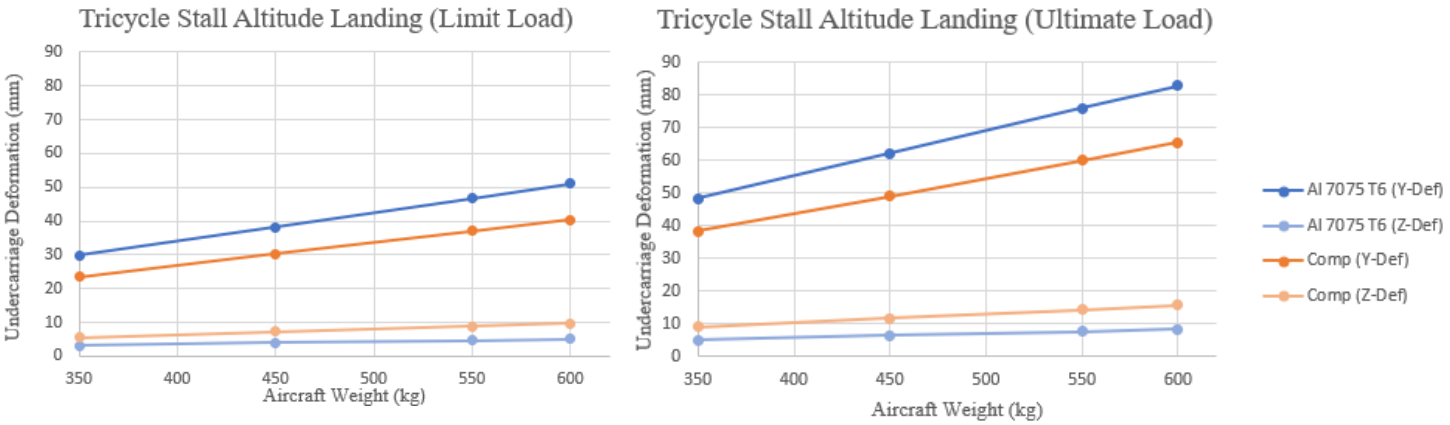


*Figure 136: Tricycle Level Stall Altitude (Al 7075 T6 vs Epoxy E-Glass UD Prepreg Undercarriage Deformations)*

## 12 FINAL COMPOSITE UNDERCARRIAGE

Figure 137, provides the assembly of Aluminium 7075 T6 and composite landing gear. The same brackets that attach to the aircraft were used for the composite gear, but the width of the plate attached to top bar bracket illustrated in Figure 138 was increased since the composite landing gear width was increased to 100 mm. This eliminated the requirement of re-designing the aircraft frame to better suit the new gear. A new bracket attachment was needed to replace the radius plates on the Aluminium 7075 T6 gear to better distribute the load across the top bar section of the composite gear. A 2 mm thick Steel alloy shims attached to the original brackets was used to contribute to the load distribution. The axle, brakes and wheel hub design remained the same to eliminate any significant changes needed to the overall design. The composite gear was 5.067 mm thicker than the Aluminium 7075 T6 alloy gear thus, needing longer bolts at the axle region. The top bolts were AN6 27A whilst the bottom bolts were AN5 27A aircraft bolts used to assemble the stub axles.

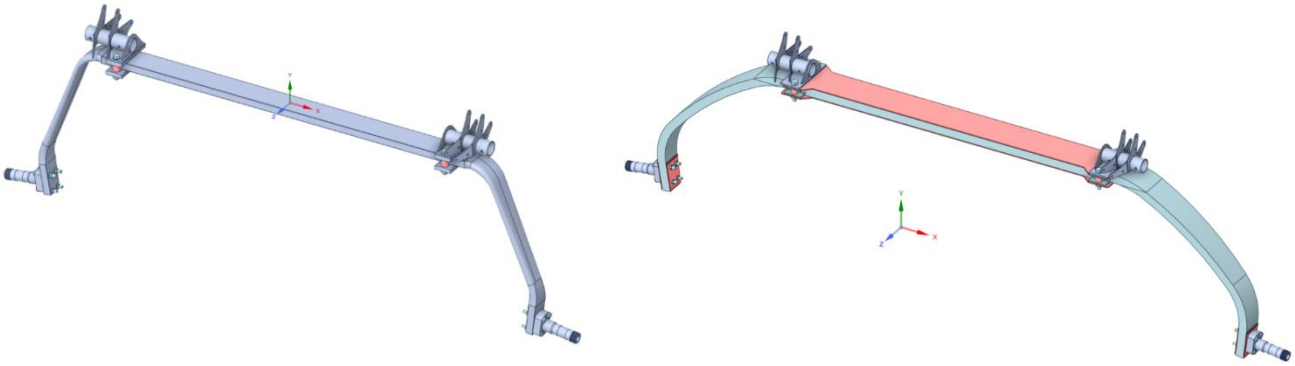

*Figure 137: Aluminium 7075 T6 (Left) vs Composite Undercarriage Assembly (Right) (Tri-metric View)*

Figure 138, provides the front view and side view comparison between the Aluminium 7075 T6 landing gear and the composite landing gear. Appendix B contains the drawings for both landing gears and their brackets.

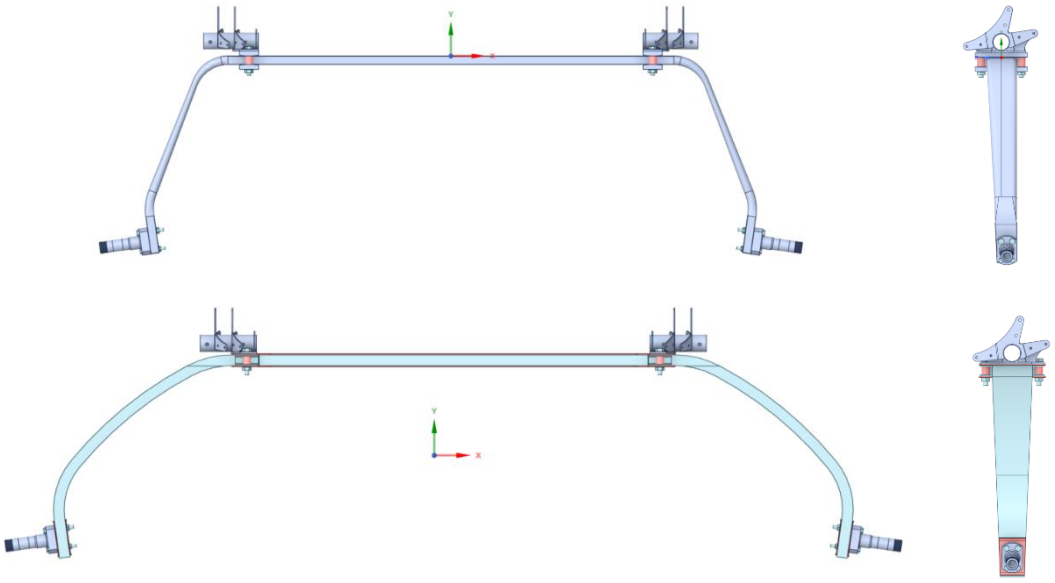

*Figure 138: Aluminium 7075 T6 (Top) vs Composite Undercarriage Assembly (Bottom) (Front and Side View)*

Figure 139 illustrates the UD Epoxy E-Glass Prepreg Landing Gear top bar section modified for the brackets. This was to prevent the landing gear from sliding side-to-side during landing. Note that this modification had no impact on the stresses and strain obtained and analysed during the FEA analysis as it was fixed during FEA analysis using a fixed constraint. Drilling into the composite landing gear to lock it in place was not preferred, thus cutting the prepreg fibre plies into a suitable shape that is aimed at keeping the composite landing gear in place between the brackets was more effective. Note that the width in this section could be increased by any amount, for this design an 8 mm width increase was used on both sides of the top bar section.

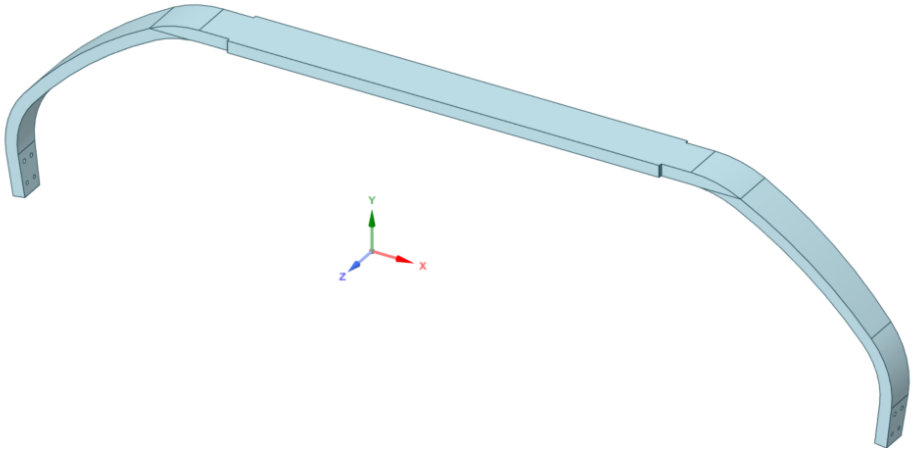

*Figure 139: UD Epoxy E-Glass Prepreg Landing Gear Bracket Slot*

Figure 140 provides the bracket attachment design for the composite undercarriage. The bolts that were used to assemble the original brackets to the attachments where M12×70 mm bolts. A c-bracket was designed to add rigidity to the assembled attachment and to house a sleeve to protect the bolts from any damage. Steel alloy shims could also be manufactured and placed between the original brackets and the top bar bracket to add extra height.

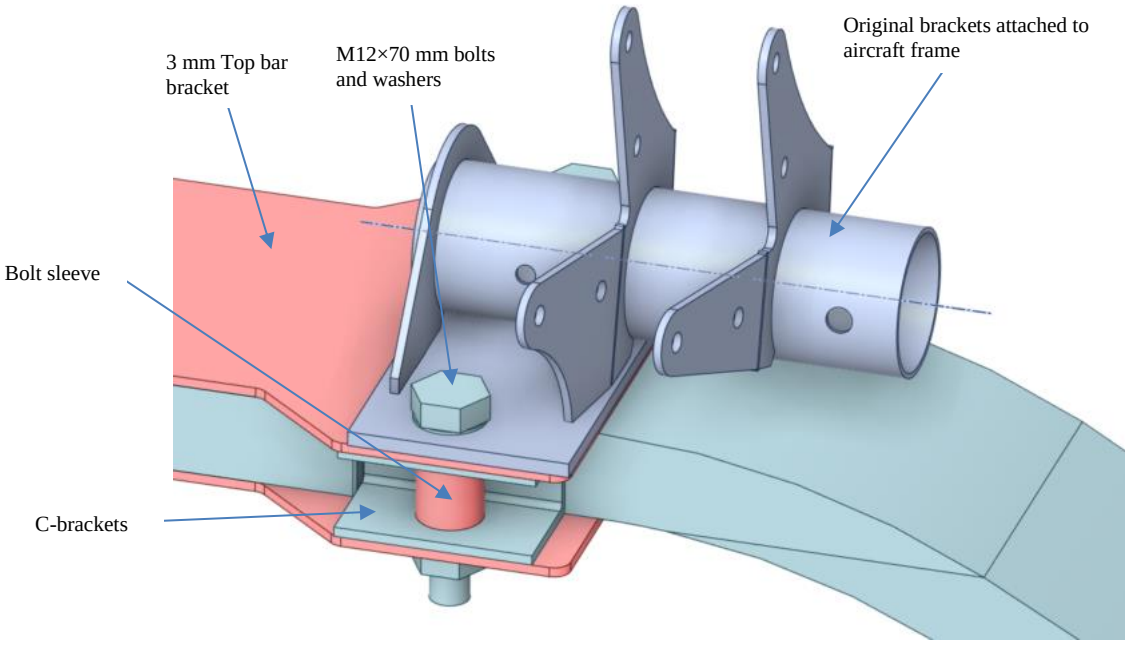


*Figure 140: Composite Undercarriage Bracket Assembly*

Table 38 provides the weight comparison between the Aluminium 7075 T6 alloy landing gear and the UD Epoxy E-Glass Prepreg landing gear. Note that the weight presented does not include the brake assembly and wheel hubs. The composite landing gear and its assembled components was approximately 6.558 kg heavier than the current design. This was due to the composite landing gear being heavier since each individual fibre ply had to withstand the ground reaction and frictional loads exerted onto the gear during limit load and ultimate load conditions. Thus, the composite gear had to occupy a greater volume by increasing the gear width, gear length and gear thickness by adding more prepreg fibre layers to increase its strength. The new attachments to the original brackets were heavier since it had to be redesigned to not exert concentrated stress areas onto the composite landing gear during landing thus, distributing the loads across a wider surface area.

*Table 38: Aluminium 7075 T6 vs UD Epoxy E-Glass Prepreg Landing Gear Weight Comparison*

| **Landing Gear** | **Top Bar Brackets** | **Aircraft Frame Brackets** | **Bolt Sleeve, Radius Plates and C Brackets** | **Bolts, Nuts Washers, and Axle Shims** | **Stub Axles** | **Total Weight** | **Units** |
|---|---|---|---|---|---|---|---|
| Al 7075 T6, UD Epoxy E-Glass Prepreg | Al 6082 T6 | Al 6082 T6 | Al 6082 T6 | 8740 Steel Alloy | Al 6061 T6 | - | - |
| **Aluminium 7075 T6 Alloy Landing Gear** | | | | | | | |
| 10.273 | - | 0.291 | 0.955 | 0.327 | 0.361 | 12.207 | kg |
| **UD Epoxy E-Glass Prepreg Landing Gear** | | | | | | | |
| 14.886 | 2.307 | 0.298 | 0.226 | 0.687 | 0.361 | 18.765 | kg |

### 12.2 Composite Undercarriage Design Summary

In conclusion, the final composite landing gear was design out of a 130 layers of 0.2159 mm thick UD Epoxy-E-Glass prepreg fibres using the Puck-failure criterion to analyse failure occurring in each fibre ply during limit load and ultimate load landing conditions. The composite landing gear was analysed and modified during each optimisation stage to create a composite alternative to the current Aluminium 7075 T6 landing gear that could withstand the same load conditions. The 1$^{st}$ stage composite landing gear was used as a reference model to determine if any modifications were needed. After analysis was conducted on the 1$^{st}$ stage composite landing gear it was found that the ±45-degree fibre plies in the core and bottom stack up failed due to matrix tensile failure at ultimate load conditions. The critical ±45-degree fibre plies were then replaced with ±15-degree fibre plies and the non-critical ±45-degree fibre plies were replaced with ±30-degree fibre plies which could withstand the flexural loads more effectively. To reduce the stress concentrations the ±15-degree and ±30-degree fibre plies, the radius of the top bend section was increased from 140 mm to 250 mm to distribute the stress across a larger surface area. The landing gear was also too stiff in comparison to the Aluminium 7075 T6 landing gear and needed dimensional adjustments. For the 2$^{nd}$ stage composite landing gear, the gear

length was increased from 1900 mm to 2060 mm to obtain a greater vertical deflection which increased the strut arc angle from 34.92° to 40.33°.

After the 2nd stage analysis was conducted, it was found that no fibre or inter-fibre failure occurred in the strut region of the landing gear at limit load and ultimate load landing conditions, but failure occurred near the bolted area at the axle region during ultimate load conditions. It was concluded during the 3rd stage analysis, that 2 mm thick Steel alloy shims should be used to distribute the stresses over a larger surface area and decrease the possibility of bolt bearing failure. It was also concluded that the wheel camber angle should be increased from a positive 5° to a positive 8° to obtain better ground contact of the wheels during landing. After analysis was conducted on the 3rd stage composite landing gear, failure still occurred near the bolted region, but was only present in the 16th fibre ply. Thus, it was concluded that inspection for any matrix failure, fibre failure or delamination were still crucial after attempting landing at ultimate (emergency) load conditions.

The 3rd stage composite landing gear deformations were also compared to the Aluminium 7075 T6 landing gear for different taildragger and tricycle aircraft take-off weight up to the MTOW of 600 kg during all landing conditions specified in the ASTM F2245 – 14 regulations. The composite landing gear had reduced vertical deflection in comparison the Aluminium 7075 T6 landing gear as more strain could result in fibre or inter-fibre failure of the composite gear. The deformations at the axle regions due to tyre frictional loads were higher for the composite landing gear in comparison the Aluminium 7075 T6 landing gear since the ±45-degree fibres were replaced with ±15-degree and ±30-degree fibre plies which is less resistant to torsional deformation in comparison to the 45-degree fibre plies.

The weight of the composite landing gear was 4.613 kg heavier whilst being 6.558 kg heavier when the brackets were assembled to both gears. This was due to the composite landing gear occupying a greater volume as the gear width, gear length and gear thickness had increased by adding more prepreg fibre layers to increase its strength. The new bracket designs were aimed at reducing any concentrated stress areas on the composite gear during landing as it could damage the composite landing gear. This new bracket design increased the overall weight of the landing gear.

In conclusion, the newly design composite landing gear was able to withstand limit load and ultimate load landing conditions without resulting in any fibre and inter-fibre failure. Thus, the composite landing gear could be used as a alternative to the current Aluminium 7075 T6 landing gear.

# 13 MANUFACTURING OF COMPOSITE LANDING GEAR

## 13.2 Introduction

This section contains the manufacturing process for a composite undercarriage alternative design that uses epoxy resin and unidirectional e-glass prepregs.

## 13.3 Manufacturing Techniques for Composite Undercarriage

Prepregs were available in unidirectional or woven fabric form. For the composite undercarriage design, the unidirectional fabrics were more preferred since the layup could be tailored to offer higher stiffness and strength along the primary load paths. The prepregs are produced with a precise amount of resin already impregnated into the fibers to ensure consistency throughout. The void content is typically below 1% which is necessary to maintain consistency during the manufacturing process [21].

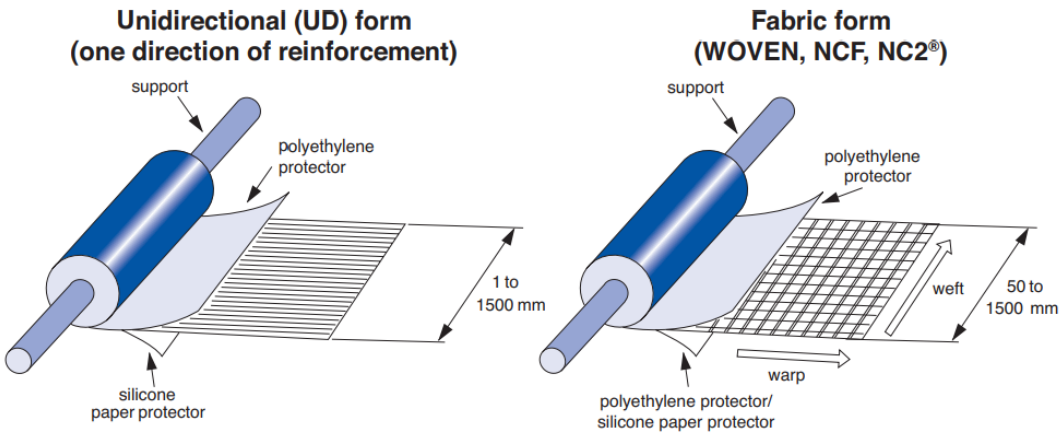


*Figure 141: Unidirectional (UD) Prepregs vs Woven Prepregs [21]*

Prepregs needs to be stored in a freezer while maintaining temperatures of approximately -18℃ to -40℃, the temperature should be recommended by the prepreg manufacturer [10]. The low temperatures will prevent the prepregs from curing during storage since they only cure at elevated temperatures. The prepregs must also be kept sealed in moisture-resistant packaging to prevent moisture build-up that can affect the curing process. The prepregs have a shelf life which should be considered, thus older materials should be used first to prevent waste. The prepregs should not pick up any contaminations such as dirt, dust, oils, or any other substances that will affect the curing process and the quality of the final manufactured undercarriage, this also includes inspection for any damage or degradation before use. When handling the prepregs during removal from storage, it should be bought to room temperature before opening the packaging which would help to prevent any condensation from occurring on the fabrics.

In Figure 142, the storage of prepreg fabrics in moisture resistant packaging at low temperatures to prevent curing of prepregs before the manufacturing process can be seen.


*Figure 142: Epoxy E-Glass Prepreg Storage [10]*

Figure 143 provides the manufacturing method followed to produce a composite component using prepregs. Each step of the process is explained:

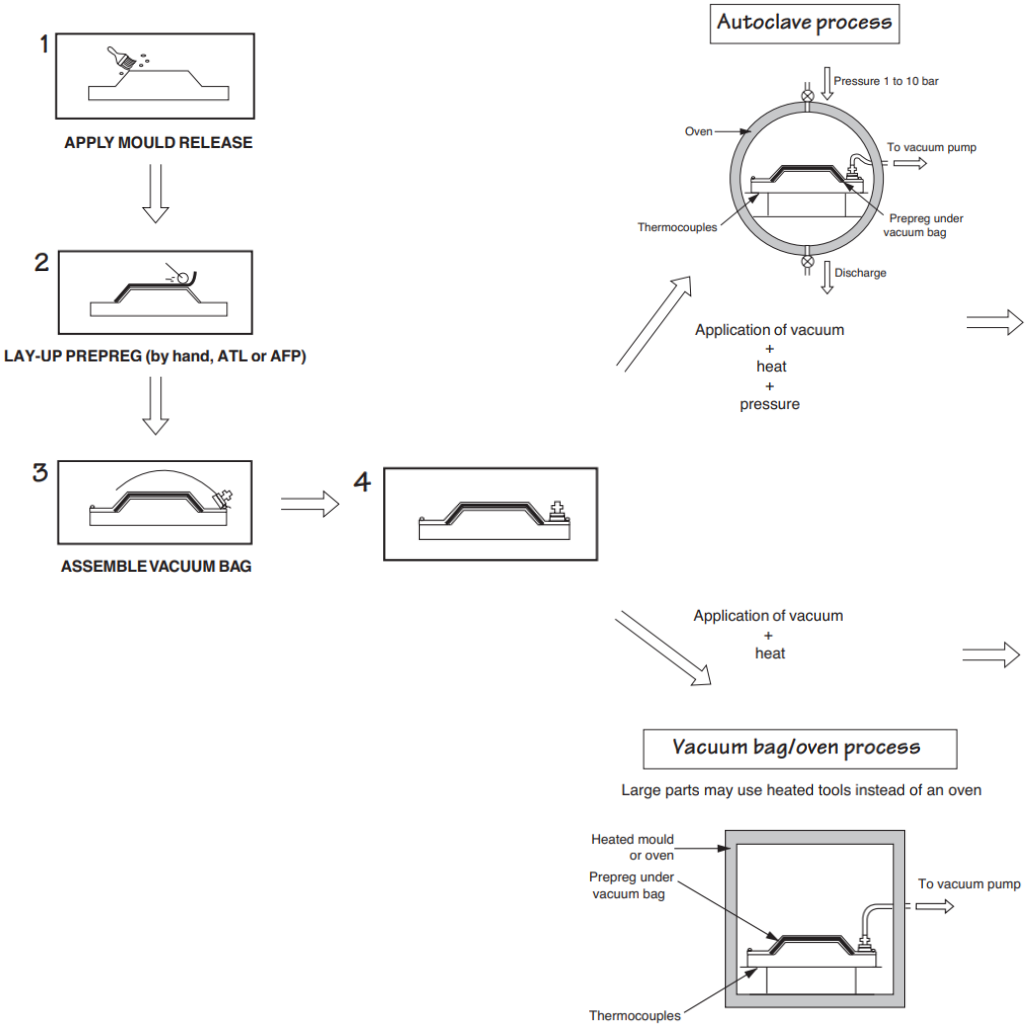


*Figure 143: Manufacturing Process Diagram for Prepreg Composite Undercarriage [21]*

**Step 1 (Apply mould release)**:

The first step is to prepare the mould surface by making sure it is clean and free of any debris, dust of residue. If needed the surface can also be waxed or polished to ensure smooth finish. The next step is to apply the mould release agent with a brush, cellulose pad, cloth, or spray cannister. Avoid over spraying or pooling of the release agent onto the mould. The manufacturer will provide instructions on the application of the mould release agent. Typically, the release agent will need some time to dry/ cure before the lay-up process begins of the composite prepregs onto the mould.

**Step 2 (Lay-up prepreg)**:

After the prepregs are taken out of storage and raised to room temperature, a CNC (Computer Numerical Control) machine could be used and programmed to cut out the desire shape and fiber orientations needed for the lay-up process. The usage of CNC to cut each fibre ply will ensure consistency and produce less waste materials during the manufacturing process. As each ply is cut, it should be numbered and labelled according to the correct layup schedule. This process of cutting the prepreg fibres could be done before step 1.

**Step 3 (Vacuum bag assembly)**:

Before the curing process of the composite components, a vacuum bag assembly of the component is done to consolidate the fibre layers, remove air and volatile compounds from the component, improve the resin distribution, enhance the surface finish and to control the part geometry during manufacturing. Figure 144 provides the components needed for the vacuum bagging process. It is recommended that new consumables are used for each component to ensure good quality is maintained during the manufacturing process of the composite undercarriage.

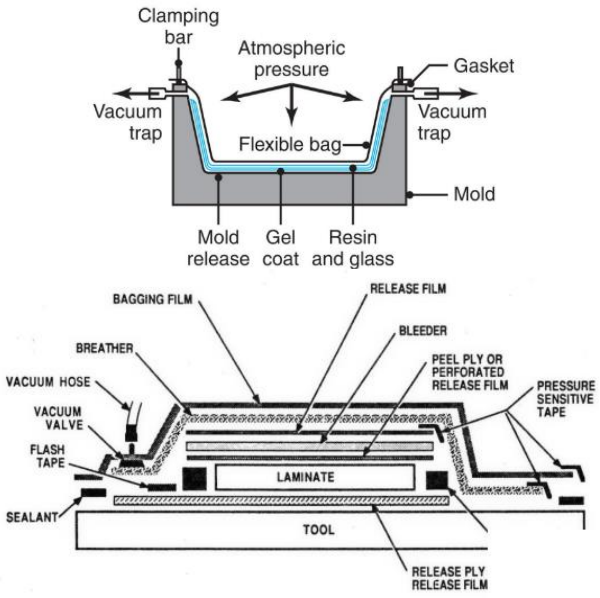


*Figure 144: Prepreg Vacuum Bagging Components [22]*

The following components of the vacuum bagging process are to be considered:

1) **Tool/ Mould**: The structure used to shape the contours and dimensions of the final composite part. Metal moulds could be used made up of steel or aluminium. There are two types of moulds which could be used, open moulds or closed moulds. Open moulds are used for flat or slightly curved parts where the composite material could be laid directly onto the mould surface. Closed moulds are also known as 'matched moulds' or 'compression moulds' where pressure is applied for consolidation. These moulds are ideal for higher production volume parts requiring precise dimensions.

2) **Laminate**: The laminate consists out composite prepreg fibres which would make up the composite landing gear.

3) **Bagging film**: Provides sealant to allow the removal of air to form a vacuum over the component.

4) **Sealant tape/ pressure sensitive tape**: The tape provides sealant to allow for the vacuum to form. It also keeps the bagging film and fabrics within the vacuums in place.

5) **Release film**: The release film will prevent any further flow of the excess resin and can be porous to allow passage of air and volatile compounds into the breather layer situated above.

6) **Bleeder fabric**: The bleeder fabric is usually felt or glass fabric to absorb the excess resin during curing. The resin flow can be regulated by the amount of bleeder fabric used.

7) **Breather fabric**: The breather fabric provides the means to apply vacuum and assist in the removal of any air and volatiles from the component and vacuum bagging assembly. When higher autoclave pressures are used during manufacturing, thicker breathers could be used.

8) **Vacuum valve**: The vacuum valve is used to prevent the vacuum from escaping the bagging assembly and attaches to the vacuum hose.

9) **Vacuum hose**: The vacuum hose is used to suck out the air of the vacuum bagging assembly.

**Step 4 (Oven/ autoclave preparation)**:

Once the composite part is sealed inside and vacuumed, the part is then ready for the autoclave or oven process. Note that the autoclave will produce higher quality parts as it controls the vacuum, temperature rate, and pressure in comparison to the oven which only controls the temperature rate and vacuum. Both methods have its advantages and are chosen based on part complexity, budget, and available equipment.

Figure 145 illustrates the vacuum bag assembly situated inside the autoclave or oven. Note that the vacuum bag assembly should be able to fit inside the autoclave or oven thus, the tooling design should consider the space requirements.

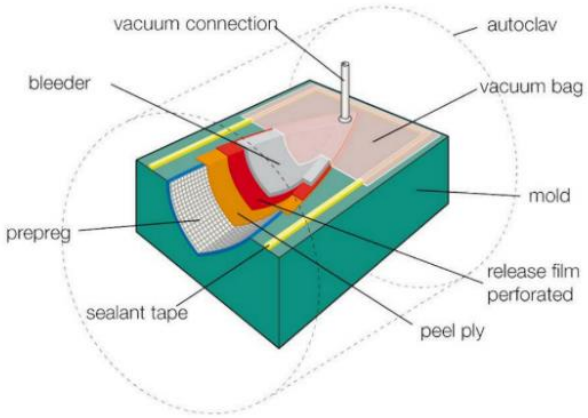


*Figure 145: Autoclave or Oven Setup Used During Manufacturing*

**Step 5 (Oven/ autoclave process)**:

When creating the composite undercarriage out of UD Epoxy E-Glass prepreg fibres, it should be considered that vacuum bag/ oven and vacuum bag/ autoclave processing are the two main methods of manufacturing components from prepregs.

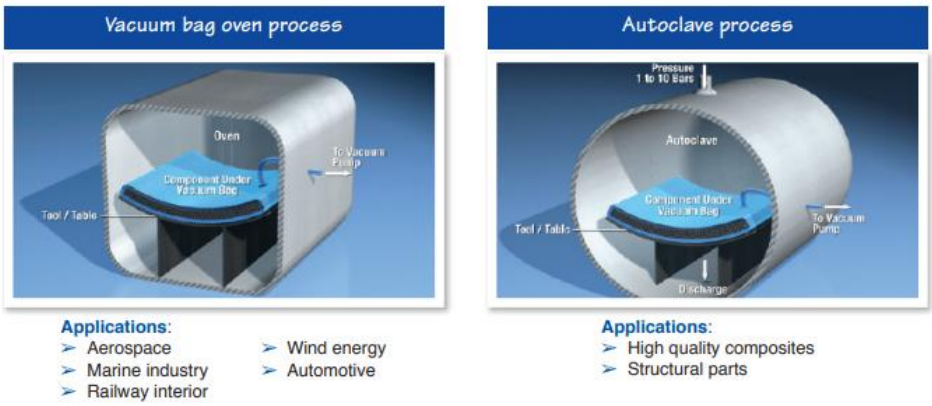


*Figure 146: Oven Vs Autoclave Process [21]*

The vacuum bagging/ oven process is well-suited for monolithic components of varying thickness. This method involves the placement and sealing of a flexible bag over the composite layup followed by the removal of all air from under the bag. The evacuation of air forces the bag down onto the layup, applying a consolidation pressure of 1 atmosphere (1 bar). Subsequently, the vacuum bagged component is placed inside an oven, initiating a brief curing cycle of the prepreg fabric within the component. By employing this technique, high performance prepregs can achieve results comparable to those produced by an autoclave, yielding components of near-autoclave quality. The autoclave process is utilised for manufacturing structural components of superior quality that contain high fibre with low void content. This process requires a similar vacuum bagging method, but the oven is replaced by an autoclave. The autoclave, functioning as a pressure vessel, provides the curing conditions needed for the composite component, regulating the vacuum, pressure, heat up rate and cure temperature. The high processing pressures will allow moulding of thicker sections with more complex component shapes. When using the autoclave process, extended cure cycles are required since the heat up rate and cool down rate will take longer. The slow heat up rates guarantee that the temperature is evenly distributed on the tooling mould of the composite component.

### 13.4 Composite Undercarriage Testing Techniques

Table 39 illustrates the techniques that could be used to analyse the composite landing gear after the manufacturing process. Visual inspections could give a clear indication of any significant damage or defects that occurred during the manufacturing process. Ultrasound or thermography could be used to inspect for any air or volatile compounds withing the composite part which could lead reduce the fatigue life of the part. Using these non-destructive should be considered as it is important that the quality of the part produces during the manufacturing process remains consistent.

*Table 39: Composite Materials Non-Destructive Techniques*

| Non Destructive Techniques | Information obtained |
|---|---|
| Visual inspection | Surface porosity |
| Ultrasound - C-scan & A-scan | Internal porosity, inclusions |
| Thermography | Internal porosity, inclusions |

Table 40, illustrates the destructive techniques used to analyse if composite part is strong enough to withstand the loads that it will endure in the field. Mechanical testing could be used to analyse the extent of the cure. The mechanical testing could include drop tests at MTOW of 600 kg at limit load and ultimate load conditions. The test can also validate if fibre failure or delamination had occurred during higher load conditions.

*Table 40: Composite Materials Destructive Techniques*

| Destructive Techniques | Information obtained |
|---|---|
| Mechanical testing | Extent of cure |
| Visual inspection | Internal porosity |

### 13.5 Manufacturing Process Summary

In conclusion, the composite landing gear should be manufactured using a vacuum bagging process which is then placed inside an autoclave or oven. It should be noted that the autoclave produces higher quality composite part which contains a higher fibre vs epoxy resin content within the laminate. The oven process could also be used to produce the composite part as both methods has its advantages and are chosen based on part complexity, budget, and available equipment.

The tooling or mould used for the composite part could consist out of steel or aluminium. There are two types of moulds which could be used, open moulds or closed mould. The open mould is used for flat parts of parts that contains curvature where the composite fibres could be laid directly onto the mould surface. Closed moulds could be used to apply pressure onto the composite part for consolidation and are ideal for higher production volume parts requiring precise dimensions.

After the manufacturing process the parts should be tested to analyse and validate if the manufacturing of the part was successful as well as if the part could withstand the applied loads without resulting in any fibre failure or delamination once it is placed in the field. Two types of testing techniques could be used, non-destructive and destructive testing. The non-destructive testing techniques consisted out of ultrasound or thermography which could be used to inspect if there are any air of volatile compounds within the laminate. This testing method is important since the quality of the manufactured part should remain consistent. Destructive testing techniques could consist out of mechanical testing such as conducting drop tests at an aircraft MTOW of 600 kg at limit load and ultimate load conditions. This test can also validate if any fibre failure or delamination had occurred during higher load conditions and that the part is safe to be used in the field of application.

# 14 CONCLUSIONS AND RECOMMENDATIONS

## 14.2 Introduction

In this section the research conducted regarding the metallic equivalent of the current Aluminium 7075 T6 alloy landing gear using composite materials was concluded. Recommended improvements that could be made on the newly designed composite landing gear are provided.

## 14.3 Conclusion

Aircraft landing gear plays an essential role in absorbing the impact energy during landing to ensure that other components of the aircraft are not damaged in the process. Shipment delays of the current Aluminium 7075 T6 alloy landing gear caused further delays in the assembly of the taildragger and tricycle aircraft. Thus, a solution was required using composite materials which could result in manufacturing the landing gear locally which would eliminate shipment costs and manufacturing delays. The composite landing gear should be able to withstand landing at limit load and ultimate load conditions specified by the ASTM F2245 -14 standards without resulting in any fibre and inter-fibre failure as well as delamination. The loads applied to the landing gear were validated using analytical methods by calculating the deflection of the landing gear strut and comparing it to FEA results. Drop tests were also conducted by the company on the current Aluminium 7075 T6 landing gear whilst it was recorded. Image processing was used to find the deflections during the drop tests where it was compared to FEA results to validate the load and constraint application to the landing gear. A mesh independence study was conducted to obtain the correct mesh element size that would provide accurate FEA results. The Aluminium 7075 T6 landing gear was then analysed for all landing conditions for both the taildragger and tricycle aircraft which were then later compared with the final composite landing gear design.

The composite materials that could be used for the aircraft landing gear was epoxy e-glass which consisted out of a wet layup or prepreg form. The wet layup fibre was approximately 34% lighter and the prepreg fibres approximately 28% lighter than the Aluminium 7075 T6 alloy when occupying the same volume. It was important to analyse the two different forms since wet layup fibres consisted out of 1-10% void content which could decrease the fatigue life of the landing gear as well as increase moisture absorption. The prepreg fibres consisted out of less than 1% void content which is carefully controlled by the manufacturer. This increases the fatigue life of the composite landing gear and decreases moisture absorption whilst being easier to use when manufacturing a composite landing gear in comparison to wet layup fibres. The wet layup fibre consisted out of out of a 50:50 resin to fibre weight ratio whereas, the prepreg fibres consisted out of a 35:65 resin to fibre weight ratio meaning that there were more fibres present to take the load. A coupon study was conducted on Aluminium 7075 T6 alloy coupons. A coupon study was also conducted on [0/90/90/0], [0/45/45/0] and [0/90/45/0] layered epoxy e-glass wet layup and prepreg fibres under tension, compression, bending and torsional loads. Note that the failure criterion used was the Puck-failure criterion which

established between fibre and inter-fibre failure of a composite laminate since it was the failure criterion used and validated during the analysis and testing of the RX1E-A aircraft composite leaf spring landing gear. The FEA results were compared to analytical results using Classical Lamination Theory. The [0/45/45/0] layered coupons obtained the best results in terms of withstanding fibre and inter-fibre failure. It was found that the prepreg layered coupons had higher safety factors for each of its individual fibres in comparison the wet layup coupons as well as having less strain during tension, compression, and torsional loads. It was thus concluded that UD Epoxy E-Glass prepreg fibres should be used to manufacture the composite landing gear and that the usage of 90-degree fibre orientated plies should be eliminated as they were the most prone to fibre and inter-fibre failure.

The final composite landing gear was design using 130 layers of 0.2159 mm thick UD Epoxy E-Glass prepreg fibres. After analysis was conducted it was found that the ±45-degree fibre plies failed due to matrix tensile failure and needed to be replaced with ±15-degree ±30-degree fibre plies to withstand the loads experienced during landing at limit load and ultimate load conditions. The landing gear dimension were also modified to increase its absorption during landing as well as distribute the stresses across a wider surface area to eliminate any stress concentrations experienced by the composite fibres. In conclusion, the newly designed landing gear was able to withstand limit load and ultimate load landing conditions without resulting in any fibre or inter-fibre failure in the strut region whereas failure had occurred in one of the fibre plies at the bolted region near the axles at ultimate load conditions. It was concluded that the composite landing gear should still be inspected for any fibre failure or delamination when attempting landing at ultimate (emergency) load conditions. The composite landing gear was approximately 4.613 kg heavier than the current Aluminium 7075 T6 landing gear. The composite landing gear made use of the original brackets attached to the aircraft frame however, new attachments had to be designed which could eliminate any concentrated stress areas introduced by the brackets. The composite landing gear in comparison the Aluminium 7075 T6 landing gear with all its assembled components were 6.558 kg heavier. The composite landing gear were also stiffer during all landing conditions at limit load and ultimate load conditions in comparison the Aluminium 7075 T6 landing gear. If the strain were increased by reducing the number of plies, the fibres would be more prone to failure.

With regards to manufacturing the composite landing gear out of prepreg fibres, it should be noted that the prepreg fibre plies had a shelf life and should be stored in a freezer at approximately -18℃ to -40℃. When cutting the prepreg fibre plies a CNC machine could be programmed to cut out the desired fibre shape as it would produce less waste and more consistent fibre layers. During the manufacturing of the composite landing gear, a vacuum bagging process were required which contained the composite part inside a vacuum to improve the resin distribution and remove any air or volatile compounds from the laminate. The vacuum bag assembly is then placed inside an oven or an autoclave where the curing process would take place. The oven can control vacuum and temperature rates where the autoclave could control the vacuum, pressure, and temperature rates. The autoclave produces higher quality parts in comparison the oven but the desired process should be chosen

based on budget and available equipment. The mould or tooling use could consist out of steel or aluminium. Note that the mould or tooling used should be able to fit inside the oven or autoclave.

### 14.4 Recommendations

The following recommendations should be considered during the analysis and design of a newly developed composite landing gear as these recommendations aim to address the identified limitations presented in the research report and enhance the reliability, performance, and development of the composite gear during future studies.

Firstly, with regards to the Puck-failure criteria used to analyse the composite landing gear during FEA analysis, ultimate strength criteria such as the (maximum-stress and maximum-strain criterion), Tsai-Wu, Tsai-hill Hoffman, and failure mode criteria such as Hashin and LaRC03 criteria should also be considered and validated though comparison between simulation and physical tests conducted. This should enable an assessment of whether failure of a composite structure will occur or not and provide a more detailed analysis with regards to the type of failures occurring in composite landing gears for light sport aircrafts [9].

Secondly, with regards to the validation process between numerical and analytical results followed during the research report, is should be pointed out that the numerical simulations only considered static load conditions. It is recommended that numerical analysis conducted should involve a dynamic study of the landing gear during load conditions presented during the different landing conditions as discussed. Data could be captured with regards to a real time landing of the BushCat aircraft as it would enable a more accurate presentation of the load magnitudes experienced during landing. Measurement devices such as strain gauges and load cells could be used to capture the necessary data.

With regards to the designed composite landing gear presented in the research report, although it could withstand all landing conditions for both the taildragger and tricycle aircraft at limit load and ultimate load conditions, it is recommended that tests should be conducted using both non-destructive and destructive static and dynamic techniques to make sure that consistency is reached within the manufacturing process and to validate that the newly developed composite landing gear could withstand all load conditions at limit load and ultimate load conditions without fibre-failure, matrix-failure and delamination occurring within the composite part.

Lastly, during the manufacturing process it should be considered that the resin produces an exothermic reaction. Thus, when placed inside the oven or autoclave the composite part could melt due to the exothermic reaction and damage the composite part. During the curing process, the landing gear should be monitored and safety measurements such as clear protocols for emergency shut down procedures and operator training to recognize signs of overheating and implement corrective actions should be in place when deciding to cure the composite part.

## 15 REFERENCES


[1] V. Jeevanantham, P. Vavidelu and P. Manigandan, “Material Based Structural Analysis of a Typical Landing Gear,” *IJISET,* vol. 4, no. 4, 2017.

[2] “Rainbow Skyreach,” Skyreach, 2023. [Online]. Available: https://www.fly-skyreach.com/. [Accessed 16 March 2023].

[3] S. Gudmundsson, “The Anatomy of the Landing Gear,” in *General Aviation Aircraft Design: Applied Methods and Procedures*, Butterworth-Heinemann, 2013.

[4] “ASTM Designation: F2245 -14: Standard Specification for Design and Performance of a Light Sport Airplane,” ASTM International, 2015.

[5] “Easy Acesss Rules for Normal, Utility, Aerobatic and Commuter Category Aeroplanes (CS-23) (Initial Issue),” European Aviation Safety Agency (EASA), 2018.

[6] “Aeronautics Guide,” February 2023. [Online]. Available: https://www.aircraftsystemstech.com/2023/02/weighing-aircraft-and-determining-empty.html. [Accessed 17 March 2023].

[7] “Gurit: Guide to Composites,” December 2022. [Online]. Available: https://www.gurit.com/wp-content/uploads/2022/12/guide-to-composites-1.pdf. [Accessed 19 March 2023].

[8] S. Rout and H. Y. Nezhad, “Development of Improved Flexural and Impact Performance of Kevlar/Carbon/Glass Fibres Reinforced Polymer Hybrid Composites,” *Journal of Composite Science,* vol. 6, no. 245, pp. 1-14, 2022.

[9] *Aircraft Structures 1: MECN3035A,* Johannesburg: University of the Witwatersrand.

[10] *Methods used to manufacture PMC's,* (AMTAS) Advanced Materials in Transport Aircraft Structures, 2012.

[11] D. LI, Z. FAN, Y. Zhang, J. Zang and F. Yang, “Optimum design and experiment of composite leaf spring landing gear for electric aircraft,” *Chinese Journal of Aeronautics,* pp. 2649-2659, 2020.

[12] R. Naveen, M. Kumar, M. Ramesh, R. Abinaya and M. Prasath, “An investigation on effect of ultravoilet (UV) rays on mechanical properties of epoxy laminates,” *Materials today,* 2023.

[13] “Maintenance Manual: For Bushcat Nose-Wheel and Tail-Dragger,” 28 June 2017. [Online]. Available: https://www.fly-skyreach.com/MaintManuals/BCMP-NT-001-000%20Detailed%20Maintenance%20Procedures%20Manual.pdf. [Accessed 25 September 2023].

[14] D. P. Raymer, Aircraft Design: A Conceptual Approach, New York: AIAA Education Series, 1999.

[15] J. D. Anderson, Introduction to Flight: Eight Edition, New York: McGraw-Hill Education, 2014.

[16] S. T. de Freitas, “Experimental research project on bolted connections in bearing for high strength steel,” p. 107, July 2005.

[17] “Grove: Aircraft Landing Gear Systems Inc.,” Grove Inc., [Online]. Available: https://www.groveaircraft.com/radiusplates.html. [Accessed 13 October 2023].

[18] T. Bingelis, *Spring Steel Landing Gears,* Experimental Aircraft Association (EAA): Sport Aviation.

[19] *ACP User's Guide,* Canonsburg: Ansys,Inc, 2023.

[20] K. Megahed, Introduction to Nonlinear Finite Element Analysis, Zenodo, 2019.

[21] H. Corporation, “Hexply Prepeg Technology,” January 2013. [Online]. Available: https://kevra.fi/wp-content/uploads/Prepreg_Technology_.pdf. [Accessed 7 November 2023].

[22] *Manufacturing of plastics and composite materials,* Johannesburg: University of the Witwatersrand, 2022.

# 16 APPENDIX A (Coupon Study Validation Tables)

Appendix A provides the FEA and analytical results validated for the [0/45/45/0] and [0/90/45/0] layered UD Epoxy E-Glass prepreg coupons during tension, compression, bending and torsion.

## 16.2 UD Epoxy E-Glass [0/45/45/0] Coupons FEA and Analytical Results

Figure 147 and Figure 148 illustrates the FEA stress results for [0/45/45/0] prepreg and wet layup coupons under beam tension. The stress, strain, and Puck-failure safety factor obtained from the FEA results for the prepreg coupon fibre layer 1 was 76.343 MPa, 0.0017018 mm/mm and 14.408 respectively. The stress, strain, and Puck-failure safety factor for the wet layup coupon fibre layer 1 was 73.374 MPa, 0.0021019 mm/mm and 10.63 respectively.

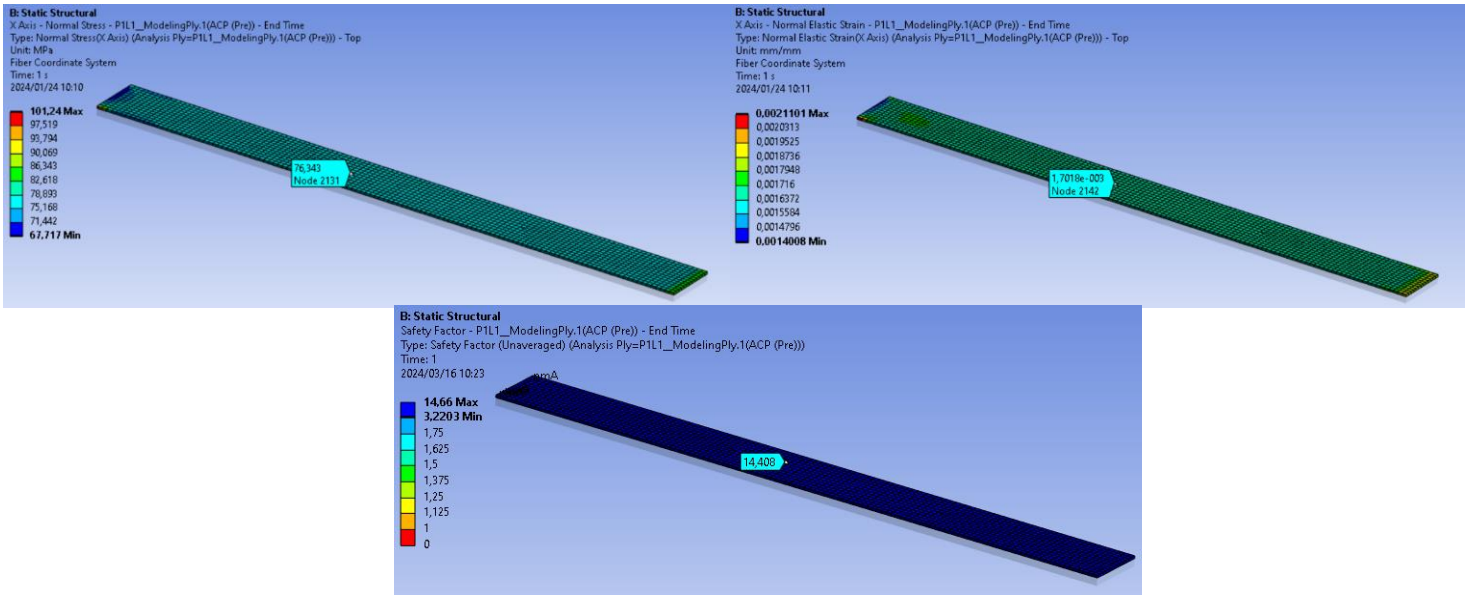


*Figure 147: [0/45/45/0] Epoxy E-Glass UD Prepreg Coupon Beam Tension Stress, Strain and Safety Factor (Fibre Layer 1)*

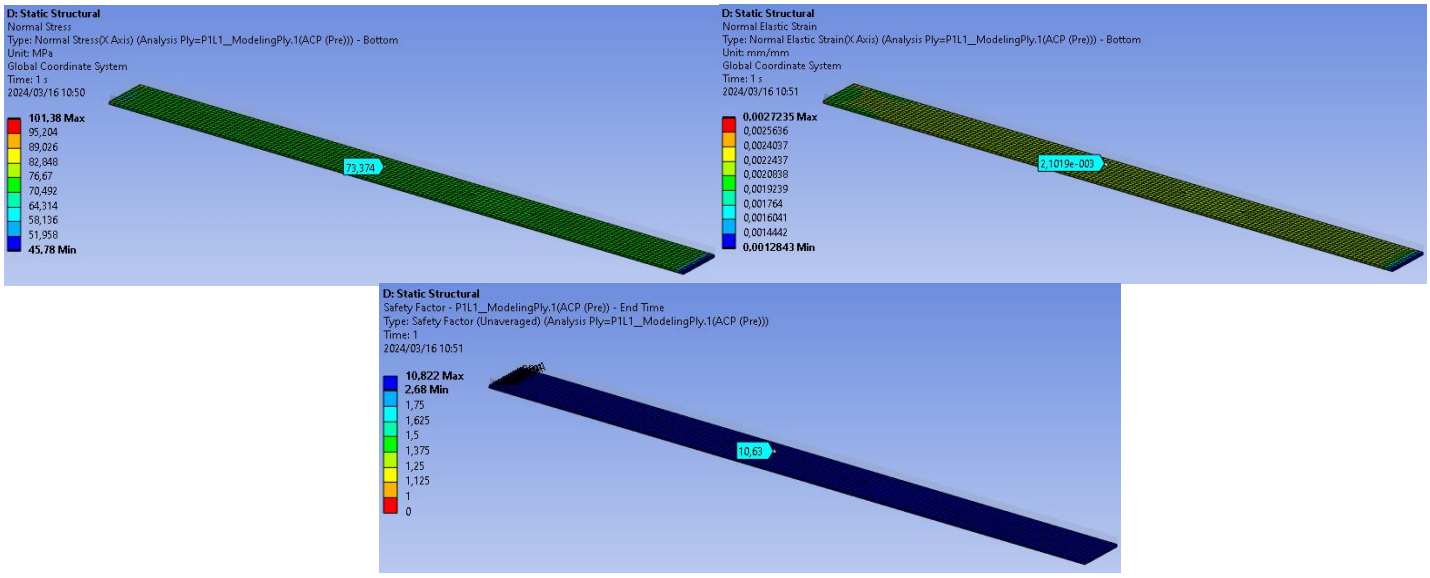


*Figure 148: [0/45/45/0] Epoxy E-Glass UD Wet Layup Coupon Beam Tension Stress, Strain and Safety Factor (Fibre Layer 1)*

Figure 149 and Figure 150 illustrates the FEA stress results for [0/45/45/0] prepreg and wet layup coupons under beam compression. The stress, strain, and Puck-failure safety factor obtained from the FEA results for the prepreg coupon fibre layer 1 was 76.343 MPa, 0.0017018 mm/mm and 8.416 respectively. The stress, strain, and Puck-failure safety factor for the wet layup coupon fibre layer 1 was 73.373 MPa, 0.002102 mm/mm and 6.5416 respectively.

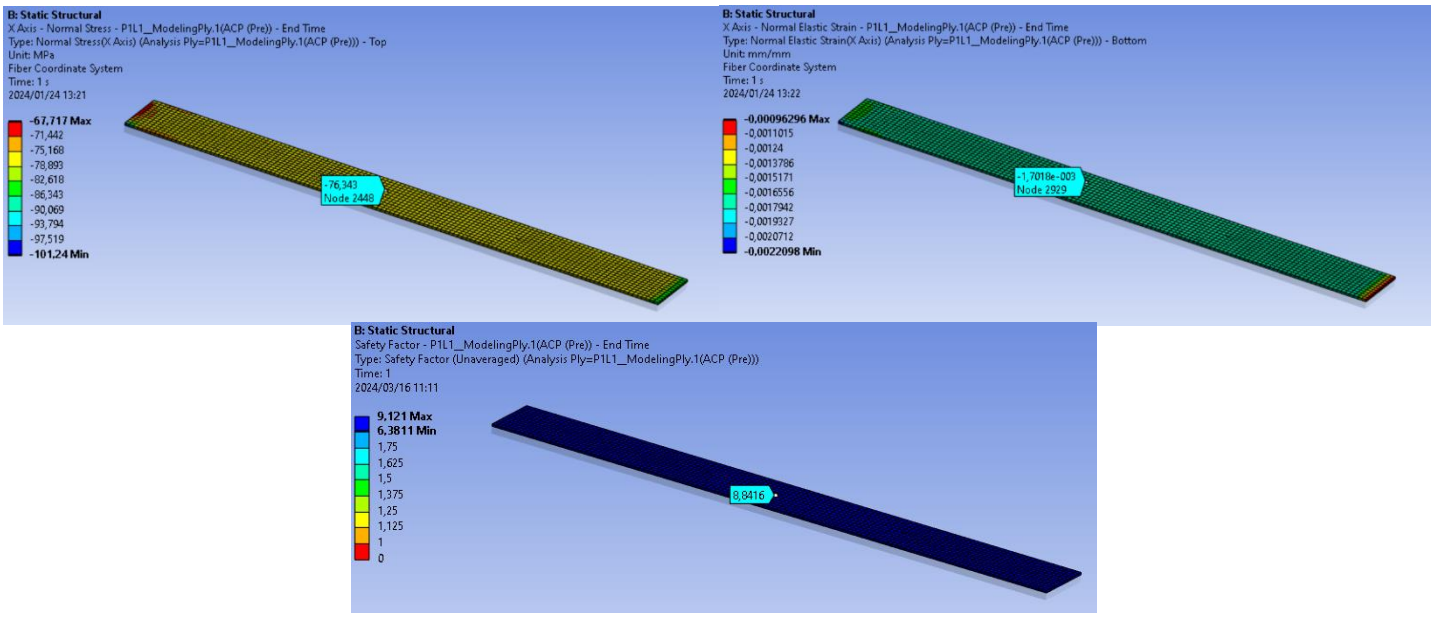


*Figure 149: [0/45/45/0] Epoxy E-Glass Prepreg Coupon Beam Compression Stress, Strain and Safety Factor (Fibre Layer 1)*

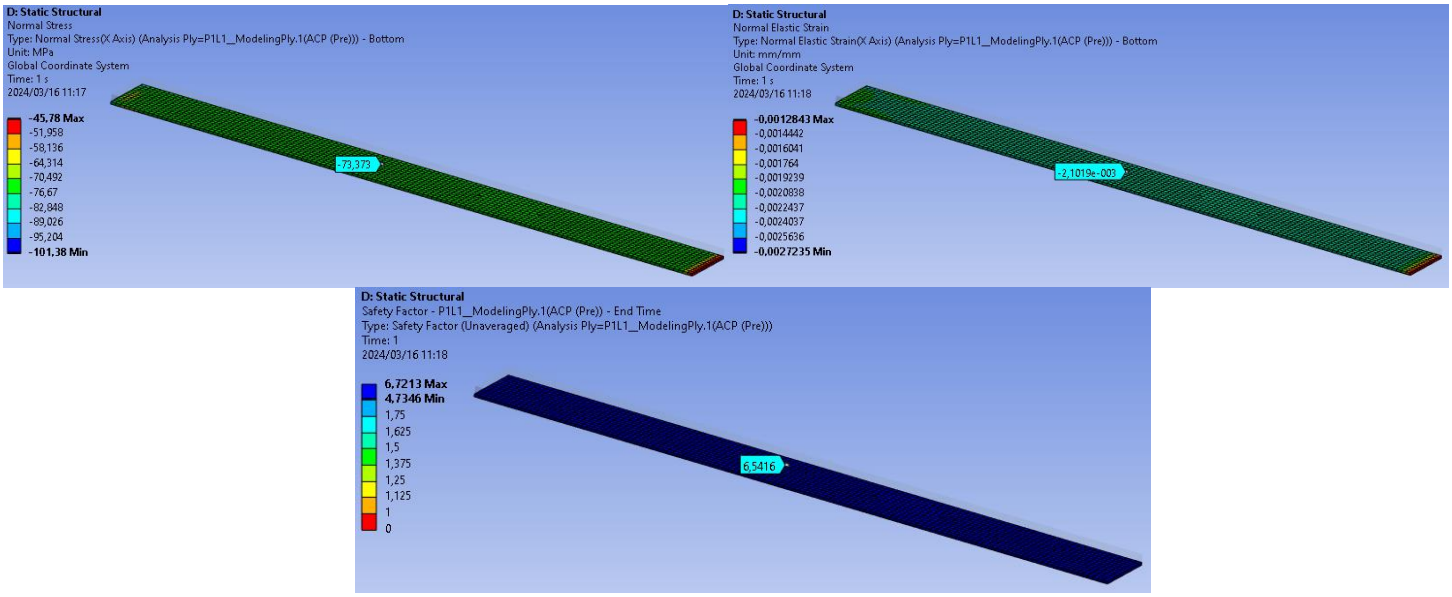


*Figure 150: [0/45/45/0] Epoxy E-Glass Wet Layup Coupon Beam Compression Stress, Strain and Safety Factor (Fibre Layer 1)*

Figure 151 and Figure 152 illustrates the FEA stress results for [0/45/45/0] prepreg and wet layup coupons under beam bending. The stress, strain, and Puck-failure safety factor obtained from the FEA results for the prepreg coupon fibre layer 1 was 153.76 MPa, 0.003398 mm/mm and 6.9666 respectively. The stress, strain, and Puck-failure safety factor for the wet layup coupon fibre layer 1 was 152.29 MPa, 0.0043669 mm/mm and 5.0382 respectively.

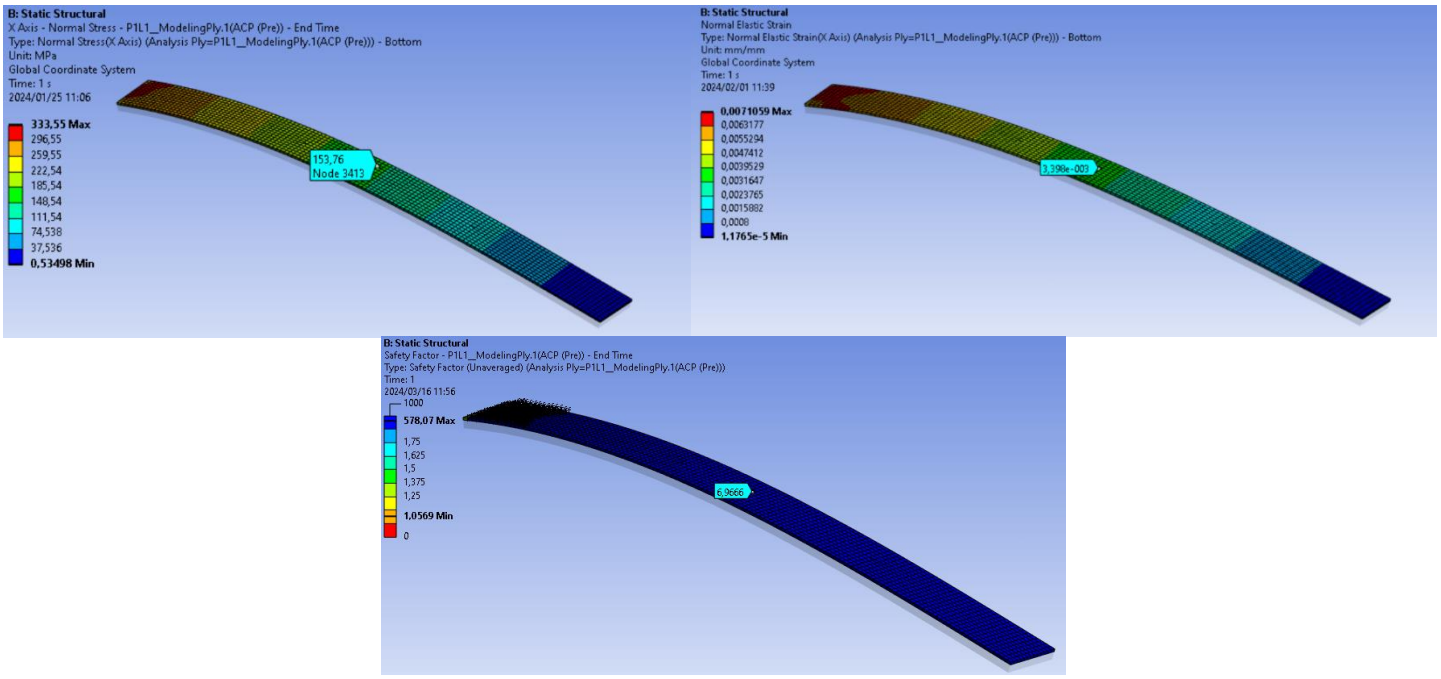


*Figure 151: [0/45/45/0] Epoxy E-Glass Prepreg Coupon Beam Bending Stress, Strain and Safety Factor (Fibre Layer 1)*

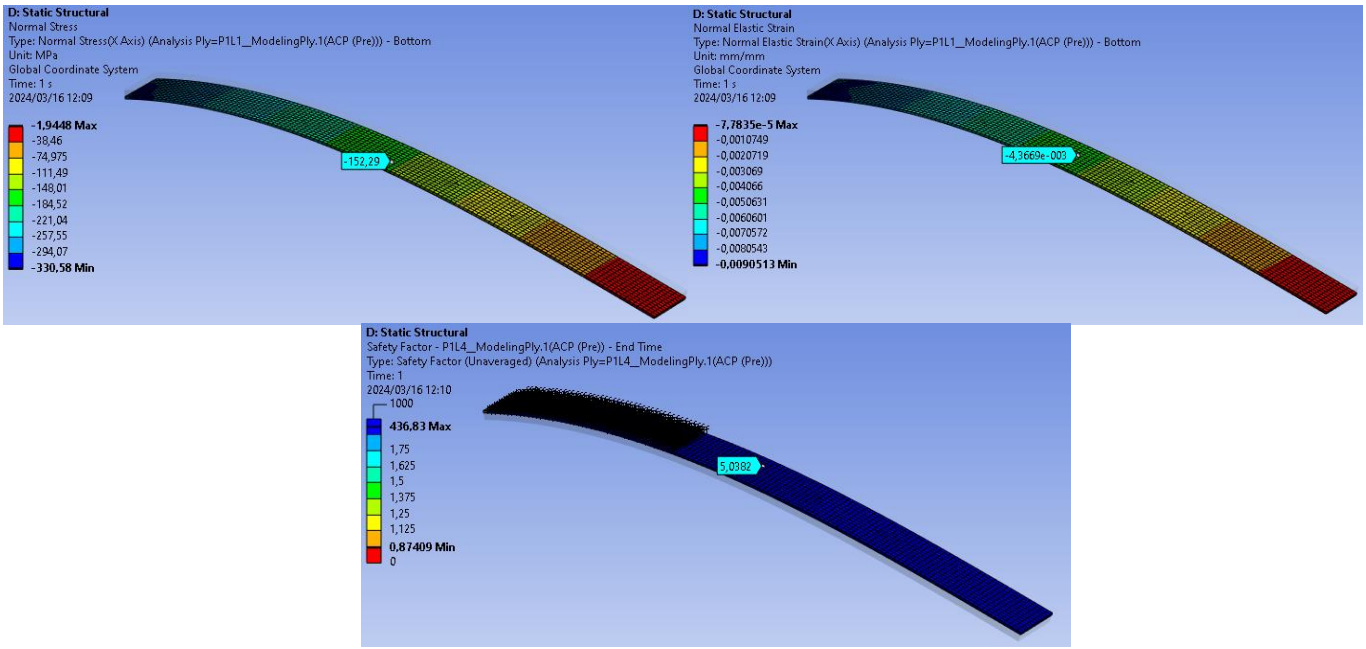


*Figure 152: [0/45/45/0] Epoxy E-Glass Wet Layup Coupon Beam Bending Stress, Strain and Safety Factor (Fibre Layer 1)*

Figure 153 and Figure 154 illustrates the FEA stress results for [0/45/45/0] prepreg and wet layup coupons under beam torsion. The stress, strain, and Puck-failure safety factor obtained from the FEA results for the prepreg coupon fibre layer 1 was 62.901 MPa, 0.0059151 mm/mm and 2.3294 respectively. The stress, strain, and Puck-failure safety factor for the wet layup coupon fibre layer 1 was 64.869 MPa, 0.0064544 mm/mm and 1.6726 respectively.

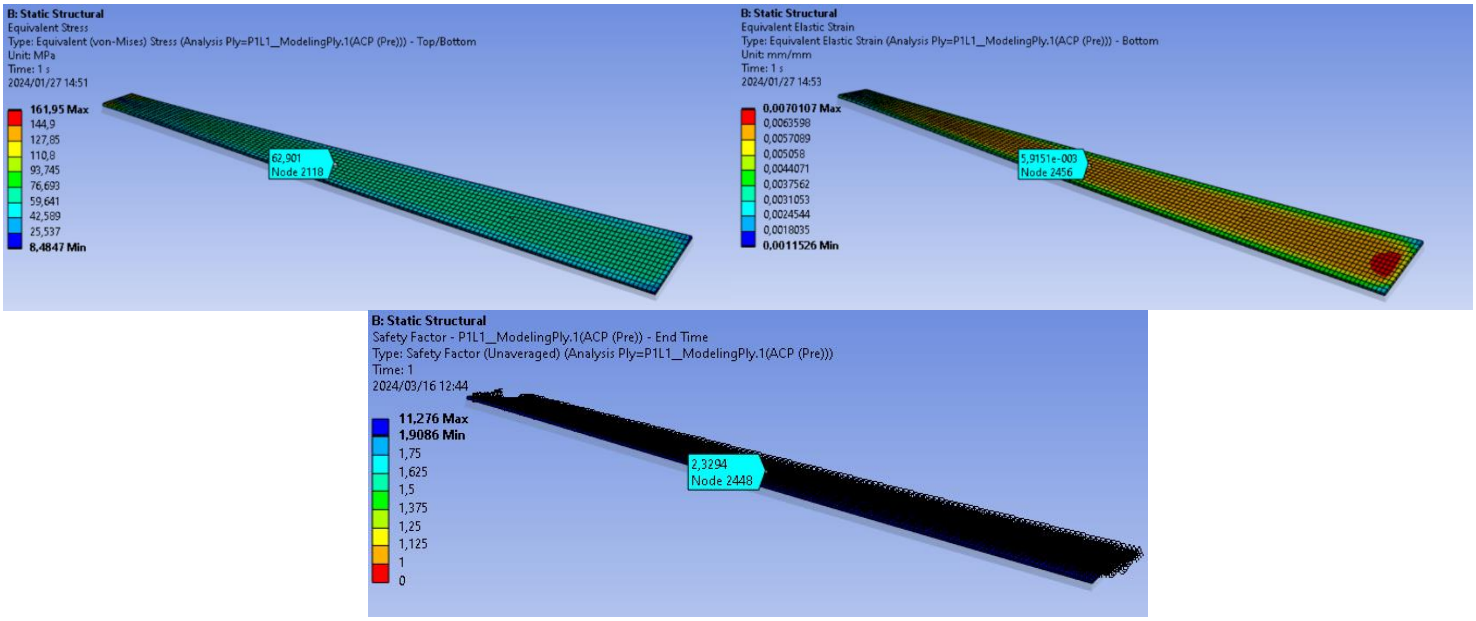


*Figure 153: [0/45/45/0] Epoxy E-Glass Prepreg Coupon Beam Torsional Stress, Strain and Safety Factor (Fibre Layer 1)*

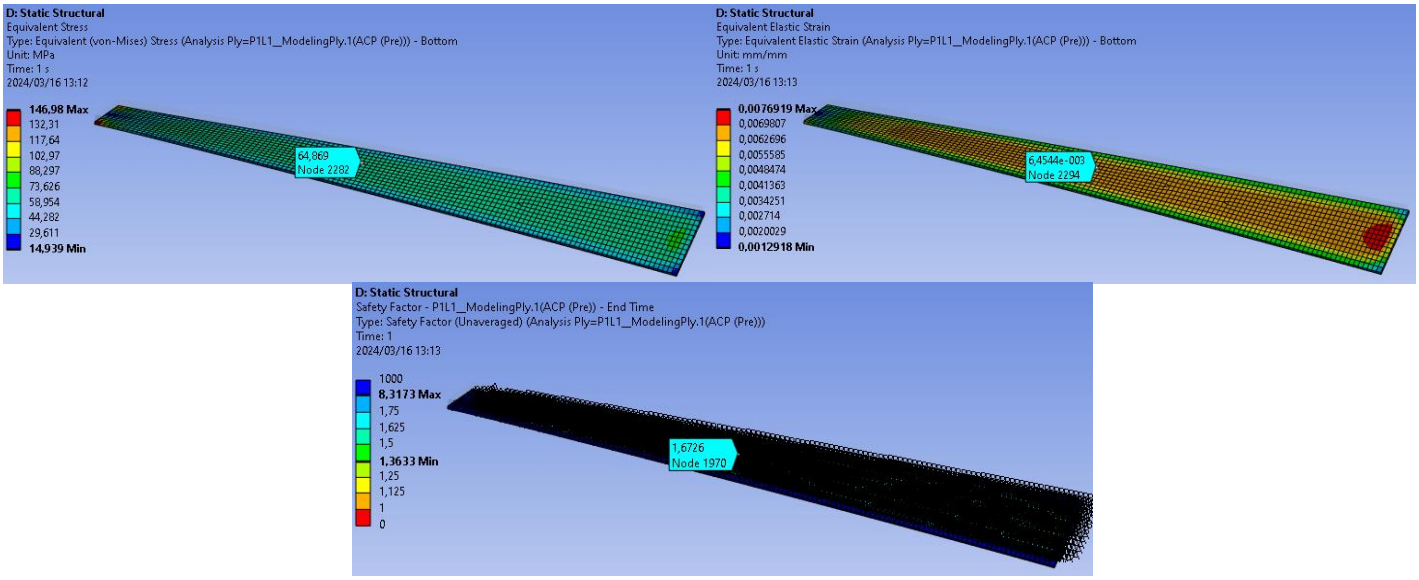


*Figure 154: [0/45/45/0] Epoxy E-Glass Wet Layup Coupon Beam Torsional Stress, Strain and Safety Factor (Fibre Layer 1)*

Table 41 to Table 44 provides the FEA and analytical results obtained for [0/45/45/0] layered Epoxy E-Glass UD prepreg and Epoxy E-Glass UD wet layup coupons during tension, compression, bending and torsion.

*Table 41: Prepreg and Wet Layup Coupon [0/45/45/0] Results (Tensile Load)*

| **Load Type** | **Stress (FEA)** | **Stress (Analytical)** | **Strain (FEA)** | **Strain (Analytical)** | **Safety Factor** |
|---|---|---|---|---|---|
| **-** | **MPa** | **MPa** | **mm/mm** | **mm/mm** | **-** |
| **[0/45/45/0] Prepreg Coupon (Tension)** | | | | | |
| Layer 1 | 76.343 | 76.309<br>0.104 % | 0.0017018 | 0.0017009<br>0.053 % | **14.408** |
| Layer 2 | 23.703 | 23.691<br>0.051 % | 0.0017018 | 0.0017009<br>0.053 % | **3.2335** |
| Layer 3 | 23.703 | 23.691<br>0.051 % | 0.0017018 | 0.0017009<br>0.053 % | **3.2335** |
| Layer 4 | 76.343 | 76.309<br>0.104 % | 0.0017018 | 0.0017009<br>0.053 % | **14.408** |
| **[0/45/45/0] Wet Layup Coupon (Tension)** | | | | | |
| Layer 1 | 73.374 | 73.300<br>0.101 % | 0.0021019 | 0.0021045<br>0.124 % | **10.63** |
| Layer 2 | 26.673 | 26.700<br>0.101 % | 0.0021019 | 0.0021045<br>0.124 % | **2.413** |
| Layer 3 | 26.673 | 26.700<br>0.101 % | 0.0021019 | 0.0021045<br>0.124 % | **2.413** |
| Layer 4 | 73.374 | 73.300<br>0.101 % | 0.0021019 | 0.0021045<br>0.124 % | **10.63** |

*Table 42: Prepreg and Wet Layup Coupon Results [0/45/45/0] (Compressive Load)*

| **Load Type** | **Stress (FEA)** | **Stress (Analytical)** | **Strain (FEA)** | **Strain (Analytical)** | **Safety Factor** |
|---|---|---|---|---|---|
| **-** | **MPa** | **MPa** | **mm/mm** | **mm/mm** | **-** |
| **[0/45/45/0] Prepreg Coupon (Compression)** | | | | | |
| Layer 1 | -76.343 | -76.309<br>0.045 % | -0.0017018 | -0.0017009<br>0.053 % | **8.8416** |
| Layer 2 | -23.703 | -23.691<br>0.051 % | -0.0017018 | -0.0017009<br>0.053 % | **7.8827** |
| Layer 3 | -23.703 | -23.691<br>0.051 % | -0.0017018 | -0.0017009<br>0.053 % | **7.8827** |
| Layer 4 | -76.343 | -76.309<br>0.045 % | -0.0017018 | -0.0017009<br>0.053 % | **8.8416** |
| **[0/45/45/0] Wet Layup Coupon (Compression)** | | | | | |
| Layer 1 | -73.373 | -73.300<br>0.099 % | -0.002102 | -0.002104<br>0.095 % | **6.5416** |
| Layer 2 | -26.673 | -26.700<br>0.101 % | -0.002102 | -0.002104<br>0.095 % | **5.3794** |
| Layer 3 | -26.673 | -26.700<br>0.101 % | -0.002102 | -0.002104<br>0.095 % | **5.3794** |
| Layer 4 | -73.373 | -73.300<br>0.099 % | -0.002102 | -0.002104<br>0.095 % | **6.5416** |

*Table 43: Prepreg and Wet Layup Coupon Results [0/45/45/0] (Bending Load)*

| Load Type | Stress (FEA) | Stress (Analytical) | Strain (FEA) | Strain (Analytical) | Safety Factor |
|---|---|---|---|---|---|
| - | MPa | MPa | mm/mm | mm/mm | - |
| **[0/45/45/0] Prepreg Coupon (Bending)** | | | | | |
| Layer 1 | 153.76 | 152.976<br>0.510 % | 0.003398 | 0.0034074<br>0.276 % | **6.9666** |
| Layer 2 | 27.343 | 27.093<br>0.914 % | 0.0017015 | 0.0017037<br>0.129 % | **3.6456** |
| Layer 3 | -27.343 | -27.093<br>0.914 % | -0.0017015 | -0.0017037<br>0.129 % | **7.8476** |
| Layer 4 | -153.76 | -152.976<br>0.510 % | -0.003398 | -0.0034074<br>0.276 % | **4.2797** |
| **[0/45/45/0] Wet Layup Coupon (Bending)** | | | | | |
| Layer 1 | 152.29 | 151.944<br>0.227 % | 0.0043669 | 0.004360<br>0.158 % | **5.0382** |
| Layer 2 | 30.919 | 30.708<br>0.682 % | 0.002176 | 0,002180<br>0.184 % | **2.442** |
| Layer 3 | -30.919 | -30.708<br>0.682 % | -0.002176 | -0.002180<br>0.184 % | **5.2499** |
| Layer 4 | -152.29 | -151.944<br>0.227 % | -0.0043669 | -0.004360<br>0.158 % | **3.1518** |

*Table 44: Prepreg and Wet Layup Coupon Results [0/45/45/0] (Torsional Load)*

| Load Type | Stress (FEA) | Stress (Analytical) | Strain (FEA) | Strain (Analytical) | Safety Factor |
|---|---|---|---|---|---|
| - | MPa | MPa | mm/mm | mm/mm | - |
| **[0/45/45/0] Prepreg Coupon (Torsion)** | | | | | |
| Layer 1 | 62.901 | 64.474<br>2.501 % | 0.0059151 | 0.006123<br>3.396 % | **2.3294** |
| Layer 2 | 74.352 | 76.704<br>3.066 % | 0.0029583 | 0.0030451<br>2.840 % | **7.7396** |
| Layer 3 | 74.352 | 76.704<br>6.163 % | 0.0029583 | 0.0030451<br>2.840 % | **7.7396** |
| Layer 4 | 62.901 | 64.474<br>2.501 % | 0.0059151 | 0.006123<br>3.396 % | **2.3294** |
| **[0/45/45/0] Wet Layup Coupon (Torsion)** | | | | | |
| Layer 1 | 64.869 | 66.819<br>2.918 % | 0.0064544 | 0.0066580<br>3.058 % | **1.6726** |
| Layer 2 | 67.728 | 67.76<br>0.047 % | 0.0032328 | 0.0033087<br>2.294 % | **6.5319** |
| Layer 3 | 67.728 | 67.76<br>0.047 % | 0.0032328 | 0.0033087<br>2.294 % | **6.5319** |
| Layer 4 | 64.869 | 66.819<br>2.918 % | 0.0064544 | 0.0066580<br>3.058 % | **1.6726** |

### 16.3 UD Epoxy E-Glass [0/90/45/0] Coupons FEA and Analytical Results

Figure 155 and Figure 156 illustrates the FEA stress results for [0/90/45/0] prepreg and wet layup coupons under beam tension. The stress, strain, and Puck-failure safety factor obtained from the FEA results for the prepreg coupon fibre layer 1 was 79.328 MPa, 0.0017435 mm/mm and 8.311 respectively. The stress, strain, and Puck-failure safety factor for the wet layup coupon fibre layer 1 was 76.915 MPa, 0.0021757 mm/mm and 7.8421 respectively.

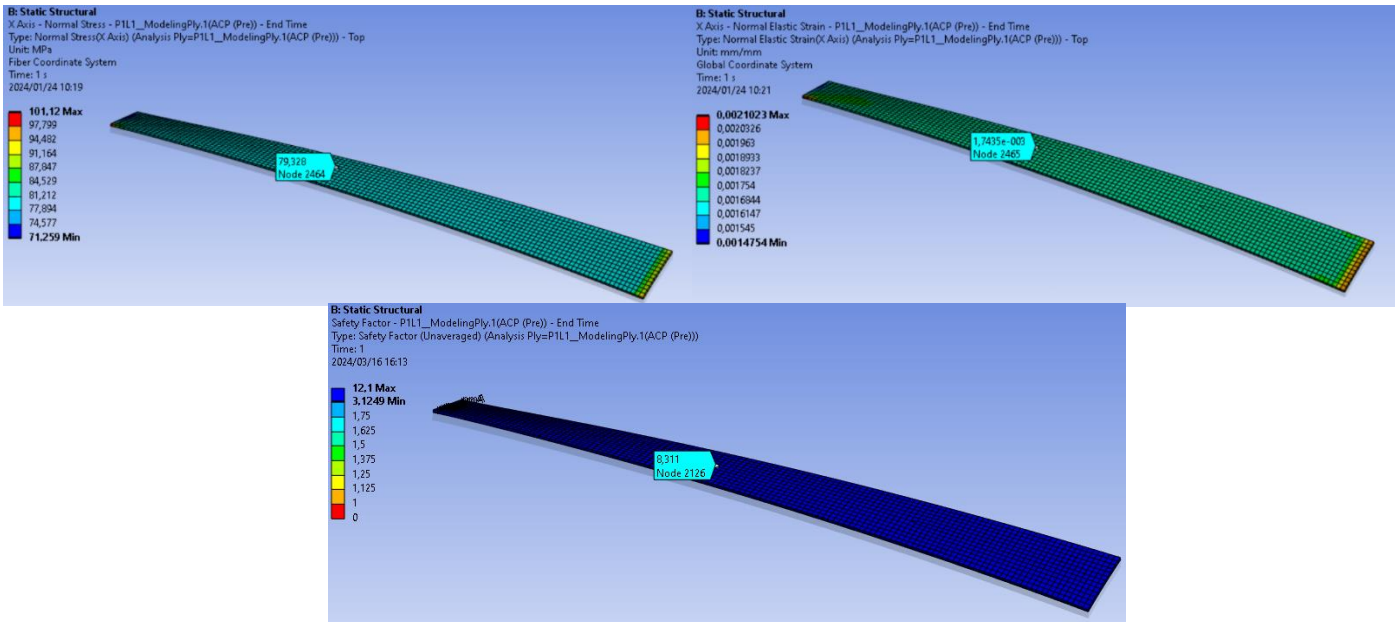


*Figure 155: [0/90/45/0] Epoxy E-Glass UD Prepreg Coupon Beam Tension Stress, Strain and Safety Factor (Fibre Layer 1)*

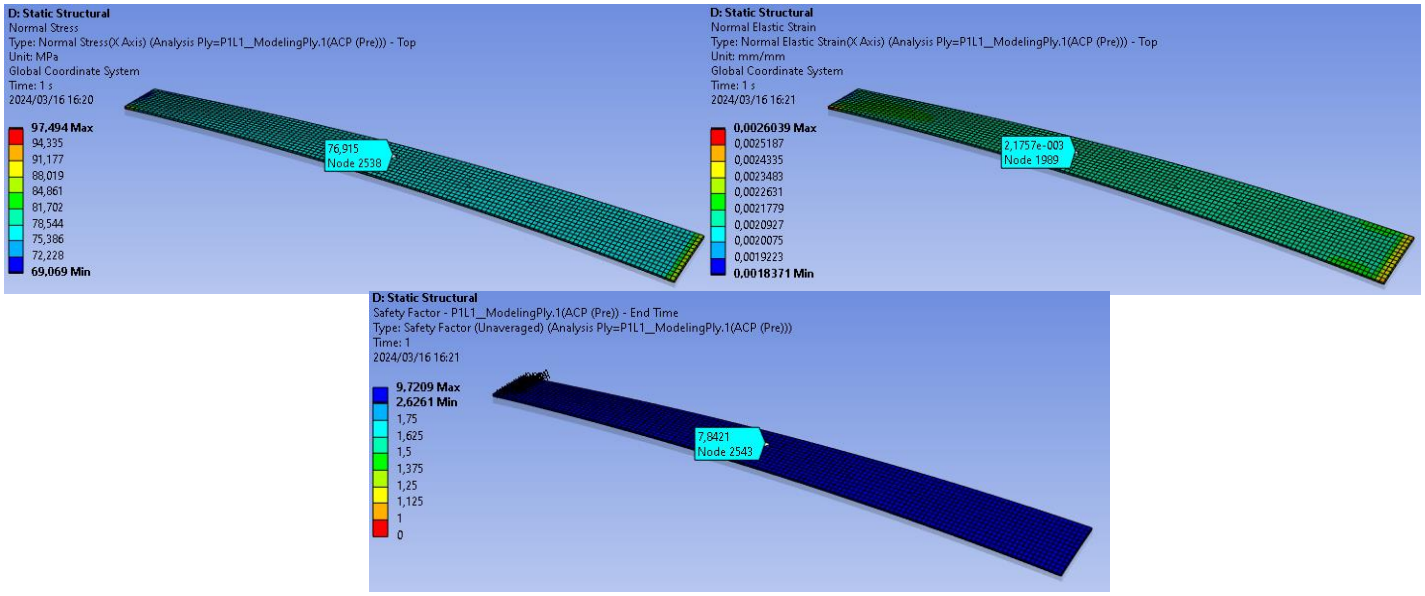


*Figure 156: [0/90/45/0] Epoxy E-Glass UD Wet Layup Coupon Beam Tension Stress, Strain and Safety Factor (Fibre Layer 1)*

Figure 157 and Figure 158 illustrates the FEA stress results for [0/90/45/0] prepreg and wet layup coupons under beam compression. The stress, strain, and Puck-failure safety factor obtained from the FEA results for the prepreg coupon fibre layer 1 was 79.33 MPa, 0.0017436 mm/mm and 8.4019 respectively. The stress, strain, and Puck-failure safety factor for the wet layup coupon fibre layer 1 was 76.915 MPa, 0.0021757 mm/mm and 6.153 respectively.

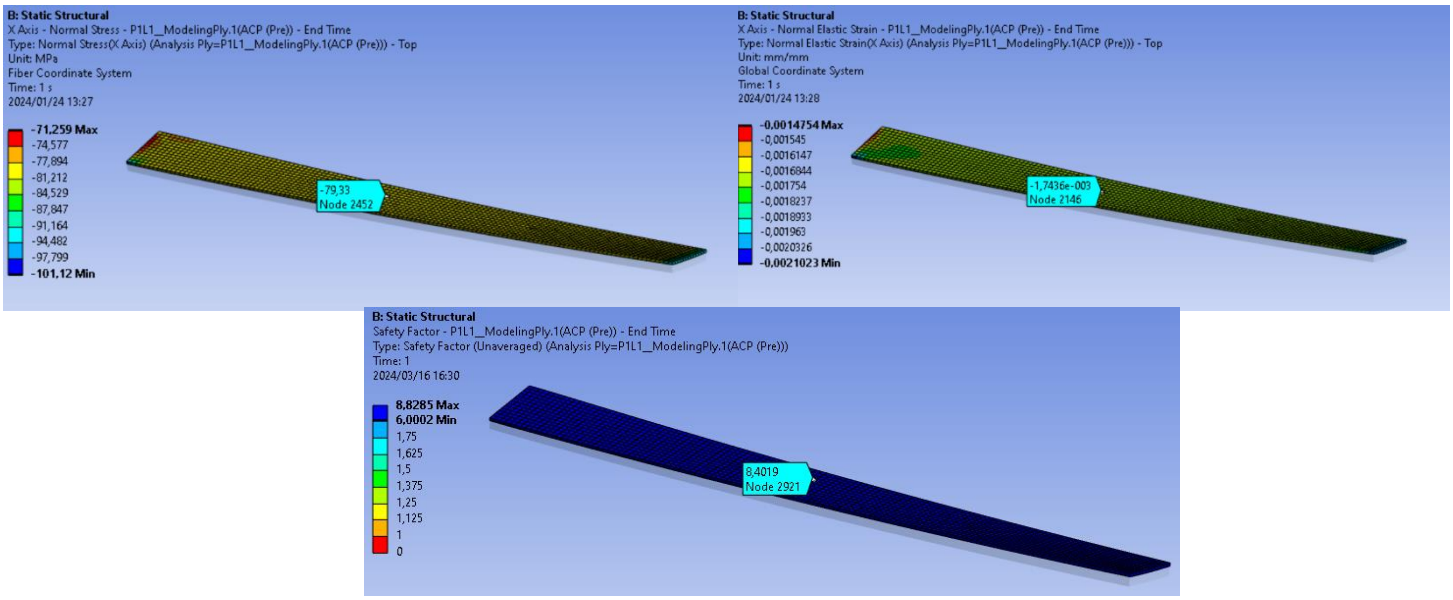


*Figure 157: [0/90/45/0] Epoxy E-Glass Prepreg Coupon Beam Compression Stress, Strain and Safety Factor (Fibre Layer 1)*

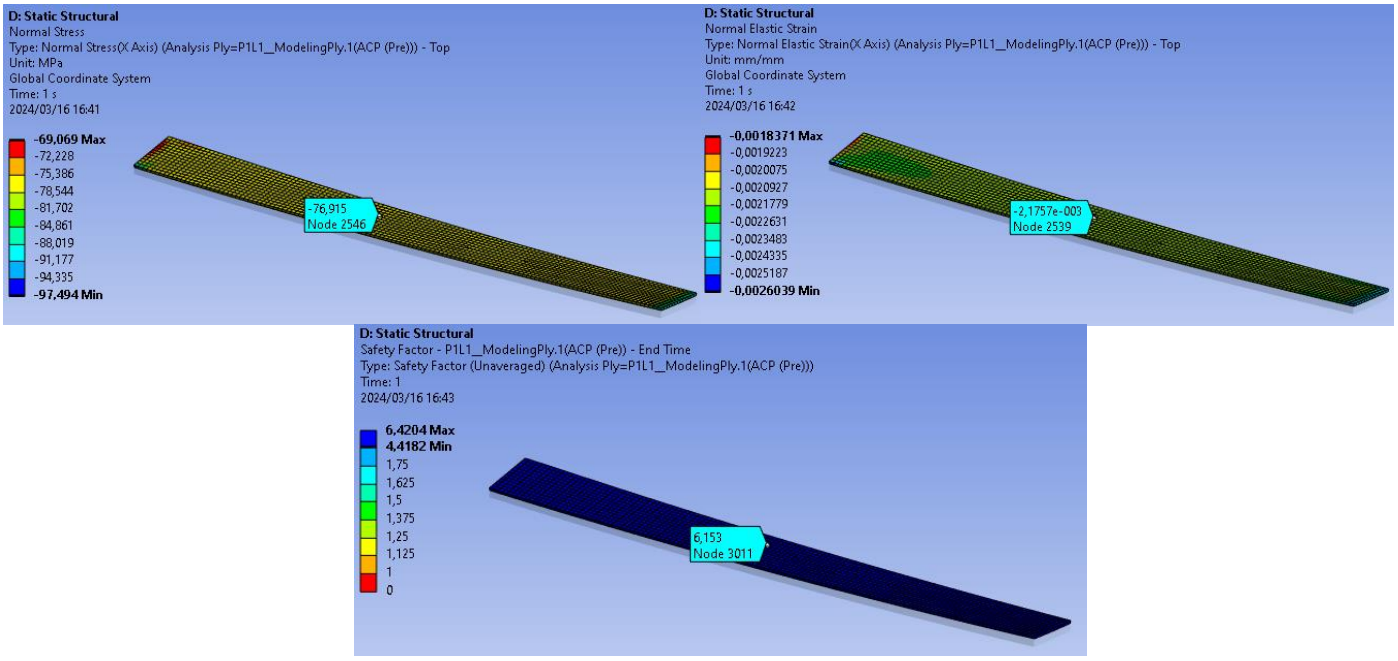


*Figure 158: [0/90/45/0] Epoxy E-Glass Wet Layup Coupon Beam Compression Stress, Strain and Safety Factor (Fibre Layer 1)*

Figure 159 and Figure 160 illustrates the FEA stress results for [0/90/45/0] prepreg and wet layup coupons under beam bending. The stress, strain, and Puck-failure safety factor obtained from the FEA results for the prepreg coupon fibre layer 1 was 157.37 MPa, 0.0033731 mm/mm and 6.8244 respectively. The stress, strain, and Puck-failure safety factor for the wet layup coupon fibre layer 1 was 155.55 MPa, 0.0044578 mm/mm and 5.1798 respectively.

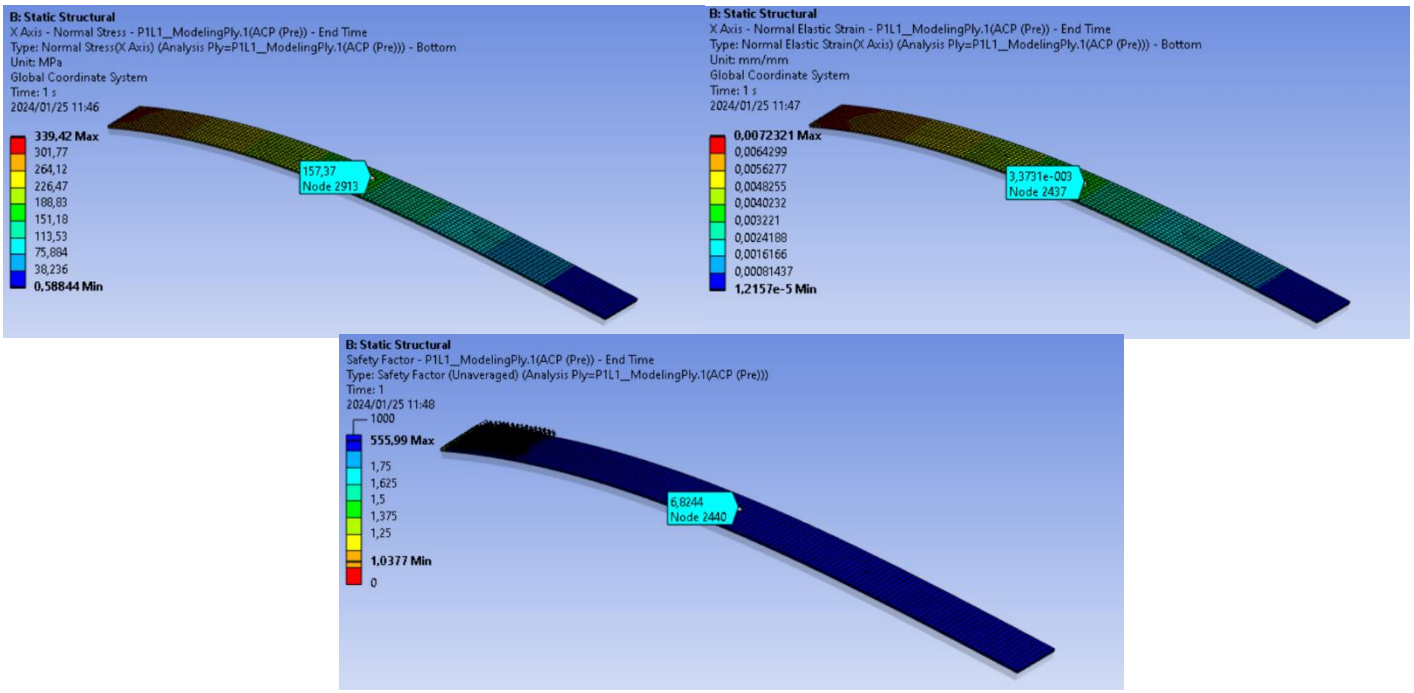


*Figure 159: [0/90/45/0] Epoxy E-Glass Prepreg Coupon Beam Bending Stress, Strain and Safety Factor (Fibre Layer 1)*

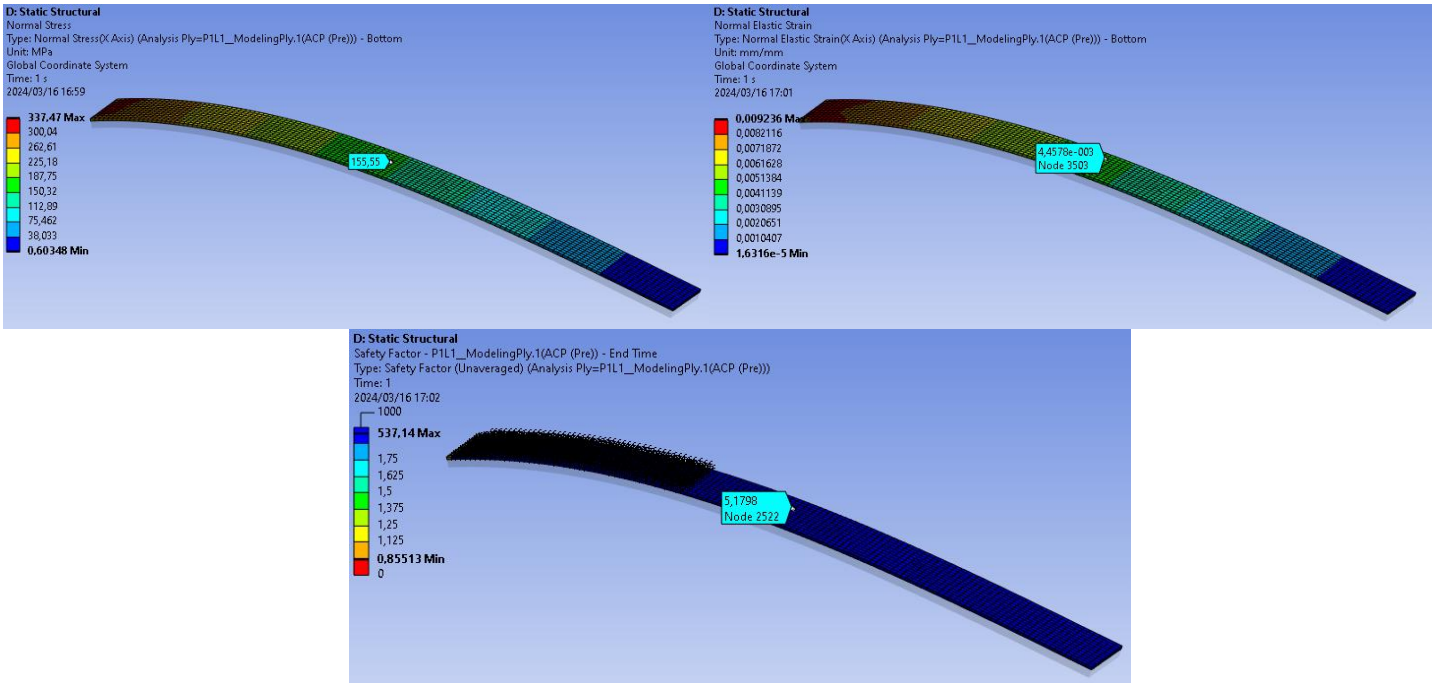


*Figure 160: [0/90/45/0] Epoxy E-Glass Wet Layup Coupon Beam Bending Stress, Strain and Safety Factor (Fibre Layer 1)*

Figure 161 and Figure 162 illustrates the FEA stress results for [0/90/45/0] prepreg and wet layup coupons under beam torsion. The stress, strain, and Puck-failure safety factor obtained from the FEA results for the prepreg coupon fibre layer 1 was 71.824 MPa, 0.0067356 mm/mm and 1.9477 respectively. The stress, strain, and Puck-failure safety factor for the wet layup coupon fibre layer 1 was 72.026 MPa, 0.0071521 mm/mm and 1.4539 respectively.

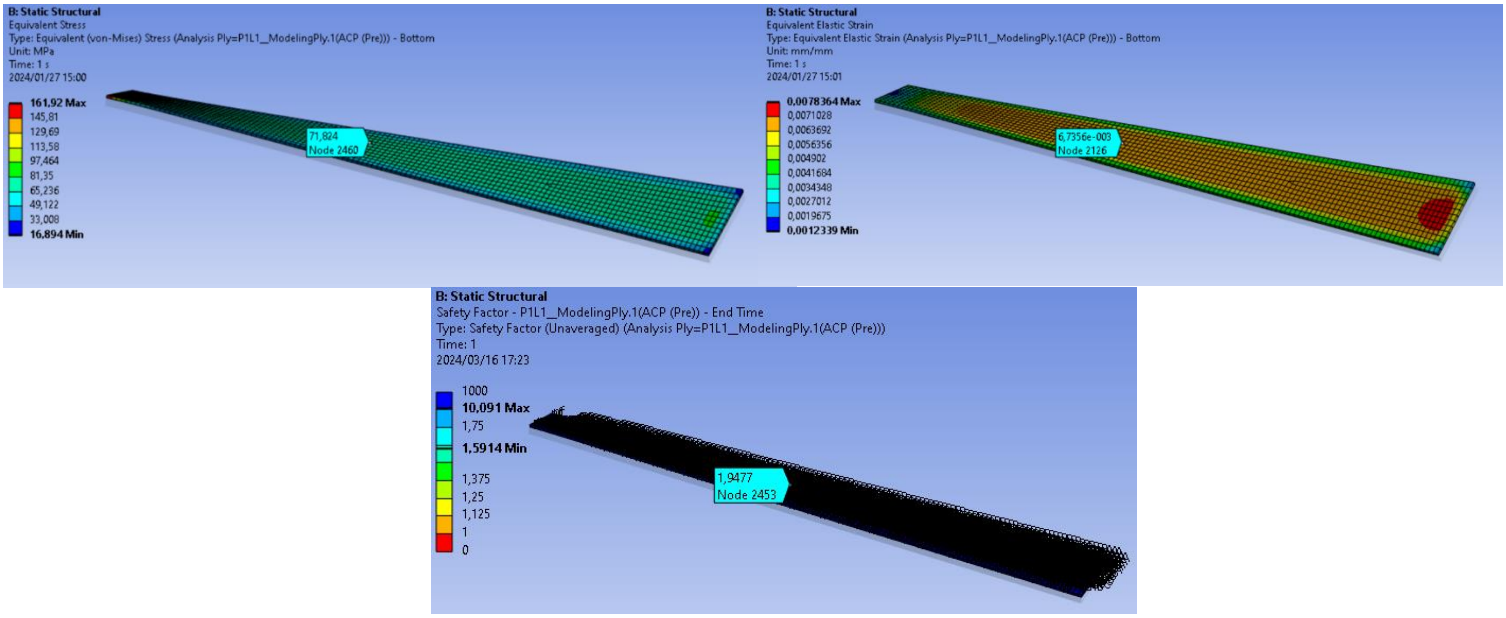


*Figure 161: [0/90/45/0] Epoxy E-Glass Prepreg Coupon Beam Torsional Stress, Strain and Safety Factor (Fibre Layer 1)*

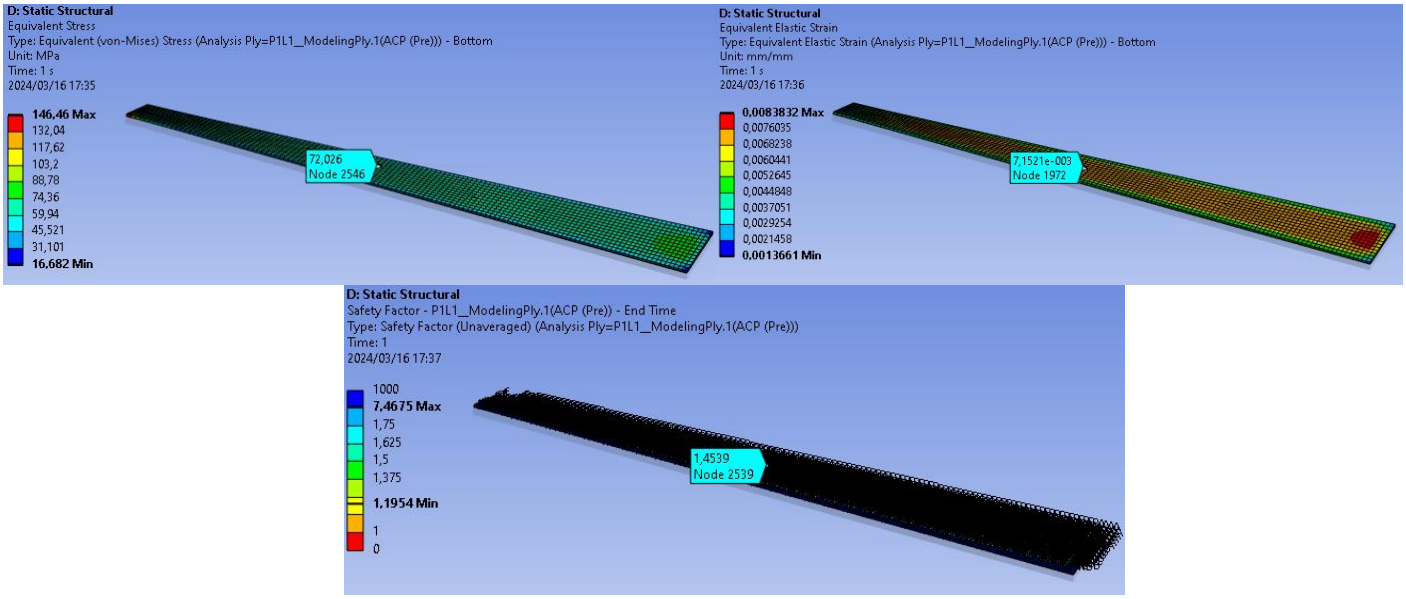


*Figure 162: [0/90/45/0] Epoxy E-Glass Prepreg Wet Layup Beam Torsional Stress, Strain and Safety Factor (Fibre Layer 1)*

Table 45 to Table 48 provides the FEA and analytical results obtained for [0/90/45/0] layered Epoxy E-Glass UD prepreg and Epoxy E-Glass UD wet layup coupons during tension, compression, bending and torsion.

*Table 45: Prepreg and Wet Layup Coupon [0/90/45/0] Results (Tensile Load)*

| Load Type | Stress (FEA) | Stress (Analytical) | Strain (FEA) | Strain (Analytical) | Safety Factor |
|---|---|---|---|---|---|
| - | MPa | MPa | mm/mm | mm/mm | - |
| **[0/90/45/0] Prepreg Coupon (Tension)** | | | | | |
| Layer 1 | 79.328 | 79.259<br>0.087 % | 0.0017435 | 0.0017418<br>0.098 % | **8.311** |
| Layer 2 | 17.06 | 17.561<br>2.937 % | 0.0017299 | 0.0017282<br>0.098 % | **2.0501** |
| Layer 3 | 25.32 | 25.267<br>0.210 % | 0.0017161 | 0.0017146<br>0.087 % | **3.3019** |
| Layer 4 | 77.317 | 77.255<br>0.080 % | 0.0017024 | 0.001701<br>0.082 % | **14.227** |
| **[0/90/45/0] Wet Layup Coupon (Tension)** | | | | | |
| Layer 1 | 76.915 | 76.823<br>0.120 % | 0.0021757 | 0.002178<br>0.106 % | **7.8421** |
| Layer 2 | 18.665 | 18.683<br>0.096 % | 0.0021542 | 0.0021564<br>0.102 % | **1.6148** |
| Layer 3 | 28.402 | 28.398<br>0.014 % | 0.0021326 | 0.0021349<br>0.108 % | **2.3144** |
| Layer 4 | 73.655 | 73.555<br>0.136 % | 0.0021111 | 0.0021133<br>0.104 % | **10.437** |

*Table 46: Prepreg and Wet Layup Coupon Results [0/90/45/0] (Compressive Load)*

| Load Type | Stress (FEA) | Stress (Analytical) | Strain (FEA) | Strain (Analytical) | Safety Factor |
|---|---|---|---|---|---|
| - | MPa | MPa | mm/mm | mm/mm | - |
| **[0/90/45/0] Prepreg Coupon (Compression)** | | | | | |
| Layer 1 | -79.328 | -80.260<br>1.175 % | -0.0017436 | -0.001755<br>0.654 % | **8.4019** |
| Layer 2 | -16.545 | -16.530<br>0.091 % | -0.0017299 | -0.0017282<br>0.098 % | **7.0162** |
| Layer 3 | -25.316 | -25.267<br>0.194 % | -0.0017162 | -0.001715<br>0.070 % | **7.9455** |
| Layer 4 | -76.312 | -76.254<br>0.076 % | -0.0017024 | -0.001701<br>0.082 % | **8.7301** |
| **[0/90/45/0] Wet Layup Coupon (Compression)** | | | | | |
| Layer 1 | -76.915 | -76.823<br>0.120 % | -0.0021757 | -0.002178<br>0.106 % | **6.153** |
| Layer 2 | -18.663 | -18.683<br>0.107 % | -0.0021542 | -0.002156<br>0.084 % | **5.2005** |
| Layer 3 | -28.402 | -28.398<br>0.014 % | -0.0021326 | -0.002135<br>0.0113 % | **5.4432** |
| Layer 4 | -73.641 | -73.555<br>0.117 % | -0.002111 | -0.002113<br>0.095 % | **6.4228** |

*Table 47: Prepreg and Wet Layup Coupon Results [0/90/45/0] (Bending Load)*

| Load Type | Stress (FEA) | Stress (Analytical) | Strain (FEA) | Strain (Analytical) | Safety Factor |
|---|---|---|---|---|---|
| - | MPa | MPa | mm/mm | mm/mm | - |
| **[0/90/45/0] Prepreg Coupon (Bending)** | | | | | |
| Layer 1 | 157.37 | 156.253<br>0.710 % | 0.003459 | 0.003457<br>0.052 % | **6.8244** |
| Layer 2 | 16.755 | 16.692<br>0.376 % | 0.001756 | 0.001742<br>0.797 % | **1.9708** |
| Layer 3 | -26.732 | -26.492<br>0.898 % | -0.001702 | -0.001690<br>0.705 % | **7.7906** |
| Layer 4 | -153.16 | -153.190<br>0.710 % | -0.003189 | -0.003174<br>0.470 % | **4.2047** |
| **[0/90/45/0] Wet Layup Coupon (Bending)** | | | | | |
| Layer 1 | 155.55 | 155.573<br>0.015 % | 0.0044578 | 0.0044377<br>0,453 % | **5.1798** |
| Layer 2 | 19.517 | 19.431<br>0.441 % | 0.0022391 | 0.0022394<br>0.013 % | **1.5735** |
| Layer 3 | -30.094 | -29.957<br>0.455 % | -0.0021556 | -0.0021582<br>0.121 % | **5.3614** |
| Layer 4 | -152.87 | -152.048<br>0.541 % | -0.0043591 | -0.0043568<br>0.053 % | **3.1552** |

*Table 48: Prepreg and Wet Layup Coupon Results [0/90/45/0] (Torsional Load)*

| Load Type | Stress (FEA) | Stress (Analytical) | Strain (FEA) | Strain (Analytical) | Safety Factor |
|---|---|---|---|---|---|
| - | MPa | MPa | mm/mm | mm/mm | - |
| **[0/90/45/0] Prepreg Coupon (Torsion)** | | | | | |
| Layer 1 | 71.824 | 74.399<br>3.585 % | 0.0067356 | 0.0069912<br>3.656 % | **1.9477** |
| Layer 2 | 37.769 | 39.119<br>3.574 % | 0.0035422 | 0.0037124<br>4.585 % | **2.3518** |
| Layer 3 | 69.786 | 71.784<br>2.863 % | 0.0028693 | 0.0030250<br>5.147 % | **3.6427** |
| Layer 4 | 64.661 | 66.723<br>3.189 % | 0.0060595 | 0.0063448<br>4.497 % | **2.0322** |
| **[0/90/45/0] Wet Layup Coupon (Torsion)** | | | | | |
| Layer 1 | 72.026 | 74.601<br>3.452 % | 0.0071521 | 0.007401<br>2.363 % | **1.4536** |
| Layer 2 | 37.533 | 38.851<br>3.512 % | 0.0037251 | 0.0038646<br>3.610 % | **2.0356** |
| Layer 3 | 63.857 | 65.092<br>1.934 % | 0.0031556 | 0.0033231<br>5.040 % | **2.7477** |
| Layer 4 | 66.152 | 68.400<br>3.398 % | 0.0065747 | 0.0067943<br>3.232 % | **1.4985** |

# 17 APPENDIX B (Aluminium 7075 T6 Alloy Gear and Composite Gear Drawings)

Appendix B provides the CAD drawings for the Aluminium 7075 T6 alloy landing gear, composite landing gear and all the assembled components.

## 17.2 Aluminium 7075 T6 Landing Gear

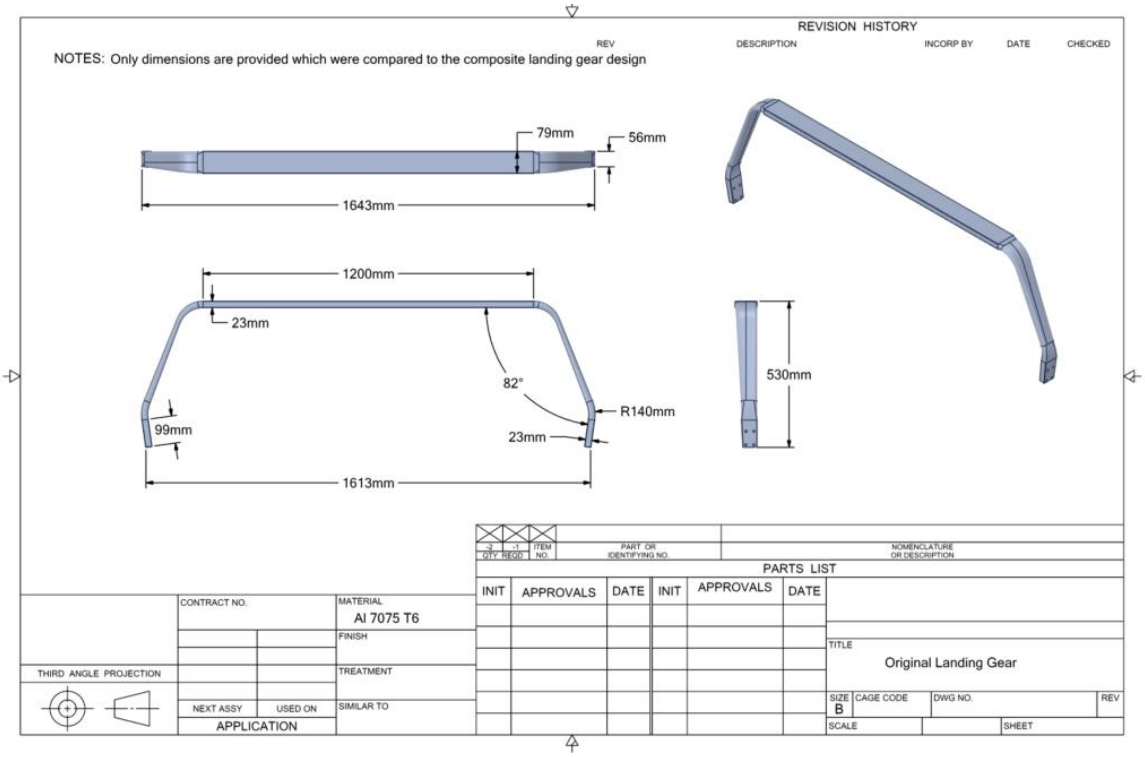


*Figure 163: Aluminium 7075 T6 Alloy Landing Gear Dimensions Drawing*

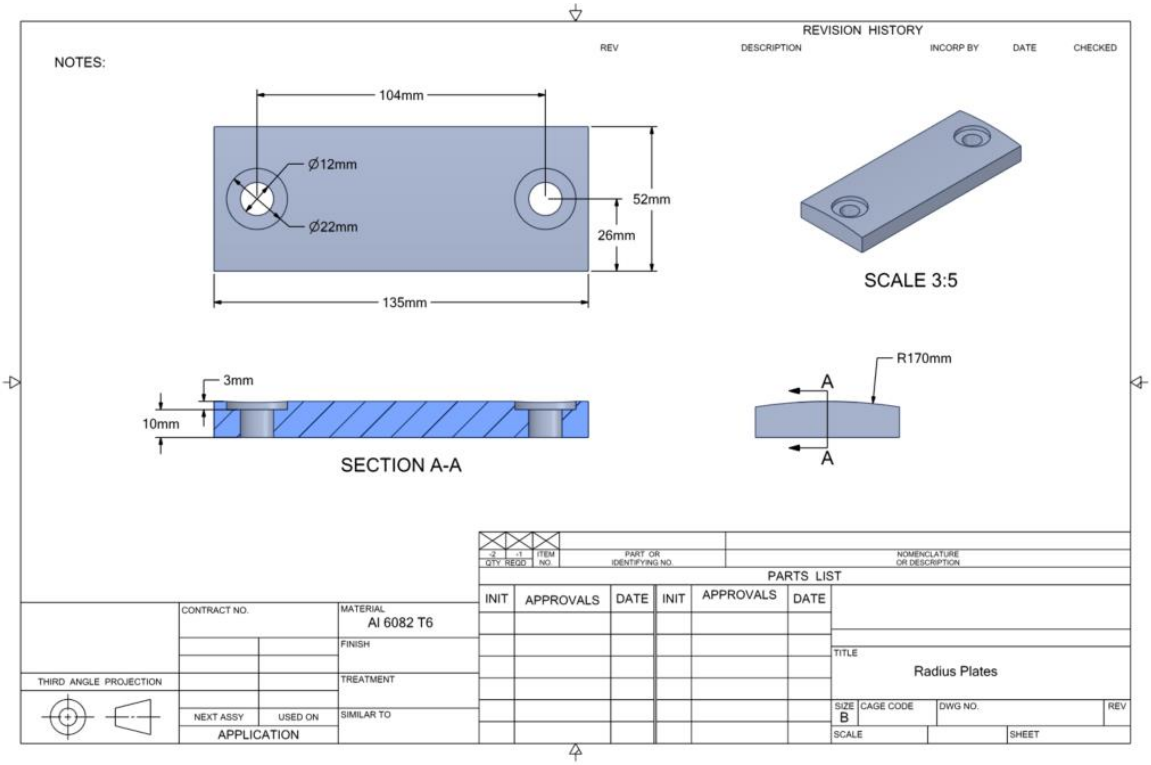


*Figure 164: Aluminium 6082 T6 Radius Plates Drawing*

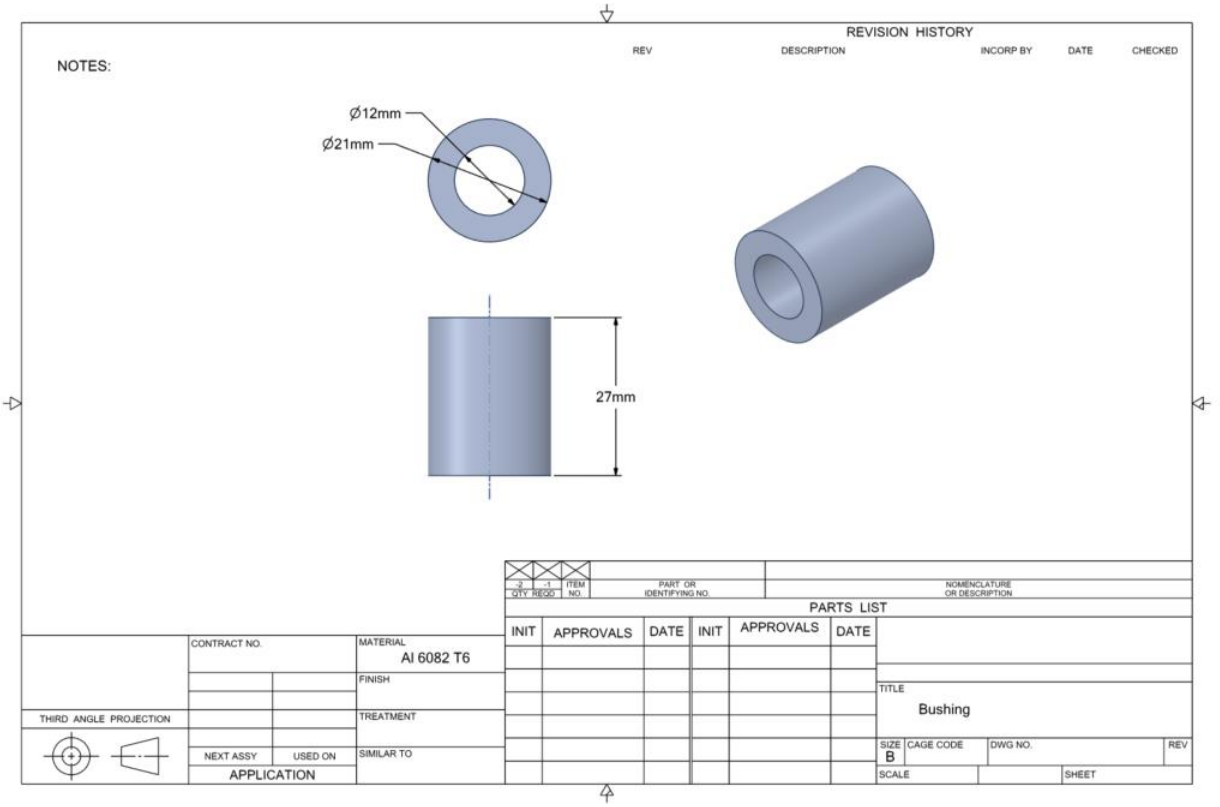


*Figure 165: Aluminium 6082 T6 Bushing (Bolt Sleeve) Drawing*

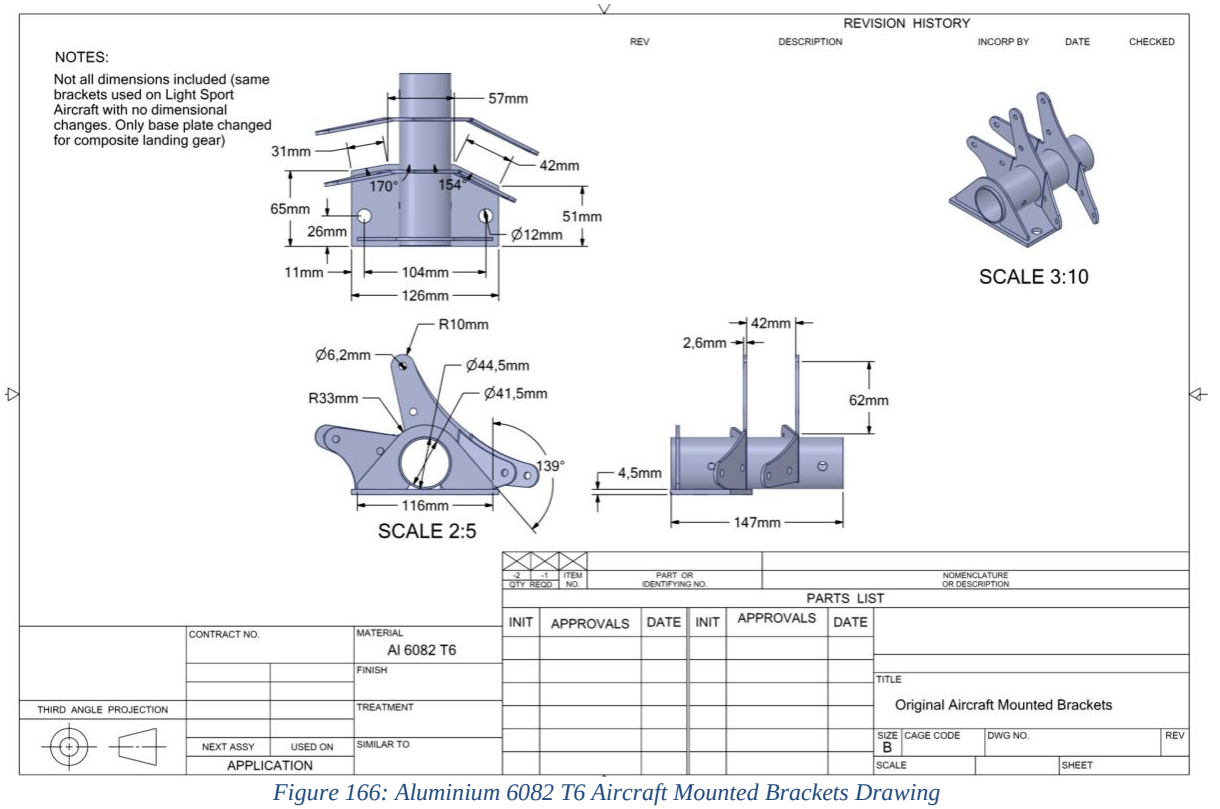


*Figure 166: Aluminium 6082 T6 Aircraft Mounted Brackets Drawing*

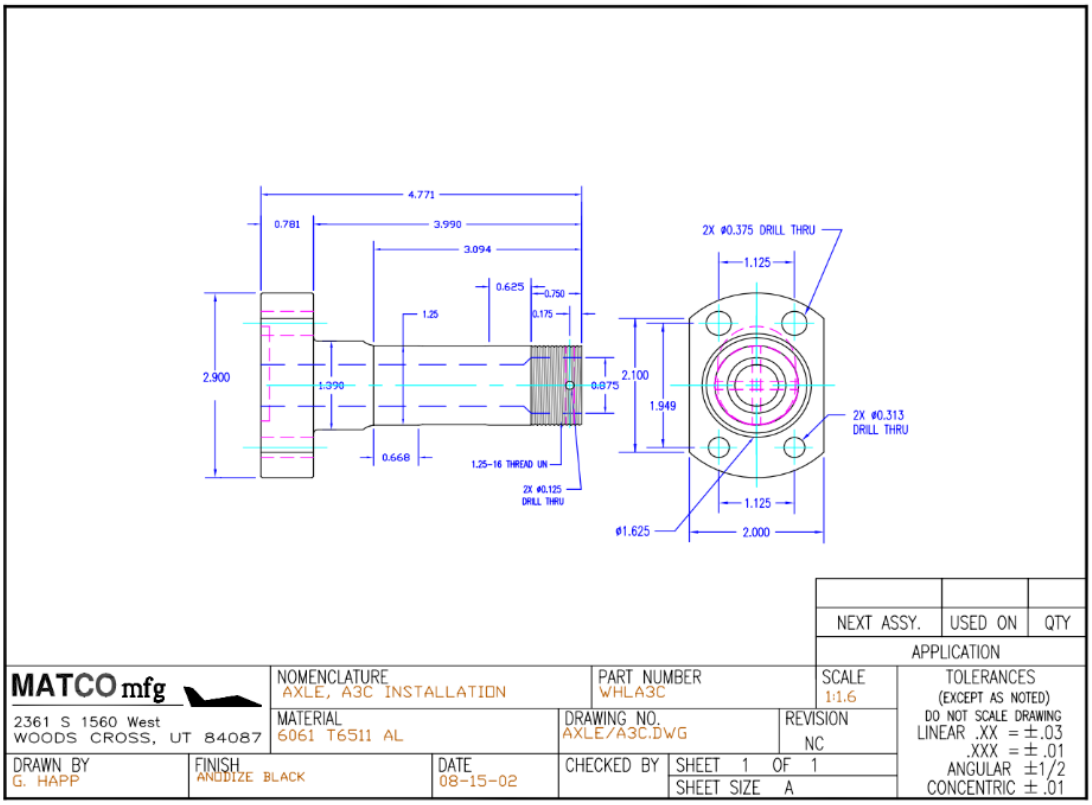


*Figure 167: MATCO A3C Stub Axle Drawing*

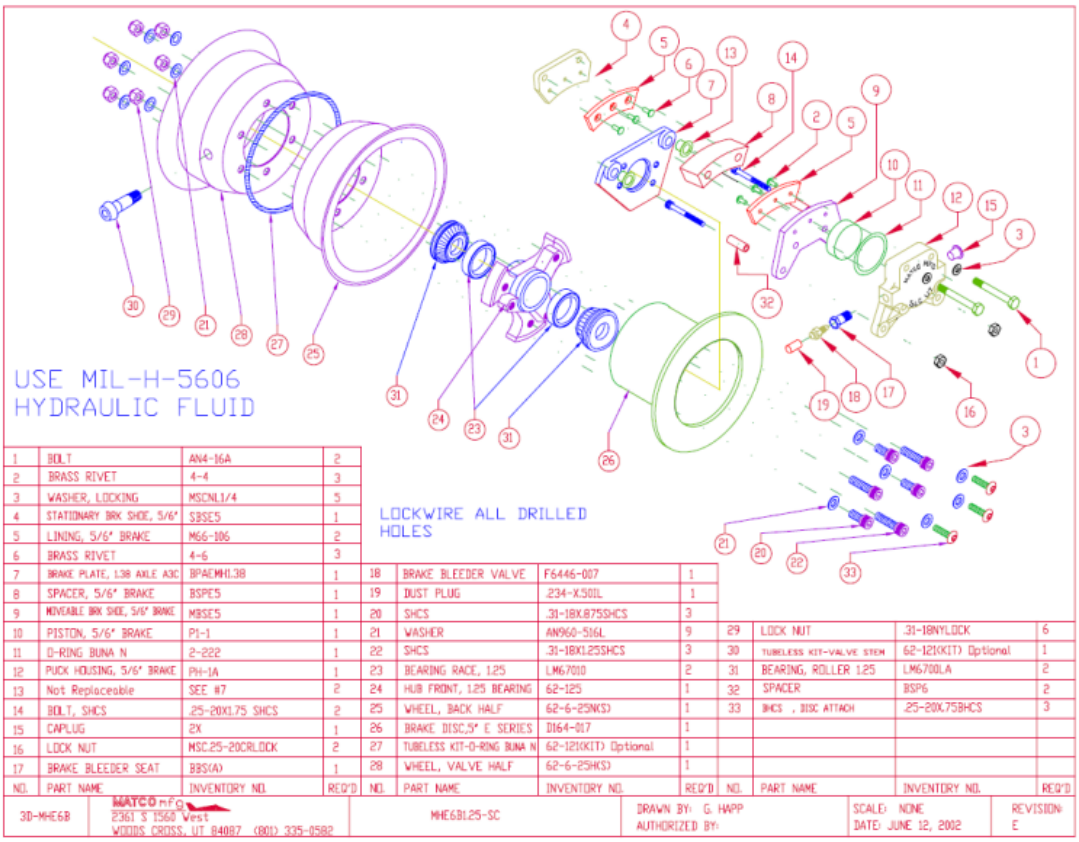


*Figure 168: Wheel Hub and Brakes Assembly Drawing*

### 17.3 Composite Landing Gear

Same stub axles and wheel hub assembly were used for the composite design.

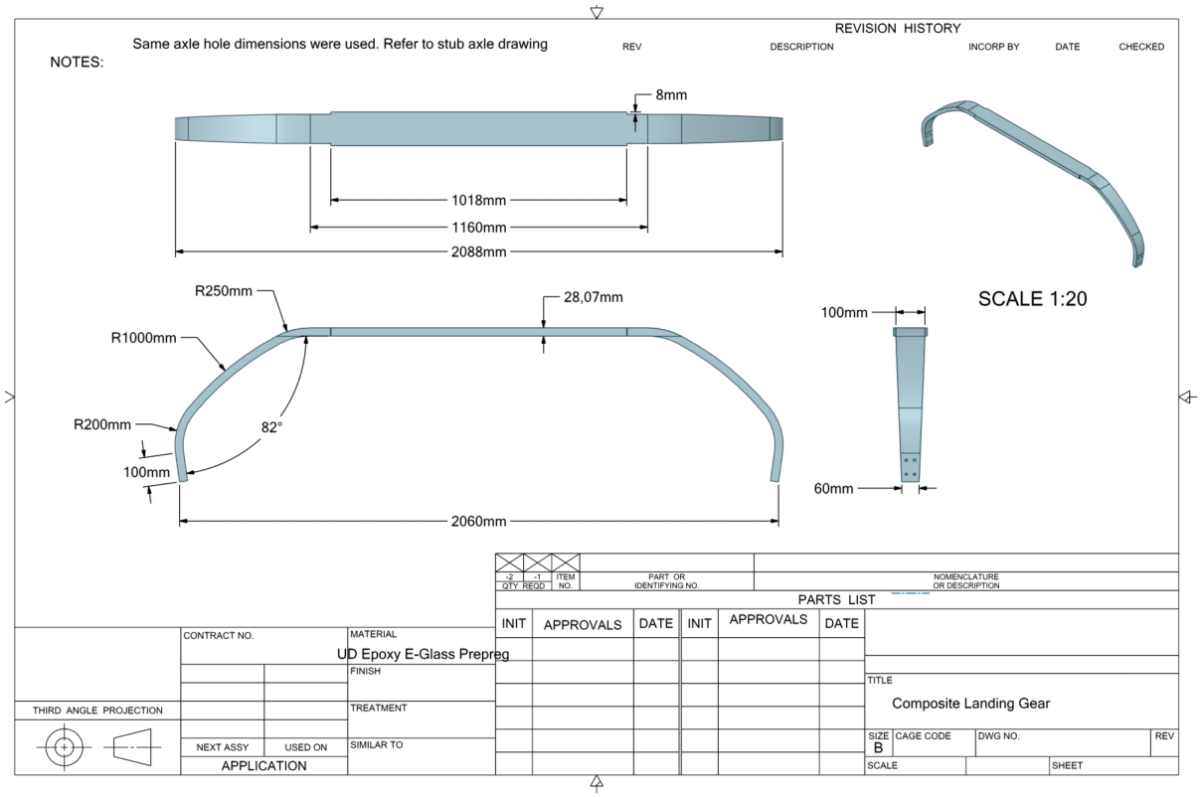


*Figure 169: UD Epoxy E-Glass Prepreg Landing Gear Dimensions Drawing*

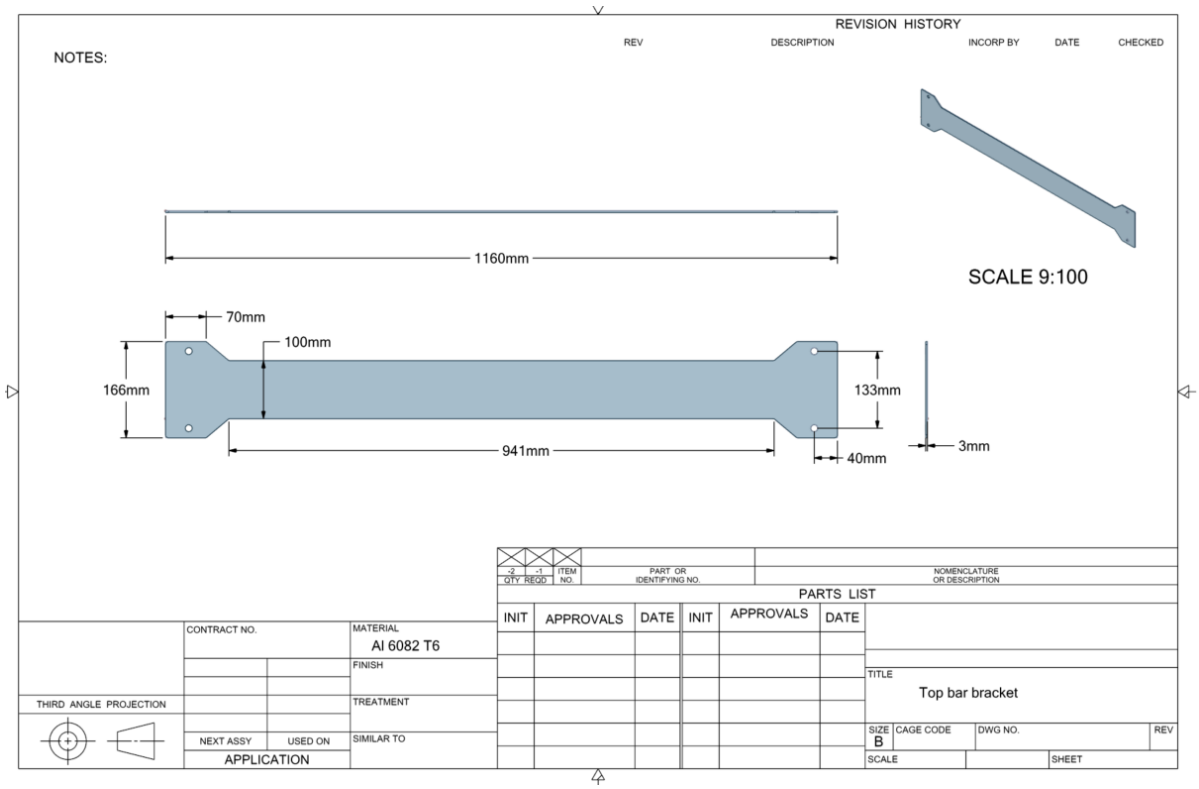


*Figure 170: Aluminium 6082 T6 Top Bar Bracket Drawing*

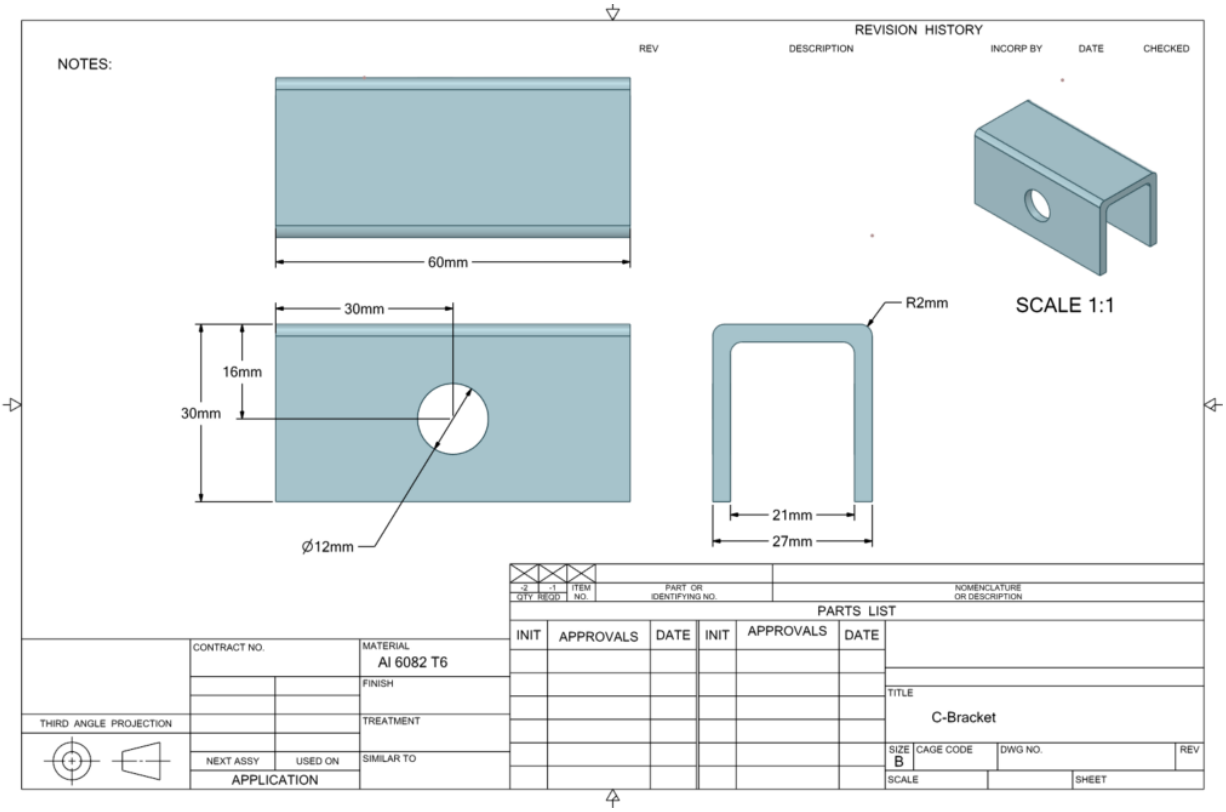


*Figure 171: Aluminium 6082 T6 C-Bracket Inserts Drawing*

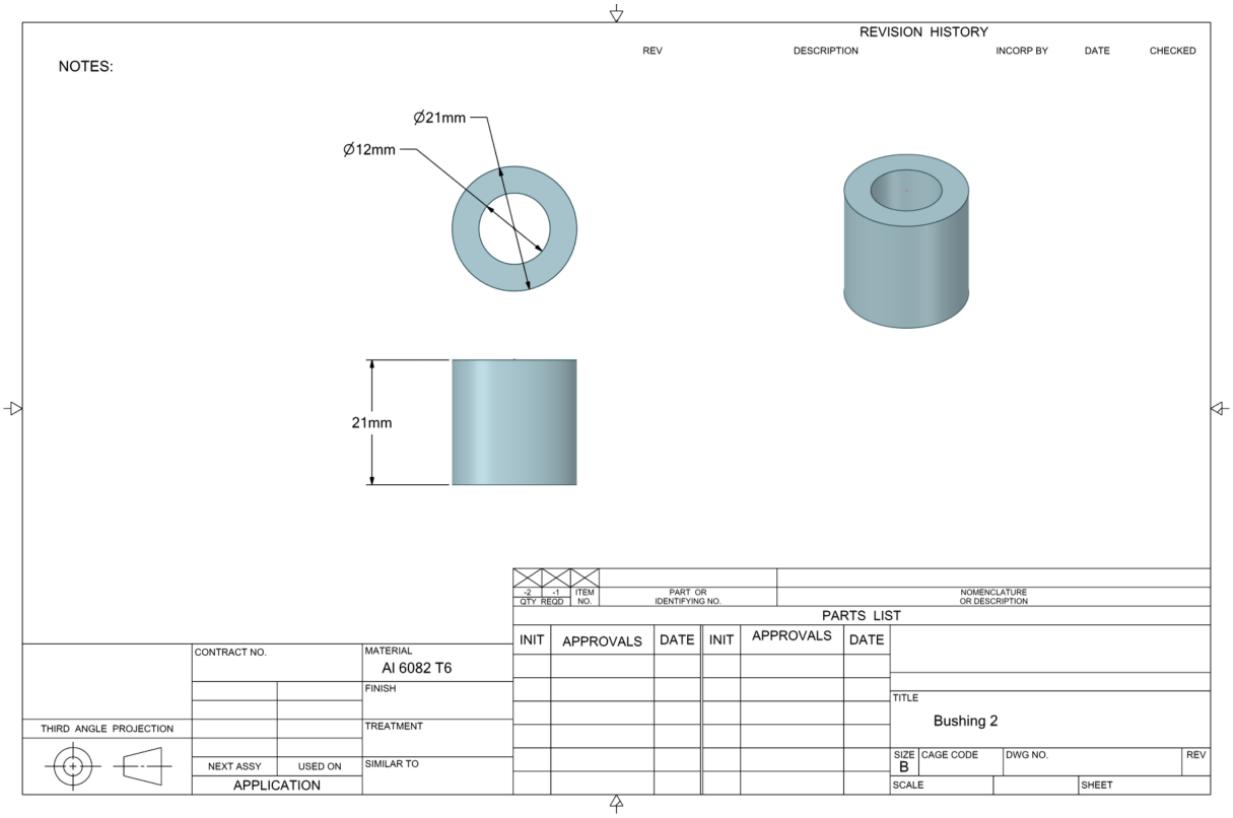


*Figure 172: Aluminium 6082 T6 Bushing 2 (Bolt Sleeve) Drawing*

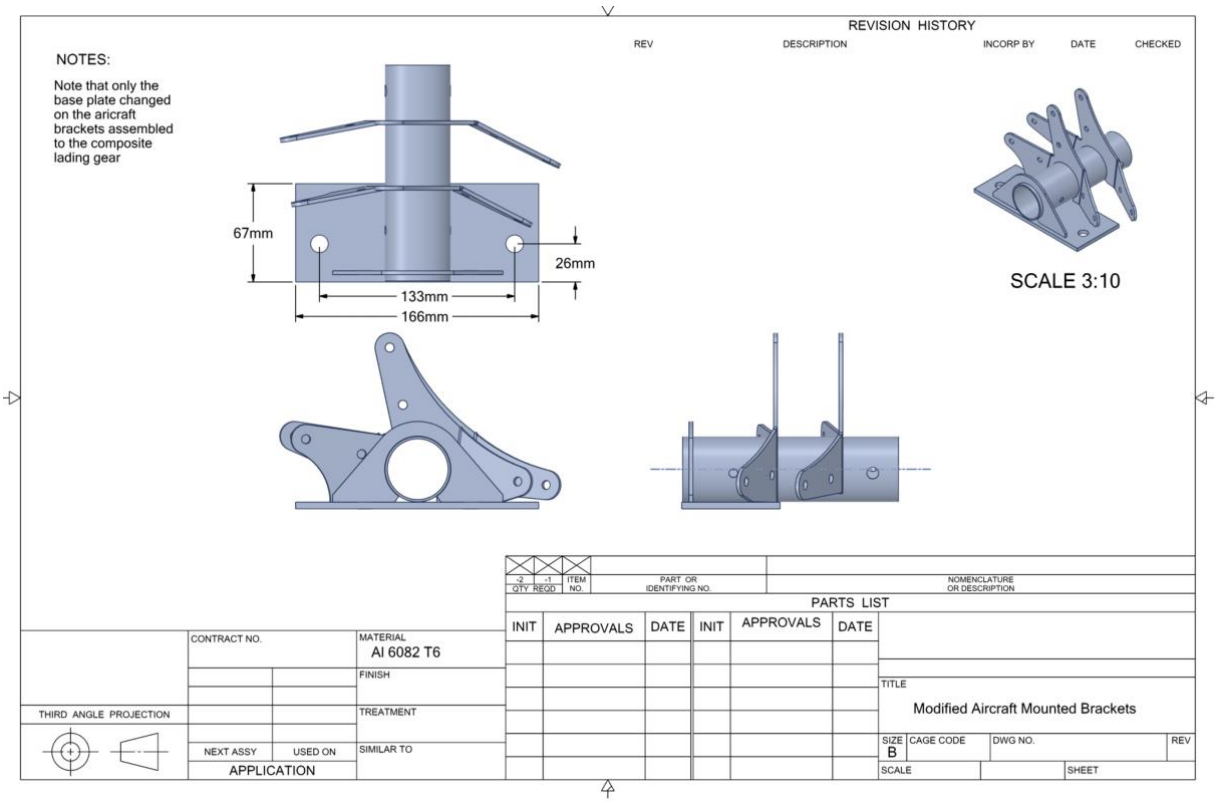


*Figure 173: Aluminium 6082 T6 Modified Aircraft Mounted Brackets Drawing*

## 18 APPENDIX C (Proof of Receipt Payment)

Note: Current Gear Batches are running 16 – 20 weeks after receipt of payment.

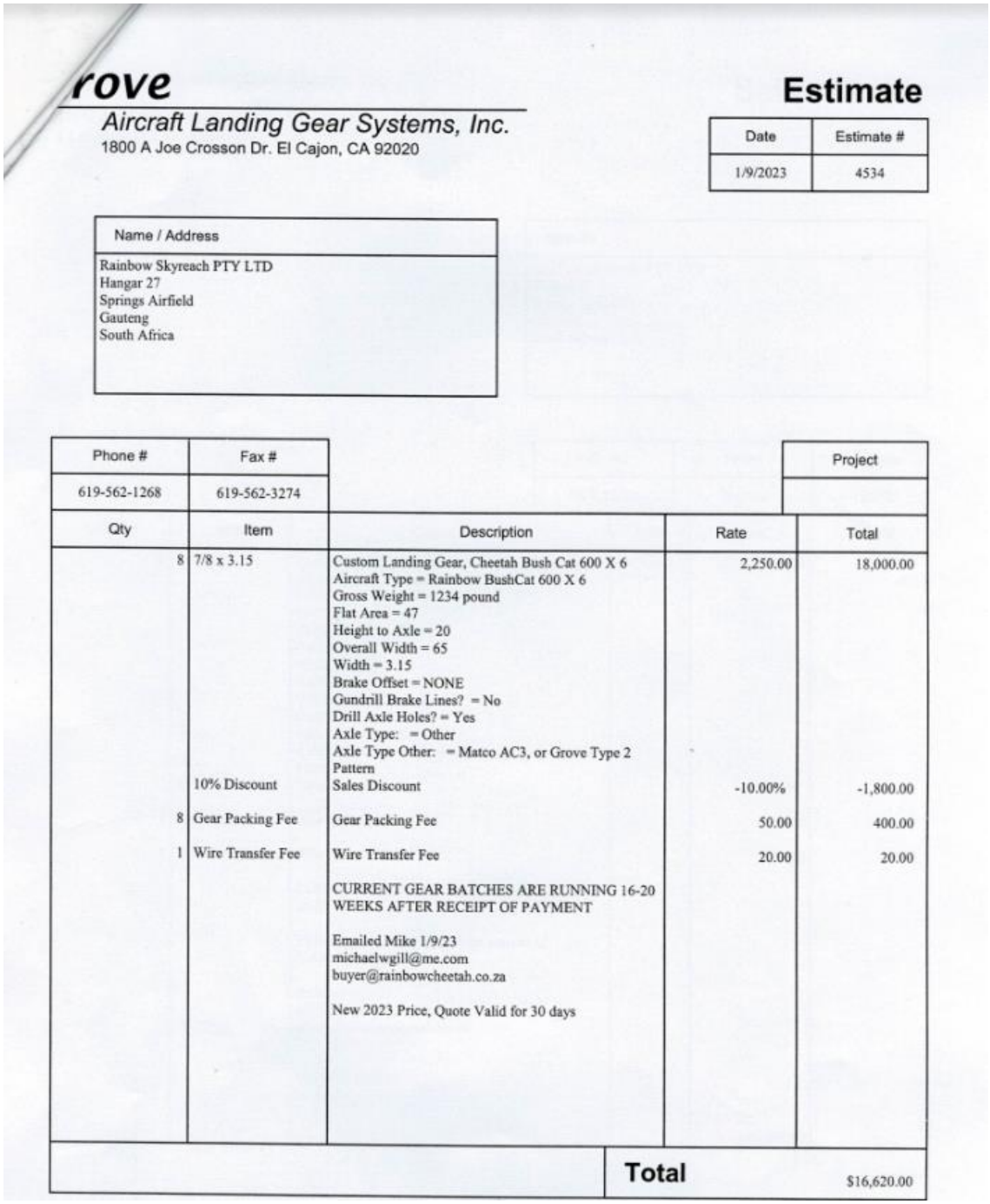

rove

Aircraft Landing Gear Systems, Inc.
1800 A Joe Crosson Dr. El Cajon, CA 92020

**Estimate**

| Date | Estimate # |
|---|---|
| 1/9/2023 | 4534 |

| Name / Address |
|---|
| Rainbow Skyreach PTY LTD<br>Hangar 27<br>Springs Airfield<br>Gauteng<br>South Africa |

| Phone # | Fax # | Project |
|---|---|---|
| 619-562-1268 | 619-562-3274 | |

| Qty | Item | Description | Rate | Total |
|---|---|---|---|---|
| 8 | 7/8 x 3.15 | Custom Landing Gear, Cheetah Bush Cat 600 X 6<br>Aircraft Type = Rainbow BushCat 600 X 6<br>Gross Weight = 1234 pound<br>Flat Area = 47<br>Height to Axle = 20<br>Overall Width = 65<br>Width = 3.15<br>Brake Offset = NONE<br>Gundrill Brake Lines? = No<br>Drill Axle Holes? = Yes<br>Axle Type: = Other<br>Axle Type Other: = Matco AC3, or Grove Type 2 Pattern | 2,250.00 | 18,000.00 |
| | 10% Discount | Sales Discount | -10.00% | -1,800.00 |
| 8 | Gear Packing Fee | Gear Packing Fee | 50.00 | 400.00 |
| 1 | Wire Transfer Fee | Wire Transfer Fee | 20.00 | 20.00 |
| | | CURRENT GEAR BATCHES ARE RUNNING 16-20 WEEKS AFTER RECEIPT OF PAYMENT<br><br>Emailed Mike 1/9/23<br>michaelwgill@me.com<br>buyer@rainbowcheetah.co.za<br><br>New 2023 Price, Quote Valid for 30 days | | |
| | | | **Total** | $16,620.00 |

## 19 ETHICAL ISSUES/CLEARANCE

**University of the Witwatersrand, Johannesburg**

***Ethics WAIVER Application Form* for *Human Research Ethics Committee (HREC Non-Medical)* (SCHOOL ETHICS COMMITTEES: Revised January 2021)**

**Instructions**

1. This form must be completed by Honours (4th year) and Masters by Coursework and Research Report students who are applying for a WAIVERED ethics clearance. Note that waivers for staff non-degree applications, PhD and research Masters students must complete the online ethics application form.
2. Completed waiver applications must be submitted to the relevant School Ethics Committee.
3. Applications may be submitted as hard or soft (electronic) copies, but the first page of the application must contain the signatures of the student and supervisor. Final revised versions must be in soft (electronic) copy as all documentation will be archived.
4. Incomplete or handwritten applications will **NOT** be considered, including where signatures are missing.

**Complete this checklist to show that you have the correct documents:**

☑ Completed ***Ethics Application Form***.
☑ Copy of the ***Research proposal***

**SIGNATURES (REQUIRED)**

***Declaration: We, the signatories, declare that all information on this form is correct and that we will strive to maintain the highest ethical standards in this research at all times, according to disciplinary and university expectations, recognising that ethical practice in research is always a continuing process.***

| | |
|---|---|
| I recognise that it is my responsibility to conduct my research in an ethical manner according to Guidelines of the University of the Witwatersrand, according to any laws and/or legal frameworks that may apply, and according to the norms and expectations of my discipline. In preparing this Application for Ethics Clearance form, I have consulted the ***Guidelines for Human Research Ethics Clearance Application/Non-Medical*** (available on this website https://www.wits.ac.za/research/researcher-support/research-ethics/ethics-committees/). In receiving ethics clearance, I agree to abide by the conditions of data collection as outlined in the *Guidelines* document. | ☑ Yes ☐ No |

**By signing this form, the researcher and supervisor of this project undertake to ensure that any amendments to this project that are required by the Human Research Ethics Committee (Non-Medical) and School Ethics Committees are made before the project commences.**

| | Date | Name | Signature* |
|---|---|---|---|
| **Student** | 26/4/2023 | Marius H. Kotze | MHKotze |
| **Supervisor** | 26/4/2023 | Mr Michael F. Boer | |

*electronic signatures are permitted

| **1. Summary of risk categories of this research project** | |
|---|---|
| **1.1** Does this project involve human participants?<br>*If YES, you need to apply for full ethics clearance through the relevant committee* | ☐ Yes ☑ No |
| **1.2** I have read and understood the risk categories table<br>*Applicants must have read the table of risk level category definitions on the final page of this document. This table is also available on the University Ethics Committee webpage.* | ☑ Yes ☐ No |

**1.3** The applicant must tick the box for the risk category that best applies to this project:

| Risk category | Tick the appropriate box |
|---|---|
| No risk | ✓ |
| Minimal risk | |
| Low risk | |
| Medium risk | |
| High risk | |

Only *No Risk* studies can be considered for a waiver

Studies falling in all other risk categories must complete ethics form and be referred to the School committee

**1.4** I confirm that I understand that if my research changes to include human participants, or secondary analysis of data collected from human participants, or a different risk category other than 'no risk', it is my responsibility to immediately apply for full ethics clearance from the relevant committee ☑ Yes ☐ No

| **2. Researcher's personal data** | |
|---|---|
| Your family name: Kotze | Your first name: Marius |
| Title: ☑ Mr ☐ Ms ☐ Other : _____ | |
| School: | School of Mechanical, Industrial and Aeronautics |
| Your student number: | 2743834 |
| Your email: | 2743834@students.wits.ac.za |
| Your tel number: | 0724822987 |
| Name of supervisor(s): | Mr Michael F. Boer |
| Your supervisor's Wits email: | michael.boer@wits.ac.za |
| Your supervisor's Wits tel number: | 0117177314 |

**3. Research project**

**3.1** Title of research project: Metallic equivalent of aircraft landing gear using composite materials

**3.2** Is this research for degree purposes? ☑ Yes ☐ No

**3.3** If YES, for what degree?

☐ Honours ☑ Masters (research report) ☐ Other (specify) _____

**3.4** Has the proposal been **approved** by the relevant School or Faculty higher degrees committee or other unit?

☑ Yes ☐ No ☐ Submitted and pending

**3.5** What are the **aims and objectives** of the research? (Please be specific)

Determine the correct design loads inflicted on the BushCat Aircraft main landing gear.
Specify a composite alternative that can withstand these calculated design application loads.

**3.6 Summary or abstract of the research** (100 words maximum)

*Give a brief outline of the research plan such that reviewers can understand what the study is about, what data you will use, how you will collect or get access to the data, and what analyses will be used*

See Open Space Below For Summary...

**3.7** Will this study reuse data that have been previously collected by other researchers? ☐ Yes ☑ No

If **YES**, do you have written permission to reuse the data? ☐ Yes ☐ No
*If you don't, you must obtain this permission from the principal investigator*

| | |
|---|---|
| **3.8** Is this application for a multi-student project (i.e. several students working on exactly the same topic under the same supervisor)?<br><br>If **YES,** list the names and student numbers of additional students working on this project: | ☐ Yes ☑ No |

Rainbow Skyreach (Pty) Ltd is a South African Civil Aviation Authority (SACAA) approved aircraft manufacturer and is known for manufacturing the BushCat Light Sport Aircraft (LSA). The BushCat Aircraft main landing gear is manufactured using Aluminium 7075 T6. The current landing gear is manufactured by Grove Aircraft Landing Gear Systems Inc. which is situated in United States of America. Due to the current landing gear being manufactured by a foreign company, Skyreach has experienced delays in shipment of this specific landing gear which causes further delays in the manufacturing of the BushCat Aircraft.
The current landing gear cannot be manufactured in South Africa due to local Aluminium manufacturers not having the correct equipment to obtain the required material properties for the main gear thus, a composite alternative is required which can be manufactured locally. Thus, an alternative composite design should be able to withstand the correct design loads inflicted upon the Bushcat Aircraft main landing gear.

The following data on various parameters needs to be collected in order to ensure the design is valid. Some of the data are collected by engineers at Skyreach such as aircraft weight, current landing gear dimensions and Pilot Operating Handbook (POH).

1) Aircraft weight - The weight is important when determining the loads on the on the landing gear. This data collection can include maximum take-off weight, empty weight, and payload weight

2) Landing gear dimensions – These dimensions are important since it directly impacts the aircrafts stability, performance, and safety during take-off. The dimensions will make sure it adheres to the ground clearance and weight distribution requirements. According to Skyreach, the new design must be the same dimensions as the Aluminum landing gear as much as possible so that minimal changes are required.

3) Landing conditions - The landing conditions are important since it determines what forces act in on the landing gear during different conditions for the taildragger and tricycle Bushcat aircrafts. These landing conditions are collected via the CS 23 amendments and ASTM F2245 – 14.

4) Regulatory requirements – The regulatory requirements include the POH. This can give information regarding the limitations at which the Bushcat aircraft can operate in. These limitations include aircraft airspeed, weight and balance which are important for calculations

5) Stress analysis – Once necessary data is collected, Ansys can be used to perform a stress analysis on the landing gear. This analysis will help to understand the forces acting on the landing gear and identify potential failure points.